KINETIC AND MECHANISTIC STUDIES OF OXYGEN SENSING FE(II)/2-OXOGLUTARATE DEPENDENT OXYGENASES



A thesis submitted to the Board of the Faculty of Physical Sciences at the University of Oxford in partial fulfilment of the requirements for the degree of Doctor of Philosophy

Hanna Tarhonskaya

St Hugh's College, Oxford

Michaelmas Term 2014

ABSTRACT

Hanna Tarhonskaya D. Phil.

St Hugh's College Michaelmas Term 2014

Kinetic and Mechanistic Studies of Oxygen Sensing Fe(II)/2-oxoglutarate Dependent Oxygenases

The Fe(II)/2-oxoglutarate (2OG) dependent oxygenases are a widespread enzyme family, which are characterised by structurally similar active sites and proposed to employ a common reaction mechanism. The work described in this thesis concerned kinetic and biophysical studies on 2OG oxygenases, with a particular focus on the hypoxia-inducible transcription factor (HIF) hydroxylases and mechanistic aspects of their reaction with oxygen.

The four human HIF hydroxylases regulate cellular levels and transcriptional activity of HIF by catalysing its post-translational hydroxylation in response to changes in oxygen availability. The three prolyl hydroxylase domain enzymes (PHDs1-3) and factor inhibiting HIF (FIH) are proposed to act as cellular oxygen sensors and provide a direct link between oxygen availability and the hypoxic response.

Previous transient kinetic studies have shown that PHD2 (the most important human PHD isoform) reacts slowly with oxygen, a factor proposed to be related to its oxygen-sensing role. The molecular mechanisms for the slow PHD2 reaction with oxygen were investigated using a range of kinetic and biophysical techniques to probe the effects of key active site substitutions. The studies reveal that a conservative substitution to an Fe(II)/H_2O binding residue results in 5-fold faster reaction with oxygen, suggesting a role for H_2O release from the active site in limiting the ability of oxygen to react with PHD2. This thesis also describes the first transient kinetic studies of FIH. The obtained results show that the rate of the FIH reaction with oxygen was significantly faster than for PHD2. Further, FIH catalyses hydroxylation not only of HIF-α, but also of proteins containing ankyrin repeat domains (ARD). The rate of the FIH reaction with oxygen was shown to be substrate dependent; faster oxygen activation of the reaction in the presence of ARD compared with HIF substrates was observed.

Mechanistic studies were performed to investigate a report that PHD2 is involved in the enzymatic oxidation of an oncometabolite (*R*)-2-hydroxyglutarate (2HG) to give 2OG, in what would be an unprecedented reaction for a 2OG oxygenase. This work found that 2HG does not substitute for 2OG in PHD2 catalysis. Instead, the non-enzymatic transformation of 2HG to 2OG was observed, which could potentially contribute to the reported 2HG-dependent PHD activation *in vivo*.

The biophysical and transient kinetic techniques used for studying the HIF hydroxylases were also applied to study the mechanism of deacetoxycephalosporin C synthase (DAOCS, the enzyme catalysing penicillin N ring expansion). Previously, it has been suggested that the DAOCS mechanism differs from the consensus 2OG oxygenase mechanism. The results described in this thesis provide strong evidence that DAOCS employs the consensus ordered mechanism characteristic of 2OG oxygenases, supporting the proposal that the consensus mechanism is a common feature of the 2OG oxygenase family.

Overall, the work described in this thesis is supportive of the proposal that most, if not all, 2OG oxygenases employ a common mechanism. However, the differences in the kinetics of their reaction with oxygen, presented throughout the thesis, suggest that different 2OG oxygenases have different rate-limiting steps. Thus, the kinetics of specific oxygenases may be adapted to their biological function, in particular that of PHD2 as the key cellular O_2 sensor.

Dedicated to my parents

Прысвячаецца маім бацькам

Acknowledgements

Firstly, I would like to thank my supervisors, Prof Christopher J. Schofield and Dr Emily Flashman. I thank Chris for giving me the opportunity to join the group and for allowing a lot of scientific freedom in pursuing research. I am very grateful to Emily for her help and advice every time when I needed them, for scientific and personal support through all my D. Phil. studies. Without this support I wouldn't be able to make it this far.

Special gratitude goes to my collaborators for their contributions to the projects: Dr Rashed Chowdhury for the crystallography work, Dr Nikita Loik for teaching me his mass spectrometry tricks, Dr Ivanhoe Leung and Dr Anna Rydzik for their NMR work, Dr Adam Hardy for useful scientific discussions and protein LC-MS, and Dr Sarah Wilkins for teaching me how to perform CD spectroscopy. I also would like to thank Wendy Sobey and Manso Jubier Herminio for providing their management in the lab and helping my experiments to go faster.

Of course, I cannot forget to thank people who created this wonderful warm and friendly atmosphere for me in this group: Inga Pfeffer, Jürgen Brem, Nikita Loik, Sander van Berkel, Carmen Domene, Ilaria Pettinati, Thomas Leißing, Shoichiro Horita, Becky Hancock and many others. Thank you for being good friends and for bringing some cheer into my everyday life. Furthermore, credit goes to people who took their time to proofread my thesis: to Leah Kearney, Carmen Domene, Becky Hancock, David Zollman, Rashed Chowdhury, Sam Cahill and Sarah Wilkins. I am very thankful for your critical comments. Overall, I would like to thank all CJS group members, past and present, for being wonderful colleagues.

I also would like to express my sincere gratitude to the Clarendon fund and to St Hugh's College for funding my D. Phil. studies. In particular I would like to thank Mr William Louey whose generous donation formed the funding body of my St Hugh's College Scholarship. This financial support gave me a life-changing opportunity to obtain my degree from the University of Oxford.

Very heartfelt thanks go to my fiancé Evgeny Kolychev for special support and continuous encouragement through all these years. Thank you for always being there for me when I needed your help.

Больш за ўсё, канешне, я хачу падзякаваць маім бацькам, яны заўсёды падтрымлівалі мяне на працягу ўсяго гэтага часу. Ваша вера і падтрымка натхнялі мяне ісці далей і здзяйсняць мае мары. Вялікі дзякуй вам за гэта.

Table of Contents

ABBREVIATIONS **i**

CHAPTER 1: Introduction **1**

1.1. Non-heme Fe(II)/2OG dependent oxygenases **1**

1.2. Mechanism of 2OG oxygenases and transient kinetic studies **3**

1.3. Deacetoxycephalosporin C synthase (DAOCS) **8**

1.4. Hypoxia-Inducible Factor (HIF) and the HIF hydroxylases **10**

1.5. Prolyl Hydroxylase Domain 2 (PHD2, EGLN1) **13**

1.6. Factor Inhibiting HIF (FIH) **15**

1.7. HIF hydroxylases as therapeutic targets and their relation to cancer **17**

1.8. Thesis objectives **19**

1.9. References **20**

CHAPTER 2: Kinetic studies on oxygen activation of PHD2-catalysed HIF-1/2α hydroxylation **29**

2.1. Introduction **29**

2.2. Results **32**

2.2.1. Steady-state kinetics of the PHD2-catalysed reaction: HIF-1α vs HIF-2α 32

2.2.2. Oxygen dependence of the PHD2-catalysed reaction 36

2.2.3. Stopped-flow kinetics of PHD2-catalysed HIF-1/2α hydroxylation 38

2.3. Discussion **49**

2.4. References **52**

CHAPTER 3: Mechanistic studies on the reaction of PHD2 with oxygen **54**

3.1. Introduction **54**

3.2. Results **57**

3.2.1. Activity of PHD2 variant enzymes 57

3.2.2. Fe(II) binding to PHD2 facial triad variants 59
3.2.3. Fe(II) and 2OG binding to PHD2 variants with altered co-substrate interactions 62
3.2.4. NODD hydroxylation catalysed by PHD2 and its variants 65
3.2.5. CD spectroscopy and amino acid analysis 67
3.2.6. pH dependence of PHD2 and its variants 69
3.2.7. Steady-state kinetics of the PHD2 variants 70
3.2.8. Steady-state oxygen dependence of the PHD2 variants 73
3.2.9. Pre-steady-state kinetic studies on PHD2 and its variants 76
3.2.10. Crystallographic analysis of the D315E variant 82

3.3. Discussion 85

3.4. References 88

CHAPTER 4: Mechanistic studies on the reaction of FIH with oxygen 91

4.1. Introduction 91

4.2. Results 94
4.2.1. FIH activity assays in the reaction with HIF-α and ARD substrates 94
4.2.2. Steady-state kinetic parameters of FIH-catalysed HIF-1/2α and ARD substrate hydroxylation 97
4.2.3. Oxygen dependence of the FIH-catalysed hydroxylation 101
4.2.4. UV-vis spectroscopy studies on the formation of FIH.Fe(II).2OG.substrate complex 103
4.2.5. Pre-steady-state kinetics of FIH-catalysed hydroxylation of CAD HIF-1/2α 105
4.2.6. Pre-steady-state studies on hydroxylation of ankyrin repeat domain substrates 111

4.3. Discussion 118

4.4. References 120

CHAPTER 5: Mechanistic studies on DAOCS-catalysed ring expansion of penicillin N 123

5.1. Introduction 123

5.2. Results 126
5.2.1. Non-denaturing mass spectrometry studies of a ternary complex formation 126
5.2.2. Presence of a substrate results in a shift of MLCT absorbance maximum 130
5.2.3. Stopped-flow kinetic studies on the DAOCS-catalysed reaction 131
5.2.4. Rapid quench-flow studies on DAOCS-catalysed reaction 135

5.3. Discussion **138**

5.4. References **142**

CHAPTER 6: Mechanism of 2-hydroxyglutarate oxidation **144**

6.1. Introduction **144**

6.2. Results **146**

6.2.1. Enzymatic assays on 2HG-promoted PHD2 catalysis of CODD hydroxylation 146

6.2.2. Studies of 2HG binding to PHD2 150

6.2.3. Non-enzymatic nature of 2HG oxidation 153

6.2.4. NMR studies on non-enzymatic 2HG oxidation 158

6.2.5. 2HG-promoted activation of other 2OG oxygenases 162

6.3. Discussion **166**

6.4. References **170**

CHAPTER 7: Materials and Methods **173**

CHAPTER 8: Summary and conclusions **198**

APPENDIX **202**

Abbreviations

(w/v) Weight to volume ratio

(v/v) Volume to volume ratio

2HG 2-hydroxyglutarate

2OG 2-oxoglutarate

2 TY 2 Tryptone/yeast medium

ACCO 1-aminocyclopropane-1-carboxylic acid oxidise

APS Ammonium persulphate

ARD Ankyrin repeat domain

Asc L-ascorbate

BBOX1 γ-butyrobetaine dioxygenase

bHLH Basic helix-loop-helix

BSA Bovine serum albumine

C Celsius

CA consensus ankyrin

CAD *C*-terminal transactivation domain

CBP CREB (cyclic adenosine monophosphate-response element binding protein) binding protein

CD Circular dichroism

cDNA Complementary DNA

CODD *C*-terminal oxygen-dependent degradation domain

CODD-OH Hydroxylated CODD

CPH Collagen prolyl hydroxylase

D-2HGDH D-2-hydroxyglutarate dehydrogenase

DACS Deacetylcephalosporin C synthase

DAOCS Deacetoxycephalosporin C synthase

DAOC Deacetoxycephalosporin C

DNA Deoxyribonucleic acid

dNTP Deoxyribonucleotide triphosphate

DSBH Double-stranded β-helix

DTT Dithiothreitol

EGF Epidermal growth factor

EPO Erythropoietin

ESI-MS Electrospray ionisation mass spectrometry

FIH Factor inhibiting hypoxia-inducible factor

FPLC Fast protein liquid chromatography

FTO The fat mass and obesity associated protein

GABA γ-aminobutyric acid

GBB γ-butyrobetaine

GBH γ-hydroxybutyrate

GSH Glutathione

GSSG Oxidised form of glutathione

h Hours

hABH2/3 Human AlkB homologue-2/3

HEPES (*N*-[2-Hydroxyethyl]piperazine-*N*'-[2-ethanesulfonicacid])

HIF Hypoxia-inducible factor

HK1/2 Hexokinase 1/2

HOT Hydroxyacidoxoacid transhydrogenase enzyme

HPLC High performance liquid chromatography

IDH1/2 Isocitrate dehydrogenase 1/2

IPNS Isopenicillin-N-synthase

IPTG Isopropyl-β-D-thiogalactoside

IOX3 (FG-2216) 2-(1-chloro-4-hydroxyisoquinoline-3-carboxamido) acetic acid

JmjC Jumonji C domain

K_d Dissociation constant

kDa Kilodalton

K_m Michaelis constant

L-2-HGDH L-2-hydroxyglutarate dehyrogenase

L5H Lysyl-5-hydroxylase

L-malIDH L-malate dehydrogenase

LB Luria Bertani broth

LC-MS Liquid chromatography mass spectrometry

LEW Lysis-equilibration-wash buffer

MALDI-TOF-MS Matrix assisted laser desorption/ionisation-time-of-flight mass spectrometry

max Maximum

MCD Magnetic circular dichroism

MES 2-Morpholinoethanesulphonic acid

MFC Mass-flow comtrollers

min Minutes

MLCT Metal to ligand charge transfer

MS Mass spectrometry

MWCO Molecular weight cut-off

m/z Mass to charge ratio

ND Not determined

NMR Nuclear magnetic resonance

NODD *N*-terminal oxygen-dependent degradation domain

NOG *N*-oxalylglycine

OD Optical density

OGFOD1 2OG and Fe(II)-dependent oxygenase domain-containing protein 1

P3H Prolyl-3-hydroxylase

PAGE Polyacrylamide gel electrophoresis

PCR Polymerase Chain Reaction

PDB Protein data bank

penG/N Penicillin G/N

Pfu Pyrococcus furiosus

PHD Prolyl hydroxylase domain

PhyH Phytanoyl-CoA 2-hydroxylase

pVHL Von Hippel-Lindau tumour suppressor protein

Q-TOF Quadrupole time-of-flight

RNA Ribonucleic acid

RPS23 40S ribosomal protein S23

ROS Reactive oxidising species

SA Succinic acid

SSA Succinic semialdehyde

SD Standard deviation

SDS Sodium dodecylsulphate

SIE Solvent isotope effect

SyrB2 Syringomycin halogenase

TauD Taurine dioxygenase

TCA Tricarboxylic acid

TED Tris-carboxymethyl ethylene diamine

TEMED *N,N,N′,N′*-Tetramethylethylene-diamine

TMLH Trimethyllysine hydroxylase

Tnkrs-1/2 Tankyrase-1/2

Tris Tris(hydroxymethylethyl)aminomethane

U Units

UV-vis Ultraviolet-visible

V Volts

VEGF Vascular endothelial growth factor

V_{max} Maximal velocity

WT Wild type

Standard abbreviations for nucleotides, standard amino acids, SI-units/prefixes and chemical elements are used throughout.

Chapter 1: Introduction

1.1. Non-heme Fe(II)/2OG dependent oxygenases

The non-heme Fe(II)/2-oxoglutarate (2OG) dependent oxygenases are a large enzyme superfamily that catalyse a variety of reactions, including chromatin/transcription factor modification, collagen biosynthesis, lipid metabolism, nucleic acid repair, etc. (**Figure 1.1**) [1-4]. In animals, 2OG oxygenases catalyse reactions of hydroxylation and demethylation (proceeding via hydroxylation), however in plants and microorganisms 2OG oxygenases catalyse a much wider range of oxidative reactions including desaturation, epimerisation, oxidative ring closure, rearrangement and halogenation [1, 2, 5]. There are also several examples of enzymes that are closely related to 2OG oxygenases based on their structure and mechanism, which do not utilise 2OG during their catalysis (e.g. isopenicillin N synthase (IPNS), which catalyses cyclisation of a tripeptide yielding the penicillin nucleus, and 1-aminocyclopropane-1-carboxylic acid oxidase (ACCO), which catalyses the production of ethylene, CO_2, and cyanide, involved in plant signalling) [1, 6].

The 2OG oxygenase family is remarkably diverse in terms of biological function, with new 2OG oxygenases still regularly being discovered and characterised [1-3, 7, 8]. Analyses of structure and sequence homology imply that 2OG oxygenases have diverged from a common ancestor, and first diversified in bacteria [9]. The identified biological functions performed by 2OG oxygenases in humans are summarised in **Figure 1.1**. 2OG oxygenases are involved in chromatin regulation by modification of nucleic acids, e.g. 5-methylcytosine oxidation, and histone tails, via N^{ϵ}-methyl lysine residue demethylation [4]. 2OG oxygenases also play important roles in the cellular and physiological responses to hypoxia [3, 8, 10], and participate in fatty acid metabolism (L-carnitine biosynthesis and degradation pathway of α-oxidation of phytanic acid) [1]. The fat mass and obesity associated protein (FTO) is a 2OG oxygenase performing *N*-methyl nucleic acid demethylation [1, 11]. Another 2OG oxygenase has been shown to have an effect on protein translational accuracy (OGFOD1, enzyme catalysing the hydroxylation of the ribosomal protein RPS23, which affects stop codon read-through) [12-14].

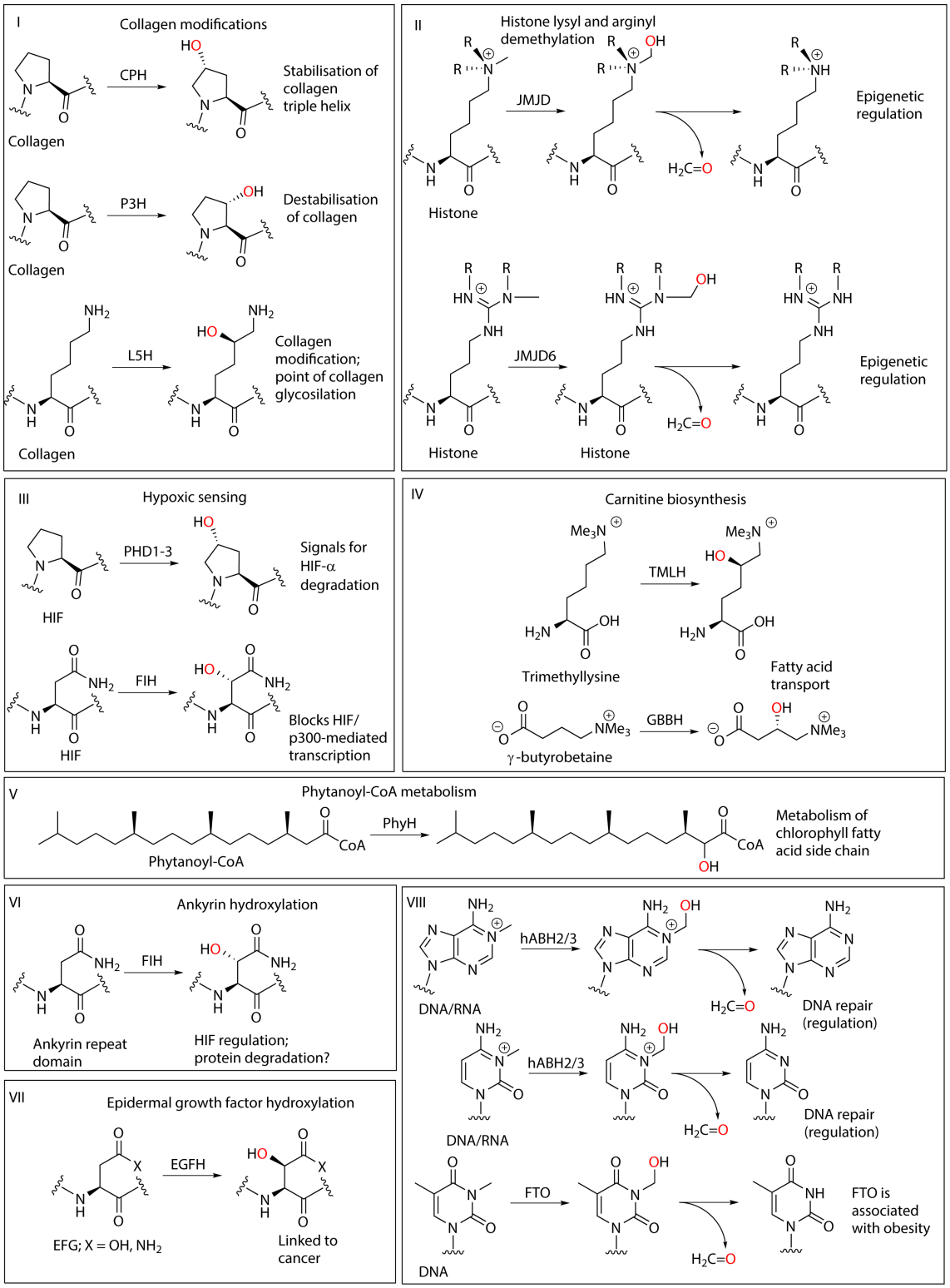


Figure 1.1. Summary of the reactions catalysed by 2OG oxygenases. (I) Collagen modifications, (II) epigenetic regulation, (III) hypoxia sensing, (IV) carnitine biosynthesis, (V) phytanoyl-CoA-metabolism, (VI) ankyrin hydroxylation, (VII) epidermal growth factor hydroxylation, (VIII) DNA repair and modification [1].

2OG oxygenases utilise Fe(II) as a co-factor and 2OG as a co-substrate to perform the 2-electron oxidation of 2OG leading to succinate formation, which is coupled to oxidative modifications of a 'prime' substrate [5, 15, 16]. Structural studies show that 2OG oxygenases have conserved active site structures and contain a double-stranded β-helix (DSBH) fold [17]. The active site Fe(II) is coordinated by two histidine residues and one carboxylate group of aspartate/glutamate from the conserved HXD/E…H motif ('facial triad') [18] (**Figure 1.2**). In the enzyme-substrate complex, 2OG is chelated by Fe(II) in a bidentate manner, and a water molecule completes the Fe(II) octahedral coordination. While a 'prime' substrate binds in the proximity of the facial triad, it is not directly coordinated to Fe(II) (see below).

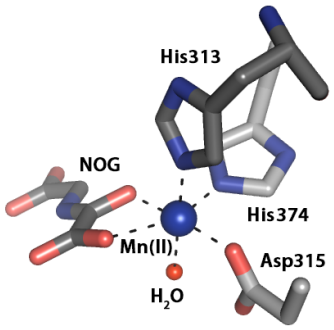


Figure 1.2. The metal ion coordination in PHD2.Mn(II).*N*-oxalylglycine (NOG).CODD structure (PDB: 3HQR) [19]. Active site metal ion has octahedral coordination and is chelated by two histidine residues and one carboxylate group of aspartate from the conserved HXD/E…H motif, NOG and a water molecule.

1.2. Mechanism of 2OG oxygenases and transient kinetic studies

It has been proposed that 2OG oxygenases employ a consensus mechanism proceeding via the formation of a ternary enzyme.Fe(II).2OG.substrate complex, in most of the studied cases with a defined order of substrate binding [5, 16, 20] (**Figure 1.3**). The first proposal of the 2OG oxygenase-catalysed hydroxylation mechanism was based on theoretical considerations [21]. Later experimental studies on taurine dioxygenase (TauD) confirmed the viability of the mechanism, albeit with some modifications [16].

Upon 2OG binding to the TauD.Fe(II) complex, there is formation of a weak absorbance feature centered in the 500 nm region (**Figure 1.3, I**). Solomon and co-workers showed by circular dichroism (CD) and magnetic circular dichroism (MCD) spectroscopy that this absorbance feature represents metal-ligand charge transfer (MLCT) due to the interaction of Fe(II) with 2OG coordinated in a bidentate manner [22]. Studies on model systems showed

that monodentate 2OG coordination is also possible, but that does not result in the appearance of an MLCT band [23, 24]. More importantly, it has been shown that Fe(II) preserves a nearly octahedral six-coordinate state with one water molecule completing the coordination. Although the binding of a 'prime' substrate does not occur via direct coordination to the active site metal, it is proposed to weaken the water Fe(II) coordination and trigger a change from a six- to a five-Fe(II) coordinate state [22].

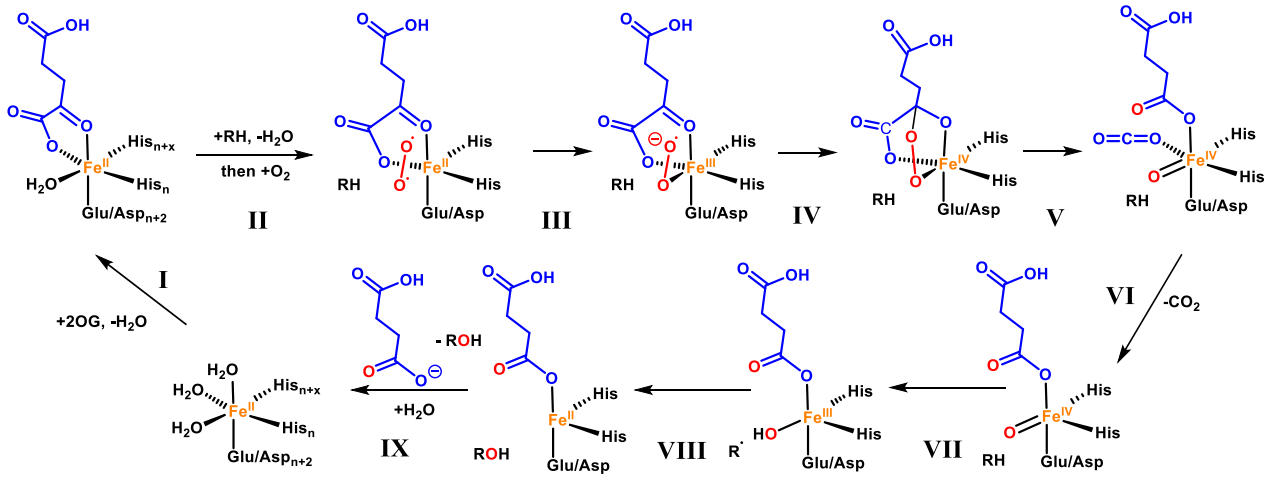


Figure 1.3. Outline of the proposed mechanism of Fe(II)/2OG dependent oxygenases. Binding of dioxygen, which occurs subsequently to enzyme-substrate complex formation, results in the oxidative decarboxylation of 2OG (step V) and generation of an Fe(IV)-oxo species (step VI) that enables hydroxylation of the C-H bond (steps VII-VIII).

Following binding events (except oxygen), the dissociation of the metal-bound water molecule occurs, which creates a vacant coordination position, where oxygen is proposed to bind [20, 25] (**Figure 1.3, I**). 2OG oxidation usually occurs at a slow rate in the absence of a 'prime' substrate [26-31]. It has been proposed that slow rates of uncoupled turnover (oxidative 2OG decarboxylation to succinate in the absence of 'prime' substrate modification) are related to difficulties in oxygen activation in the absence of a 'prime' substrate [5, 32, 33]. Thus, it has been shown that binding of a 'prime' substrate triggers faster reaction with oxygen due to the facilitated release of the metal-bound water molecule [27-29, 34]. Furthermore, the incorrect positioning of a substrate leads to an increased uncoupled turnover [16].

Computational and model system studies coupled with related experiments on the interaction of NO with Fe(II) have suggested that addition of oxygen to the coordinatively unsaturated Fe(II) leads to formation of an Fe(III)-superoxo complex, the reactive nature of which has so far precluded its direct observation [16, 35-38]. The proposed Fe(III)-superoxo species performs a nucleophilic attack on the C-2 of 2OG forming the bicyclic species (**Figure 1.3**, **IV**), with subsequent oxidative decarboxylation of 2OG, succinate and CO_2 formation. The studies on model systems, whereby electron-withdrawing substituents on the α-ketoacid were introduced, led to the acceleration of a decarboxylation rate, which was consistent with the proposed mechanism [23].

The next key step in catalysis is the formation of an Fe(IV)-oxo intermediate, performing H-abstraction from the 'prime' substrate and yielding an Fe(III)-OH complex. Although most of the mechanistic studies were conducted using model systems, the first direct observation of the proposed consensus mechanism reaction intermediates was reported in 2004 by Bollinger, Krebs and co-workers based on studies of TauD [16, 27]. Kinetic and spectroscopic studies on TauD led to the observation of two reaction intermediates (**Figure 1.4b**). In stopped-flow experiments, upon mixing anaerobic TauD.Fe(II).2OG.taurine complex with oxygen-saturated buffer, a strong absorbance feature with maximum at 318 nm was apparent. The 318 nm species then degraded with the decrease of absorbance at 520 nm, which corresponded to loss of an MLCT band of the reactant complex (i.e. TauD.Fe(II).2OG.substrate). The 318 nm intermediate was shown to absorb in a visible region, thus the development of a second intermediate, lacking the absorbance properties of the initial complex, could only have been observed after degradation of this 318 nm species. Notably, kinetic isotope effect studies with deuterium-labelled substrates revealed that the 318 nm intermediate is involved in the H-abstraction step of the catalysis [27, 39].

Further spectroscopic characterisation of the 318 nm reaction intermediate was conducted using rapid freeze-quench Mössbauer spectroscopy. Analyses of isomer shift values and quadrupole splitting parameters were different compared to any previously reported shifts for model Fe(IV)-oxo complexes [27]. However, the intermediate decomposition after exposure to γ-radiation yielded a high-spin Fe(III) species, thus it was concluded that the iron oxidation state of the intermediate was +IV. Further structural characterization (by resonance Raman

and X-ray absorption spectroscopy) showed that the 318 nm intermediate is a high-spin Fe(IV) species proposed to participate in the 2OG oxygenase catalysis (reviewed in reference [16]).

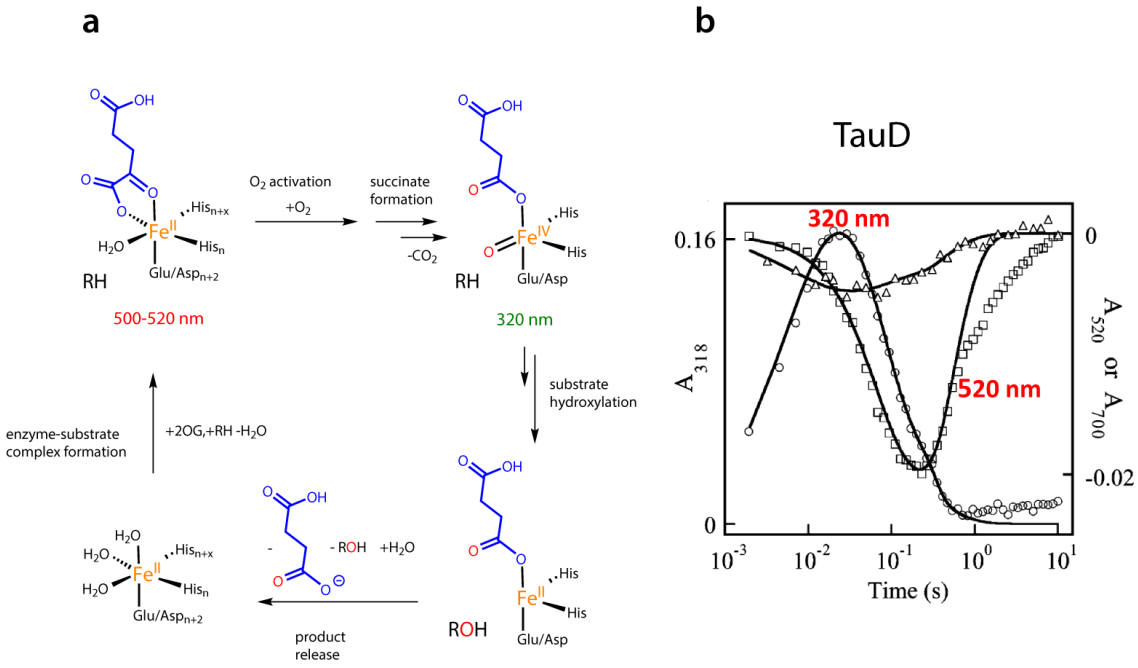


Figure 1.4. Pre-steady state kinetic studies on 2OG oxygenases. (a) An abbreviated scheme of the proposed 2OG oxygenase mechanism. **(b)** The kinetic traces representing depletion of the initial enzyme-substrate complex (520 nm) and formation of Fe(IV)-oxo intermediate (320 nm) for TauD [27]. Figure is adapted with permission from Price *et al.* (2003) Biochemistry 42, 7497-7508. Copyright (2003) American Chemical Society.

The second intermediate (520 nm absorbance decay) was a product of the 318 nm species degradation and had spectral characteristics allowing its assignment as a high-spin Fe(II) complex [27]. Rapid quench-flow (CO_2 and sulfite release in the TauD-catalysed reaction) together with solvent viscosity experiments provided further support for the intermediate assignment as an Fe(II)-product(s) complex [34]. Although 2OG oxygenase catalysis must involve other intermediate species, the kinetics of their formation as well as their highly reactive nature appeared to be unfavorable for their accumulation and therefore experimental observation, at least for systems studied to date.

The subsequent hydroxylation step was proposed to proceed via a radical mechanism, where a substrate radical reacts with Fe(III)-OH complex [5]. This has been in accord with a number of studies using $^{18}O_2$, when isotope labelled oxygen was incorporated into succinate and into

the hydroxylated product (reviewed in reference [5]). Interestingly, for some 2OG oxygenases the ratio of ^{18}O incorporation into hydroxylated product was shown to be less than stoichiometric suggesting that some of the catalytic intermediates may undergo oxygen exchange with solvent water [40]. The proposed mechanism of this exchange has included a 'ferryl-flip' step (**Figure 1.5**). This is when the Fe(IV)-oxo intermediate is protonated and coordinates a hydroxide, with subsequent release of a water molecule and return to the Fe(IV)-oxo intermediate step prior to substrate hydroxylation [5, 41].

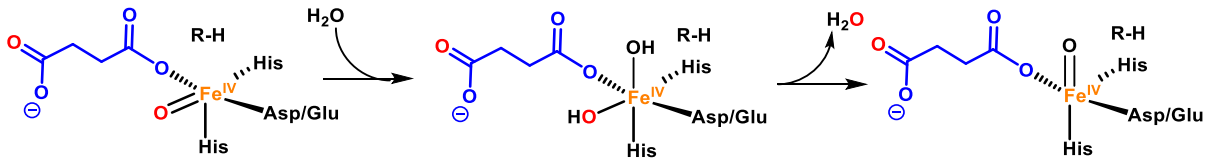


Figure 1.5. Scheme outlining the proposed 'ferryl-flip' mechanistic step. Binding of a water molecule results in Fe(IV)-oxo intermediate protonation. Subsequent release of a water molecule results in return to the Fe(IV)-oxo intermediate step.

After the pioneering studies on TauD, similar analyses on other 2OG oxygenases have been performed [28-31]. Accumulation of two intermediates in the reaction of viral collagen prolyl-4-hydroxylase (vCPH) with a close similarity to those observed in TauD catalysis was reported [28], again with a large kinetic isotope effect of the reaction. The mechanistic studies were expanded onto halogenases (CytC3 and SyrB2) showing that they employ the consensus mechanism common for 2OG oxygenases [29, 39]. Interestingly, for CytC3 two high-spin Fe(IV) intermediates were shown to exist in an equilibrium [39]. Notably, all these studies showed very fast oxygen activation of the reaction, with Fe(IV)-oxo intermediate maximum accumulation times around 10-100 ms.

The direct observation and characterisation of an Fe(IV)-oxo intermediate, together with isotope exchange studies, showing incorporation of oxygen atoms into succinate and a product, provided the first experimental evidence for the proposed sequence of the catalytic events utilised in the catalysis by 2OG oxygenases [16, 27]. However, mechanistic differences related to the biological function of each member of the enzymatic family in particular still remain to be identified. Further clarification of the mechanistic details, and 'case' kinetic studies on 2OG oxygenases are therefore required.

1.3. Deacetoxycephalosporin C synthase (DAOCS)

Deacetoxycephalosporin C synthase (DAOCS) catalyses the chemically interesting oxidative ring expansion of penicillin N (penN) to deacetoxycephalosporin C, which is a committed step in the biosynthesis of the medicinally important cephalosporin antibiotics [42-48]. There is a subsequent enzymatic reaction leading to the C-3' hydroxylation of deacetoxycephalosporin C. In some eukaryotic species, there is a DAOCS homolog (DAOC/deacetylcephalosporin C synthase (DACS)), a bifunctional enzyme, which is able to catalyse both penicillin ring expansion and further hydroxylation. However, in prokaryotic organisms, such as *S. clavuligerus*, containing the 'monofunctional' DAOCS, another enzyme (DACS) catalyses the subsequent hydroxylation reaction [44, 47, 49]. These enzymes are interesting from the perspective of their practical application in the biosynthesis of antimicrobial therapeutic agents (cephalosporins), which requires a ring expansion step of hydrophobic penicillins, such as penicillin G (penG). The more hydrophobic cephalosporins can be more efficiently extracted than the natural cephalosporins possessing the polar D-δ-(α-aminoadipoyl) side chain [49-58].

The mechanistic studies on the DAOC/DACS included isotope effect experiments to elucidate the penicillin ring expansion mechanism during catalysis. These studies, where penN was labelled with deuterium at the (*pro-S*) *β*-methyl group, suggested reversibility of penN binding to the Fe(IV)-oxo complex [42, 49, 59]. Competition experiments, in which both deuterated and protiated substrates were simultaneously present, showed that the protiated penN is selectively transformed into the product relative to the deuterated penN. In contrast, such an effect was not observed in the analogous experiments with C-2 labelled deuterated penN [49]. In the case of C-2 deuteration DAOC/DACS promotes formation of a 3*β*-hydroxycepham 'shunt' product that arises from hydroxylation rather than desaturation of the cephem radical intermediate [49, 59]. It was proposed that the isotope effect observations reflect a mechanism in which the C-2 C-H bond is cleaved after the reaction of the Fe(IV)-oxo species with the (*pro-S*) *β*-methyl group. Furthermore, previous isotopic studies using labelled $^{18}O_2$ or $H_2{}^{18}O$ showed that in the case of DAOCS incorporation of ^{18}O into the hydroxylated product was only ~50 % [40, 42]. It has been proposed that the Fe(IV)-oxo intermediate can undergo an oxygen exchange with solvent water during the reaction (**Figure 1.5**)

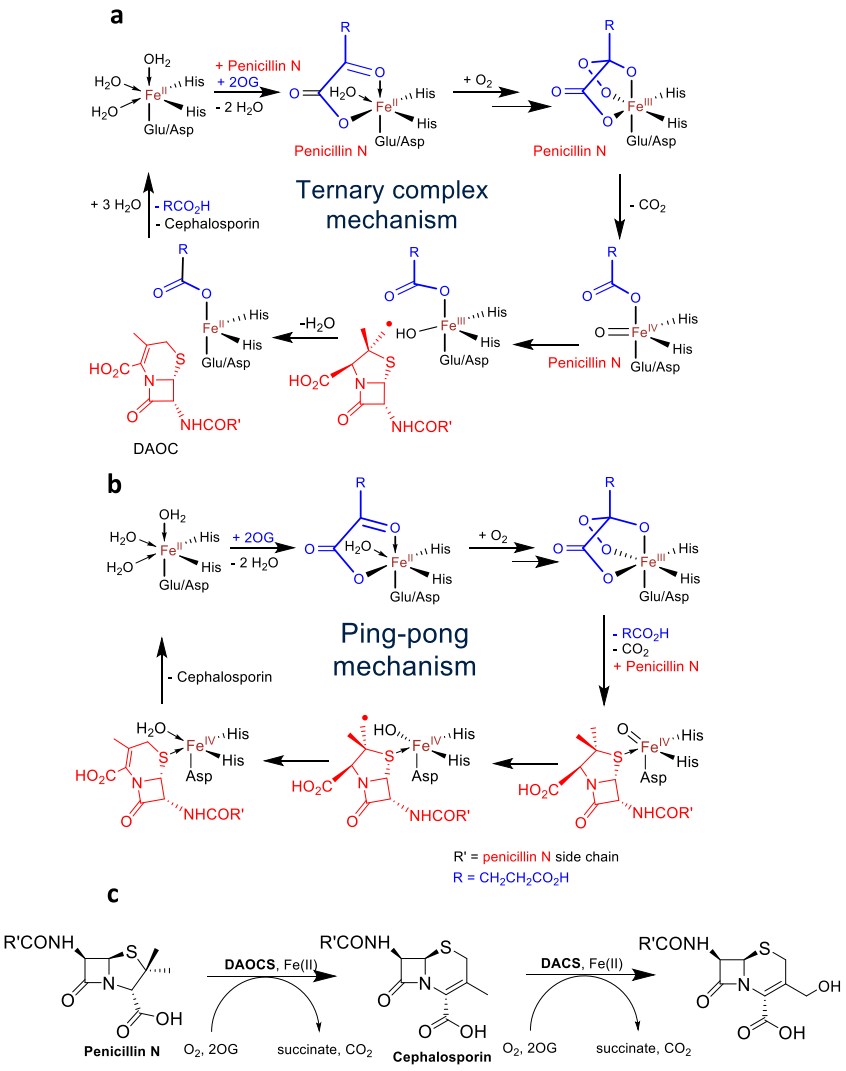


Figure 1.6. The outline of the proposed consensus mechanism of 2OG oxygenases, as applied to DAOC, in comparison with an alternative 'ping-pong' mechanism. (a) Binding of dioxygen to a DAOCS.Fe(II).2OG.penN complex results in the oxidative decarboxylation of 2OG and generation of Fe(IV)-oxo species that enables oxidative rearrangement of the substrate via initial hydrogen abstraction on the methyl group of the penicillin. **(b)** Binding of dioxygen to a DAOCS.Fe(II).2OG complex occurs with subsequent release of succinate and CO_2 followed by penicillin binding. **(c)** Scheme of the DAOCS-catalysed oxidative ring expansion of penN to deacetoxycephalosporin C and the second DACS-catalysed hydroxylation of deacetoxycaphalosporin C. Figure and figure legend are adapted with permission from Tarhonskaya *et al.* (2014) Biochemistry **53**, 2483-2493 [60]. Copyright (2014) American Chemical Society.

Despite the paradigm that all 2OG oxygenases employ a very similar consensus mechanism, there has been a proposal that DAOCS utilises a 'ping-pong' mechanism where a 'prime' substrate (penG) binds to an Fe(IV)-oxo intermediate after succinate release (**Figure 1.6**) [43]. A crystal structure of DAOCS in complex with Fe(II) and 2OG was the first reported for 2OG

oxygenases [46]. The overall folding and co-substrate binding mode were consistent with the 2OG oxygenase structures published afterwards [17]. However, in 2004 further crystallographic studies on DAOCS using unnatural DAOCS substrates - such as ampicillin and penicillin G - identified unusual 'prime' substrate binding modes, where penicillin had more than one binding orientation, and penicillin binding sites were overlapping with 2OG binding. Based on this crystallographic data and kinetic analyses showing substrate inhibition for both 2OG and penG, a novel mechanism was proposed. It suggested the release of a succinate byproduct and formation of an Fe(IV)-oxo intermediate prior to penicillin binding [43]. The proposed mechanism was unprecedented in 2OG oxygenase catalysis, where the common mechanism predicts formation of an Fe(IV)-oxo intermediate from a ternary complex [16], but it was in agreement with the previous isotope effect studies. However, while crystallographic studies suggested this novel mechanism, validation of the proposal by more detailed mechanistic studies on the DAOCS catalysis was not provided in order to clarify whether DAOCS indeed employs an unusual mechanism in solution.

1.4. Hypoxia-Inducible Factor (HIF) and the HIF hydroxylases

The hypoxic response is the reaction of an organism to the challenge of low availability of oxygen. The chronic hypoxic response is mediated by accumulation of the hypoxia-inducible transcriptional factor (HIF) in cells, which activates the transcription of an array of several hundred genes that enable production of erythropoietin (EPO), vascular endothelial growth factor (thus promoting angiogenesis), glucose uptake and metabolism, amongst many other processes [61, 62]. HIF consists of two subunits: HIF-α and HIF-β. Although, HIF-α has three isoforms, only levels of HIF-1α and HIF-2α depend on oxygen availability [63]. HIF-β is expressed constitutively, and dimerisation of the subunits, which occurs via a basic helix-loop-helix domain, is required for transcription of the hypoxia controlled genes [64].

Both the cellular levels of HIF-1/2α and its transcriptional activity are regulated via HIF post-translational modifications as a response to changes in oxygen concentrations. Under normoxic conditions (sufficient cellular oxygen concentrations), human HIF-1/2α undergoes hydroxylation catalysed by four enzymes (the HIF hydroxylases): three prolyl hydroxylases (prolyl hydroxylase domain 1-3, PHDs/EGLN 1-3) and one asparaginyl hydroxylase (factor inhibiting HIF-1, FIH-1) [8, 65]. These enzymes have been proposed to act as cellular oxygen

sensors reacting to changes in oxygen availability and linking them with HIF levels in cells [66]. PHDs and FIH belong to the enzymatic family of 2OG oxygenases, thus they are proposed to employ a similar mechanism as other members of the group [67, 68].

The PHDs catalyse hydroxylation of one or both of two prolyl residues in HIF-1/2α (Pro402 and Pro564 in HIF-1α, and Pro405 and Pro531 in HIF-2α in *C*-terminal oxygen dependent degradation domain, CODD, and *N*-terminal oxygen dependent degradation domain, NODD) triggering the proteosomal degradation of HIF [3, 7]. The HIF degradation occurs via the pathway of recognition by the E3 ubiquitin ligase complex containing the von Hippel–Lindau tumour suppressor protein (pVHL). FIH catalyses hydroxylation of an asparaginyl residue in HIF-1/2α (Asn803 in human HIF-1α and Asn851 in HIF-2α in *C*-terminal transactivation domain, CAD), which blocks its interaction with the transcriptional co-activator p300/CBP and therefore the transcription of hypoxic genes [8, 67, 69].

Although HIF-1α and HIF-2α are very similar in their structure, it has been suggested that overexpression of HIF-1α and HIF-2α isoforms can regulate activation of the pro-agiogenic genes in a different way when expressed in the same cell types. This causes differences in the overall effects of upregulated HIF levels on angiogenesis [70-72]. The pro-angiogenic factors, the expression of which is regulated by HIF, include vascular endothelial factor (VEGF, factor which is responsible for stimulation of the proliferation of new blood vessels), interleukin-8 (IL-8), placental growth factor (PIGF) [73-75]. Previously, hypoxia-triggered HIF-α upregulation has been shown to promote angiogenesis in certain tumours and therefore proposed to be related to tumorigenesis (reviewed in [76]). However, in certain cases the effects of HIF-α upregulation were shown to be the opposite, suggesting that in fact HIF could also act as a tumour suppressor, with HIF-1α and HIF-2α causing the opposite effects in the same cell type [70, 71, 77, 78]. Thus, HIF-1α, but not HIF-2α, was found to act as a tumour suppressor in renal carcenoma, while HIF-2α showed tumour suppressor effects in lung adenocarcenoma [70, 71]. The difference in the HIF-1α and HIF-2α functioning is proposed to reflect multiple factors including independent target gene regulation, and direct/indirect interactions of HIF with complexes containing tumour suppressors (reviewed in [76]).

It has been shown that the human HIF hydroxylases are non-redundant, including different PHD isoforms. PHDs have homology in their *C*-terminal regions, however, they show

differences in their *N*-terminal sequences, as well as in their function and cellular localisation [79]. PHD1 is found exclusively in the nucleus, while PHD2 exists predominantly in the cytoplasm, however, can also be found in the nucleus. PHD3 is expressed in both the nucleus and the cytoplasm with uniform distribution [80]. In addition, availability of a particular PHD isoform is variable depending on the type of tissue [81] (e.g. PHD3 has the highest level of expression in the heart, and PHD1 was the only PHD isoform found in testis [82, 83]). PHDs were also found to show different activity towards hydroxylation of the two prolyl hydroxylation sites (CODD and NODD) in HIF-1α and HIF-2α: all three isoforms are able to hydroxylate the CODD site, while hydroxylation of NODD was more specific for PHD1 and PHD2 [80]. Biochemical studies on PHD2 selectivity in the hydroxylation of the CODD or NODD sites showed (in competition experiments) that CODD has a higher hydroxylation rate compared to NODD [84], and mutation analyses showed that β2β3 loop (residues 237-254) could be a determinant feature for the observed PHD2 substrate selectivity [84].

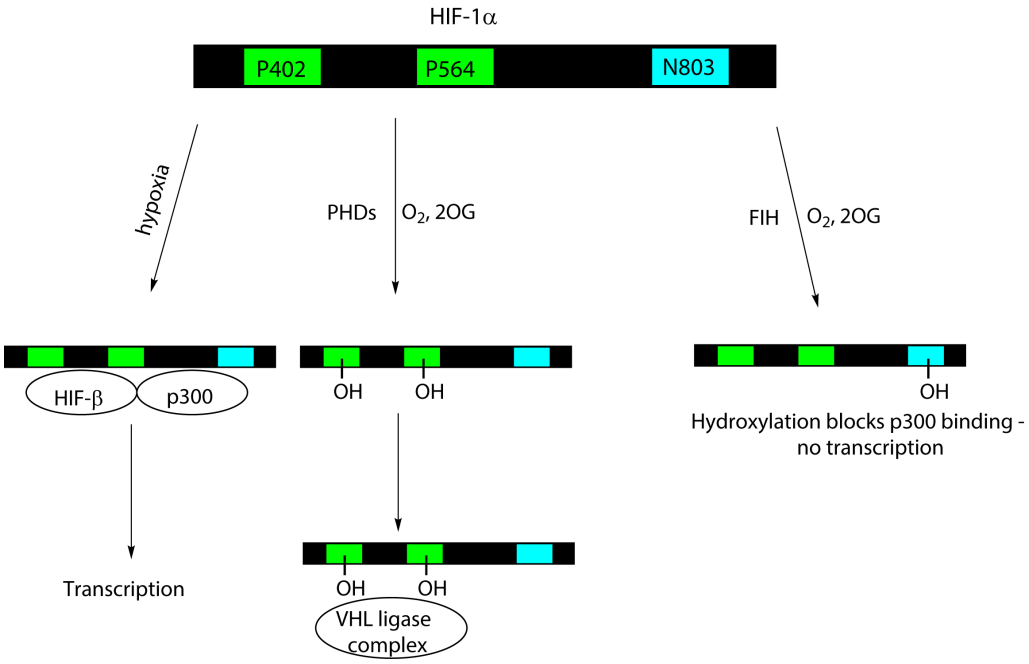


Figure 1.7. Mechanism of the HIF-mediated response and its regulation by the HIF hydroxylases. The hydroxylation of CODD and NODD sites by PHDs leads to proteosomal degradation of HIF, while hydroxylation of CAD site by FIH results in reduced transcription due to blocked interactions with the transcriptional co-activator.

As discussed above, the PHDs and FIH are proposed to act as oxygen sensors in cells based on their low affinity for oxygen as well as on cell based experiments [85]. The PHDs are reported to have high K_m values for oxygen (~250 μM, as reported), substantially above the physiological range of oxygen concentrations (~100 μM) [86, 87]. In the case of FIH, the reported K_m values for oxygen are lower compared to PHD2 (~100 μM [86, 88]). This suggests that PHD is highly tuned to react to small changes in oxygen concentrations in the whole range of physiological oxygen levels, while FIH may be more responsive under hypoxic conditions [86, 88]. Cell based experiments support this proposal, showing a much more graded dependence of PHD-catalysed HIF hydroxylation on oxygen concentration, compared to FIH [66], i.e. FIH is shown to be active in cells at lower oxygen concentrations.

1.5. Prolyl Hydroxylase Domain 2 (PHD2, EGLN1)

PHD2 is the most abundant PHD isoform in humans, ablation of which was shown to increase embryonic lethality in mice, thus suggesting that among prolyl hydroxyases, PHD2 is the most important cellular oxygen sensor [89, 90]. It was also found that PHD2, as well as other hypoxic sensing enzymes, exhibits very low activity in tumour tissues, which results in HIF up-regulation and promoted vascularisation of certain cancers [75]. PHD2 is therefore an important therapeutic target.

A number of crystal structures of the PHD2 catalytic domain have been reported [19, 68], including in complex with the substrate (a 19-mer peptide representing HIF-1α CODD site) [19] (**Figure 1.8**). It has been shown that PHD2 has a mobile β2β3 loop, and HIF-α binding is accompanied by a conformational change such as that the β2β3 loop encloses the substrate [19]. In addition, the prolyl residue of the CODD site undergoes a conformational bias from C^4-endo to C^4-exo yielding *trans*-4-prolyl-hydroxylation [91].

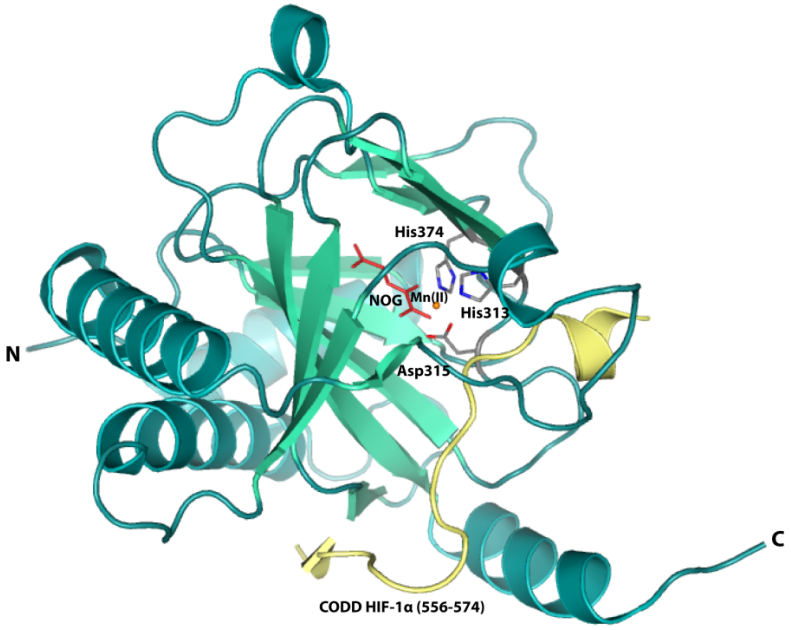


Figure 1.8. A view of the PHD2 structure (cyan) in complex with Mn(II), *N*-oxalylglycine (NOG) and the substrate HIF-1α (yellow, residues 556-574) outlining active site coordination (PDB: 3HQR) [19].

The design of selective inhibitors for the HIF hydroxylases, including PHDs, has been the subject of medicinal chemistry activity in recent years [92]. PHD inhibition has therapeutic potential for the treatment of cardiovascular diseases and cancer (see Section 1.7). Three PHD inhibitors are currently in clinical trials [93]. Most of the reported inhibitors include glycinamide or related motifs, selectivity of which however is not usually high enough to prevent inhibition of other 2OG oxygenases [93]. Alternative groups of PHD inhibitors include 8-hydroxyquinolines [94], pyrazolopyridines [95], pyridinyldihydropyrazolones [96], carboxymethyl-N-hydroxythiazoles [97] (reviewed in [92]).

Although PHD2 was proposed to be the most important human PHD isoform, the mechanistic features making it unique compared to other 2OG oxygenases and enabling its action as an oxygen-sensor (if any), are still not identified. A report on PHD2 transient kinetic studies showed that unlike for other 2OG oxygenases, accumulation of an Fe(IV)-oxo intermediate was not observed during the PHD2 catalysis [30]. In addition, the PHD2 oxygen activation was found to be abnormally slow for an enzymatic reaction, which was suggested to be related to its oxygen sensing function in cells [30]. A later report, where an inverse solvent isotope

effect (SIE) was observed for catalysis by PHD2, suggested that release of an iron-bound water molecule from the active site precedes a rate-limiting step of the reaction [27]. The SIE experiments also suggested that, consistent with the reported pre-steady-state kinetic studies, the enzymatic turnover of PHD2 may be, at least in part, limited by the rate of oxygen binding or activation step [27].

Although, a clear link between oxygen activation rates of 2OG oxygenases, and the biological oxygen sensing properties is not established, the slow kinetics of PHD2 reaction with oxygen merits further investigation. Recent studies on JMJD2E, a histone demethylase, have been reported and show formation of a similar absorbance 320 nm species, as reported for TauD [31], with relatively slow formation and degradation rates (maximum time of accumulation was ~11 s compared to 10-100 ms for other 2OG oxygenases) [27-29, 39]. Thus, a better understanding of the reaction of PHD2 with oxygen may enable rationalisation of its ability to act as an oxygen sensor.

1.6. Factor Inhibiting HIF (FIH)

FIH was one of the first enzymes to be identified as being involved in hypoxia sensing and regulation of HIF transcriptional activity [8, 69]. FIH catalyses the hydroxylation of Asn803 in human HIF-1α and Asn851 in HIF-2α [98]. This enzyme is ubiquitously expressed in all tissues, predominantly in the cytoplasm [99, 100]. Upon changes in oxygen availability, FIH modifies HIF-α which switches off HIF transcriptional ability. Studies on the molecular mechanism of CAD HIF-1α binding to p300/CBP showed that the Asn803 is the most deeply buried residue of the binding interface of CAD HIF-1α and p300/CBP, and it is positioned in a hydrophobic pocket [101, 102]. Therefore, addition of a hydroxyl group to Asn803 disrupts interactions of HIF-1α with CBP/p300 and acts as a molecular switch of HIF related transcription at normoxia. Interestingly, it has been shown that FIH has a higher affinity for HIF-1α compared to HIF-2α [72].

Structural studies reveal that FIH is a homodimer. NMR studies on HIF-α binding to FIH showed that unstructured HIF-1α CAD (residues 776-826) become structured upon binding to FIH, which is also accompanied by a conformational change in FIH itself [101-103]. A number of FIH crystal structures, including those with peptides representing CAD HIF-1α and ankyrin repeat domain (ARD) substrates, are available [101, 103]. They reveal that CAD

binds by forming hydrogen bonds and hydrophobic interactions with FIH. The inverse γ-turn of Asn803 and Ala804 is stabilised by a hydrogen bond between the backbone carbonyl of Val802 and NH of Ala804 [103].

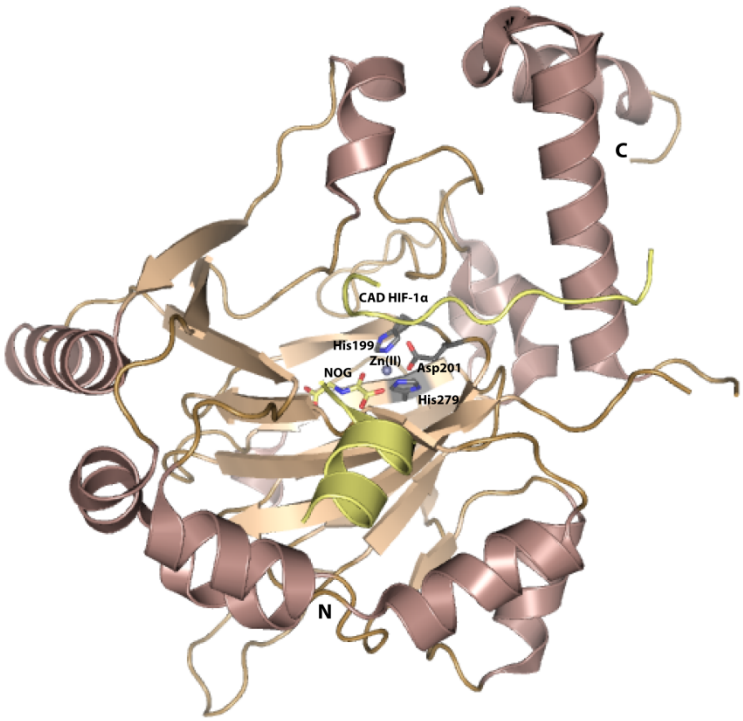


Figure 1.9. A view of the FIH (salmon) crystal structure in complex with Zn(II), NOG and substrate HIF-1α (yellow, residues 775-826) outlining active site coordination (PDB: 1H2M) [103].

Although FIH was identified first as a HIF hydroxylase, it is in fact highly promiscuous. Thus, FIH hydroxylates not only HIF, but also proteins containing ankyrin repeat domains (ARD). Ankyrin substrates were shown to bind in a similar manner as CAD HIF-1α with similar hydrogen bond interactions [104]. Furthermore, FIH has been shown to modify not only Asn (in ARDs), but also His, Leu and Ser residues [104-106]. Interestingly, it has also been reported that FIH-catalysed ARD substrate hydroxylation of Notch1-3 (an ARD protein) is characterised by much lower K_m values for oxygen compared to HIF-1α (e.g. 10 μM in the presence of Notch1-3 proteins compared to 100 μM for CAD HIF-1α) [107]. This raises the possibility that the reaction of FIH with ARDs is less oxygen sensitive than with HIF substrates, however, kinetic studies on other ARD substrates in addition to Notch1-3 are required. The differences in the oxygen sensitivity of the FIH-catalysed hydroxylation

reactions are of interest from both a mechanistic perspective as well as for obtaining new insights into the biological function of FIH [107].

Although FIH is proposed to employ a 2OG oxygenase consensus mechanism, mechanistic studies performed on this enzyme are relatively limited [108, 109]. Recently, it has been shown that similar to TauD, the Fe(II) in the FIH active site undergoes change from six- to five-coordinate state upon CAD HIF-1α substrate binding [109]. In addition, studies on SIE for FIH suggest that the rate-limiting step of catalysis occurs between the release of an iron bound water molecule from the active site and 2OG oxidative decarboxylation [108]. Interestingly, it has also been proposed that FIH can undergo auto-hydroxylation during uncoupled turnover, based on UV-vis and mass spectrometric analyses [110]. More detailed mechanistic studies and investigation of pre-steady-state rates of oxygen activation of FIH catalysis would contribute to knowledge on the mechanisms and action of the HIF hydroxylases.

1.7. HIF hydroxylases as therapeutic targets and their relation to cancer

The HIF hydroxylases are attractive therapeutic targets, and their selective inhibition is interesting with respect to modulating the hypoxic response. Activation of the HIF system could be used for treatment of such conditions as ischemia (including preconditioning before surgery), stroke, heart attack, wound healing and inflammation (reviewed in reference [111]). In addition, modulation of EPO production is attractive from the perspective of renal anemia treatment [111, 112]. HIF upregulation can promote angiogenesis, enhancing vascularisation of tumours, thus, activity of the HIF hydroxylases has been reported to be related to the development of certain cancers [111, 113]. Activation of the HIF hydroxylases could promote inhibition of angiogenesis and inhibit tumour growth.

It has been proposed that inhibition of the HIF hydroxylases by tricarboxylic acid (TCA) cycle metabolites and (*R*)-2HG, which is an oncometabolite produced due to mutations in IDH1/2 isoforms, may be linked to tumour development [114]. Although previous reports have indicated that (*R*)- and (*S*)-2HG are only weak inhibitors for the HIF hydroxylases (IC_{50} values for PHD2 7.3 mM and 0.4 mM for (*R*)- and (*S*)-2HG, respectively [115, 116]), elevated (*R*)-2HG levels caused by IDH mutations may indeed inhibit PHD action in cells resulting in HIF activated transcription [117].

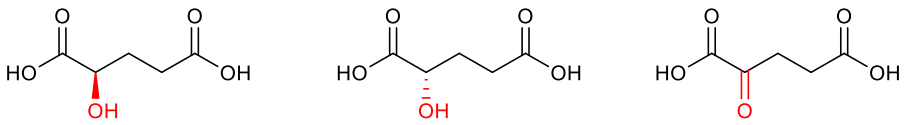


Figure 1.10. Structures of (*R*)-2HG, (*S*)-2HG and 2OG.

In contrast to the paradigm that TCA cycle metabolite- and (*R*)-2HG-mediated inhibition of 2OG dependent oxygenases is pathogenic, it has been recently reported that (*R*)-, but not (*S*)-2HG, actually stimulates PHD activity, both *in vitro* and in cells, so reducing HIF levels, and leading to enhanced proliferation of astrocytes [118]. (*R*)-2HG was proposed to be enzymatically oxidised to 2OG, which then can be utilised as a co-substrate by PHDs. The proposed mechanism of (*R*)-2HG oxidation to 2OG in the active site of the PHDs includes H-abstraction from the co-substrate by Fe(III)-peroxo species. This results in the formation of 2OG, which is then subsequently utilised in the PHDs catalysis using a common mechanism [118]. Co-substrate oxidation in such manner is unprecedented in 2OG oxygenase catalysis, thus this experimental observation is of interest from the perspective of the mechanism of 2OG oxygenases as well as its relation to tumourigenesis.

1.8. Thesis objectives

The existing experimental and theoretical data on the mechanism of 2OG oxygenases are sufficient to propose a consensus mechanism, defining the sequence of the catalytic events for the 2OG oxygenase catalysis. However, it is unclear how the mechanism of the individual enzymes within the family can be tailored to their biological function, e.g. oxygen sensing. Understanding the mechanism of the 2OG oxygenases, and the HIF hydroxylases in particular, is therefore of interest both from an enzymology perspective and from the perspective of the design of new selective inhibitors for therapeutic treatment of a whole range of pathological conditions.

Therefore, the objectives of this thesis were:

1. Investigations of the reaction of PHD2 with oxygen, and identification of molecular features responsible for its slow oxygen activation.
2. Mechanistic studies of FIH and its reaction with oxygen, aiming to establish whether slow oxygen activation is a common feature for catalysis of the oxygen-sensing HIF-hydroxylases.
3. Studies on the influence of enzyme-substrate interactions on the rate of oxygen activation in HIF hydroxylase catalysis.
4. Investigation of the mechanism of DAOCS catalysis and testing of the proposed 'ping-pong' mechanism. Comparison of the pre-steady-state kinetics of a small molecule modifying enzyme to the protein hydroxylases (the HIF hydroxylases).
5. Understanding a potential mechanism for 2HG conversion to 2OG as catalyse by PHD2.

1.9. References

1. Loenarz, C. and C.J. Schofield (2011) *Physiological and biochemical aspects of hydroxylations and demethylations catalyzed by human 2-oxoglutarate oxygenases.* Trends Biochem. Sci. **36**, 7-18.
2. Hutton Jr, J.J., A. Kaplan, and S. Udenfriend (1967) *Conversion of the amino acid sequence Gly-Pro-Pro in protein to Gly-Pro-Hyp by collagen proline hydroxylase.* Arch. Biochem. Biophys. **121**, 384-391.
3. Ivan, M., K. Kondo, H. Yang, W. Kim, J. Valiando, M. Ohh, A. Salic, J.M. Asara, W.S. Lane, and W.G. Kaelin Jr. (2001) *HIFα Targeted for VHL-Mediated Destruction by Proline Hydroxylation: Implications for O_2 Sensing.* Science **292**, 464-468.
4. Walport, L.J., R.J. Hopkinson, and C.J. Schofield (2012) *Mechanisms of human histone and nucleic acid demethylases.* Curr. Opin. Chem. Biol. **16**, 525-534.
5. Hausinger, R.P. (2004) *Fe(II)/α-Ketoglutarate-Dependent Hydroxylases and Related Enzymes.* Crit. Rev. Biochem. Mol. Biol. **39**, 21-68.
6. Roach, P.L., I.J. Clifton, V. Fulop, K. Harlos, G.J. Barton, J. Hajdu, I. Andersson, C.J. Schofield, and J.E. Baldwin (1995) *Crystal structure of isopenicillin N synthase is the first from a new structural family of enzymes.* Nature **375**, 700-704.
7. Jaakkola, P., D.R. Mole, Y.-M. Tian, M.I. Wilson, J. Gielbert, S.J. Gaskell, A.v. Kriegsheim, H.F. Hebestreit, M. Mukherji, C.J. Schofield, P.H. Maxwell, C.W. Pugh, and P.J. Ratcliffe (2001) *Targeting of HIF-α to the von Hippel-Lindau Ubiquitylation Complex by O_2-Regulated Prolyl Hydroxylation.* Science **292**, 468-472.
8. Lando, D., D.J. Peet, D.A. Whelan, J.J. Gorman, and M.L. Whitelaw (2002) *Asparagine Hydroxylation of the HIF Transactivation Domain: A Hypoxic Switch.* Science **295**, 858-861.
9. Iyer, L.M., S. Abhiman, R.F. de Souza, and L. Aravind (2010) *Origin and evolution of peptide-modifying dioxygenases and identification of the wybutosine hydroxylase/hydroperoxidase.* Nucleic Acids Res. **38**, 5261-5279.
10. Semenza, G.L. (2001) *HIF-1 and mechanisms of hypoxia sensing.* Curr. Opin. Cell Biol. **13**, 167-171.
11. Aik, W., M. Demetriades, M.K.K. Hamdan, E.A.L. Bagg, K.K. Yeoh, C. Lejeune, Z. Zhang, M.A. McDonough, and C.J. Schofield (2013) *Structural Basis for Inhibition of the Fat Mass and Obesity Associated Protein (FTO).* J. Med. Chem. **56**, 3680-3688.
12. Loenarz, C., R. Sekirnik, A. Thalhammer, W. Ge, E. Spivakovsky, M.M. Mackeen, M.A. McDonough, M.E. Cockman, B.M. Kessler, P.J. Ratcliffe, A. Wolf, and C.J. Schofield (2014) *Hydroxylation of the eukaryotic ribosomal decoding center affects translational accuracy.* Proc. Natl. Acad. Sci. U. S. A. **111**, 4019-4024.
13. Singleton, R.S., P. Liu-Yi, F. Formenti, W. Ge, R. Sekirnik, R. Fischer, J. Adam, P.J. Pollard, A. Wolf, A. Thalhammer, C. Loenarz, E. Flashman, A. Yamamoto, M.L. Coleman, B.M. Kessler, P. Wappner, C.J. Schofield, P.J. Ratcliffe, and M.E. Cockman (2014) *OGFOD1 catalyzes prolyl hydroxylation of RPS23 and is involved in translation control and stress granule formation.* Proc. Natl. Acad. Sci. U. S. A. **111**, 4031-4036.
14. Katz, M.J., J.M. Acevedo, C. Loenarz, D. Galagovsky, P. Liu-Yi, M. Pérez-Pepe, A. Thalhammer, R. Sekirnik, W. Ge, M. Melani, M.G. Thomas, S. Simonetta, G.L. Boccaccio, C.J. Schofield, M.E. Cockman, P.J. Ratcliffe, and P. Wappner (2014) *Sudestada1, a Drosophila ribosomal prolyl-hydroxylase required for mRNA*

translation, cell homeostasis, and organ growth. Proc. Natl. Acad. Sci. U. S. A. **111**, 4025-4030.

15. Clifton, I.J., M.A. McDonough, D. Ehrismann, N.J. Kershaw, N. Granatino, and C.J. Schofield (2006) *Structural studies on 2-oxoglutarate oxygenases and related double-stranded β-helix fold proteins.* J. Inorg. Biochem. **100**, 644-669.
16. Bollinger, J.M., J.C. Price, L.M. Hoffart, E.W. Barr, and C. Krebs (2005) *Mechanism of Taurine: α-Ketoglutarate Dioxygenase (TauD) from Escherichia coli.* Eur. J. Inorg. Chem. **2005**, 4245-4254.
17. Aik, W., M.A. McDonough, A. Thalhammer, R. Chowdhury, and C.J. Schofield (2012) *Role of the jelly-roll fold in substrate binding by 2-oxoglutarate oxygenases.* Curr. Opin. Struct. Biol. **22**, 691-700.
18. Koehntop, K., J. Emerson, and L. Que, Jr. (2005) *The 2-His-1-carboxylate facial triad: a versatile platform for dioxygen activation by mononuclear non-heme iron(II) enzymes.* J. Biol. Inorg. Chem. **10**, 87-93.
19. Chowdhury, R., M.A. McDonough, J. Mecinović, C. Loenarz, E. Flashman, K.S. Hewitson, C. Domene, and C.J. Schofield (2009) *Structural Basis for Binding of Hypoxia-Inducible Factor to the Oxygen-Sensing Prolyl Hydroxylases.* Structure **17**, 981-989.
20. Solomon, E.I., T.C. Brunold, M.I. Davis, J.N. Kemsley, S.-K. Lee, N. Lehnert, F. Neese, A.J. Skulan, Y.-S. Yang, and J. Zhou (1999) *Geometric and Electronic Structure/Function Correlations in Non-Heme Iron Enzymes.* Chem. Rev. **100**, 235-350.
21. Hanauske-Abel, H.M. and V. Günzler (1982) *A stereochemical concept for the catalytic mechanism of prolylhydroxylase: Applicability to classification and design of inhibitors.* J. Theor. Biol. **94**, 421-455.
22. Pavel, E.G., J. Zhou, R.W. Busby, M. Gunsior, C.A. Townsend, and E.I. Solomon (1998) *Circular dichroism and magnetic circular dichroism spectroscopic studies of the non-heme ferrous active site in clavaminate synthase and its interaction with α-ketoglutarate cosubstrate.* J. Am. Chem. Soc. **120**, 743-753.
23. Mehn, M.P., K. Fujisawa, E.L. Hegg, and L. Que (2003) *Oxygen Activation by Nonheme Iron(II) Complexes: α-Keto Carboxylate versus Carboxylate.* J. Am. Chem. Soc. **125**, 7828-7842.
24. Ho, R.Y.N., M.P. Mehn, E.L. Hegg, A. Liu, M.J. Ryle, R.P. Hausinger, and L. Que (2001) *Resonance Raman Studies of the Iron(II)−α-Keto Acid Chromophore in Model and Enzyme Complexes.* J. Am. Chem. Soc. **123**, 5022-5029.
25. Costas, M., M.P. Mehn, M.P. Jensen, and L. Que (2004) *Dioxygen Activation at Mononuclear Nonheme Iron Active Sites: Enzymes, Models, and Intermediates.* Chem. Rev. **104**, 939-986.
26. Ryle, M.J., K.D. Koehntop, A. Liu, L. Que, and R.P. Hausinger (2003) *Interconversion of two oxidized forms of taurine/α-ketoglutarate dioxygenase, a non-heme iron hydroxylase: Evidence for bicarbonate binding.* Proc. Natl. Acad. Sci. U. S. A. **100**, 3790-3795.
27. Price, J.C., E.W. Barr, B. Tirupati, J.M. Bollinger, and C. Krebs (2003) *The First Direct Characterization of a High-Valent Iron Intermediate in the Reaction of an α-Ketoglutarate-Dependent Dioxygenase: A High-Spin Fe(IV) Complex in Taurine/α-*

Ketoglutarate Dioxygenase (TauD) from Escherichia coli. Biochemistry **42**, 7497-7508.

28. Hoffart, L.M., E.W. Barr, R.B. Guyer, J.M. Bollinger, and C. Krebs (2006) *Direct spectroscopic detection of a C-H-cleaving high-spin Fe(IV) complex in a prolyl-4-hydroxylase.* Proc. Natl. Acad. Sci. U. S. A. **103**, 14738-14743.
29. Matthews, M.L., C.M. Krest, E.W. Barr, F.H. Vaillancourt, C.T. Walsh, M.T. Green, C. Krebs, and J.M. Bollinger (2009) *Substrate-Triggered Formation and Remarkable Stability of the C−H Bond-Cleaving Chloroferryl Intermediate in the Aliphatic Halogenase, SyrB2.* Biochemistry **48**, 4331-4343.
30. Flashman, E., L.M. Hoffart, R.B. Hamed, J.M. Bollinger Jr, C. Krebs, and C.J. Schofield (2010) *Evidence for the slow reaction of hypoxia-inducible factor prolyl hydroxylase 2 with oxygen.* FEBS J. **277**, 4089-4099.
31. Sánchez-Fernández, E.M., H. Tarhonskaya, K. Al-Qahtani, R.J. Hopkinson, J.S.O. McCullagh, C.J. Schofield, and E. Flashman (2013) *Investigations on the oxygen dependence of a 2-oxoglutarate histone demethylase.* Biochem. J **449**, 491-496.
32. Liu, A., R.Y.N. Ho, L. Que, M.J. Ryle, B.S. Phinney, and R.P. Hausinger (2001) *Alternative Reactivity of an α-Ketoglutarate-Dependent Iron(II) Oxygenase: Enzyme Self-Hydroxylation.* J. Am. Chem. Soc. **123**, 5126-5127.
33. Henshaw, T.F., M. Feig, and R.P. Hausinger (2004) *Aberrant activity of the DNA repair enzyme AlkB.* J. Inorg. Biochem. **98**, 856-861.
34. Price, J.C., E.W. Barr, L.M. Hoffart, C. Krebs, and J.M. Bollinger (2005) *Kinetic Dissection of the Catalytic Mechanism of Taurine:α-Ketoglutarate Dioxygenase (TauD) from Escherichia coli.* Biochemistry **44**, 8138-8147.
35. Schenk, G., M.Y.M. Pau, and E.I. Solomon (2003) *Comparison between the Geometric and Electronic Structures and Reactivities of $\{FeNO\}_7$ and $\{FeO_2\}_8$ Complexes: A Density Functional Theory Study.* J. Am. Chem. Soc. **126**, 505-515.
36. Arciero, D.M., A.M. Orville, and J.D. Lipscomb (1985) *[^{17}O]Water and nitric oxide binding by protocatechuate 4,5-dioxygenase and catechol 2,3-dioxygenase. Evidence for binding of exogenous ligands to the active site Fe^{2+} of extradiol dioxygenases.* J. Biol. Chem. **260**, 14035-14044.
37. Chen, V.J., A.M. Orville, M.R. Harpel, C.A. Frolik, K.K. Surerus, E. Münck, and J.D. Lipscomb (1989) *Spectroscopic studies of isopenicillin N synthase. A mononuclear nonheme Fe^{2+} oxidase with metal coordination sites for small molecules and substrate.* J. Biol. Chem. **264**, 21677-21681.
38. Pohl, K., K. Wieghardt, B. Nuber, and J. Weiss (1987) *Preparation and magnetism of the binuclear iron(II) complexes $[\{Fe(C_9H_{21}N_3)X_2\}_2]$(X = NCS, NCO, or N_3) and their reaction with NO. Crystal structures of $[\{Fe(C_9H_{21}N_3)(NCS)_2\}_2]$ and $[Fe(C_9H_{21}N_3)(NO)(N_3)_2]$.* J. Chem. Soc., Dalton Trans., 187-192.
39. Galonic, D.P., E.W. Barr, C.T. Walsh, J.M. Bollinger, and C. Krebs (2007) *Two interconverting Fe(IV) intermediates in aliphatic chlorination by the halogenase CytC3.* Nat. Chem. Biol. **3**, 113-116.
40. Baldwin, J.E., R.M. Adlington, N.P. Crouch, and I.A.C. Pereira (1993) *Incorporation of ^{18}O-labelled water into oxygenated products produced by the enzyme deacetoxy/deacetylcephalosporin C synthase.* Tetrahedron **49**, 7499-7518.

41. Zhang, Z., J.-s. Ren, K. Harlos, C.H. McKinnon, I.J. Clifton, and C.J. Schofield (2002) *Crystal structure of a clavaminate synthase–Fe(II)–2-oxoglutarate–substrate–NO complex: evidence for metal centred rearrangements.* FEBS Lett. **517**, 7-12.
42. Baldwin, J.E., R.M. Adlington, R.T. Aplin, N.P. Crouch, G. Knight, and C.J. Schofield (1987) *Cephalosporin C biosynthesis; a branched pathway sensitive to a kinetic isotope effect.* J. Chem. Soc., Chem. Commun., 1651-1654.
43. Valegård, K., A.C.T. van Scheltinga, A. Dubus, G. Ranghino, L.M. Oster, J. Hajdu, and I. Andersson (2004) *The structural basis of cephalosporin formation in a mononuclear ferrous enzyme.* Nat. Struct. Mol. Biol. **11**, 95-101.
44. Baldwin, J.E., R.M. Adlington, J.B. Coates, M.J. Crabbe, N.P. Crouch, J.W. Keeping, G.C. Knight, C.J. Schofield, H.H. Ting, and C.A. Vallejo (1987) *Purification and initial characterization of an enzyme with deacetoxycephalosporin C synthetase and hydroxylase activities.* Biochem. J. **245**, 831-841.
45. Lloyd, M.D., H.-J. Lee, K. Harlos, Z.-H. Zhang, J.E. Baldwin, C.J. Schofield, J.M. Charnock, C.D. Garner, T. Hara, A.C. Terwisscha van Scheltinga, K. Valegård, J.A.C. Viklund, J. Hajdu, I. Andersson, Å. Danielsson, and R. Bhikhabhai (1999) *Studies on the active site of deacetoxycephalosporin C synthase.* J. Mol. Biol. **287**, 943-960.
46. Valegård, K., A.C.T. van Scheltinga, M.D. Lloyd, T. Hara, S. Ramaswamy, A. Perrakis, A. Thompson, H.-J. Lee, J.E. Baldwin, C.J. Schofield, J. Hajdu, and I. Andersson (1998) *Structure of a cephalosporin synthase.* Nature **394**, 805-809.
47. Dotzlaf, J.E. and W.K. Yeh (1987) *Copurification and characterization of deacetoxycephalosporin C synthetase/hydroxylase from Cephalosporium acremonium.* J. Bacteriol. **169**, 1611-1618.
48. Kovacevic, S., B.J. Weigel, M.B. Tobin, T.D. Ingolia, and J.R. Miller (1989) *Cloning, characterization, and expression in Escherichia coli of the Streptomyces clavuligerus gene encoding deacetoxycephalosporin C synthetase.* J. Bacteriol. **171**, 754-760.
49. Hamed, R.B., J.R. Gomez-Castellanos, L. Henry, C. Ducho, M.A. McDonough, and C.J. Schofield (2013) *The enzymes of β-lactam biosynthesis.* Nat. Prod. Rep. **30**, 21-107.
50. Ji, J., X. Tian, K. Fan, and K. Yang (2012) *New strategy of site-directed mutagenesis identifies new sites to improve Streptomyces clavuligerus deacetoxycephalosporin C synthase activity toward penicillin G.* Appl. Microbiol. Biotechnol. **93**, 2395-2401.
51. Wei, C.-L., Y.-B. Yang, W.-C. Wang, W.-C. Liu, J.-S. Hsu, and Y.-C. Tsai (2003) *Engineering Streptomyces clavuligerus Deacetoxycephalosporin C Synthase for Optimal Ring Expansion Activity toward Penicillin G.* Appl. Environ. Microbiol. **69**, 2306-2312.
52. Lee, H.-J., C.J. Schofield, and M.D. Lloyd (2002) *Active Site Mutations of Recombinant Deacetoxycephalosporin C Synthase.* Biochem. Biophys. Res. Commun. **292**, 66-70.
53. Lee, H.-J., M.D. Lloyd, K. Harlos, I.J. Clifton, J.E. Baldwin, and C.J. Schofield (2001) *Kinetic and crystallographic studies on deacetoxycephalosporin C synthase (DAOCS).* J. Mol. Biol. **308**, 937-948.
54. Chin, H.S., J. Sim, and T.S. Sim (2001) *Mutation of N304 to Leucine in Streptomyces clavuligerus Deacetoxycephalosporin C Synthase Creates an Enzyme with Increased Penicillin Analogue Conversion.* Biochem. Biophys. Res. Commun. **287**, 507-513.

55. Sim Goo, K., C. Song Chua, and T.-S. Sim (2008) *A complete library of amino acid alterations at R306 in Streptomyces clavuligerus deacetoxycephalosporin C synthase demonstrates its structural role in the ring-expansion activity.* Proteins: Struct., Funct., Bioinf. **70**, 739-747.
56. Goo, K.S., C.S. Chua, and T.-S. Sim (2008) *Relevant Double Mutations in Bioengineered Streptomyces clavuligerus Deacetoxycephalosporin C Synthase Result in Higher Binding Specificities Which Improve Penicillin Bioconversion.* Appl. Environ. Microbiol. **74**, 1167-1175.
57. Lloyd, M.D., S.J. Lipscomb, K.S. Hewitson, C.M.H. Hensgens, J.E. Baldwin, and C.J. Schofield (2004) *Controlling the Substrate Selectivity of Deacetoxycephalosporin/deacetylcephalosporin C Synthase.* J. Biol. Chem. **279**, 15420-15426.
58. Goo, K.-S., C.-S. Chua, and T.-S. Sim (2009) *Directed evolution and rational approaches to improving Streptomyces clavuligerus deacetoxycephalosporin C synthase for cephalosporin production.* J. Ind. Microbiol. Biotechnol. **36**, 619-633.
59. Baldwin, J.E., R.M. Adlington, N.P. Crouch, C.J. Schofield, N.J. Turner, and R.T. Aplin (1991) *Cephalosporin biosynthesis: A branched pathway sensitive to an isotope effect.* Tetrahedron **47**, 9881-9900.
60. Tarhonskaya, H., A. Szöllössi, I.K.H. Leung, J.T. Bush, L. Henry, R. Chowdhury, A. Iqbal, T.D.W. Claridge, C.J. Schofield, and E. Flashman (2014) *Studies on Deacetoxycephalosporin C Synthase Support a Consensus Mechanism for 2-Oxoglutarate Dependent Oxygenases.* Biochemistry **53**, 2483-2493.
61. Huang, L.E. and H.F. Bunn (2003) *Hypoxia-inducible Factor and Its Biomedical Relevance.* J. Biol. Chem. **278**, 19575-19578.
62. Ratcliffe, P.J. (2002) *From Erythropoietin to Oxygen: Hypoxia-Inducible Factor Hydroxylases and the Hypoxia Signal Pathway.* Blood Purif. **20**, 445-450.
63. Wang, G.L., B.H. Jiang, E.A. Rue, and G.L. Semenza (1995) *Hypoxia-inducible factor 1 is a basic-helix-loop-helix-PAS heterodimer regulated by cellular O_2 tension.* Proc. Natl. Acad. Sci. U. S. A. **92**, 5510-5514.
64. Hara, S., J. Hamada, C. Kobayashi, Y. Kondo, and N. Imura (2001) *Expression and Characterization of Hypoxia-Inducible Factor (HIF)-3α in Human Kidney: Suppression of HIF-Mediated Gene Expression by HIF-3α.* Biochem. Biophys. Res. Commun. **287**, 808-813.
65. Bruick, R.K. and S.L. McKnight (2001) *A Conserved Family of Prolyl-4-Hydroxylases That Modify HIF.* Science **294**, 1337-1340.
66. Tian, Y.-M., K.K. Yeoh, M.K. Lee, T. Eriksson, B.M. Kessler, H.B. Kramer, M.J. Edelmann, C. Willam, C.W. Pugh, C.J. Schofield, and P.J. Ratcliffe (2011) *Differential Sensitivity of Hypoxia Inducible Factor Hydroxylation Sites to Hypoxia and Hydroxylase Inhibitors.* J. Biol. Chem. **286**, 13041-13051.
67. Hewitson, K.S., L.A. McNeill, M.V. Riordan, Y.-M. Tian, A.N. Bullock, R.W. Welford, J.M. Elkins, N.J. Oldham, S. Bhattacharya, J.M. Gleadle, P.J. Ratcliffe, C.W. Pugh, and C.J. Schofield (2002) *Hypoxia-inducible Factor (HIF) Asparagine Hydroxylase Is Identical to Factor Inhibiting HIF (FIH) and Is Related to the Cupin Structural Family.* J. Biol. Chem. **277**, 26351-26355.
68. McDonough, M.A., V. Li, E. Flashman, R. Chowdhury, C. Mohr, B.M.R. Liénard, J. Zondlo, N.J. Oldham, I.J. Clifton, J. Lewis, L.A. McNeill, R.J.M. Kurzeja, K.S.

Hewitson, E. Yang, S. Jordan, R.S. Syed, and C.J. Schofield (2006) *Cellular oxygen sensing: Crystal structure of hypoxia-inducible factor prolyl hydroxylase (PHD2).* Proc. Natl. Acad. Sci. U. S. A. **103**, 9814-9819.

69. Mahon, P.C., K. Hirota, and G.L. Semenza (2001) *FIH-1: a novel protein that interacts with HIF-1α and VHL to mediate repression of HIF-1 transcriptional activity.* Genes Dev. **15**, 2675-2686.
70. Maranchie, J.K., J.R. Vasselli, J. Riss, J.S. Bonifacino, W.M. Linehan, and R.D. Klausner (2002) *The contribution of VHL substrate binding and HIF1-α to the phenotype of VHL loss in renal cell carcinoma.* Cancer Cell **1**, 247-255.
71. Kondo, K., W.Y. Kim, M. Lechpammer, and W.G. Kaelin, Jr. (2003) *Inhibition of HIF2α Is Sufficient to Suppress pVHL-Defective Tumor Growth.* PLoS Biol. **1**, e83.
72. Loboda, A., A. Jozkowicz, and J. Dulak (2012) *HIF-1 versus HIF-2 — Is one more important than the other?* Vasc. Pharmacol. **56**, 245-251.
73. Semenza, G.L., *Hypoxia. Cross talk between oxygen sensing and the cell cycle machinery*, ed. G.L. Semenza. Vol. 301. 2011. C550-C552.
74. Semenza, G.L. (2011) *Oxygen Sensing, Homeostasis, and Disease.* New Engl. J. Med. **365**, 537-547.
75. Chowdhury, R., A. Hardy, and C.J. Schofield (2008) *The human oxygen sensing machinery and its manipulation.* Chem. Soc. Rev. **37**, 1308-1319.
76. Keith, B., R.S. Johnson, and M.C. Simon (2012) *HIF1α and HIF2α: sibling rivalry in hypoxic tumour growth and progression.* Nat. Rev. Cancer **12**, 9-22.
77. Acker, T., A. Diez-Juan, J. Aragones, M. Tjwa, K. Brusselmans, L. Moons, D. Fukumura, M.P. Moreno-Murciano, J.-M. Herbert, A. Burger, J. Riedel, G. Elvert, I. Flamme, P.H. Maxwell, D. Collen, M. Dewerchin, R.K. Jain, K.H. Plate, and P. Carmeliet (2005) *Genetic evidence for a tumor suppressor role of HIF-2α.* Cancer Cell **8**, 131-141.
78. Mazumdar, J., M.M. Hickey, D.K. Pant, A.C. Durham, A. Sweet-Cordero, A. Vachani, T. Jacks, L.A. Chodosh, J.L. Kissil, M.C. Simon, and B. Keith (2010) *HIF-2α deletion promotes Kras-driven lung tumor development.* Proc. Natl. Acad. Sci. U. S. A. **107**, 14182-14187.
79. Huang, J., Q. Zhao, S.M. Mooney, and F.S. Lee (2002) *Sequence Determinants in Hypoxia-inducible Factor-1α for Hydroxylation by the Prolyl Hydroxylases PHD1, PHD2, and PHD3.* J. Biol. Chem. **277**, 39792-39800.
80. Appelhoff, R.J., Y.-M. Tian, R.R. Raval, H. Turley, A.L. Harris, C.W. Pugh, P.J. Ratcliffe, and J.M. Gleadle (2004) *Differential Function of the Prolyl Hydroxylases PHD1, PHD2, and PHD3 in the Regulation of Hypoxia-inducible Factor.* J. Biol. Chem. **279**, 38458-38465.
81. Siddiq, A., L. Aminova, and R. Ratan (2007) *Hypoxia Inducible Factor Prolyl 4-Hydroxylase Enzymes: Center Stage in the Battle Against Hypoxia, Metabolic Compromise and Oxidative Stress.* Neurochem. Res. **32**, 931-946.
82. Cioffi, C.L., X. Qin Liu, P.A. Kosinski, M. Garay, and B.R. Bowen (2003) *Differential regulation of HIF-1α prolyl-4-hydroxylase genes by hypoxia in human cardiovascular cells.* Biochem. Biophys. Res. Commun. **303**, 947-953.
83. Lieb, M.E., K. Menzies, M.C. Moschella, R. Ni, and M.B. Taubman (2002) *Mammalian EGLN genes have distinct patterns of mRNA expression and regulation.* Biochem. Cell Biol. **80**, 421-426.

84. Flashman, E., E.A.L. Bagg, R. Chowdhury, J. Mecinović, C. Loenarz, M.A. McDonough, K.S. Hewitson, and C.J. Schofield (2008) *Kinetic Rationale for Selectivity toward N- and C-terminal Oxygen-dependent Degradation Domain Substrates Mediated by a Loop Region of Hypoxia-Inducible Factor Prolyl Hydroxylases.* J. Biol. Chem. **283**, 3808-3815.
85. Aragonés, J., P. Fraisl, M. Baes, and P. Carmeliet (2009) *Oxygen Sensors at the Crossroad of Metabolism.* Cell Metab. **9**, 11-22.
86. Ehrismann, D., E. Flashman, D.N. Genn, N. Mathioudakis, K.S. Hewitson, P.J. Ratcliffe, and C.J. Schofield (2007) *Studies on the activity of the hypoxia-inducible-factor hydroxylases using an oxygen consumption assay.* Biochem. J. **401**, 227-234.
87. Hirsilä, M., P. Koivunen, V. Günzler, K.I. Kivirikko, and J. Myllyharju (2003) *Characterization of the Human Prolyl 4-Hydroxylases That Modify the Hypoxia-inducible Factor.* J. Biol. Chem. **278**, 30772-30780.
88. Koivunen, P., M. Hirsilä, V. Günzler, K.I. Kivirikko, and J. Myllyharju (2004) *Catalytic Properties of the Asparaginyl Hydroxylase (FIH) in the Oxygen Sensing Pathway Are Distinct from Those of Its Prolyl 4-Hydroxylases.* J. Biol. Chem. **279**, 9899-9904.
89. Takeda, K., V.C. Ho, H. Takeda, L.-J. Duan, A. Nagy, and G.-H. Fong (2006) *Placental but Not Heart Defects Are Associated with Elevated Hypoxia-Inducible Factor α Levels in Mice Lacking Prolyl Hydroxylase Domain Protein 2.* Mol. Cell. Biol. **26**, 8336-8346.
90. Berra, E., E. Benizri, A. Ginouvès, V. Volmat, D. Roux, and J. Pouysségur, *HIF prolyl hydroxylase 2 is the key oxygen sensor setting low steady-state levels of HIF-1α in normoxia*. Vol. 22. 2003. 4082-4090.
91. Loenarz, C., J. Mecinović, R. Chowdhury, L.A. McNeill, E. Flashman, and C.J. Schofield (2009) *Evidence for a Stereoelectronic Effect in Human Oxygen Sensing.* Angew. Chem. Int. Ed. **48**, 1784-1787.
92. Rose, N.R., M.A. McDonough, O.N.F. King, A. Kawamura, and C.J. Schofield (2011) *Inhibition of 2-oxoglutarate dependent oxygenases.* Chem. Soc. Rev. **40**, 4364-4397.
93. Yan, L., V.J. Colandrea, and J.J. Hale (2010) *Prolyl hydroxylase domain-containing protein inhibitors as stabilizers of hypoxia-inducible factor: small molecule-based therapeutics for anemia.* Expert Opin. Ther. Targets **20**, 1219-1245.
94. Warshakoon, N.C., S. Wu, A. Boyer, R. Kawamoto, J. Sheville, S. Renock, K. Xu, M. Pokross, S. Zhou, C. Winter, R. Walter, M. Mekel, and A.G. Evdokimov (2006) *Structure-based design, synthesis, and SAR evaluation of a new series of 8-hydroxyquinolines as HIF-1α prolyl hydroxylase inhibitors.* Bioorg. Med. Chem. Lett. **16**, 5517-5522.
95. Warshakoon, N.C., S. Wu, A. Boyer, R. Kawamoto, S. Renock, K. Xu, M. Pokross, A.G. Evdokimov, S. Zhou, C. Winter, R. Walter, and M. Mekel (2006) *Design and synthesis of a series of novel pyrazolopyridines as HIF 1-α prolyl hydroxylase inhibitors.* Bioorg. Med. Chem. Lett. **16**, 5687-5690.
96. Warshakoon, N.C., S. Wu, A. Boyer, R. Kawamoto, J. Sheville, R.T. Bhatt, S. Renock, K. Xu, M. Pokross, S. Zhou, R. Walter, M. Mekel, A.G. Evdokimov, and S. East (2006) *Design and synthesis of substituted pyridine derivatives as HIF-1α prolyl hydroxylase inhibitors.* Bioorg. Med. Chem. Lett. **16**, 5616-5620.

97. Tegley, C.M., V.N. Viswanadhan, K. Biswas, M.J. Frohn, T.A.N. Peterkin, C. Chang, R.W. Bürli, J.H. Dao, H. Veith, N. Rogers, S.C. Yoder, G. Biddlecome, P. Tagari, J.R. Allen, and R.W. Hungate (2008) *Discovery of novel hydroxy-thiazoles as HIF-α prolyl hydroxylase inhibitors: SAR, synthesis, and modeling evaluation.* Bioorg. Med. Chem. Lett. **18**, 3925-3928.
98. McNeill, L.A., K.S. Hewitson, T.D. Claridge, J.F. Seibel, L.E. Horsfall, and C.J. Schofield (2002) *Hypoxia-inducible factor asparaginyl hydroxylase (FIH-1) catalyses hydroxylation at the beta-carbon of asparagine-803.* Biochem. J. **367**, 571-575.
99. Stolze, I.P., Y.-M. Tian, R.J. Appelhoff, H. Turley, C.C. Wykoff, J.M. Gleadle, and P.J. Ratcliffe (2004) *Genetic Analysis of the Role of the Asparaginyl Hydroxylase Factor Inhibiting Hypoxia-inducible Factor (HIF) in Regulating HIF Transcriptional Target Genes.* J. Biol. Chem. **279**, 42719-42725.
100. Bracken, C.P., A.O. Fedele, S. Linke, W. Balrak, K. Lisy, M.L. Whitelaw, and D.J. Peet (2006) *Cell-specific Regulation of Hypoxia-inducible Factor (HIF)-1α and HIF-2α Stabilization and Transactivation in a Graded Oxygen Environment.* J. Biol. Chem. **281**, 22575-22585.
101. Dames, S.A., M. Martinez-Yamout, R.N. De Guzman, H.J. Dyson, and P.E. Wright (2002) *Structural basis for Hif-1α/CBP recognition in the cellular hypoxic response.* Proc. Natl. Acad. Sci. U. S. A. **99**, 5271-5276.
102. Freedman, S.J., Z.-Y.J. Sun, F. Poy, A.L. Kung, D.M. Livingston, G. Wagner, and M.J. Eck (2002) *Structural basis for recruitment of CBP/p300 by hypoxia-inducible factor-1α.* Proc. Natl. Acad. Sci. U. S. A. **99**, 5367-5372.
103. Elkins, J.M., K.S. Hewitson, L.A. McNeill, J.F. Seibel, I. Schlemminger, C.W. Pugh, P.J. Ratcliffe, and C.J. Schofield (2003) *Structure of Factor-inhibiting Hypoxia-inducible Factor (HIF) Reveals Mechanism of Oxidative Modification of HIF-1α.* J. Biol. Chem. **278**, 1802-1806.
104. Yang, M., R. Chowdhury, W. Ge, R.B. Hamed, M.A. McDonough, T.D. Claridge, B.M. Kessler, M.E. Cockman, P.J. Ratcliffe, and C.J. Schofield (2011) *Factor-inhibiting hypoxia-inducible factor (FIH) catalyses the post-translational hydroxylation of histidinyl residues within ankyrin repeat domains.* FEBS J. **278**, 1086-1097.
105. Cockman, M.E., J.D. Webb, and P.J. Ratcliffe (2009) *FIH-dependent asparaginyl hydroxylation of ankyrin repeat domain-containing proteins.* Ann. N Y Acad. Sci. **1177**, 9-18.
106. Yang, M., A.P. Hardy, R. Chowdhury, N.D. Loik, J.S. Scotti, J.S. McCullagh, T.D. Claridge, M.A. McDonough, W. Ge, and C.J. Schofield (2013) *Substrate selectivity analyses of factor inhibiting hypoxia-inducible factor.* Angew. Chem. Int. Ed. Engl. **52**, 1700-1704.
107. Wilkins, S.E., J. Hyvärinen, J. Chicher, J.J. Gorman, D.J. Peet, R.L. Bilton, and P. Koivunen (2009) *Differences in hydroxylation and binding of Notch and HIF-1α demonstrate substrate selectivity for factor inhibiting HIF-1 (FIH-1).* Int. J. Biochem. Cell Biol. **41**, 1563-1571.
108. Hangasky, J.A., E. Saban, and M.J. Knapp (2013) *Inverse Solvent Isotope Effects Arising from Substrate Triggering in the Factor Inhibiting Hypoxia Inducible Factor.* Biochemistry **52**, 1594-1602.

109. Light, K.M., J.A. Hangasky, M.J. Knapp, and E.I. Solomon (2013) *Spectroscopic Studies of the Mononuclear Non-Heme FeII Enzyme FIH: Second-Sphere Contributions to Reactivity.* J. Am. Chem. Soc. **135**, 9665-9674.
110. Chen, Y.-H., L.M. Comeaux, S.J. Eyles, and M.J. Knapp (2008) *Auto-hydroxylation of FIH-1: an Fe(II), α-ketoglutarate-dependent human hypoxia sensor.* Chem. Commun., 4768-4770.
111. Hewitson, K.S. and C.J. Schofield (2004) *The HIF pathway as a therapeutic target.* Drug Discovery Today **9**, 704-711.
112. Shyu, K.-G., M.-T. Wang, B.-W. Wang, C.-C. Chang, J.-G. Leu, P. Kuan, and H. Chang (2002) *Intramyocardial injection of naked DNA encoding HIF-1α/VP16 hybrid to enhance angiogenesis in an acute myocardial infarction model in the rat.* Cardiovasc. Res. **54**, 576-583.
113. Carmeliet, P., Y. Dor, J.-M. Herbert, D. Fukumura, K. Brusselmans, M. Dewerchin, M. Neeman, F. Bono, R. Abramovitch, P. Maxwell, C.J. Koch, P. Ratcliffe, L. Moons, R.K. Jain, D. Collen, and E. Keshet (1998) *Role of HIF-1a in hypoxia-mediated apoptosis, cell proliferation and tumour angiogenesis.* Nature **394**, 485-490.
114. Hewitson, K.S., B.M.R. Liénard, M.A. McDonough, I.J. Clifton, D. Butler, A.S. Soares, N.J. Oldham, L.A. McNeill, and C.J. Schofield (2007) *Structural and Mechanistic Studies on the Inhibition of the Hypoxia-inducible Transcription Factor Hydroxylases by Tricarboxylic Acid Cycle Intermediates.* J. Biol. Chem. **282**, 3293-3301.
115. Sasaki, M., C.B. Knobbe, M. Itsumi, A.J. Elia, I.S. Harris, I.I.C. Chio, R.A. Cairns, S. McCracken, A. Wakeham, J. Haight, A.Y. Ten, B. Snow, T. Ueda, S. Inoue, K. Yamamoto, M. Ko, A. Rao, K.E. Yen, S.M. Su, and T.W. Mak (2012) *D-2-hydroxyglutarate produced by mutant IDH1 perturbs collagen maturation and basement membrane function.* Genes Dev. **26**, 2038-2049.
116. Williams, S., M. Karajannis, L. Chiriboga, J. Golfinos, A. von Deimling, and D. Zagzag (2011) *R132H-mutation of isocitrate dehydrogenase-1 is not sufficient for HIF-1α upregulation in adult glioma.* Acta Neuropathol. **121**, 279-281.
117. Zhao, S., Y. Lin, W. Xu, W. Jiang, Z. Zha, P. Wang, W. Yu, Z. Li, L. Gong, Y. Peng, J. Ding, Q. Lei, K.-L. Guan, and Y. Xiong (2009) *Glioma-Derived Mutations in IDH1 Dominantly Inhibit IDH1 Catalytic Activity and Induce HIF-1α.* Science **324**, 261-265.
118. Koivunen, P., S. Lee, C.G. Duncan, G. Lopez, G. Lu, S. Ramkissoon, J.A. Losman, P. Joensuu, U. Bergmann, S. Gross, J. Travins, S. Weiss, R. Looper, K.L. Ligon, R.G.W. Verhaak, H. Yan, and W.G. Kaelin Jr (2012) *Transformation by the (R)-enantiomer of 2-hydroxyglutarate linked to EGLN activation.* Nature **483**, 484-488.

Chapter 2: Kinetic studies on oxygen activation of PHD2-catalysed HIF-1/2α hydroxylation

2.1. Introduction

The aim of the work described in this Chapter was to investigate the influence of the nature of the substrate on the kinetics of the PHD2 reaction with oxygen, and whether this could rationalise the unusually slow oxygen activation of the catalytic events. Detailed steady-state and transient (pre-steady-state) kinetic studies of the PHD2-catalysed hydroxylation of CODD and NODD HIF-1α, as well as its comparison to hydroxylation of HIF-2α, were carried out.

The HIF-1/2α isoforms have similar structures and characteristics, however some differences in their properties have been identified showing that they are not redundant (see Chapter 1, Section 1.4, reviewed in [1]). The structural differences are mostly located in the *N*-terminal region, which has been proposed to contribute to the differences in HIF target gene specificity [2]. While HIF-1α is mostly responsible for activation of glycolytic pathway genes (e.g. HK1 (hexokinase1), HK2 (hexokinase2)), HIF-2α is involved in regulation of genes responsible for cell cycle progression (e.g. cyclin D1), tumour growth, erythropoesis (e.g. EPO (erythropoietin)) and maintaining stem cell pluripotency amongst others [3, 4]. In addition, HIF-1/2α can both act as either pro-oncogenic factors or tumour suppressors depending on the cell type [1, 5, 6].

The PHDs are known to hydroxylate two different prolyl sites within both HIF-1α and HIF-2α, (CODD and NODD, Pro402 and Pro564 in HIF-1α, and Pro405 and Pro531 in HIF-2α). There are therefore four potential HIF prolyl sites for hydroxylation by the PHDs, raising the possibility that the kinetics of these hydroxylation reactions may vary with implications for their biological function. It has previously been shown that PHD2 has a preference for CODD hydroxylation over NODD hydroxylation based on both *in vitro* and cell-based studies [7-9]. The reported steady-state kinetic parameters suggested a stronger affinity of PHD2 for CODD compared to NODD (the reported K_m values are presented in the **Table 2.1**) [7, 8, 10, 11]. However, the absolute reported K_m values for CODD/NODD HIF-1α vary significantly

depending on the experimental technique and conditions used (**Table 2.1**). Techniques used for K_m determination have included [^{14}C] 2OG turnover or oxygen consumption assay, which unfortunately cannot differentiate between substrate modification and uncoupled 2OG turnover [10, 11]. In addition, differences in conditions, such as use of crude cell extracts [10] and absence of reducing agents required for optimum PHD2 activity [11], could affect the obtained results. To date, the most reliable and reproducible techniques for steady-state studies on PHD2-catalysed peptide hydroxylation have included matrix-assisted-laser-desorption-time-of-flight-mass spectrometry (MALDI-TOF-MS) based assays [7, 8]. However, these techniques have only been applied for kinetic studies with HIF-1α (determinations of K_m values for 2OG and CODD/NODD peptides). Therefore, systematic determination of the K_m values for both CODD/NODD sites of HIF-1/2α using a technique such as MALDI-TOF-MS, which would also help to eliminate the influence of uncoupled 2OG turnover, is required. This data could then be used to optimise conditions to determine $K_m(O_2)$ values for PHD2 in the presence of its different substrates.

Table 2.1. The reported kinetic parameters for PHD2-catalysed HIF-α hydroxylation. ND – not determined.

Enzyme	Substrate	K_m(2OG), μM	K_m(substrate), μM	$K_m(O_2)$, μM	Ref.
$PHD2_{181-426}$	HIF-$1\alpha_{556-574}$CODD	55±11	22±7	229±60	[11]
H_6-$PHD2_{181-426}$	H_6-HIF-$1\alpha_{530-652}$CODD	ND	2.3±0.3	76±11	[11]
H_6-$PHD2_{181-426}$	H_6-HIF-$2\alpha_{502-697}$CODD	267±34	15±2	67±10	[11]
H_6-$PHD2_{181-426}$	H_6-HIF-$1\alpha_{344-503}$NODD	58±20	24±7	85±17	[11]
$PHD2_{181-426}$	HIF-$1\alpha_{556-574}$CODD	ND	37±9	ND	[7]
$PHD2_{181-426}$	HIF-$1\alpha_{395-413}$NODD	ND	44±8	ND	[7]
PHD2 full length	HIF-$1\alpha_{556-574}$CODD	60	7	250	[10]
PHD2 full length	HIF-$1\alpha_{395-413}$NODD	ND	130	ND	[10]
PHD2 full length	HIF-$2\alpha_{522-541}$CODD	ND	30	ND	[10]
PHD2 full length	HIF-$2\alpha_{396-415}$NODD	ND	60	ND	[10]
$PHD2_{178-426}$	HIF-$1\alpha_{556-574}$CODD	ND	1.0±0.3	ND	[8]
$PHD2_{178-426}$	HIF-$1\alpha_{395-414}$NODD	ND	14±3	ND	[8]
PHD2 full length	HIF-$1\alpha_{558-574}$CODD	0.34±0.03	7.3±1.3	1746±574	[12]

Previous pre-steady-state studies on oxygen activation of the PHD2-catalysed CODD HIF-1α hydroxylation using stopped-flow UV-vis analyses have shown transient accumulation of a strongly absorbing 318-320 nm species, as assigned to the Fe(IV)-oxo intermediate for other 2OG oxygenases [13-16]. Mössbauer spectroscopy did not reveal the presence of an Fe(IV)-oxo intermediate as a major intermediate species during the catalysis [17], suggesting the observed 320 nm absorbance feature for PHD2 was attributable to a different species. The previous pre-steady-state studies had been carried out in the presence of L-ascorbate (Asc), known to stimulate PHD2 activity *in vitro* [17]. L-ascorbate forms an absorbing species with Fe(II) which is centered in the 500 nm region [18]. Due to the proposed slow reaction of PHD2 with oxygen, formation of an Asc-Fe(II)/(III) species during the timeframe of the reaction could interfere with the observation of the enzymatic reaction intermediates during stopped-flow UV-vis spectroscopic analyses (Asc-Fe(II)/(III) absorbs in the same wavelength region as (proposed) intermediates in PHD2 catalysis [17, 18]). Thus, further studies on the transient kinetics of the PHD2 reaction with oxygen were conducted in the absence of ascorbate. Furthermore, spectroscopic and kinetic analyses were used to investigate the effects of ascorbate on PHD2 catalysis.

2.2. Results

2.2.1. Steady-state kinetics of the PHD2-catalysed reaction: HIF-1α vs HIF-2α

The catalytic domain of human PHD2 (truncated $PHD2_{181-426}$, hereafter PHD2) was produced in *E. coli* and purified using cation exchange chromatography followed by size-exclusion chromatography, as described in *Materials and Methods* (Chapter 7) [19]. The purity of the protein was assessed at each stage by SDS-PAGE (>90 % final purity, **Figure 2.1a,b**) and the molecular weight of the enzyme was confirmed by LC-MS (**Figure 2.1c**).

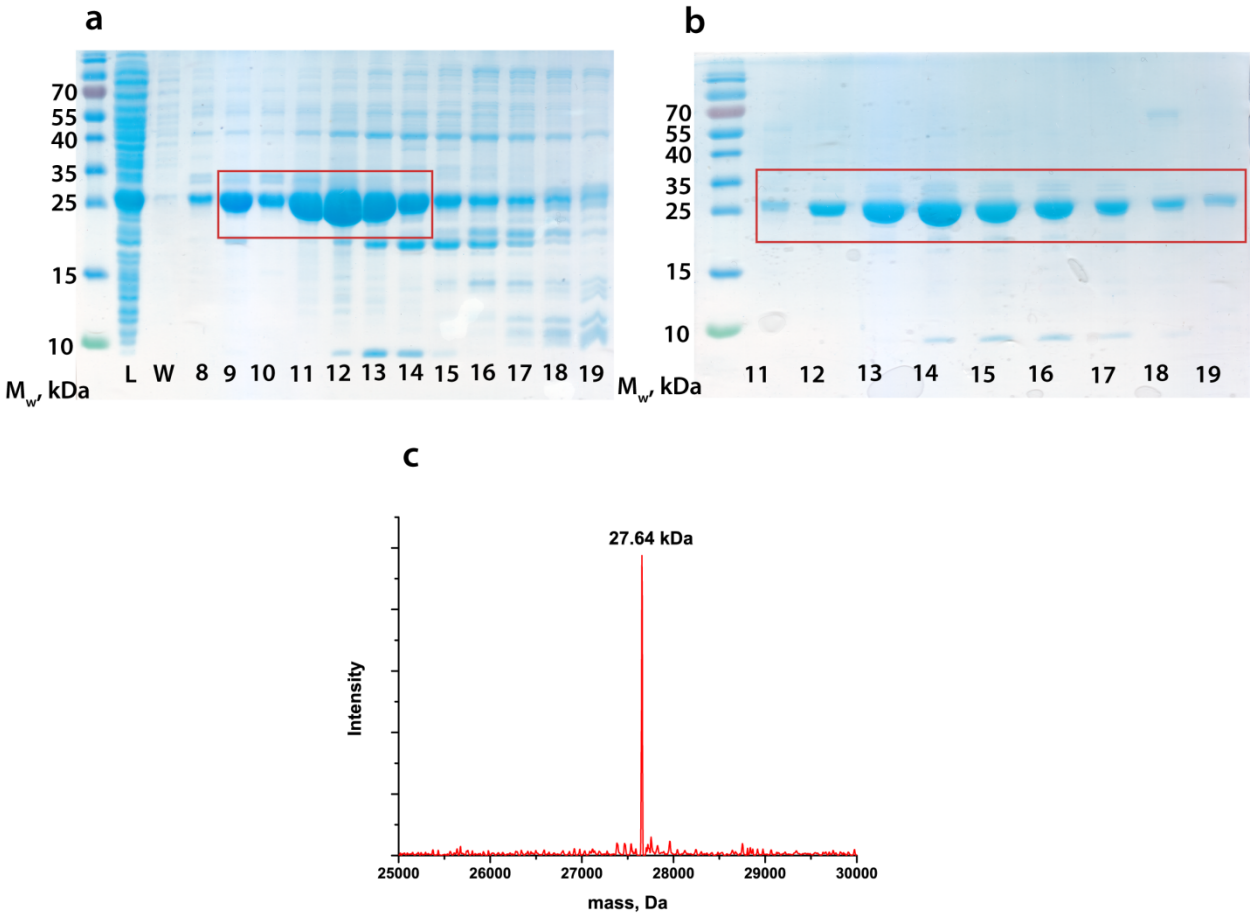


Figure 2.1. PHD2 purification. SDS-PAGE gels and deconvoluted protein LC-MS spectrum. (a) PHD2 (27.64 kDa) purification using cation exchange chromatography. L – lysate, W – column wash after lysate loading, 8-19 – numbers representing collected fractions. Fractions 9-14 were selected for further chromatography step. **(b)** PHD2 purification using size exclusion chromatography (subsequent to the cation exchange). 11-19 – collected fractions. **(c)** The deconvoluted LC-MS spectrum of the purified PHD2.·

· The LC-MS analyses confirming purity of the proteins used for the work described in this thesis were carried out by Dr A. Hardy (University of Oxford, Schofield group).

To assess the activity of PHD2, hydroxylation of CODD/NODD HIF-1/2α 19-mer peptides (the sequences are given in *Materials and Methods*) was studied under standard conditions previously optimised in the Schofield group (see *Materials and Methods* **Table 7.14**, [7]) using MALDI-TOF-MS based assays. The ratio between hydroxylated and unhydroxylated peptide was analysed (**Figure 2.2a**, the limit of detection ~3 % hydroxylation). A time course of CODD HIF-1/2α hydroxylation showed almost no difference between the two HIF-α isoforms (**Figure 2.2**). However, consistent with a previous report [7], hydroxylation of the NODD peptide was significantly slower compared to CODD for both HIF-1/2α (**Figure 2.2**). NODD HIF-1α hydroxylation was faster compared to NODD HIF-2α (50 % and 20 % hydroxylation after 15 min, respectively). In the case of CODD HIF-1/2α, there was a consistent level of background oxidation, which is likely a Met oxidation under the assay conditions, observed in the absence of the enzyme (~8-10 %). The background hydroxylation/oxidation was subtracted from the results of subsequent CODD hydroxylation assays.

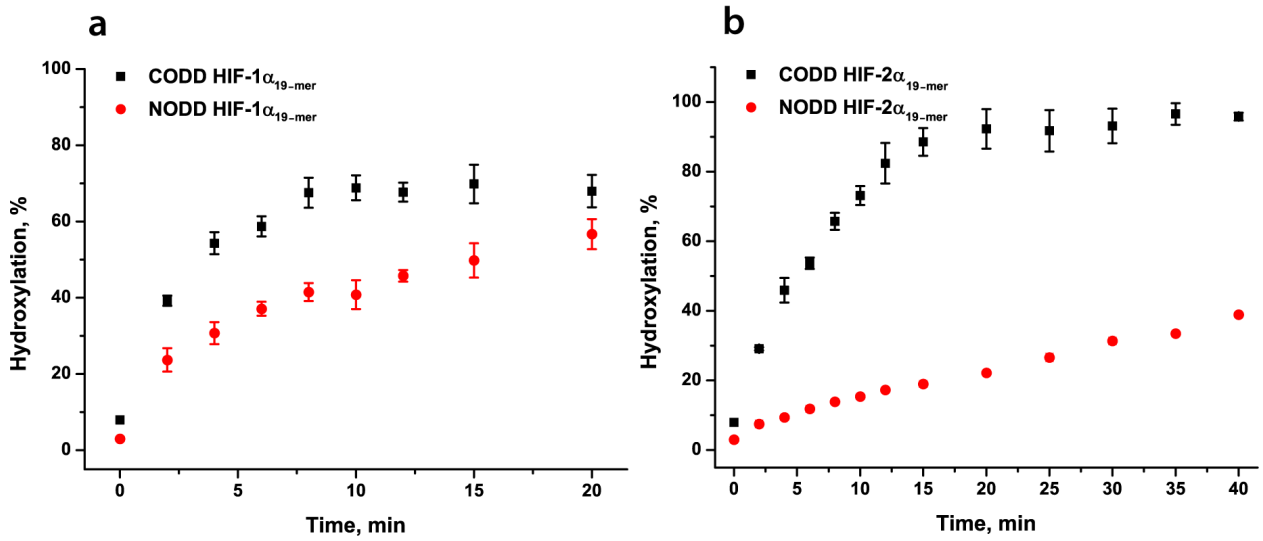


Figure 2.2. Time course activity assays of PHD2-catalysed CODD/NODD HIF-1/2α hydroxylation. Conditions: samples containing 4 μM PHD2, 300 μM 2OG, 100 μM peptide, 50 μM Fe(II), 4 mM ascorbate in 50 mM Tris·HCl (pH 7.5) buffer were incubated at 37 °C and then quenched with 1 % formic acid at defined time points (1:1 ratio). The peptide hydroxylation was analysed by MALDI-TOF-MS. The error bars represent standard deviation (SD) of triplicate assays. **(a)** Time course of HIF-1α CODD and NODD hydroxylation. **(b)** Time course of HIF-2α CODD and NODD hydroxylation.

Due to the variability in the reported kinetic parameters, it was envisaged that determination of the steady-state kinetic parameters (K_m, k_{cat}) for all substrates was required. This would

enable the use of saturating substrate and co-substrate concentrations (>2K_m) in the kinetic studies with oxygen, thus ensuring that PHD2 activity is only limited by oxygen availability. Time courses for PHD2 catalysis with different peptide/2OG concentrations were used to determine initial rates of the reaction. The dependence of the initial rates on (co-)substrate concentration was analysed using Michaelis-Menten kinetics (non-linear regression fitting). In the case of CODD peptides, the determined K_m for HIF-1α was lower compared to that for HIF-2α, which suggests a higher affinity of PHD2 for the former (10±6 μM and 34±9 μM for CODD HIF-1α and CODD HIF-2α, respectively, **Table 2.2, Figure 2.3**). However, the k_{cat} values were equivalent within error (0.060±0.006 s^{-1} and 0.069±0.006 s^{-1} for CODD HIF-1α and CODD HIF-2α, respectively), consistent with the activity time courses (**Figure 2.2**). The same tendency was observed for NODD HIF-1/2α peptides. Thus, the K_m for NODD HIF-1α was lower than for NODD HIF-2α (11±2 μM and 50±8 μM for HIF-1α and HIF-2α, respectively). However, the k_{cat} value was twice as high (0.028±0.001 s^{-1} and 0.013±0.001 s^{-1} for HIF-1α and HIF-2α, respectively), suggesting that NODD HIF-1α is a more efficient substrate than NODD HIF-2α (**Figure 2.3, Table 2.2**). The K_m values for 2OG were similar within error, with slightly higher values for NODD peptides compared to CODD. Overall, K_m(2OG) values were in agreement with the high affinity of 2OG binding to PHD2, (previously determined kinetic parameters suggested relatively tight co-substrate binding for PHD2 (**Table 2.1**) [7, 8, 10, 11], which is consistent with the observation that PHD2 forms a very stable complex with Fe(II) and 2OG [20]).

Table 2.2. Kinetic parameters of PHD2-catalysed CODD/NODD HIF-1/2α hydroxylation. Conditions: samples containing 4 μM PHD2, 2OG/peptide (varied), 50 μM Fe(II), 4 mM ascorbate in 50 mM Tris·HCl (pH 7.5) buffer were incubated at 37 °C. Peptide hydroxylation was analysed by MALDI-TOF-MS. To determine k_{cat} values, V_{max} rates were divided to PHD2 concentration (4 μM) assuming that $[E]_{active}=[E]_0$.

Substrate	K_m 2OG, μM	K_m peptide, μM	k_{cat}^{app}, s^{-1}
HIF-1α $CODD_{19\text{-mer}}$	13±2	10±6	0.060±0.006
HIF-1α $NODD_{19\text{-mer}}$	30±9	11±2	0.028±0.001
HIF-2α $CODD_{19\text{-mer}}$	9±2	34±9	0.069±0.006
HIF-2α $NODD_{19\text{-mer}}$	17±5	50±8	0.013±0.001

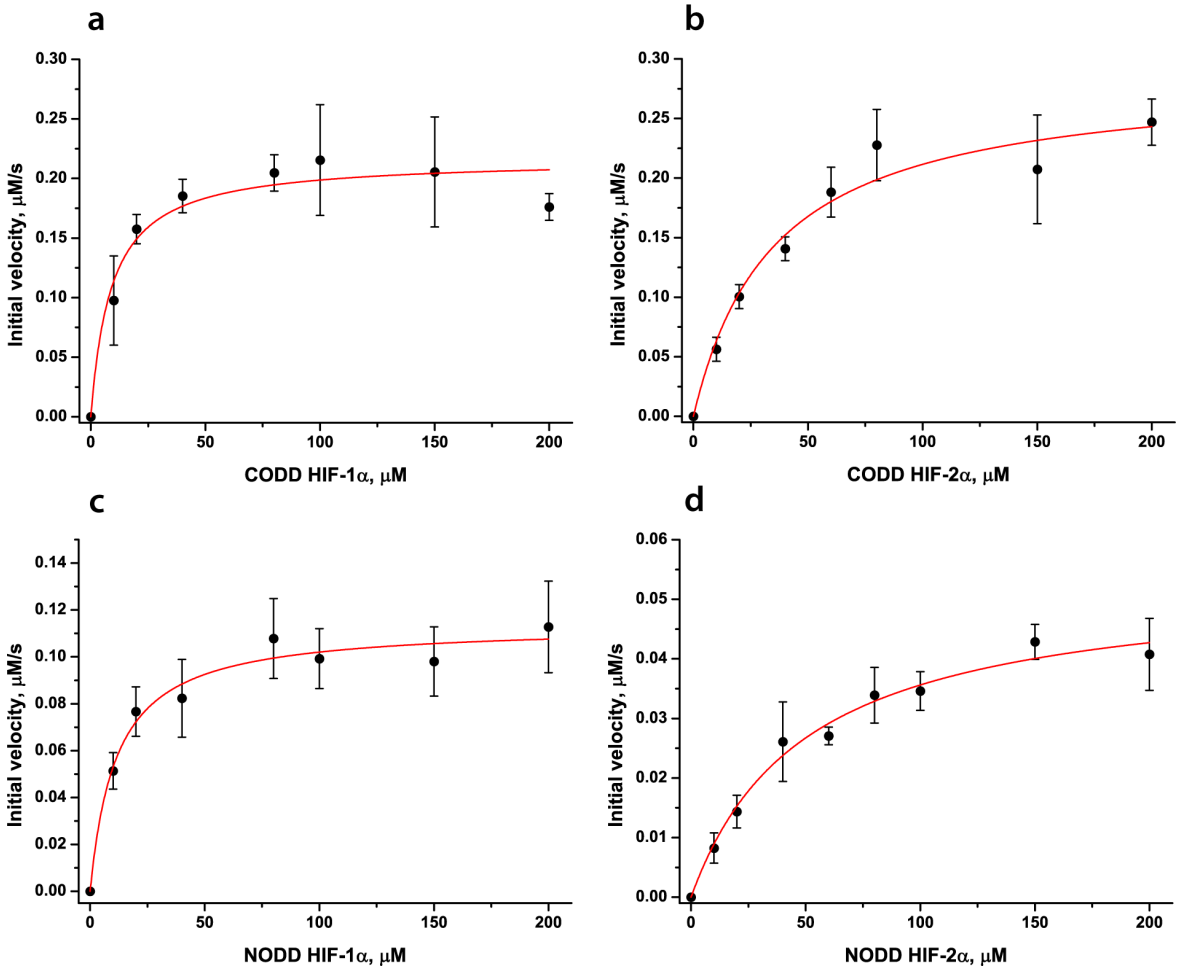


Figure 2.3. Peptide substrate K_m determination for PHD2-catalysed CODD/NODD HIF-1/2α hydroxylation. Conditions: samples containing 4 μM PHD2, peptide (varied), 300 μM 2OG, 50 μM Fe(II), 4 mM ascorbate in 50 mM Tris·HCl (pH 7.5) buffer were incubated at 37 °C. The peptide hydroxylation was analysed by MALDI-TOF-MS. The error bars represent SD of triplicate assays. The data were fitted using the Michaelis-Menten kinetic equation. The following peptide substrates were used: **(a)** CODD HIF-1α, **(b)** CODD HIF-2α, **(c)** NODD HIF-1α, **(d)** NODD HIF-2α.

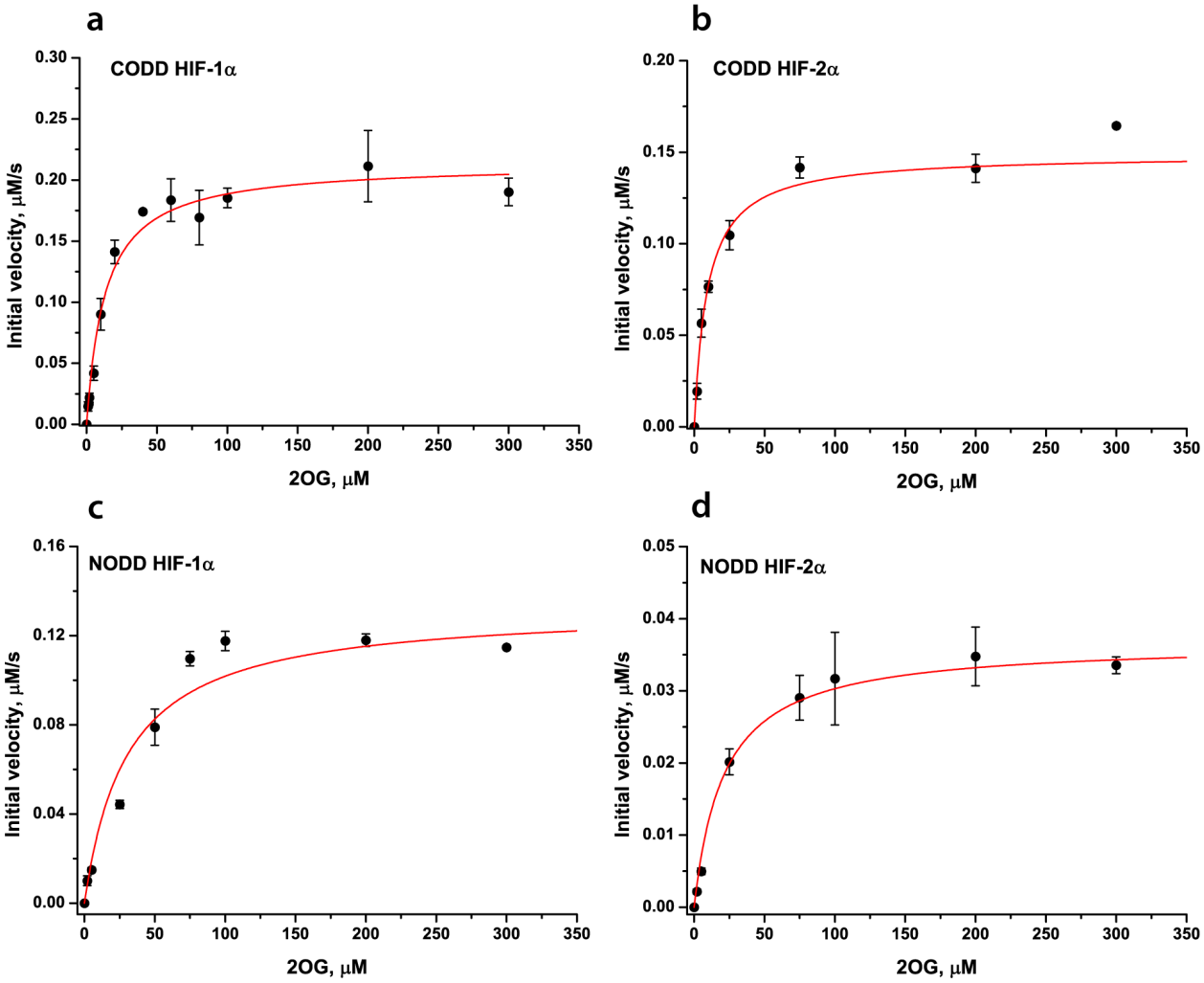


Figure 2.4. 2OG K_m determination for the PHD2-catalysed hydroxylation of CODD/NODD HIF-1/2α . Conditions: samples containing 4 μM PHD2, 100 μM peptide, 2OG (varied) 50 μM Fe(II), 4 mM ascorbate in 50 mM Tris·HCl (pH 7.5) buffer were incubated at 37 °C. The peptide hydroxylation was analysed by MALDI-TOF-MS. The error bars represent SD of triplicate assays. The data were fitted using the Michaelis-Menten kinetic equation. The following peptide substrates were used: **(a)** CODD HIF-1α, **(b)** CODD HIF-2α, **(c)** NODD HIF-1α, **(d)** NODD HIF-2α.

2.2.2. Oxygen dependence of the PHD2-catalysed reaction

Previous studies of PHD2-catalysed CODD HIF-1α hydroxylation have indicated a very high $K_m(O_2)$ for PHD2 which is in agreement with its oxygen-sensing function [9-11]. Thus, the O_2-dependence of HIF-α hydroxylation activity was shown to be linear over the whole 'physiological' range of oxygen concentrations, i.e. PHD2 activity is responsive to subtle changes in O_2 concentration. Therefore, it was necessary to use an assay in which O_2 concentrations could be controlled even to 'supra-physiological' levels. To compare the

oxygen dependence of CODD/NODD HIF-1/2α hydroxylation catalysed by PHD2, assays were therefore performed in sealed vials with a solution of peptide being pre-equilibrated under different O_2/N_2 gas mixes (up to 80 % O_2, the O_2/N_2 ratio was controlled by mass-flow controllers (MFC)) prior to addition of the remaining assay components (see *Materials and Methods*). The concentration of the dissolved O_2 was confirmed by a FOXY electrode [11]. To determine initial rates of the PHD2 reaction with each substrate at varied O_2 concentrations, the assay mixture was quenched at defined time points with 1 % formic acid. Interestingly, no sufficient saturation for CODD HIF-1/2α peptides or NODD HIF-1α was observed, suggesting that the K_m for O_2 is significantly higher than previously reported (>450 μM O_2, **Figure 2.5a-c**). Hydroxylation of NODD HIF-2α was characterised with a lower K_m for O_2, 414±82 μM (**Figure 2.5d**) [9].

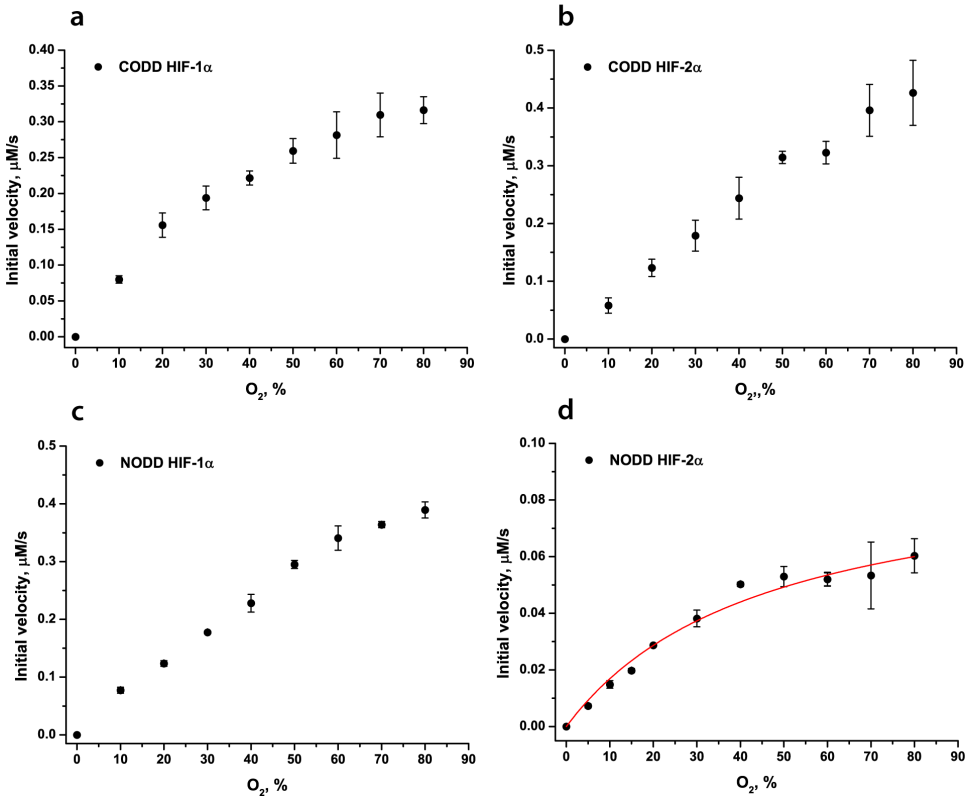


Figure 2.5. Oxygen dependence of PHD2-catalysed CODD/NODD HIF-1/2α hydroxylation. Conditions: samples containing 4 μM PHD2, 100 μM peptide, 300 μM 2OG, 50 μM Fe(II), 4 mM ascorbate in 50 mM HEPES (pH 7.5) buffer were incubated at 37 °C in septa-sealed vials under different N_2/O_2 gas mixes and then quenched by 1 % formic acid at defined time points. The peptide hydroxylation was analysed by MALDI-TOF-MS. The error bars represent SD of triplicate assays. The following substrates were used: **(a)** CODD HIF-1α, **(b)** CODD HIF-2α, **(c)** NODD HIF-1α, **(d)** NODD HIF-2α.

2.2.3. Stopped-flow kinetics of PHD2-catalysed HIF-1/2α hydroxylation·

2.2.3.1. Requirement of ascorbate for PHD2 catalysis under pre-steady-state conditions

To study the pre-steady-state kinetics of PHD2, interference of L-ascorbate with the observation of the catalytic intermediates was first investigated. An anaerobically prepared mixture of L-ascorbate, Fe(II) and 2OG was rapidly mixed with O_2-saturated buffer in a stopped-flow apparatus (Applied Photophysics SX20). Interestingly, the time course of formation and degradation of the absorbance features had a similar profile to those previously reported in studies on the PHD2 reaction with oxygen [17]. Positive transient absorbance species were observed as centered at 320 and 550 nm (**Figure 2.6**), which could affect observation of catalytic intermediates in the PHD2-catalysed reaction. Thus, it was necessary either to exclude ascorbate from the assay mixture in order to observe intermediates in PHD2 catalysis or to replace it with another reducing agent.

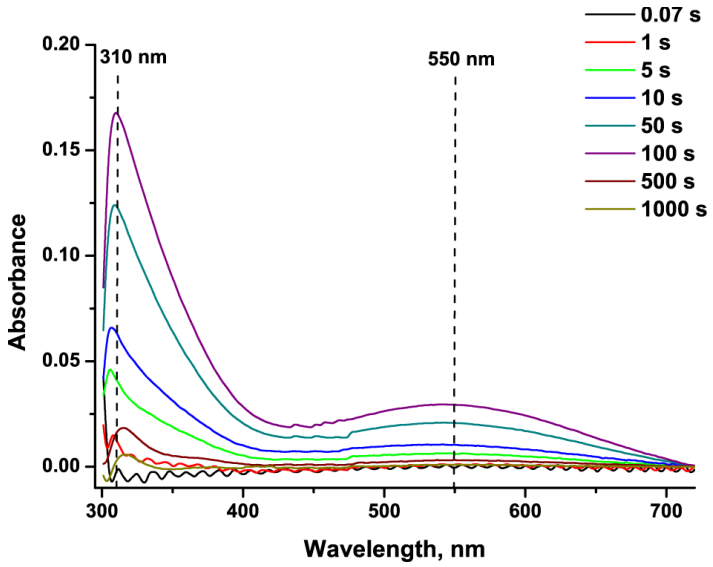


Figure 2.6. Stopped-flow absorbance spectra showing transient species formed due to the reaction of ascorbate with Fe(II). Difference spectra (O_2-free buffer spectra were subtracted from O_2-saturated buffer spectra) obtained after reaction of 0.5 mM Fe(II), 5 mM 2OG and 5 mM L-ascorbate at 5 °C.

· Part of the work described in this section has been published in Tarhonskaya, H., Chowdhury, R., Leung, I.K.H., Loik, N.D., McCulagh, J.S.O., Claridge, T.D.W., Schofield, C.J., Flashman E. (2014) *Investigating the contribution of the active site environment to the slow reaction of hypoxia-inducible factor prolyl hydroxylase with oxygen.* Biochemical Journal, **463**, 363-372.

The role of L-ascorbate in the stimulation of 2OG oxygenase activity is unclear, however, it has been proposed that L-ascorbate may be required to prevent inactivation of 2OG oxygenases over several reaction cycles due to uncoupled 2OG turnover and oxidative damage [21, 22]. Therefore, under conditions close to single turnover, one would not expect the enzymatic reaction to be significantly affected by the presence or absence of reducing agents [23]. To investigate the influence of L-ascorbate on PHD2 activity under pre-steady-state conditions, rapid quench-flow experiments were carried out comparing CODD hydroxylation in the presence and absence of L-ascorbate. An anaerobically prepared solution of a PHD2.Fe(II).2OG.CODD complex (+/- L-ascorbate) was rapidly mixed with O_2-saturated buffer, and the reaction was quenched at defined time points by 1 % CF_3COOH. The levels of CODD hydroxylation were analysed using MALDI-TOF-MS, and the pre-steady-state time course of CODD-OH accumulation was fitted with a single exponential equation as described [17] to determined the pseudo-first order rate constants of the reaction (**Figure 2.7**). The determined rate constants of product accumulation (fitting parameters) were very similar (0.0180 s^{-1} and 0.0155 s^{-1} with and without Asc, respectively). Thus, it has been demonstrated that it is possible to exclude L-ascorbate from the assay mixture for further studies without ablation of PHD2 enzymatic activity. L-ascorbate was therefore excluded from all subsequent pre-steady-state studies on PHD2.

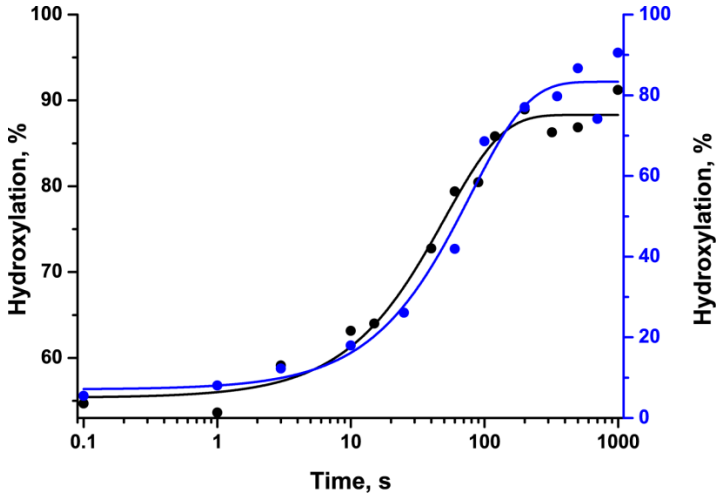


Figure 2.7. Rapid quench-flow experiments showing PHD2-catalysed CODD hydroxylation in the presence and absence of L-ascorbate. The reaction mixture containing 0.8 mM apo-PHD2, 0.5 mM Fe(II), 5 mM 2OG, 1 mM CODD (blue circles) and with 5 mM ascorbate (black circles) in 50 mM HEPES (pH 7.5) was rapidly mixed with O_2 buffer in 1:1 ratio at 5 °C and then quenched with 1 % (v/v) CF_3COOH at defined time points. The data were fitted with $y=a\cdot(1-exp(-bx))+c$ function.

2.2.3.2. Formation of 310 nm absorbance feature

To investigate the pre-steady-state reaction of PHD2, the PHD2.Fe(II).2OG.CODD HIF-1α assay mixture was prepared in an anaerobic glove box (without Asc or other reducing agents being added to the assay) and either mixed with O_2-free or with O_2-saturated buffer in 1:1 ratio (5 °C). The reaction was observed using a photodiode array detector and the difference spectra array was subsequently analysed (spectra with O_2-free buffer were subtracted to eliminate influences of absorbance changes which are not due to catalytic events). Although Asc was excluded from the assay mixture, upon introducing O_2 to the reaction formation and degradation of a relatively strong positive absorbance feature at 305-310 nm was again observed (**Figure 2.8c**). In addition, a weakly absorbing negative feature (also transient) centred at 520 nm was apparent (**Figure 2.8**). This absorbance decay at 520 nm was not observed previously for PHD2 catalysis [17], which is explained by stronger absorption of Asc-Fe(II)/(III) in the same region (see positive absorbance feature centered at 550 nm, **Figure 2.6**), however it was reported for other studied 2OG oxygenases [13, 14, 16, 17, 24]

Previous reports have shown that a high spin Fe(IV)-oxo reactive intermediate, observed for other 2OG oxygenases, has characteristic absorbance at 320 nm [13, 14, 16, 17, 24]. However, free Fe(III) in solution is also known to absorb at ~300 nm [25]. The observed absorbance features could therefore represent either an Fe(IV)-oxo intermediate, which is apparent in the absence of L-ascorbate, or transient changes in unbound iron oxidation states. Notably, formation and degradation of the 310 nm species was still slow compared to other 2OG oxygenase [13-16, 26]. To investigate the nature of the 310 nm species, Fe(II) oxidation in enzyme-free control experiments was studied. The results showed that spectral changes as a result of free-Fe(II) oxidation overlap with the observed 310 nm species, and free iron in solution could contribute to the observed changes of absorbance at this wavelength (**Figure 2.9b**). This implied that, even in the absence of Asc, the observed 310 nm absorbance species may not represent the proposed formation of an Fe(IV)-oxo intermediate. This was in agreement with a previous report indicating no accumulation of an Fe(IV)-oxo intermediate in a PHD2 catalytic cycle (note, that ascorbate was present in the assay mixture in previous studies on PHD2 [17]). Attempts were made to determine rates of formation and degradation of the observed 310 nm species by fitting curves. Analytical fitting of the individual kinetic traces (310 nm) using exponential functions gave a poor fit, which suggests either

heterogeneity of the observed species or complexity of the analysed processes. Moreover, the estimated rate constants of the formation and degradation of the 310 nm species were very low (0.0092±0.0001 s^{-1} and 0.0004±0.0001 s^{-1}, respectively, in the reaction of PHD2.Fe(II).2OG.CODD HIF-1α complex with oxygen), which suggested that this species might not be formed on a catalytically relevant timeframe of the reaction and could represent non-enzymatic processes.

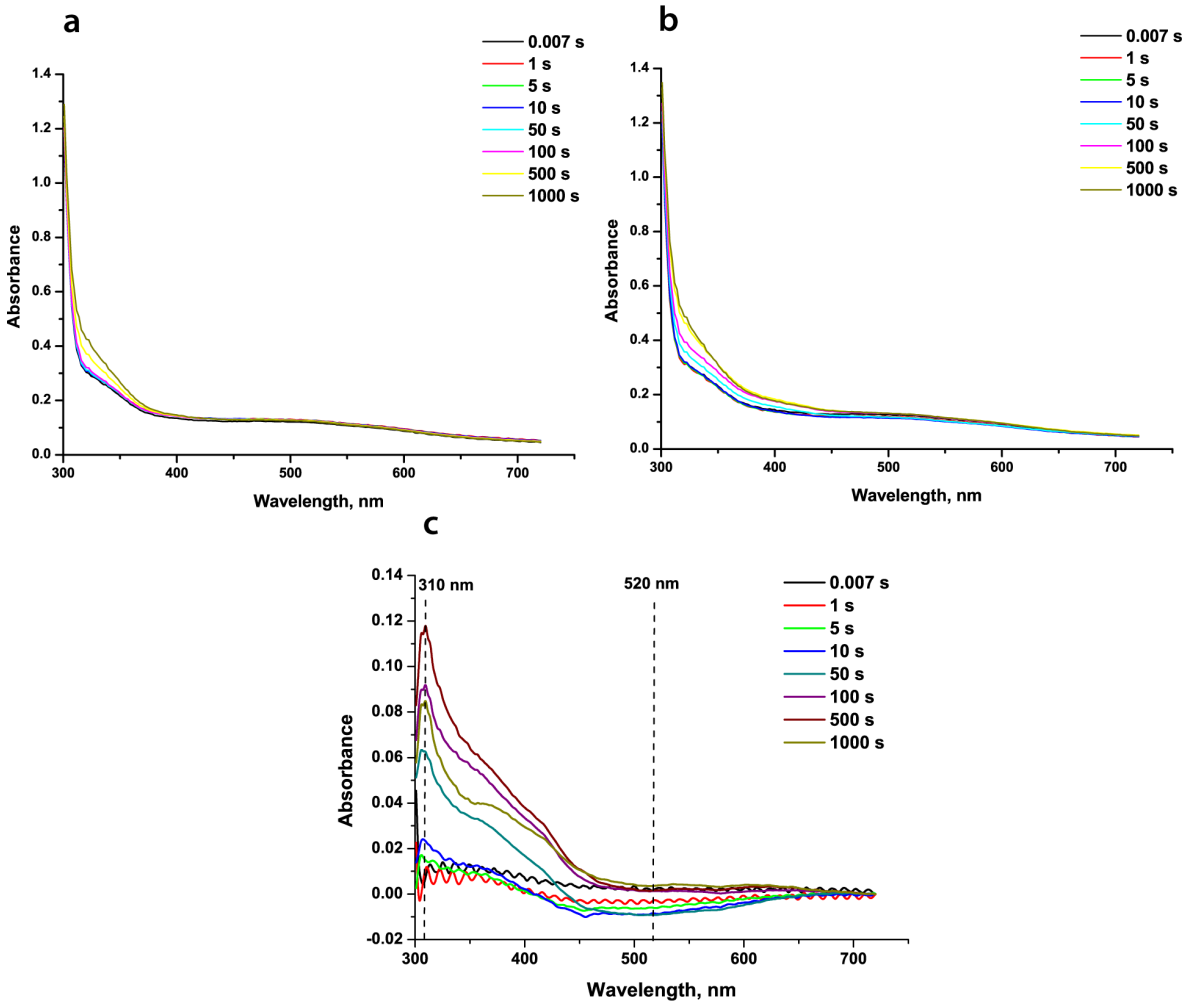


Figure 2.8. Stopped-flow absorbance spectra showing time course of the PHD2-catalysed reaction without ascorbate. The reaction mixture containing 0.8 mM apo-PHD2, 0.5 mM Fe(II), 5 mM 2OG, 1 mM peptide in 50 mM HEPES (pH 7.5) was rapidly mixed with O_2-free/O_2-saturated buffer in 1:1 ratio at 5 °C. **(a)** The absorbance spectra representing reaction after mixing PHD2.Fe(II).2OG.CODD complex with O_2-free buffer. **(b)** The absorbance spectra representing reaction after mixing PHD2.Fe(II).2OG.CODD complex with O_2-saturated buffer. **(c)** The difference spectra: O_2-free buffer spectra were subtracted from O_2-saturated buffer spectra.

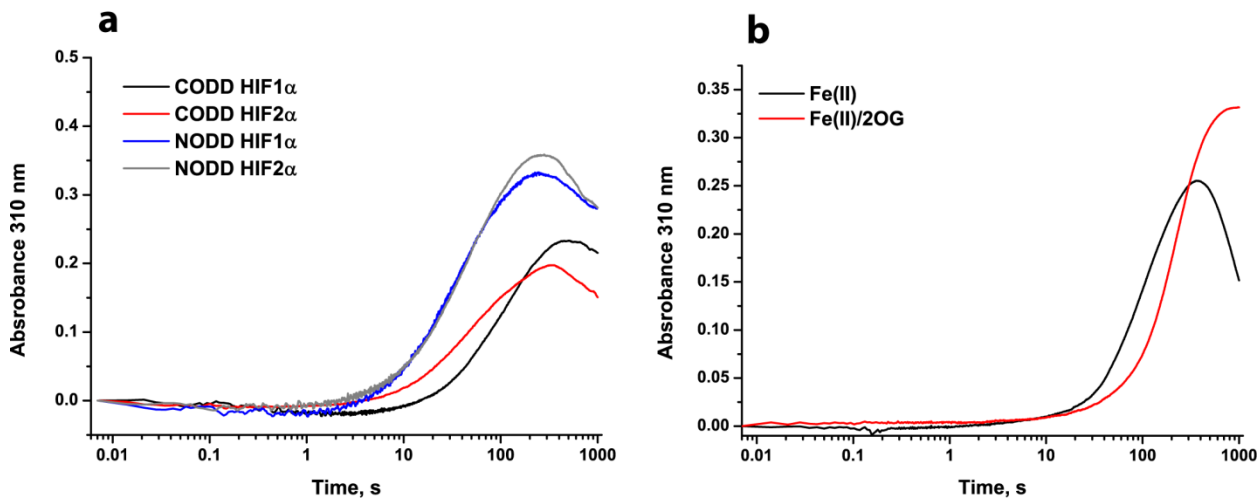


Figure 2.9. Stopped-flow kinetic traces at 310 nm showing absorbance species formed in the PHD2-catalysed HIF-1/2α hydroxylation. (a) The reaction mixture containing 0.8 mM apo-PHD2, 0.5 mM Fe(II), 5 mM 2OG, 1 mM peptide in 50 mM HEPES (pH 7.5) was rapidly mixed with O_2-saturated buffer in 1:1 ratio at 5 °C. The kinetic traces at 310 nm were analysed. These kinetic traces represent the average of triplicate assays. **(b)** The reaction mixture containing 0.5 mM Fe(II), 5 mM 2OG (if present) in 50 mM HEPES (pH 7.5) was rapidly mixed with O_2-saturated buffer in 1:1 ratio at 5 °C. Kinetic traces at 310 nm were analysed.

2.2.3.3. Formation of the 520 nm absorbance decay feature in stopped-flow experiments

It has been reported (including for PHD2) that formation of an enzyme-substrate complex for 2OG oxygenases can be characterised by a weak absorbance band at 520-530 nm due to metal ligand charge transfer (MLCT) representing the interaction of Fe(II) with 2OG [13, 17]. In accord with this, prior to the formation of the 310 nm species, a decay in absorbance at 520 nm was observed. Previously this decay has been associated with the depletion of the initial enzyme-substrate complex and accumulation of a high spin enzyme.Fe(II).product(s) complex, which does not possess the same absorbance characteristic [13]. Notably, for other 2OG oxygenases formation of the negative absorbance feature was usually visible only after/simultaneously with degradation of the 318-320 nm intermediate due to the mutual absorbance of the Fe(IV)-oxo species in the 300 nm and 500 nm region [13]. In the studies described in this Chapter, the decay in the 500 nm region was observed prior to the formation of the 310 nm absorbance species, again suggesting that the 310 nm species observed for PHD2 is not a catalytically relevant species, and that accumulation of the reactive Fe(IV)-oxo intermediate does not occur in PHD2 catalysis. The observed 520 nm absorbance species

likely represents an analogous catalytic intermediate (a high-spin enzyme.Fe(II).product(s)) and may be used for the assessment of the oxygen activation rates in PHD2 catalysis [13].

The rates of the PHD2.Fe(II).2OG.CODD HIF-1α complex absorbance depletion at 520 nm were investigated using the same conditions as in the previous study (except excluding Asc from the assay) [17]. The formation rate of the observed absorbance decay feature was rather slow, and the absorbance reached a minimum (likely reflecting maximum accumulation of the reaction intermediate) at ~22 s. It has been shown for other 2OG oxygenases, that oxygen activation is faster in the presence of a 'prime' substrate ('substrate triggering') [13-16, 26]. To ensure that the oxygen activation rates are not limited by insufficient substrate binding, the concentration of the CODD HIF-1α peptide was increased twice. This did not result in a significant change in the rate of the 520 nm absorbance depletion giving the same 22 s maximum intermediate accumulation, however, the amplitude of the observed feature (**Figure 2.10**) doubled. Thus, the initially chosen conditions provide sufficient formation of a PHD2.Fe(II).2OG.CODD complex and efficiently trigger O_2-activation.

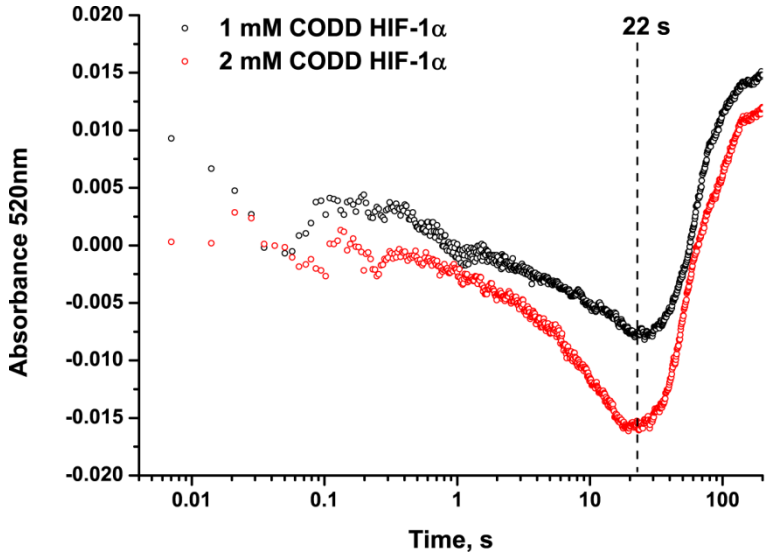


Figure 2.10. Comparison of 520 nm absorbance decay species in the reaction of PHD2-catalysed CODD hydroxylation in dependence on CODD HIF-1α concentration. The reaction mixture containing 0.8 mM apo-PHD2, 0.5 mM Fe(II), 5 mM 2OG, 1 mM peptide in 50 mM HEPES (pH 7.5) was rapidly mixed with O_2-free/O_2-saturated buffer in 1:1 ratio at 5 °C and then observed using a photodiode array detector. Difference spectra were analysed and time-dependent absorbance changes at λ=520 nm are presented.

2.2.3.4. Investigation of the influence of substrate nature on the reaction of PHD2 with oxygen

Having chosen the observed 520 nm absorbance decay as a feature to monitor PHD2 reaction with oxygen, the influence of the substrate nature on the kinetics of PHD2 catalysis was studied. The reaction of PHD2.Fe(II).2OG.CODD/NODD HIF-1/2α complexes with oxygen was investigated using stopped-flow spectroscopy. Experiments were set up under anaerobic conditions, and the enzymatic reaction was initiated by mixing the assay mixture with O_2-saturated buffer. The results are seen in **Figure 2.9a** and **Figure 2.11**. In all cases, formation and degradation of a 310 nm species was observed, characterised by similarly slow kinetics as for CODD HIF-1α. Analyses of the 520 nm feature showed little/no difference in the rates of the 520 nm absorbance decay for CODD and NODD HIF-1α. Interestingly, CODD HIF-2α peptide showed faster oxygen-activation compared to CODD HIF-1α, while there was no difference in the reaction with oxygen for NODD HIF-1α and NODD HIF-2α.

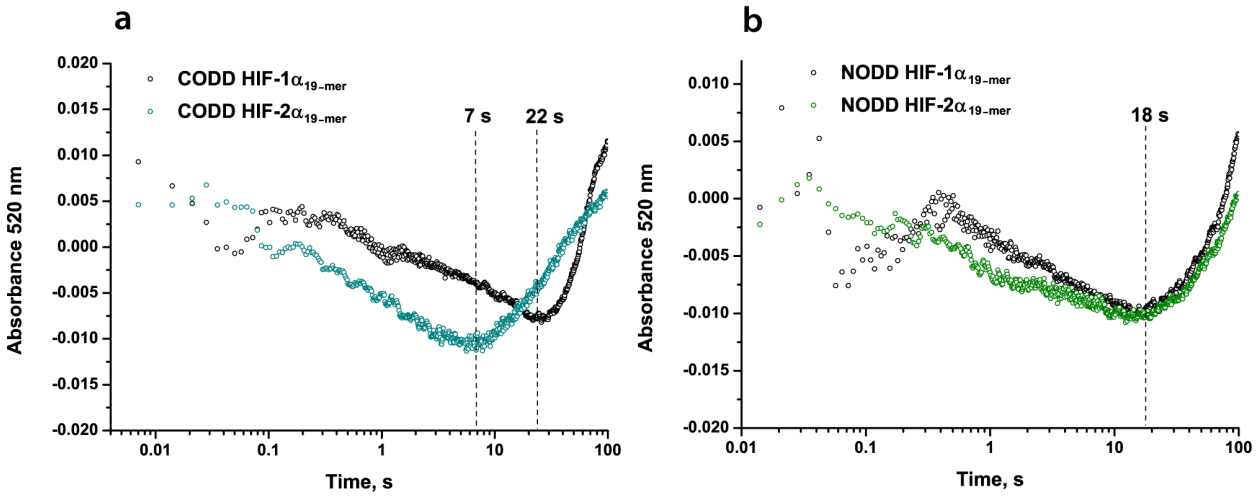


Figure 2.11. Comparison of 520 nm absorbance decay species in the reaction of PHD2-catalysed peptide hydroxylation with CODD/NODD HIF-1/2α substrates. The reaction mixture containing 0.8 mM apo-PHD2, 0.5 mM Fe(II), 5 mM 2OG, 1 mM substrate in 50 mM HEPES (pH 7.5) was rapidly mixed with O_2-free/O_2-saturated buffer in 1:1 ratio at 5 °C and then observed using a photodiode array detector. Difference spectra were analysed and time-dependent absorbance changes at 520 nm are presented.

Although, the presence of 19-mer peptides was sufficient to trigger the pre-steady-state reaction of PHD2 with oxygen, higher binding affinity of longer HIF-α fragments could result in alteration of the reaction rates. Previously, it had been shown that the reaction with CODD HIF-1α and recombinant CODD HIF-1α was characterised by the same pre-steady-state

kinetics [17]. To investigate whether the studied peptides adequately represent rates of the reaction in the case of NODD hydroxylation, stopped-flow experiments with recombinant NODD HIF-1$\alpha_{344\text{-}503}$ were carried out. Recombinant NODD HIF-1$\alpha_{344\text{-}503}$ showed the same kinetics of transient (with a negative absorbance change) species accumulation, after mixing PHD2.Fe(II).2OG.NODD complex as with O_2-saturated buffer, as observed in the presence of the 19-mer NODD HIF-1$\alpha_{395\text{-}414}$ peptide (**Figure 2.12**).

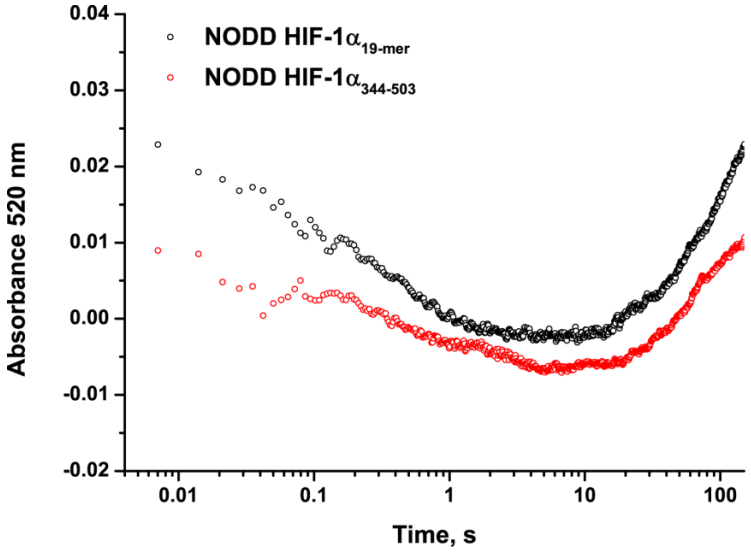


Figure 2.12. Comparison of 520 nm absorbance decay species in the reaction of PHD2-catalysed NODD HIF-1$\alpha_{395\text{-}414}$ hydroxylation and recombinant NODD HIF-1$\alpha_{344\text{-}503}$. The reaction mixture containing 0.8 mM apo-PHD2, 0.5 mM Fe(II), 5 mM 2OG, 1 mM substrate (NODD HIF-1$\alpha_{395\text{-}414}$ or HIF-1$\alpha_{344\text{-}503}$) in 50 mM HEPES (pH 7.5) was rapidly mixed with O_2-free/O_2-saturated buffer in 1:1 ratio and then observed using a photodiode array detector. Difference spectra were analysed and time-dependent absorbance changes at 520 nm are presented.

To investigate the correlation of 520 nm absorbance decay and peptide hydroxylation, pre-steady-state rates of product accumulation were studied. Anaerobically prepared PHD2.Fe(II).2OG.peptide complexes were mixed with O_2-saturated buffer at 1:1 ratio (same conditions as in stopped-flow experiments), and the reaction was quenched at defined time points with 1 % CF_3COOH. The ratio of hydroxylation was assessed by MALDI-TOF-MS. In the case of CODD HIF-1/2α the reaction proceeded up to 80 % which is consistent with PHD2:peptide ratio (0.8:1.0). This result was also in agreement with the assumption of a single catalytic turnover in the PHD2-catalysed reaction under these conditions (and good coupling efficiency as previously reported [17]). However, in the case of NODD HIF-1/2α hydroxylation, lower final hydroxylation levels were observed (~60 % and ~30 %, for NODD

HIF-1α and HIF-2α respectively). This may reflect lower levels of the enzyme-substrate complex in the assay mixture due to lower affinity of the peptides to PHD2, and correlates with the lower levels of hydroxylation observed in the steady-state studies (**Figure 2.2**).

To assess the pseudo-first order rates of product accumulation, the obtained results were fitted with a single exponential equation. Unlike the kinetics of intermediate formation observed in stopped-flow experiments, no significant difference was observed in the kinetics of product formation for the CODD HIF-α isoforms. NODD HIF-2α was hydroxylated slightly faster than NODD HIF-1α. The obtained rate constants are summarised in **Table 2.3.** Thus, studies of product accumulation in the oxygen-triggered reaction under pre-steady-state conditions did not reveal any significant difference in the kinetics of hydroxylation of CODD and NODD sites in HIF-1α and HIF-2α.

Table 2.3. The determined kinetic parameters of pre-steady-state PHD2-catalysed hydroxylation of HIF-1/2α CODD/NODD. Conditions: anaerobically prepared mixture of 0.8 mM apo-PHD2, 1 mM peptide substrate, 5 mM 2OG, 0.5 mM Fe(II) in 50 mM HEPES (pH 7.5) was rapidly mixed with O_2-saturated buffer at 5 °C. ND – not determined. The data were fitted either with a single or a double exponential function using Origin 8.51.

Substrate	Stopped-flow, 520 nm		Rapid quench-flow	
	$k_{fall\ phase}$, s^{-1}	$k_{rise\ phase}$, s^{-1}	$k_{hydroxylation}$, s^{-1}	$k_{succinate}$, s^{-1}
CODD HIF-1α	0.040±0.007	0.015±0.005	0.0155±0.0012	0.0130±0.0020
CODD HIF-2α	0.450±0.010	0.027±0.001	0.0124±0.0030	0.0120±0.0070
NODD HIF-1α	0.178±0.006	0.002±0.001	0.0080±0.0020	0.0060±0.0010
NODD HIF-2α	0.195±0.009	0.003±0.001	0.0199±0.0032	0.0270±0.0060

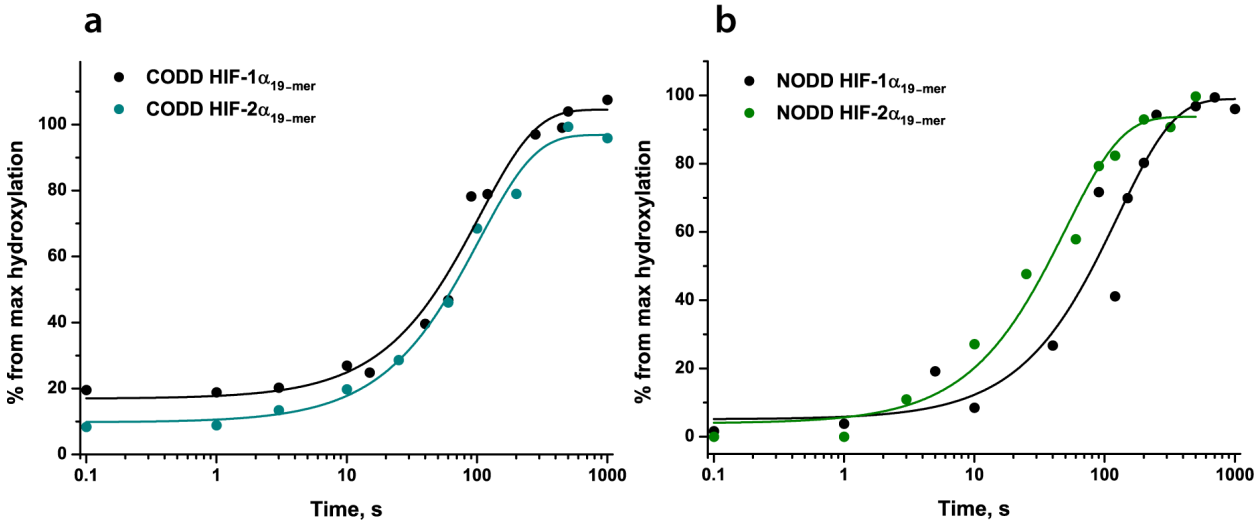


Figure 2.13. Comparison of the product accumulation time courses in the PHD2-catalysed hydroxylation of CODD/NODD HIF-1/2α. The reaction mixture containing 0.8 mM apo-PHD2, 0.5 mM Fe(II), 5 mM 2OG, 1 mM peptide in 50 mM HEPES (pH 7.5) was rapidly mixed with O_2-saturated buffer in 1:1 ratio at 5 °C and then quenched at defined time points by 1 % CF_3COOH. The peptide hydroxylation was analysed by MALDI-TOF-MS. **(a)** CODD site hydroxylation in HIF-1α and HIF-2α. **(b)** NODD site hydroxylation in HIF-1α and HIF-2α.

To investigate coupling of 2OG decarboxylation to hydroxylation, succinate formation during the reaction was investigated using liquid chromatography – mass spectrometry (LC-MS). The succinate concentration was determined by comparison with an external calibration curve. The data were fitted with a single exponential function and the determined kinetic parameters of succinate formation are summarised in **Table 2.3**. The 2OG oxidation was relatively tightly coupled to hydroxylation for all PHD2 substrates (determined rate constants were same within calculated error) (**Figure 2.14**).

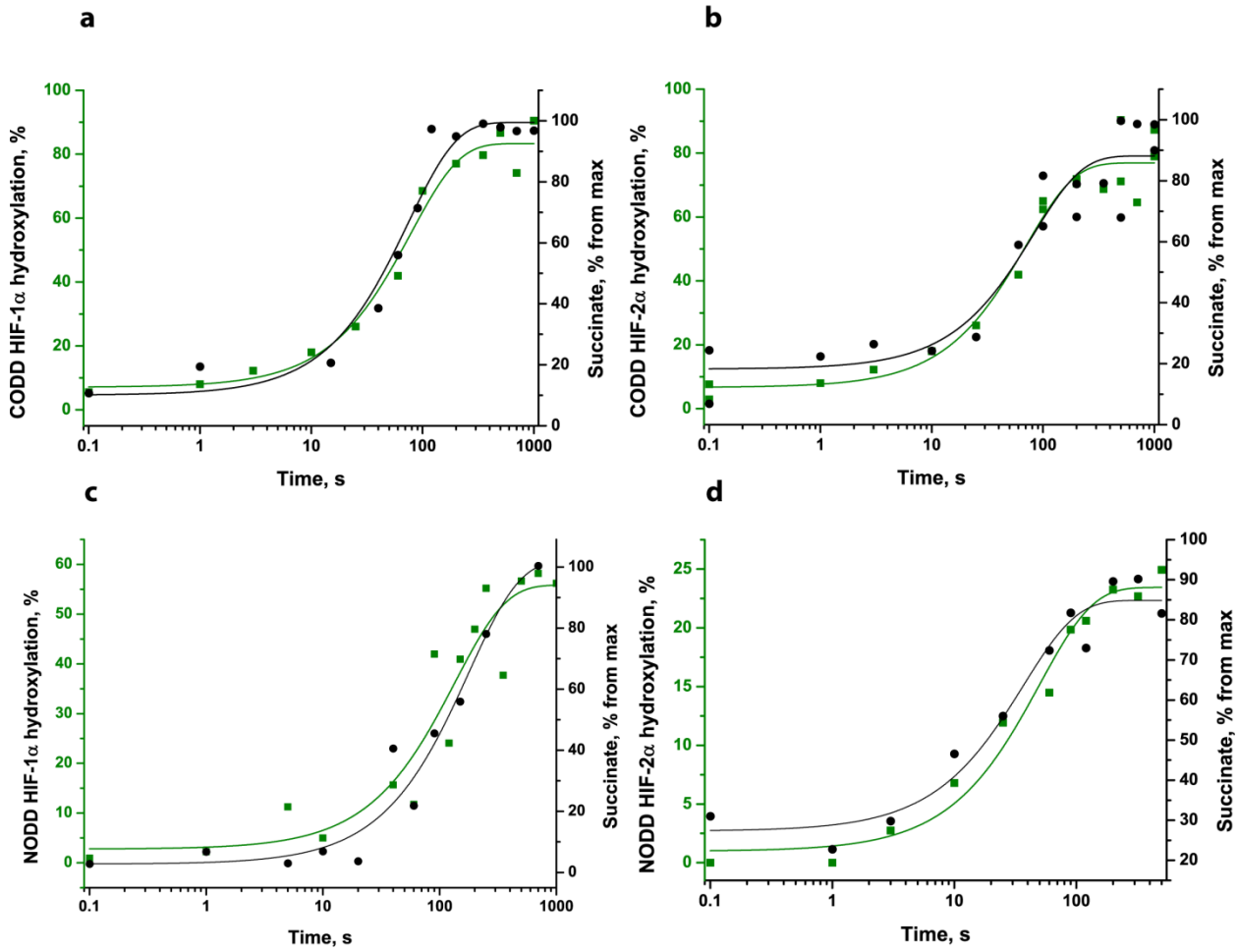


Figure 2.14. Rapid flow-quench studies of the PHD2-catalysed HIF-1/2α hydroxylation comparing hydroxylation and succinate formation. The reaction mixture containing 0.8 mM apo-PHD2, 0.5 mM Fe(II), 5 mM 2OG, 1 mM peptide in 50 mM HEPES (pH 7.5) was rapidly mixed with O_2 buffer in 1:1 ratio and then quenched with 1 % CF_3COOH at defined time points. The hydroxylation levels (green) were assessed by MALDI-TOF-MS and succinate accumulation (black) by LC-MS. The data was fitted with *y=a·(1-exp(-bx))+c* function. **(a)** CODD HIF-1α, **(b)** CODD HIF-2α, **(c)** NODD HIF-1α, **(d)** NODD HIF-2α.

2.3. Discussion

Previous studies of the pre-steady-state kinetics of PHD2 showed very slow oxygen-triggered activation of CODD HIF-1α hydroxylation [17]. In addition to the graded response to changes in the whole range 0-20.6 % of oxygen concentrations, this kinetic characteristic of PHD2 catalysis was proposed to be related to its biological function as an oxygen sensor in cells [9, 17]. It was of interest to investigate whether PHD2-catalysed hydroxylation of the HIF-1α NODD site, as well as hydroxylation of HIF-2α NODD and CODD, are characterised by the same slow oxygen activation as in the case of CODD HIF-1α. It was also important to acquire a full set of steady-state kinetic studies on PHD2, conducted using the optimum method, including determination of K_m values for CODD and NODD HIF-2α.

The determined kinetic parameters using MALDI-TOF-MS assays showed the same trend as previously published values [7, 8, 10, 11] for more efficient turnover of CODD over NODD (0.060±0.006 s^{-1} and 0.028±0.001 s^{-1} for HIF-1α CODD and NODD, respectively). In addition, the determined K_m values suggested higher affinity for HIF-1α, compared to HIF-2α (10±6 μM and 34±9 μM for CODD HIF-1α and CODD HIF-2α, respectively, **Table 2.2, Figure 2.3**). Interestingly, the steady-state kinetic parameters determined for oxygen dependence showed that the PHD2 K_m for O_2 may be higher than previously reported (i.e. >250 μM [10, 11]). However, this result is consistent with reported kinetic studies using a time-resolved fluorescence resonance energy transfer-based assay where the determined $K_m(O_2)$ for PHD2 was 1.7 mM [12]. This discrepancy in the results could arise from differences in the conditions used for K_m determination. One of the reported studies describes kinetic analyses using crude cell extracts with over-expressed full-length PHD2 [10], while the current study was done using the purified catalytic domain of PHD2 (note, that only determined values were presented in the published study making it is impossible to assess the goodness of the fit [10]). Another study was performed using an oxygen consumption assay, where ascorbate was excluded from the assay mixture to prevent its oxidation and contribution to the observed oxygen consumption [11]. It is known that ascorbate is required to maintain optimum activity of PHDs in steady state *in vitro* assays [17]. In addition, the presented kinetic curves and the fitting of the data obtained using the oxygen consumption assay suggest that the saturation was not reliably obtained up to 400 μM O_2. Thus, given the data obtained in this study using the optimised MFC/MALDI-TOF-MS based assay that enables direct product

hydroxylation rates to be calculated at O_2 concentrations up to 80 %, it is probable that PHD2 has an even more graded response to changes in O_2 *in vitro* than was previously reported.

Previously published pre-steady-state kinetics showed formation of a 320 nm species during catalysis which was not possible to assign to an Fe(IV)-oxo intermediate [17]. Here it was shown that the reported absorbance species, observed in the presence of ascorbate, most likely represents the reaction of Fe(II) with ascorbate. In addition, no change of absorbance over time in the 500 nm region was observed previously, which also could be explained by overlapping absorbance species from both the enzymatic and/or non-enzymatic reactions. When ascorbate was excluded from the assay mixture, a new negative (relatively weak) absorbance feature became apparent. A similar absorbance decay was also observed for other studied 2OG oxygenases [13, 14, 24], and most likely represents consumption of the initial PHD2.Fe(II).2OG.CODD/NODD complex. While the determined rates of the absorbance decay are associated with the beginning of the reaction, the analysis of the rise phase should be carried out with care due to the influence of the 310 nm species absorbance in the 500 nm region.

PHD2 has been shown to have preference for hydroxylation of the CODD site in HIF-1α, compared to NODD [7, 9, 27]. However, the kinetic analyses conducted in this study on the PHD2 oxygen dependence, including both pre-steady-state and steady-state phases of the catalysis, did not show significant differences neither between CODD and NODD hydroxylation, nor between HIF-1α and HIF-2α. Although the oxygen-triggered absorbance decay at 520 nm (PHD2.Fe(II).2OG.substrate consumption) was faster in the case of CODD HIF-2α hydroxylation (~10 fold) compared to CODD HIF-1α, suggesting faster oxygen activation for the former, there was no difference in the pre-steady-state time course of product accumulation. In addition, the determined k_{cat} values for both substrates were the same within error. These results suggest that although the initial step of oxygen activation may proceed faster, the impact of the further catalytic steps diminishes this effect of faster oxygen activation. Thus, the overall kinetics of CODD HIF-2α hydroxylation are very similar to CODD HIF-1α. A slight difference for NODD HIF-1/2α was also accompanied by much lower k_{cat} values, compared to the CODD site hydroxylation, which suggests less efficient hydroxylation and may make it less significant from the biological perspective.

Overall, the very slow reaction of PHD2 with oxygen was validated in this study. In addition, it was shown that PHD2-catalysed hydroxylation is slow, when oxygen is limiting, regardless of which substrate is used (whether it is the CODD or NODD site in either HIF-1α or HIF-2α). Accumulation of another transient species was observed, characterised by lower absorbance than the initial enzyme-substrate complex, which was previously masked by the non-enzymatic reaction of ascorbate with iron. Thus, the nature of the PHD2 interaction with its substrate does not significantly influence the kinetics of catalysis, and the molecular mechanism of this slow oxygen activation requires further investigation.

2.4. References

1. Loboda, A., A. Jozkowicz, and J. Dulak (2012) *HIF-1 versus HIF-2 — Is one more important than the other?* Vasc. Pharmacol. **56**, 245-251.
2. Hu, C.-J., L.-Y. Wang, L.A. Chodosh, B. Keith, and M.C. Simon (2003) *Differential Roles of Hypoxia-Inducible Factor 1α (HIF-1α) and HIF-2α in Hypoxic Gene Regulation.* Mol. Cell. Biol. **23**, 9361-9374.
3. Raval, R.R., K.W. Lau, M.G.B. Tran, H.M. Sowter, S.J. Mandriota, J.-L. Li, C.W. Pugh, P.H. Maxwell, A.L. Harris, and P.J. Ratcliffe (2005) *Contrasting Properties of Hypoxia-Inducible Factor 1 (HIF-1) and HIF-2 in von Hippel-Lindau-Associated Renal Cell Carcinoma.* Mol. Cell. Biol. **25**, 5675-5686.
4. Hu, C.-J., A. Sataur, L. Wang, H. Chen, and M.C. Simon (2007) *The N-Terminal Transactivation Domain Confers Target Gene Specificity of Hypoxia-inducible Factors HIF-1α and HIF-2α.* Mol. Biol. Cell **18**, 4528-4542.
5. Maranchie, J.K., J.R. Vasselli, J. Riss, J.S. Bonifacino, W.M. Linehan, and R.D. Klausner (2002) *The contribution of VHL substrate binding and HIF1-α to the phenotype of VHL loss in renal cell carcinoma.* Cancer Cell **1**, 247-255.
6. Kondo, K., W.Y. Kim, M. Lechpammer, and W.G. Kaelin, Jr. (2003) *Inhibition of HIF2α Is Sufficient to Suppress pVHL-Defective Tumor Growth.* PLoS Biol. **1**, e83.
7. Flashman, E., E.A.L. Bagg, R. Chowdhury, J. Mecinović, C. Loenarz, M.A. McDonough, K.S. Hewitson, and C.J. Schofield (2008) *Kinetic Rationale for Selectivity toward N- and C-terminal Oxygen-dependent Degradation Domain Substrates Mediated by a Loop Region of Hypoxia-Inducible Factor Prolyl Hydroxylases.* J. Biol. Chem. **283**, 3808-3815.
8. Pektas, S. and M.J. Knapp (2013) *Substrate preference of the HIF-prolyl hydroxylase-2 (PHD2) and substrate-induced conformational change.* J. Inorg. Biochem. **126**, 55-60.
9. Tian, Y.-M., K.K. Yeoh, M.K. Lee, T. Eriksson, B.M. Kessler, H.B. Kramer, M.J. Edelmann, C. Willam, C.W. Pugh, C.J. Schofield, and P.J. Ratcliffe (2011) *Differential Sensitivity of Hypoxia Inducible Factor Hydroxylation Sites to Hypoxia and Hydroxylase Inhibitors.* J. Biol. Chem. **286**, 13041-13051.
10. Hirsilä, M., P. Koivunen, V. Günzler, K.I. Kivirikko, and J. Myllyharju (2003) *Characterization of the Human Prolyl 4-Hydroxylases That Modify the Hypoxia-inducible Factor.* J. Biol. Chem. **278**, 30772-30780.
11. Ehrismann, D., E. Flashman, D.N. Genn, N. Mathioudakis, K.S. Hewitson, P.J. Ratcliffe, and C.J. Schofield (2007) *Studies on the activity of the hypoxia-inducible-factor hydroxylases using an oxygen consumption assay.* Biochem. J. **401**, 227-234.
12. Dao, J.H., R.J.M. Kurzeja, J.M. Morachis, H. Veith, J. Lewis, V. Yu, C.M. Tegley, and P. Tagari (2009) *Kinetic characterization and identification of a novel inhibitor of hypoxia-inducible factor prolyl hydroxylase 2 using a time-resolved fluorescence resonance energy transfer-based assay technology.* Anal. Biochem. **384**, 213-223.
13. Price, J.C., E.W. Barr, B. Tirupati, J.M. Bollinger, Jr., and C. Krebs (2003) *The first direct characterization of a high-valent iron intermediate in the reaction of an α-ketoglutarate-dependent dioxygenase: a high-spin Fe(IV) complex in taurine/α-ketoglutarate dioxygenase (TauD) from Escherichia coli.* Biochemistry **42**, 7497-508.

14. Hoffart, L.M., E.W. Barr, R.B. Guyer, J.M. Bollinger, and C. Krebs (2006) *Direct spectroscopic detection of a C-H-cleaving high-spin Fe(IV) complex in a prolyl-4-hydroxylase.* Proc. Natl. Acad. Sci. U. S. A. **103**, 14738-14743.
15. Galonić, D.P., E.W. Barr, C.T. Walsh, J.M. Bollinger, and C. Krebs (2007) *Two interconverting Fe(IV) intermediates in aliphatic chlorination by the halogenase CytC3.* Nat. Chem. Biol. **3**, 113-116.
16. Matthews, M.L., C.M. Krest, E.W. Barr, F.H. Vaillancourt, C.T. Walsh, M.T. Green, C. Krebs, and J.M. Bollinger (2009) *Substrate-Triggered Formation and Remarkable Stability of the C−H Bond-Cleaving Chloroferryl Intermediate in the Aliphatic Halogenase, SyrB2.* Biochemistry **48**, 4331-4343.
17. Flashman, E., S.L. Davies, K.K. Yeoh, and C.J. Schofield (2010) *Investigating the dependence of the hypoxia-inducible factor hydroxylases (factor inhibiting HIF and prolyl hydroxylase domain 2) on ascorbate and other reducing agents.* Biochem. J. **427**, 135-142.
18. Keypour, H., J. Silver, M.T. Wilson, and M.Y. Hamed (1986) *Studies on the reactions of ferric iron with ascorbic acid. A study of solution chemistry using Mössbauer spectroscopy and stopped-flow techniques.* Inorg. Chim. Acta **125**, 97-106.
19. Chowdhury, R., M.A. McDonough, J. Mecinović, C. Loenarz, E. Flashman, K.S. Hewitson, C. Domene, and C.J. Schofield (2009) *Structural Basis for Binding of Hypoxia-Inducible Factor to the Oxygen-Sensing Prolyl Hydroxylases.* Structure **17**, 981-989.
20. McNeill, L.A., E. Flashman, M.R.G. Buck, K.S. Hewitson, I.J. Clifton, G. Jeschke, T.D.W. Claridge, D. Ehrismann, N.J. Oldham, and C.J. Schofield (2005) *Hypoxia-inducible factor prolyl hydroxylase 2 has a high affinity for ferrous iron and 2-oxoglutarate.* Mol. BioSyst **1**, 321-324.
21. Myllylä, R., K. Majamaa, V. Günzler, H.M. Hanauske-Abel, and K.I. Kivirikko (1984) *Ascorbate is consumed stoichiometrically in the uncoupled reactions catalyzed by prolyl 4-hydroxylase and lysyl hydroxylase.* J. Biol. Chem. **259**, 5403-5405.
22. Hausinger, R.P. (2004) *Fe(II)/α-Ketoglutarate-Dependent Hydroxylases and Related Enzymes.* Crit. Rev. Biochem. Mol. Biol. **39**, 21-68.
23. De Jong, L., S.P.J. Albracht, and A. Kemp (1982) *Prolyl 4-hydroxylase activity in relation to the oxidation state of enzyme-bound iron: The role of ascorbate in peptidyl proline hydroxylation.* BBA-Protein. Struct. M **704**, 326-332.
24. Tarhonskaya, H., A. Szöllössi, I.K.H. Leung, J.T. Bush, L. Henry, R. Chowdhury, A. Iqbal, T.D.W. Claridge, C.J. Schofield, and E. Flashman (2014) *Studies on Deacetoxycephalosporin C Synthase Support a Consensus Mechanism for 2-Oxoglutarate Dependent Oxygenases.* Biochemistry **53**, 2483-2493.
25. Knight, R.J. and R.N. Sylva (1975) *Spectrophotometric investigation of iron(III) hydrolysis in light and heavy water at 25°C.* J. Inorg. Nucl. Chem. **37**, 779-783.
26. Sánchez-Fernández, E.M., H. Tarhonskaya, K. Al⁻Qahtani, R.J. Hopkinson, J.S.O. McCullagh, C.J. Schofield, and E. Flashman (2013) *Investigations on the oxygen dependence of a 2-oxoglutarate histone demethylase.* Biochem. J. **449**, 491-496.
27. Chan, D.A., P.D. Sutphin, S.-E. Yen, and A.J. Giaccia (2005) *Coordinate Regulation of the Oxygen-Dependent Degradation Domains of Hypoxia-Inducible Factor 1α.* Mol. Cell. Biol. **25**, 6415-6426.

Chapter 3: Mechanistic studies on the reaction of PHD2 with oxygen*

3.1. Introduction

PHD2 was the first 2OG oxygenase for which a relatively slow reaction with oxygen was observed [1-4]. Although the slow oxygen activation shown for PHD2 was not directly linked to its biological function, it was proposed that this kinetic feature may be related to the oxygen sensing function of this enzyme [5]. Thus, identification of the molecular features responsible for the low affinity of PHD2 for oxygen and/or its slow reaction with oxygen was interesting from the perspective of better understanding the molecular mechanism of the reaction of PHD2 with oxygen.

Previous attempts at investigating the mechanistic strategies of PHD2 included steady-state kinetic analyses and solvent isotope effect (SIE) experiments [6]. Steady-state kinetic studies on the pH dependence of k_{cat} and SIE experiments for PHD2-catalysed CODD hydroxylation suggested that release of an iron-bound water molecule occurs after CODD binding [6]. The kinetic parameters of the reaction were also measured using D_2O as a solvent, and showed inverse solvent isotope effect, which implies that the release of a metal-bound water molecule may precede a rate-limiting step of the reaction [6]. In addition, the pH dependence of PHD2 activity suggested higher turnover under moderately acidic conditions, rather than at high pH. This was proposed to have a physiological implication in pH sensing by the PHDs in addition to the oxygen sensing function [6]. However, the reported results of the studies on the pH dependence of PHD2 turnover could also be a manifestation of other factors such as instability of the enzyme *in vitro* at higher pH values (which would therefore affect the calculated k_{cat} values), as well as faster oxidation of Fe(II) to Fe(III) in solution.

* Part of the work described in this Chapter has been published in Tarhonskaya, H., Chowdhury, R., Leung, I.K.H., Loik, N.D., McCulagh, J.S.O., Claridge, T.D.W., Schofield, C.J., Flashman E. (2014) *Investigating the contribution of the active site environment to the slow reaction of hypoxia-inducible factor prolyl hydroxylase with oxygen*. Biochemical Journal, **463**, 363-372.

Crystallographic analyses of a PHD2.Mn(II).*N*-oxaloglycine(NOG).CODD complex suggested that 2OG is coordinated to the active site iron such that oxygen cannot bind in the optimum position for HIF-α hydroxylation [7]. Coupled with the fact that PHD2 is known to bind Fe(II) and 2OG unusually tightly (K_d for 2OG<1 μM, for Fe(II)<2 μM) [8], this suggests that 2OG rearrangement at the active site prior to efficient oxygen binding may be slow and rate-limiting (**Figure 3.1**).

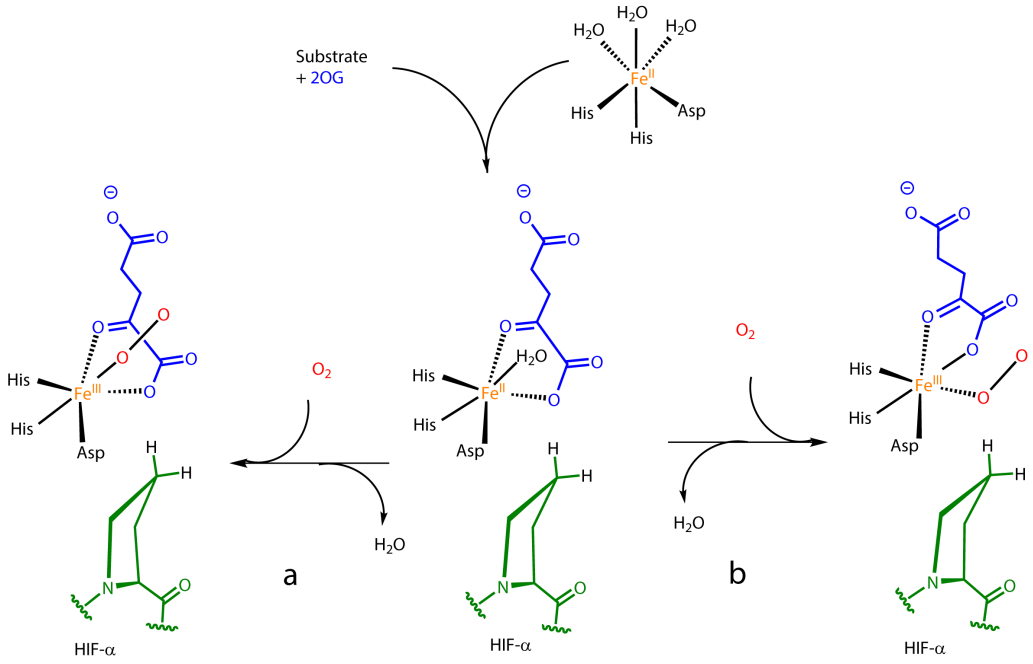


Figure 3.1. Scheme illustrating two possible conformations for oxygen binding during the PHD2-catalysed reaction. Oxygen either binds in **(a)** a sterically hindered site or **(b)** 2OG molecule coordination is rearranged during the reaction.

According to the PHD2.Mn(II).NOG.CODD crystal structure, 2OG binding is stabilised by electrostatic interactions with R383, and hydrogen bonds with Y329 [7] (**Figure 3.2**). R383 is usually conserved across the 2OG dependent oxygenases. However, there are also members of the enzymatic family which possess a Lys residue in this position [9]. In addition, 2OG creates hydrogen bonds with the network of water molecules as well as Y303. It is also known that Y303 substitution to A decreases the catalytic activity of hydroxylation [7]. Substitution of the named residues could therefore influence the 2OG binding mode and thus potentially the PHD2 reaction with oxygen (if indeed 2OG rearrangement precedes O_2 binding).

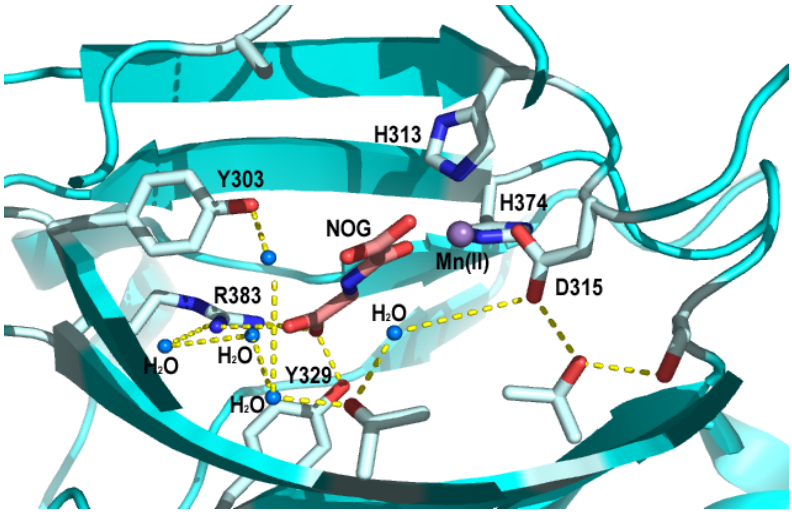


Figure 3.2. Overview of the active site structure and interactions in the crystal structure of PHD2.Mn(II).NOG.CODD complex (PDB: 3HQR). 2OG forms electrostatic interactions with a conserved R383 residue and an H-bond with Y329, while metal ion is coordinated by facial triad residues (D315, H313, H374). There is also a network of H-bonds which includes a metal-coordinated water molecule and Y303. In addition, the metal-coordinated water molecule is also stabilised by an H-bond with D315.

The metal-coordinated H_2O is known to be stabilised by its interaction with D315 in PHD2, one of the Fe(II) binding residues, possibly reducing the rate at which it can be replaced with O_2 [7]. It is known that binding of a 'prime' substrate triggers a shift from iron six- to five-coordinate state, whereby the bond between the iron and the coordinated water molecule is weakened, thus allowing binding of oxygen [10]. The higher affinity of PHD2 to water ligand, rather than to oxygen could explain its slow oxygen activation [5, 6]. This is consistent with the proposals that the dissociation of the metal-bound water molecule precedes the rate-limiting step of the reaction [6]. Interestingly, it has been shown that substitution of the aspartate to glycine in the FIH facial triad does not ablate enzymatic activity [11]. The fact that there is apparent flexibility and tolerance to changes in Fe(II) coordinating residues amongst the 2OG dependent oxygenases raises the possibility of making substitutions of the iron binding residues without complete loss of enzymatic activity. As a consequence, these changes may influence the oxygen binding properties of the enzyme.

The above mentioned structural factors, such as stabilisation of a metal-bound H_2O by an H-bond with D315E, and the influence of tight Fe(II)/2OG binding were investigated using site-directed mutagenesis, kinetic and spectroscopic techniques to determine whether they contribute to the slow reaction of PHD2 with O_2.

3.2. Results

3.2.1. Activity of PHD2 variant enzymes

To investigate the influence of the key active site residues on the rate of the reaction with O_2, a range of PHD2 variants were cloned (Fe(II) binding - H313D, D315H, D315E, H374E, H374R; 2OG coordination – Y303F, Y329F, R383K (**Figure 3.2**)), produced in *E. coli* and purified (as described in *Materials and Methods*). The purity of the variants was assessed using SDS-PAGE and LC-MS analyses (**Figure 3.3**).

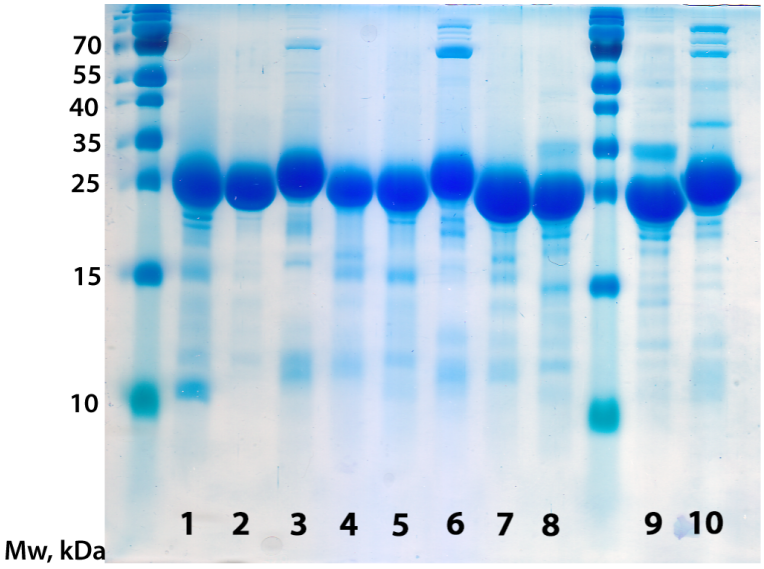


Figure 3.3. SDS-PAGE gel of purified WT PHD2 and its variants. 1. Y303F, 2. H313D, 3. D315H-His_6, 4. D315E, 5. Y329F, 6. H374E-His_6, 7. H374R, 8. R383K, 9. WT, 10. D315E R383K-His_6. D315H, H374E, D315E R383K were left with His_6 tag due to the low levels of production. Figure and figure legend are adopted with permission from Tarhonskaya *et al.* Biochem. J. **463**, 363-372.

The activity of the variant enzymes in the reaction of CODD HIF-1α hydroxylation was first assessed using MALDI-TOF-MS based time course assays [12, 13]. To study changes to the kinetics of the reaction with O_2, variants with altered co-substrate/co-factor binding, which also would have sufficient enzymatic activity to conduct further studies, were required. The time course assays showed that Y303F and Y329F did not have a significant change in the rate of catalysis of CODD hydroxylation compared to wild-type (WT) PHD2, while most of the facial triad mutations led to complete loss of enzymatic activity (**Figure 3.4**). Thus H313D, D315H, H374E, H374R were not active under the standard assay conditions (**Figure 3.4c**). However, the conservative D315E variant (E is present in some 2OG oxygenases at this position as a part of the HXD/E…H motif coordinating Fe(II)) [14] showed similar activity to

WT PHD2 in a time-course assay (**Figure 3.4**). Notably, substitution of the conservative 2OG coordinating residue R383 to K resulted in only a reduced rate of CODD hydroxylation with completion of the reaction after 30 min of incubation with PHD2 at 37 °C. (Note that K is present in some 2OG dependent oxygenases as a 2OG-binding residue [14], and substitution of R at this position to K has been shown to ablate full-length PHD1 activity (under different assay conditions: using crude extracts of insect cells, assessing 2OG turnover) [15].)

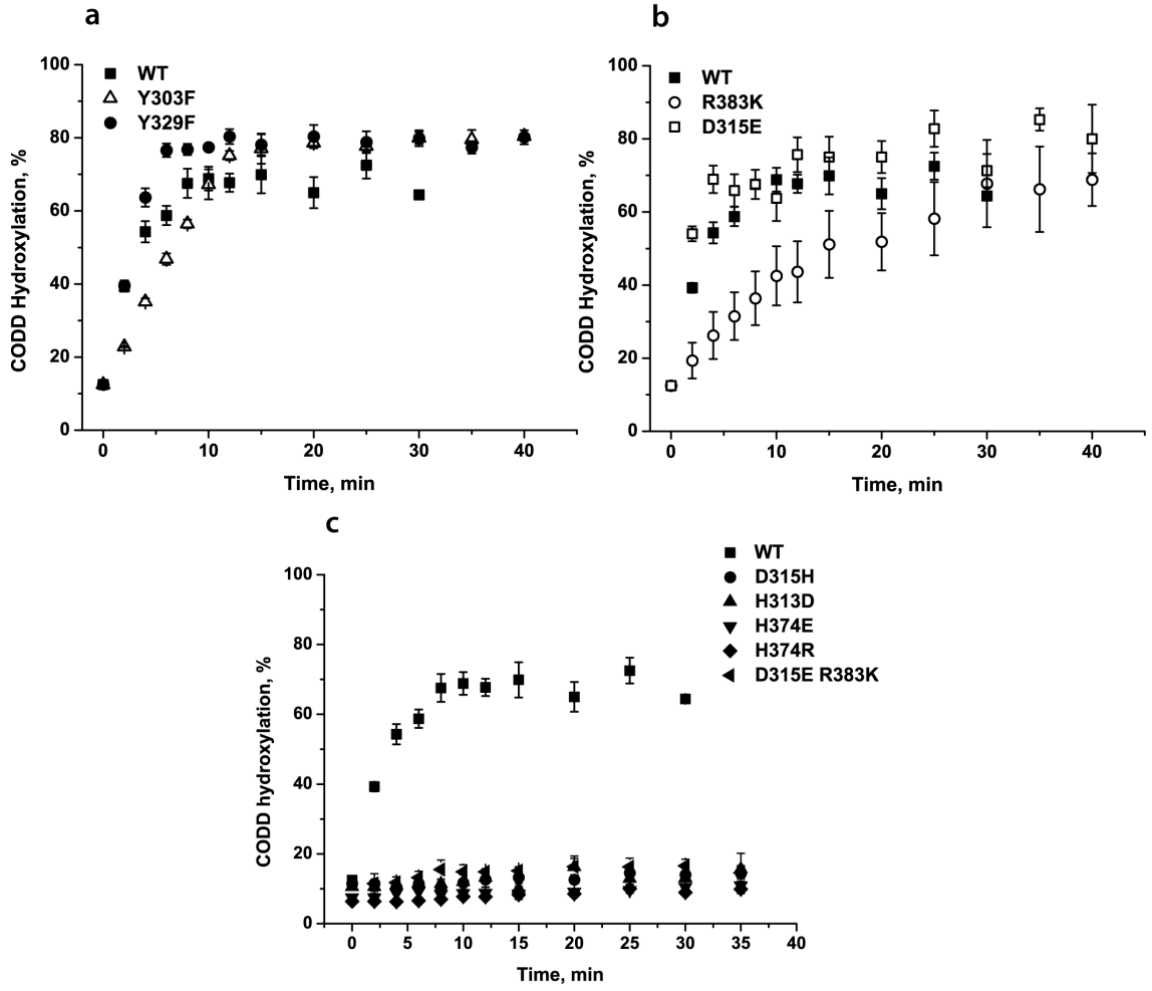


Figure 3.4. Activity of the PHD2 variant enzymes in the reaction of CODD hydroxylation. PHD2-catalysed reaction of CODD hydroxylation. **(a)** -■- PHD2 WT, -Δ- Y303F, -●- Y329F; **(b)** -■- PHD2 WT, -○-R383K, -□- D315E. **(c)** D315H, H313D, H374E, H374R, D315E R383K in comparison with WT PHD2. Conditions: 4 µM PHD2, 100 µM HIF-1α CODD 19-mer peptide, 50 µM Fe(II), 300 µM 2OG, 4 mM L-ascorbate in 50 mM Tris·HCl (pH 7.5) were incubated at 37 °C. Note: ~10 % background hydroxylation/oxidation was observed in the absence of enzyme. Figure and figure legend are adopted with permission from Tarhonskaya *et al.* Biochem. J. **463**, 363-372.

3.2.2. Fe(II) binding to PHD2 facial triad variants

To investigate Fe(II) binding to the PHD2 active site variants (H313D, D315H, D315E, H374E, H374R), non-denaturing ESI-MS (electrospay ionisation-mass spectrometry) studies were performed using an assay mixture of PHD2, Fe(II) and 2OG taken at equivalent concentrations. The results reveal that none of the facial triad variants (D315, H374 and H313) co-purified with Fe(II), in contrast to PHD2 WT [8], (**Figure 3.5, Figure 3.9**). Adding Fe(II) also did not lead to the detectable formation of PHD2.Fe(II) complex (**Figure 3.5**), thus rationalising the absence of activity observed with the D315, H374 and H313 variants as due to weak metal binding (except D315E, see below). This implies that PHD2, unlike several other 2OG oxygenases, requires both H residues and D residue for efficient Fe(II) coordination [14, 16]. 2OG binding to these variant enzymes was not observed, consistent with Fe(II) binding being required prior to 2OG binding for formation of PHD2.Fe(II).2OG complex [8] (**Figure 3.5a**).

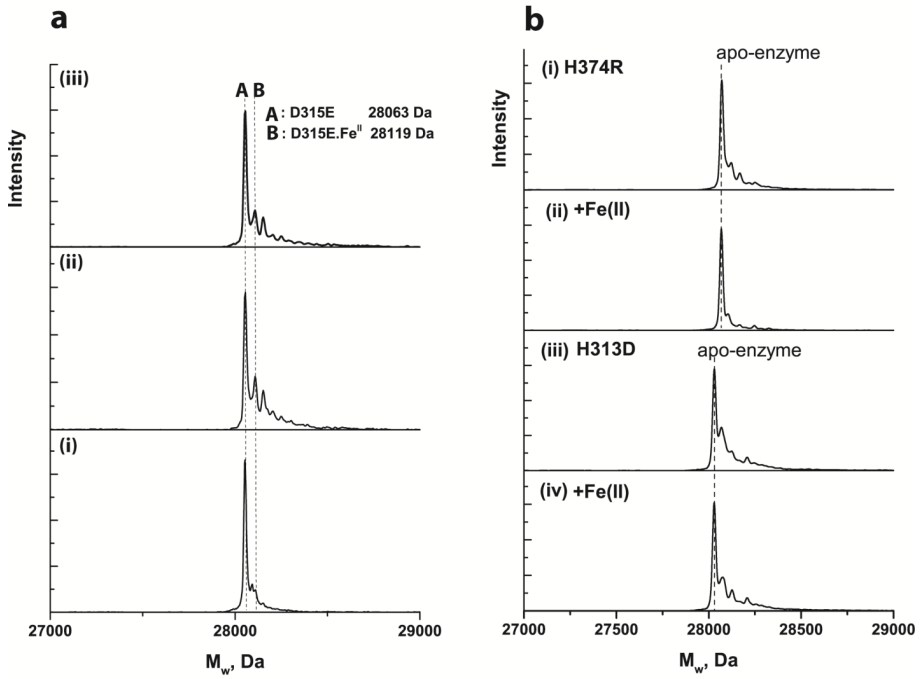


Figure 3.5. Non-denaturing ESI-MS of the PHD2 variants. (a) Deconvoluted ESI-MS spectra of D315E. The assay mixtures contained: (i) 15 µM D315E; (ii) 15 µM D315E with 15 µM Fe(II); (iii) 15 µM D315E, 15 µM Fe(II), 15 µM 2OG. **(b)** (i) 15 µM H374R, (ii) 15 µM H374R, 15 µM Fe(II), (iii) 15 µM H313D, (iv) 15 µM H313D, 15 µM Fe(II). Peaks: only apo-enzyme was observed (28072 for H374R, 28032 for H313D). Cone voltage: 60 V. Figure and figure legend are adopted with permission from Tarhonskaya *et al.* Biochem. J. **463**, 363-372.

Interestingly, substitution of D315 to E, results in a decrease in the stability of the PHD2.Fe(II) complex (**Figure 3.5a**), but does not significantly affect enzymatic activity (**Figure 3.4**). To further investigate the metal binding properties of D315E, NMR studies were performed using a paramagnetic water relaxation and ligand displacement technique· [17, 18], where Mn(II) was used as a substitute for Fe(II). The K_d for Mn(II) of D315E was found to be 243±30 μM, whereas that of WT was found to be 0.6±0.4 μM (**Figure 3.6**). This result further supports the proposal of weak metal binding to this variant and provides quantification of metal binding affinity.

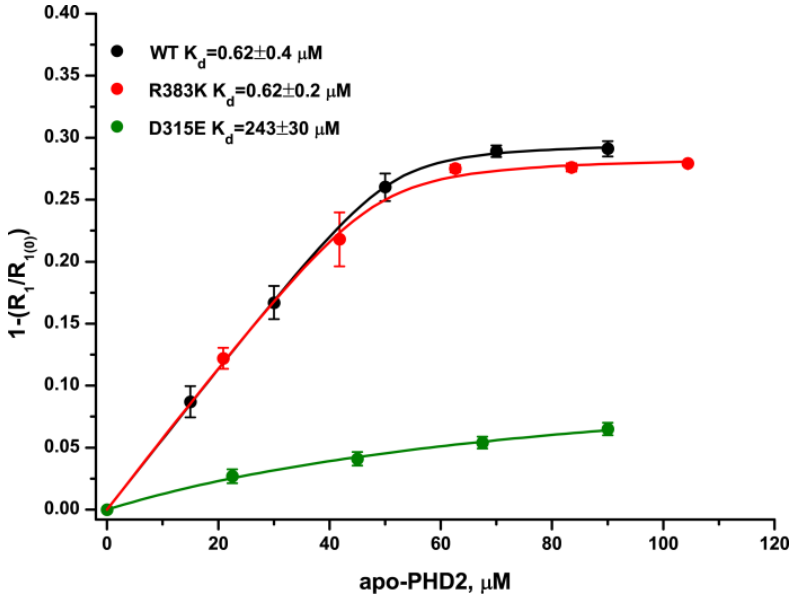


Figure 3.6. Binding of Mn(II) to apo-PHD2 as determined by NMR water relaxation technique. Samples contained 50 μM $MnCl_2$, 125 mM NaCl and 50 mM Tris-*d11* (pH 7.5) dissolved in 90 % H_2O and 10 % D_2O. The titratant stock solutions of *apo*-PHD2 (and its variants) were then titrated directly into the NMR tube. The error bars represent SD of triplicate assays.

Upon formation of an enzyme-(co-)substrate complex, 2OG oxygenases usually exhibit a weakly absorbing feature in the UV-vis range [19]. This feature can be observed for the PHD2.Fe(II).2OG complex under anaerobic conditions and represents metal ligand charge transfer (MLCT) transitions for Fe(II) and 2OG bound in a bidentate manner [5, 10]. The formation of MLCT features for D315E variant was also investigated (using UV-vis spectroscopy). An anaerobic PHD2.Fe(II).2OG complex formation, which usually appears as a broad feature at 500-530 nm [5] was not observed for the D315E variant (**Figure 3.7**). This

· NMR experiments were performed by Dr I. K. H. Leung (University of Oxford, Schofield group).

is consistent with an inability of this variant to form a stable PHD2.Fe(II).2OG complex under the standard conditions and/or suggests that the D315E variant may have altered Fe(II)-2OG coordination (**Figure 3.7**).

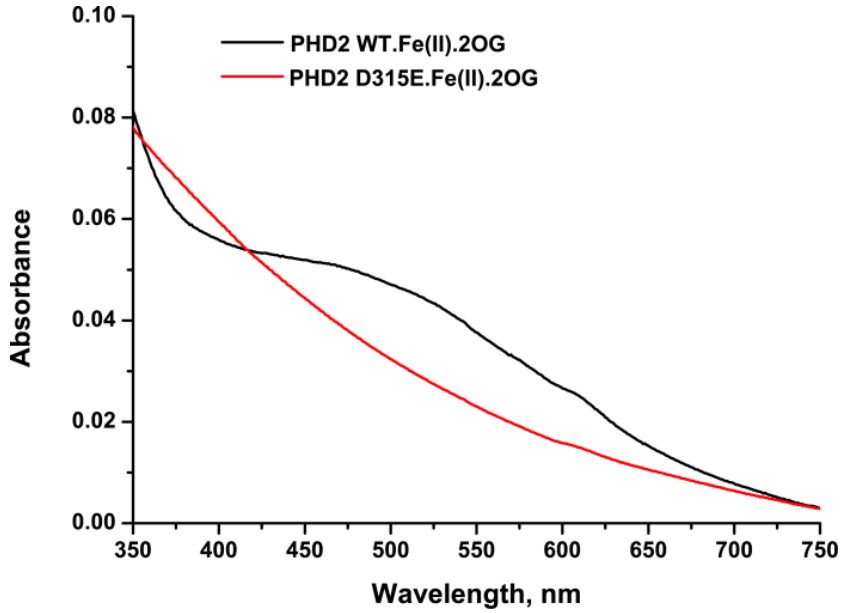


Figure 3.7. UV-vis spectroscopy of PHD2 D315E.Fe(II).2OG complex formation. The samples contained **(black trace)** 100 µM PHD2 wild-type, 120 µM Fe(II), 1 mM 2OG in 50 mM HEPES buffer (pH 7.5), **(red trace)** 100 µM PHD2 D315E, 120 µM Fe(II), 1 mM 2OG in 50 mM HEPES buffer (pH 7.5). All solutions were prepared anaerobically as previously described [1, 5]. Figure and figure legend are adopted with permission from Tarhonskaya *et al.* Biochem. J. **463**, 363-372.

To further investigate the influence of metal binding properties on the reaction, studies of the dependence of D315E PHD2 catalysis on Fe(II) concentration were carried out. The results revealed no difference compared to WT enzyme (saturation at ~10 µM Fe(II)), suggesting that Fe(II) binding is not limiting for CODD hydroxylation under steady-state conditions, when excess of Fe(II) is used (**Figure 3.8a)**. In addition to this, D315E dependence on L-ascorbate, which is known to stimulate activity of PHD2 *in vitro* (one of the proposed functions of L-ascorbate in 2OG oxygenase catalysis is maintenance of an Fe(II) pool in solution) [12], was studied. The D315E variant showed similar L-ascorbate dependence as was reported for WT PHD2 [12] (**Figure 3.8b**).

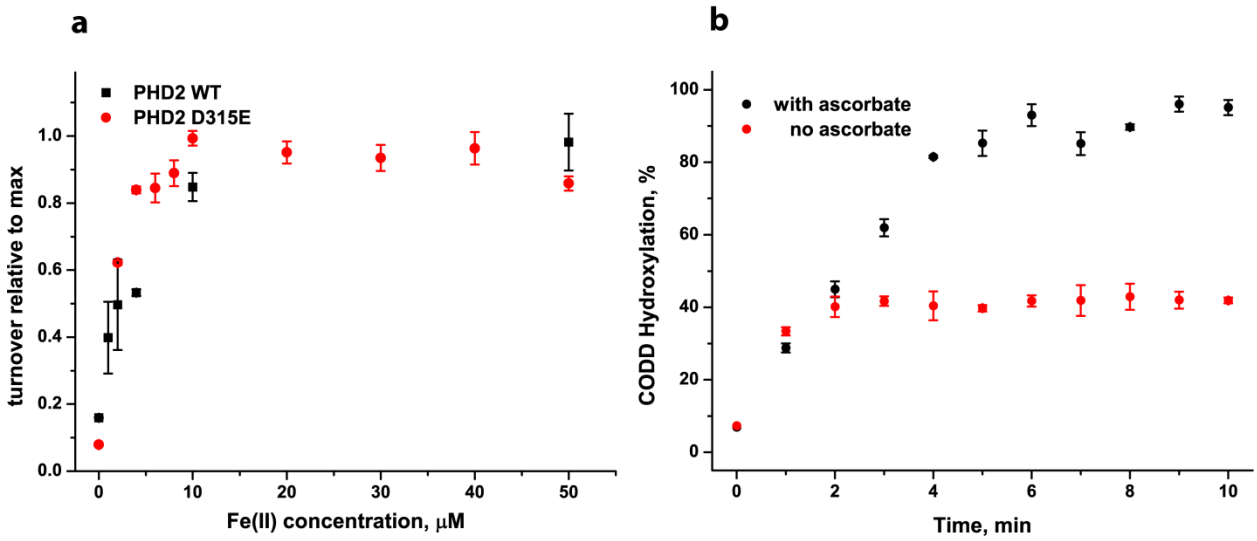


Figure 3.8. Fe(II) and L-ascorbate dependence of PHD2 D315E. (a) Fe(II) dependence. **(b)** PHD2 D315E-catalysed reaction in the presence (black circles) and absence of ascorbate (red circles). Conditions: 4 μM PHD2, 100 μM HIF-1α CODD 19-mer peptide, Fe(II) (varied), 300 μM 2OG, 4 mM L-ascorbate (if applicable) in 50 mM Tris·HCl (pH 7.5) were incubated at 37 °C. The error bars represent SD of triplicate assays.

3.2.3. Fe(II) and 2OG binding to PHD2 variants with altered co-substrate interactions

In contrast to the Fe(II)-binding variants, the 2OG-binding variants (R383K, Y303F, Y329F) showed a similar affinity for Fe(II) as WT (**Figure 3.9**) [8]. However, some alterations in 2OG binding were observed. Notably, non-denaturing ESI-MS studies showed a low affinity for 2OG to the R383K variant (a PHD2 R383K.Fe(II).2OG complex was not observed by ESI-MS, **Figure 3.9b**), while Y303F and Y329F variants bound 2OG with the same affinity as WT (**Figure 3.9c,d**).

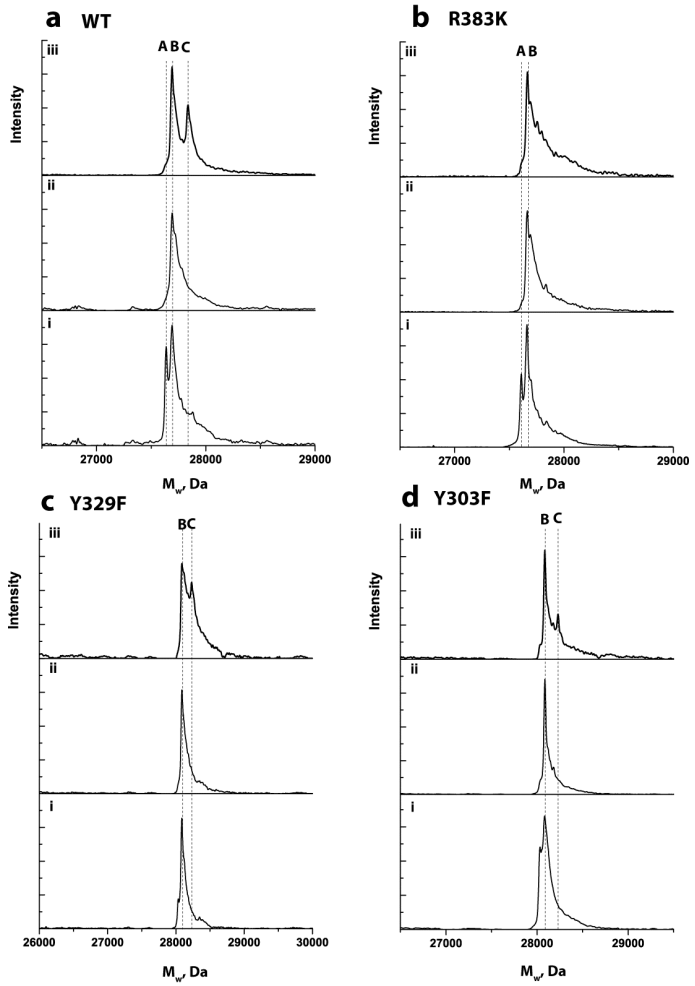


Figure 3.9. The PHD2 R383K variant has altered 2OG binding properties. Non-denaturing ESI-MS studies of Fe(II) and 2OG binding (deconvoluted spectra), **(a)** PHD2 WT, **(b)** R383K, **(c)** Y329F, **(d)** Y303F. The assay mixtures contained: **(i)** 15 μM enzyme; **(ii)** 15 μM enzyme with 15 μM Fe(II); **(iii)** 15 μM enzyme, 15 μM Fe(II), 15 μM 2OG. Cone voltage: 60 V. A – apo-PHD2, B – PHD2.Fe(II), C – PHD2.Fe(II).2OG. Figure and figure legend are adopted with permission from Tarhonskaya *et al.* Biochem. J. **463**, 363-372.

Determination of K_d(2OG) using UV-vis spectroscopy (measuring MLCT absorbance for the PHD2.Fe(II).2OG complex (λ_{max} vs 2OG concentration)) suggested that 2OG binds weakly to R383K compared to WT (K_d>100 μM for R383K, 5 μM for WT) [17] (**Figure 3.10**). Interestingly, for R383K 2OG binding depended on the presence of CODD (K_d(2OG) was 550±150 μM and 110±10 μM, in the absence and presence of CODD respectively, **Table 3.1**). This suggests possible conformational changes upon CODD binding and/or the importance of a substrate binding order. Although, it was shown that CODD indeed can bind to PHD2 in the absence of 2OG (see Chapter 6, **Figure 6.6**), CODD binding was not previously shown to

affect 2OG binding for WT PHD2 (K_d for 2OG was not dependent on the presence or absence of CODD for WT PHD2) [17]. The R383K K_d for Mn(II), as determined by NMR water relaxation studies, was the same as for WT (0.6±0.2 μM), consistent with non-denaturing ESI-MS (**Figure 3.6**). To quantify the change in 2OG affinity and to determine K_d for 2OG binding the NMR ligand displacement technique was employed [18]. 2OG binding to R383K was very weak and revealed dependence not only on the presence of CODD, but also on the nature of the metal (**Table 3.1**). Thus, it was shown that 2OG binds better to R383K in the presence of Zn(II), rather than Mn(II), which indicates different abilities of the metals to stabilise the complex with PHD2.

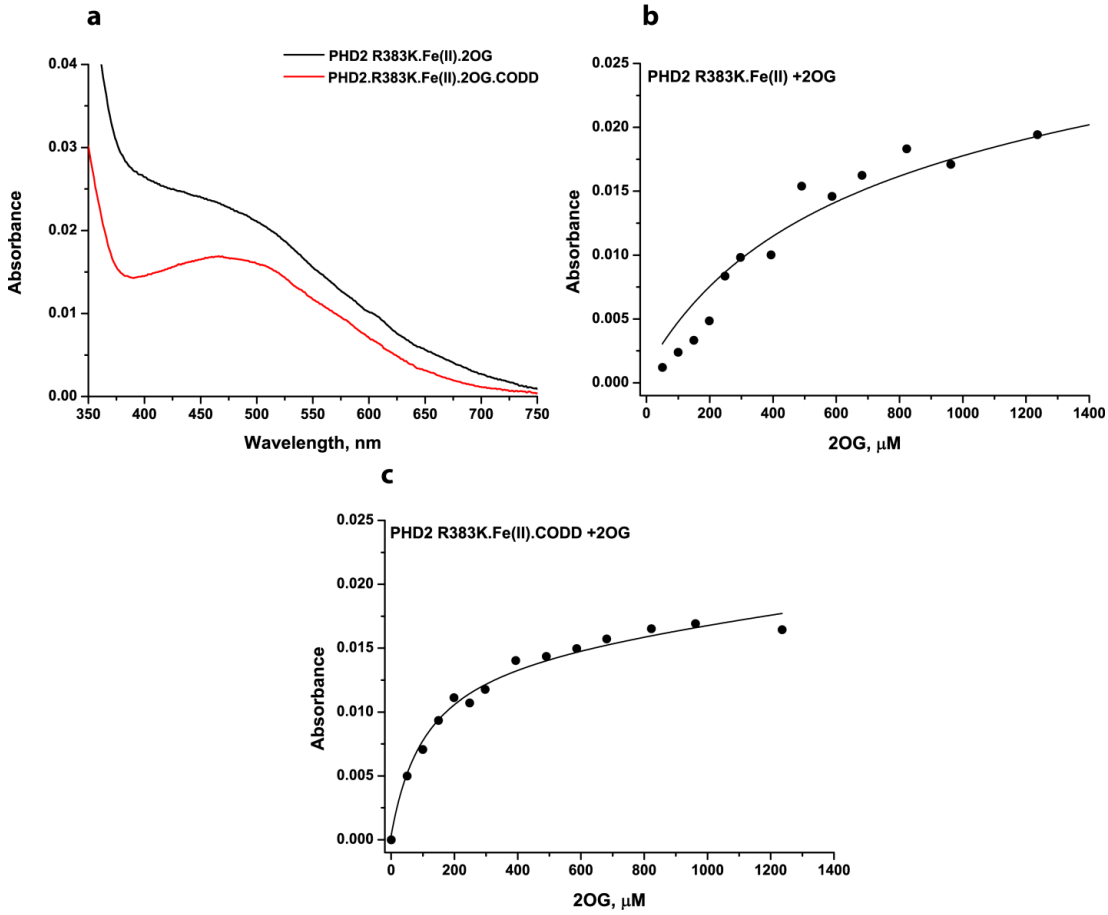


Figure 3.10. UV-vis spectroscopy studies of PHD2 R383K.Fe(II).2OG complex formation. The samples contained 100 μM PHD2 R383K, 120 μM Fe(II), 1 mM or varied 2OG, 125 μM CODD (where applicable) in 50 mM HEPES buffer (pH 7.5). All solutions were prepared anaerobically as previously described [1, 5]. **(a)** MLCT for R383K.Fe(II).2OG(+/- CODD) complexes; **(b)** R383K.Fe(II) titration with 2OG (absorbance at 520 nm); **(c)** R383K.Fe(II).CODD titration with 2OG (absorbance at 520 nm). Figure and figure legend are adopted with permission from Tarhonskaya *et al.* Biochem. J. **463**, 363-372.

Table 3.1. Binding parameters of the PHD2 variants. K_d(2OG) was determined either by analysis of a metal to ligand charge transfer feature of anaerobic PHD2.Fe(II).2OG complexes [1] or using NMR water relaxation/ligand displacement techniques [17, 18]. Table and table legend are adopted with permission from Tarhonskaya *et al.* Biochem. J. **463**, 363-372.

Complex	Ligand	K_d, μM	method
WT.Fe(II).2OG	2OG	5±3	UV-vis
R383K.Fe(II).2OG	2OG	550±150	UV-vis
R383K.Fe(II).2OG.CODD	2OG	105±5	UV-vis
WT.Mn(II).2OG	2OG	0.9±0.1	NMR [17]
R383K.Mn(II).2OG	2OG	>10000	NMR
R383K.Mn(II).2OG.CODD	2OG	430±30	NMR
R383K.Zn(II).2OG	2OG	110±20	NMR
R383K.Zn(II).2OG.CODD	2OG	<10	NMR
WT.Mn(II)	Mn(II)	0.6±0.4	NMR
R383K.Mn(II)	Mn(II)	0.6±0.2	NMR
D315E.Mn(II)	Mn(II)	240±30	NMR

3.2.4. NODD hydroxylation catalysed by PHD2 and its variants

The activity of the R383K, Y303F, Y329F and D315E variants in the reaction with NODD HIF-1α substrate was also tested. For D315E, in contrast to the reaction with CODD where it showed comparable to WT or higher activity, D315E catalysed NODD hydroxylation less efficiently (10 % after 15 min of the reaction, **Figure 3.11**). Interestingly, no activity was observed in the reaction with the R383K variant, while the Y303F and Y329F variants revealed the same level of changes as in the reaction with CODD. While for CODD the reaction was typically complete after 10 min, for NODD there was only 50 % hydroxylation after 15 min, suggesting slower turnover rates in the case of the latter. Thus, the difference in catalysis by PHD2 and its variants could be explained by the difference in NODD and CODD turnover rates or their different abilities to stabilise the enzyme-substrate complex (see UV-vis spectroscopy results for R383K, **Table 3.1**).

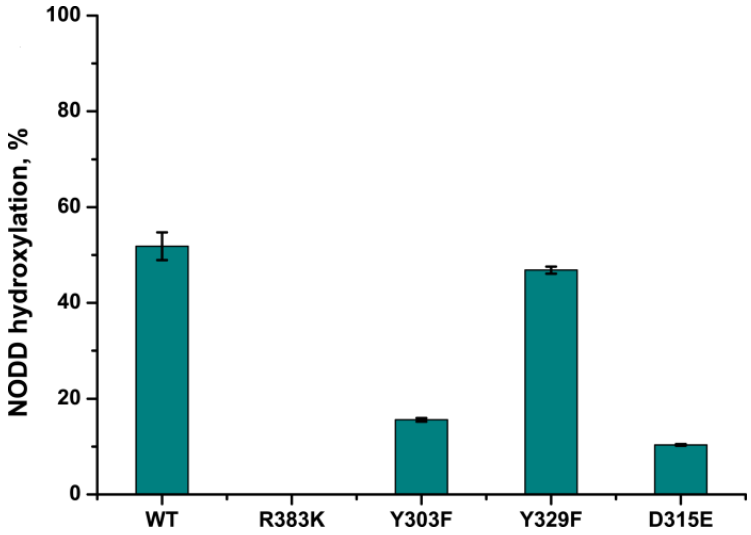


Figure 3.11. NODD hydroxylation catalysed by PHD2 and its variants. Conditions: 4 µM PHD2, 100 µM HIF-1α NODD 19-mer peptide, 50 µM Fe(II), 300 µM 2OG, 4 mM L-ascorbate in Tris·HCl 50 mM (pH 7.5) were incubated for 15 min at 37 °C and then analysed by MALDI-TOF-MS. The error bars represent SD of triplicate assays.

Due to the differences in the structure of Arg and Lys residues, the R383K mutation could result in reduced 2OG binding, as electrostatic interactions depend on the distance between charged functional groups. Therefore, 2OG analogues, such as 2-oxoadipate and oxaloacetate, were tested to investigate how the length of the C-chain in co-substrate affects the PHD2-catalysed reaction. The assay mixtures were incubated for 15 min with PHD2 under standard assay conditions (**Figure 3.12**). Oxaloacetate did not substitute for 2OG in the reaction of CODD/NODD hydroxylation, as assessed after 15 min of incubation with the enzyme at 37 °C. At the same time 2-oxoadipate acted as a co-substrate both for WT and R383K variant with no difference compared to 2OG (in the case of CODD hydroxylation) and consistent with a previous report [20]. This result suggests that oxaloacetate is likely not sufficiently coordinated by PHD2, while 2-oxoadipate still fits into the 2OG binding pocket.

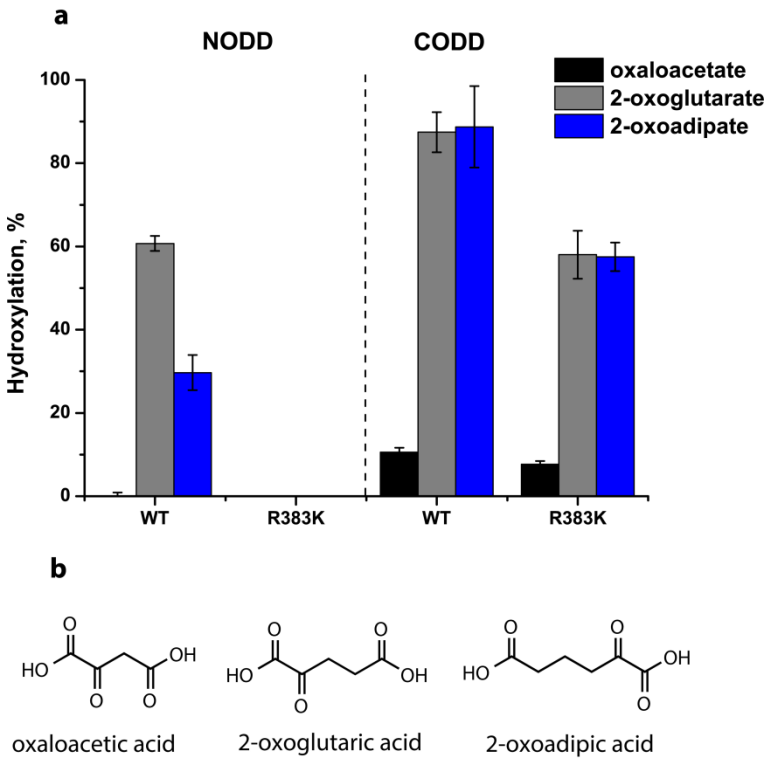


Figure 3.12. NODD/CODD hydroxylation catalysed by PHD2 and R383K using 2OG analogues as a co-substrate. (a) Comparison of the activities of PHD2 and its variants when 2OG analogues were used as a co-substrate. Conditions: 4 μM PHD2, 100 μM HIF-1α NODD or CODD 19-mer peptide, 50 μM Fe(II), 300 μM 2OG/oxaloacetate/2-oxoadipate, 4 mM L-ascorbate in 50 mM Tris·HCl (pH 7.5) were incubated for 15 min at 37 °C and then analysed by MALDI-TOF-MS. The ~7-10 % background in the reaction with CODD peptide is due to Met oxidation under the assay conditions. **(b)** Structures of the compounds used for the comparison.

3.2.5. CD spectroscopy and amino acid analysis·

To investigate whether R383K and D315E mutations introduce any changes to the overall folding of the enzyme and/or its stability, circular dichroism (CD) spectroscopy experiments were performed. CD spectroscopy showed no change in folding for the variants compared with WT PHD2. (**Figure 3.13a**). Thermostability of the R383K and D315E variants was also studied (**Figure 3.13b**). The determined T_m values were 44.1±0.1 °C (PHD2 WT), 44.9±0.2 °C (D315E), 46.0±0.2 °C (R383K), revealing no significant changes in the stability of the variants.

· The amino acid analyses were performed by Dr N. D. Loik (University of Oxford, Schofield group).

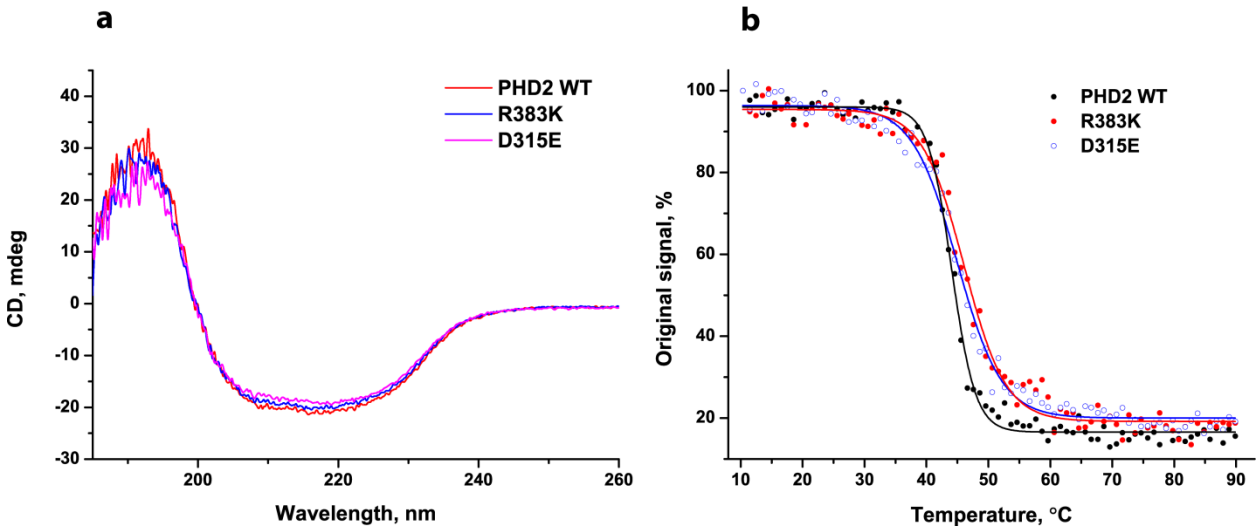


Figure 3.13. CD spectra and thermal stability of PHD2 and its variants. CD spectroscopy was used to analyse the folding and the thermal denaturation of PHD2 WT and its variants. **(a)** Far-UV CD spectra of PHD2 WT, R383K, D315E variants. The concentration of the proteins was 0.125 mg/mL in 5 mM sodium phosphate pH 8.0. Data represent the average of three independent scans. **(b)** Thermal denaturation of PHD2 WT and its variants (the ellipticity at 220 nm (θ_{220}) was monitored from 10 to 90 °C). Data are expressed as a % of the θ_{220} at 10 °C. Figure and figure legend are adopted with permission from Tarhonskaya *et al.* Biochem. J. **463**, 363-372.

To exclude the possibility that the observed modification of CODD peptide by D315E (+16 Da shift in MALDI-TOF-MS spectra) was caused by non-specific Met oxidation (performed by reactive oxidising species (ROS), which could be produced as a result of an incomplete reaction cycle due to altered coordination of the metal), amino acid analysis of the assay mixtures was performed. The results validated the product as *trans*-4-hydroxyproline (**Figure 3.14).** An attempt to combine the observed effects of both D315E and R383K substitutions by producing a double variant enzyme resulted in the ablation of PHD2 enzymatic activity (**Figure 3.4**).

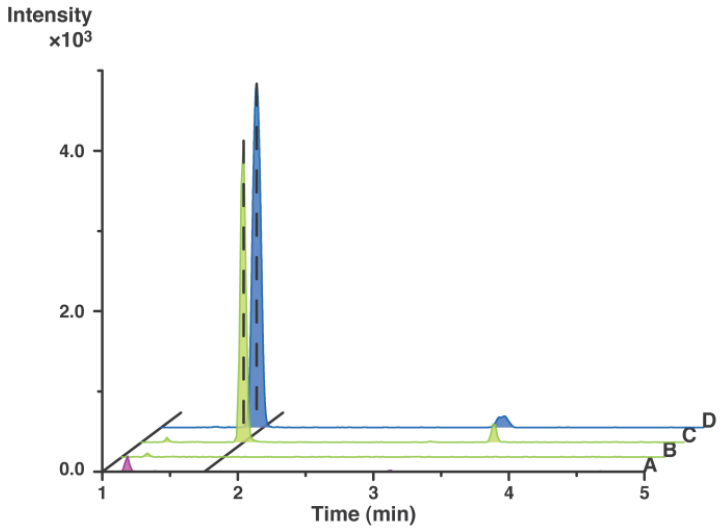


Figure 3.14. Amino acid analysis of the assay mixture of PHD2 D315E-catalysed CODD hydroxylation. Conditions: the assay mixture containing 4 µM PHD2, 50 µM Fe(II), 4 mM L-ascorbate, 100 µM CODD, 300 µM 2OG in 50 mM HEPES (pH 7.5) was incubated at 37 °C for 30 min and subsequently analysed for the presence of Pro-OH. **A.** PHD2 D315E, Fe(II), L-ascorbate; **B.** CODD, Fe(II), 2OG, L-ascorbate; **C.** PHD2 D315E, CODD, Fe(II), 2OG, L-ascorbate; **D.** a standard containing *trans*-4-hydroxyproline amino acid. The figure was provided by Dr N. D. Loik.

3.2.6. pH dependence of PHD2 and its variants

The importance of the deprotonation of the active site acid during PHD2 catalysis and pH dependence of the turnover has been previously reported [6]. To investigate a potential difference in the ability of the PHD2 variants for deprotonation, studies on the pH dependence of the activity of PHD2 and its variants in the reaction of CODD hydroxylation were carried out. No major difference in the trend of changes in activity versus pH was observed. This suggests that if deprotonation of an active site acid in PHD2 is one of the steps of PHD2-catalysis (as previously suggested [6]), the introduced substitutions either do not significantly affect the rate of this step or deprotonation is not rate-limiting for PHD2 turnover (**Figure 3.15**). A slight difference for the activity of the D315E variant compared with WT at high pH (9-10) likely reflects reduced Fe(II) binding by this variant, because free Fe(II) is prompted to oxidise rapidly in solution at high pH reducing the pool of Fe(II) available to maintain PHD2 activity.

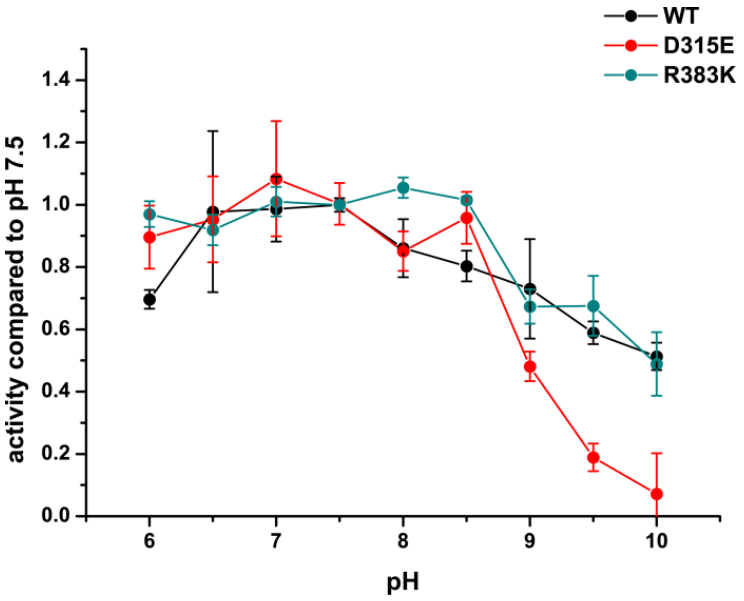


Figure 3.15. pH dependence of the PHD2-catalysed reaction. Conditions: 4 µM PHD2, 100 µM HIF-1α CODD 19-mer peptide, 50 µM Fe(II), 300 µM 2OG, 4 mM L-ascorbate in 50 mM buffer with different pH, incubated at 37 °C for 2 min, 1 min and 8 min for WT, D315E and R383K respectively, and then analysed by MALDI-TOF-MS.

3.2.7. Steady-state kinetics of the PHD2 variants

To investigate the effects of reduced Fe(II) and 2OG binding observed in the variants on their catalytic activity in more details, steady-state kinetic parameters of the D315E and R383K variants were determined. Despite the difference in the binding characteristics, major differences in the kinetic parameters were not observed. The determined R383K K_m(2OG) was ~3-fold higher compared to WT (45±10 µM and 13±2 µM, respectively, **Table 2**), consistent with the expected effects of the reduced 2OG binding. Consistent with the time course experiments, R383K also had a lower k_{cat} value than WT (**Figure 3.16**). D315E kinetic parameters were similar to those of WT PHD2, however k_{cat} for D315E variant was slightly higher compared to WT PHD2, again consistent with time course experiments. Other variant enzymes did not show any significant differences in steady-state kinetic parameters, except Y303F, which also had a higher K_m(2OG) and lower k_{cat} value. Determination of K_m(CODD) for the variants did not reveal any change compared to WT implying that the introduced substitutions do not interfere with CODD substrate binding (**Figure 3.17**).

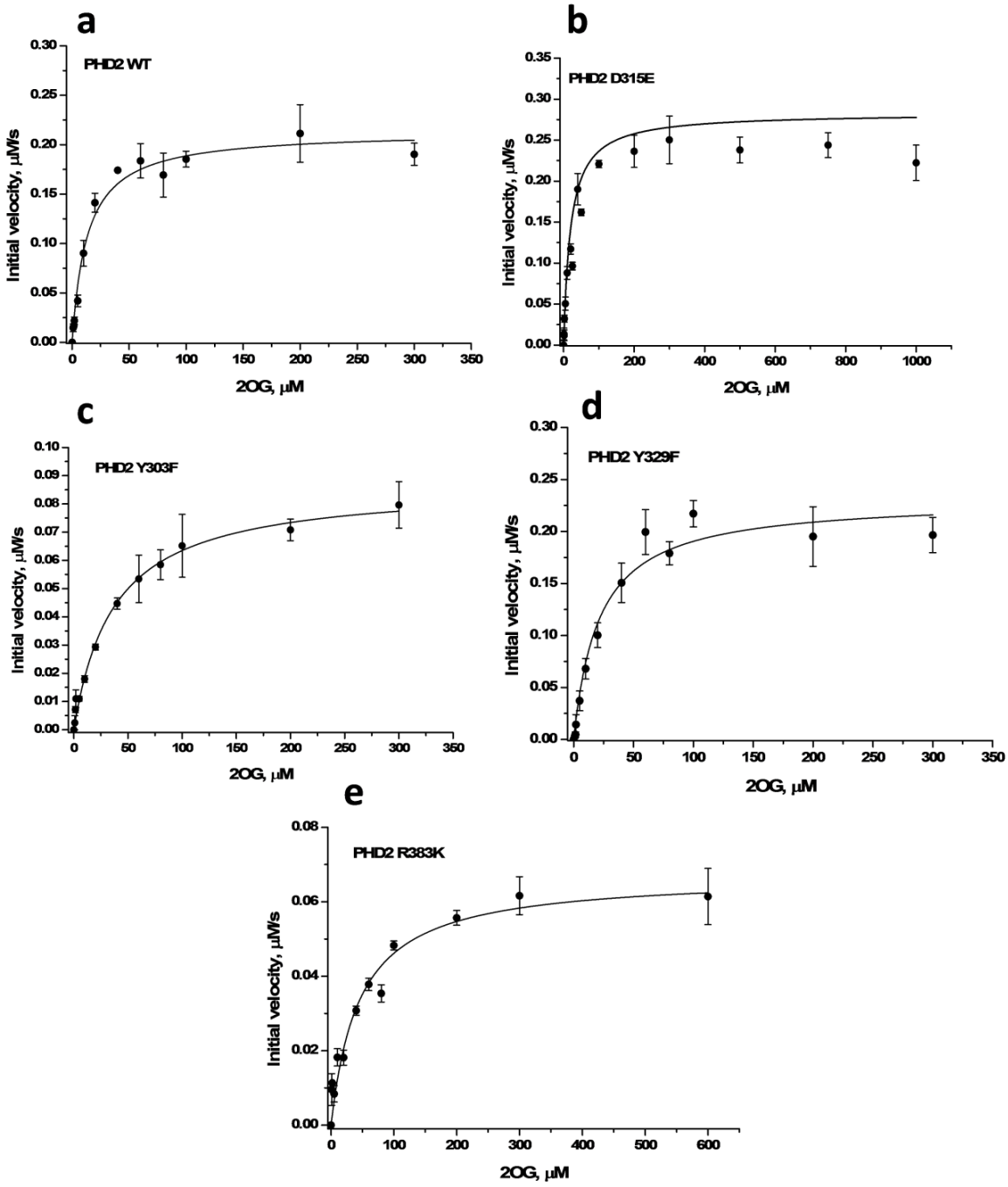


Figure 3.16. Determination of kinetic parameters of PHD2 and its variants (K_m(2OG)). (a) WT PHD2, **(b)** D315E, **(c)** Y303F, **(d)** Y329F, **(e)** R383K. Conditions: 4 µM PHD2, 100 µM CODD, 50 µM Fe(II), 4 mM L-ascorbate, various concentrations of 2OG. CODD hydroxylation was analysed by MALDI-TOF-MS, background Met oxidation (~8 %) was subtracted. Figure and figure legend are adopted with permission from Tarhonskaya *et al.* Biochem. J. **463**, 363-372.

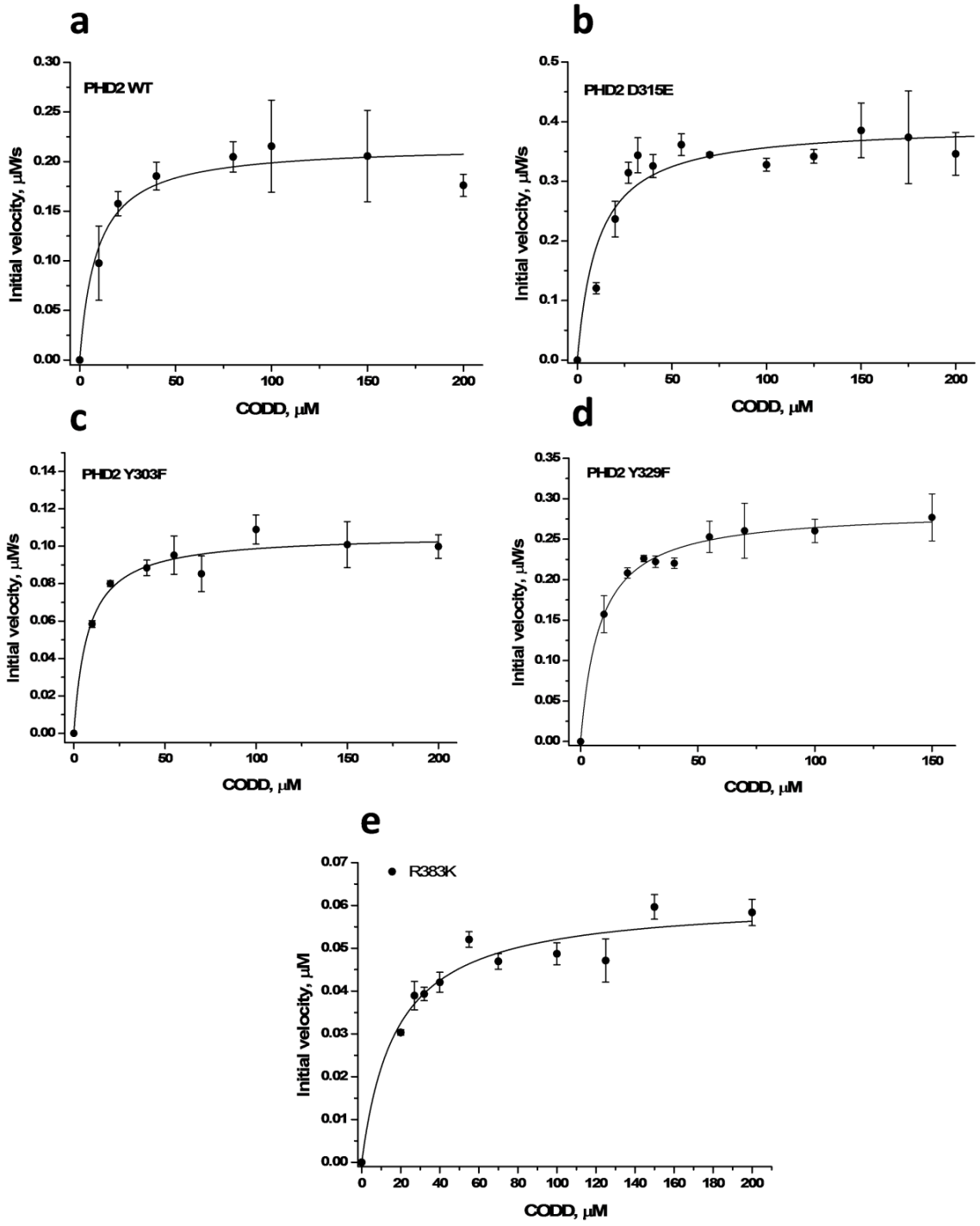


Figure 3.17. Determination of kinetic parameters of PHD2 and its variants (K_m(CODD)). (a) WT PHD2, **(b)** D315E, **(c)** Y303F, **(d)** Y329F, **(e)** R383K. Conditions: 4 µM PHD2, 50 µM Fe(II), 300 µM 2OG, 4 mM L-ascorbate, various concentrations of CODD. CODD hydroxylation was analysed by MALDI-TOF-MS, background Met oxidation (~8 %) was subtracted. Figure and figure legend are adopted with permission from Tarhonskaya *et al.* Biochem. J. **463**, 363-372.

Table 3.2. Steady-state kinetic parameters of the PHD2 variants. 4 µM PHD2, 50 µM Fe(II), 4 mM L-ascorbate, 2OG (varied) and HIF-1α CODD 19-mer peptide (varied) in Tris·HCl 50 mM (pH 7.5) were incubated at 37 °C. The initial rates of the reaction were determined by analysis of CODD hydroxylation levels using MALDI-TOF-MS. Table and table legend are adopted with permission from Tarhonskaya *et al.* Biochem. J. **463**, 363-372.

	K_m(2OG), µM	K_m(CODD), µM	k_{cat}^{app}, s^{-1}
WT	13±2	9±3	0.060±0.007
R383K	45±10	18±4	0.017±0.001
Y303F	37±4	8±2	0.027±0.001
Y329F	21±4	8±2	0.072±0.002
D315E	20±7	11±3	0.099±0.007

3.2.8. Steady-state oxygen dependence of the PHD2 variants

To study the O_2-dependence of the variant enzymes under steady-state conditions, assays were performed in a hypoxic workstation using buffer prior pre-equilibrated under different pO_2 (for 24 hours, 37 °C). All PHD2 variants showed a graded response to changes in O_2-concentrations, similar to WT PHD2, and consistent with the previously reported high K_m for O_2 for WT PHD2 [15]. These results suggest no major influence of alteration in Fe(II)/2OG binding affinities on steady-state O_2-dependence, at least in a physiologically relevant O_2-concentration range (0-20 %) (**Figure 3.18**).

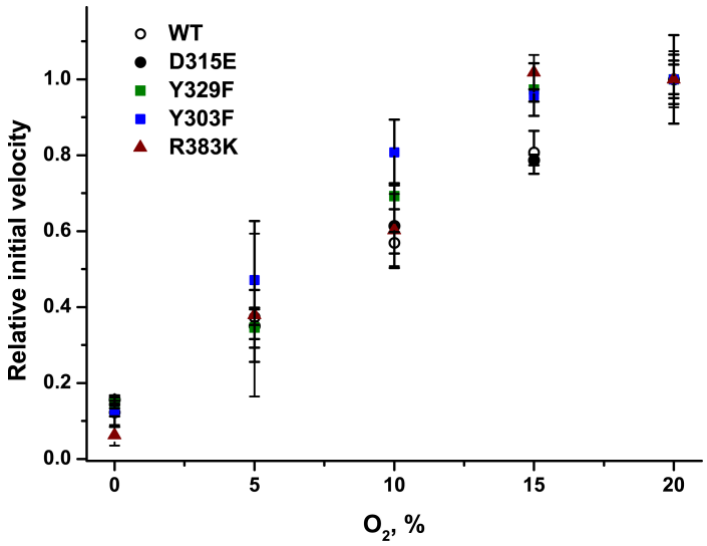


Figure 3.18. Steady-state oxygen dependence of PHD2 WT and its variants (up to 20 % O_2). Conditions: 4 μM PHD2, 100 μM HIF-1α CODD 19-mer peptide, 50 μM Fe(II), 300 μM 2OG, 4 mM L-ascorbate in 50 mM Tris·HCl (pH 7.5) were incubated at 37 °C in Hypoxia workstation under different pO_2. The different hydroxylation levels were analysed by MALDI-TOF-MS. The error bars represent SD of triplicate assays. The determined initial velocities were normalised to the initial velocity at 20 % O_2. Figure and figure legend are adopted with permission from Tarhonskaya *et al.* Biochem. J. **463**, 363-372.

Although there were no apparent differences in the steady-state rates of catalysis by PHD2 and its variants in the 0-20 % O_2 range, it was considered possible that the differences could be more evident by the determination of the initial rates at saturating O_2 concentrations. To further investigate the oxygen dependence of the R383K and D315E variants at oxygen concentrations higher than atmospheric (up to 80 % O_2), the assays were conducted in sealed glass vials, which were incubated under different O_2/N_2 gas mixes. The results (**Figure 3.19**) suggested that the K_m for O_2 in the case of the R383K variant is the same within error as for the WT PHD2 (>450 μM), while the D315E variant has a lower K_m of 200±30 μM. The latter observation suggests potential alteration in the reaction with oxygen for this variant rendering it potentially less sensitive to O_2 than WT.

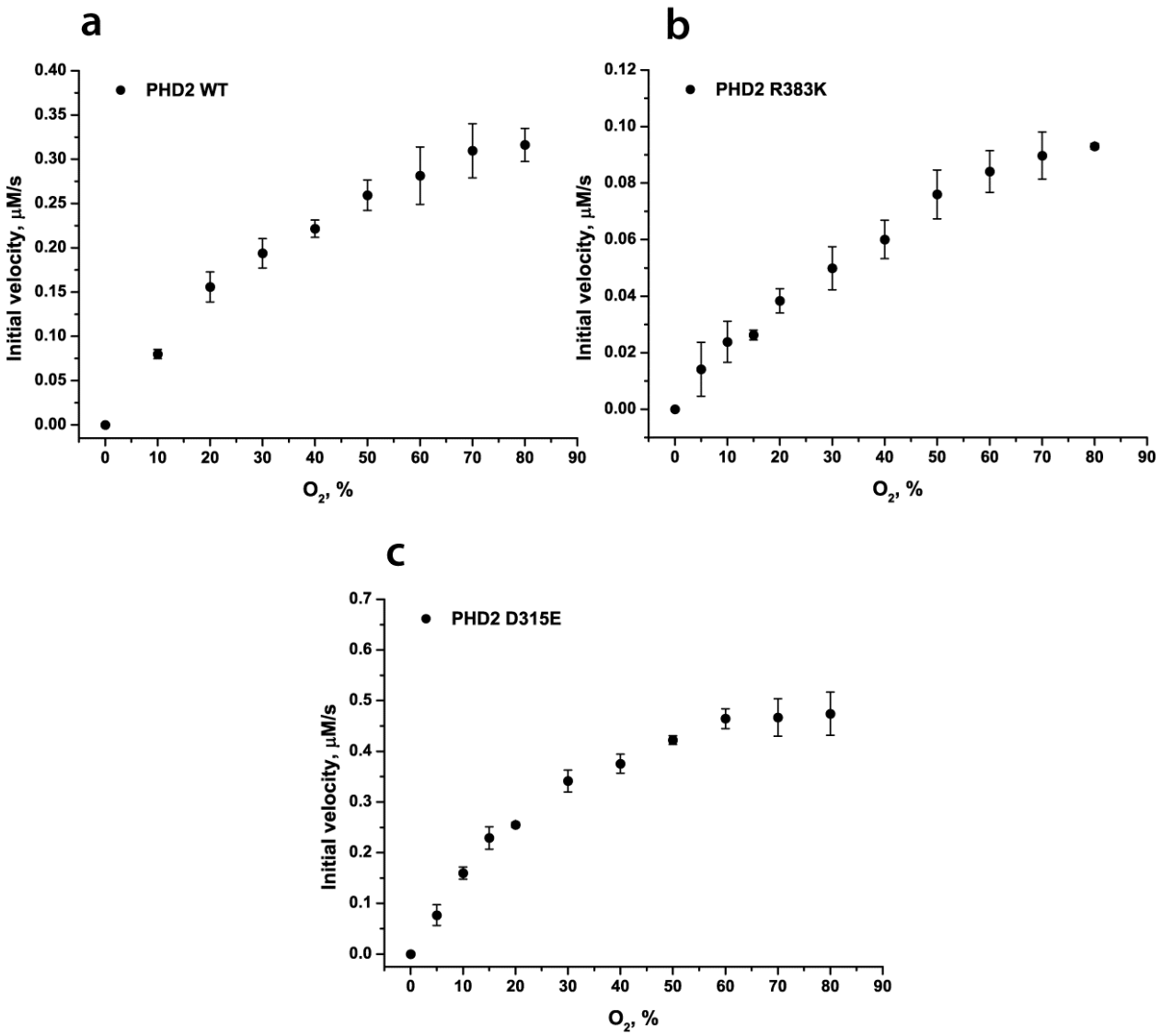


Figure 3.19. Steady-state oxygen dependence of PHD2 WT and the R383K, D315E variants (up to 80 % O_2). (a) WT PHD2, **(b)** R383K, **(c)** D315E. Conditions: 4 μM PHD2, 100 μM HIF-1α CODD 19-mer peptide, 50 μM Fe(II), 300 μM 2OG, 4 mM L-ascorbate in 50 mM HEPES (pH 7.5) were incubated at 37 °C in sealed glass vials under different pO_2. The different hydroxylation levels were analysed by MALDI-TOF-MS. The error bars represent SD of triplicate assays. Figure and figure legend are adopted with permission from Tarhonskaya *et al.* Biochem. J. **463**, 363-372.

The D315E and R383K variants demonstrate greatest differences compared to WT PHD2 in terms of Fe(II)/2OG binding, yet they remain active. To probe in more detail the effect of weakened Fe(II)/2OG binding on the catalytic step of O_2-activation, further kinetic characterisation was conducted using methods of rapid mixing to observe the pre-steady-state phase of the enzymatic catalysis.

3.2.9. Pre-steady-state kinetic studies on PHD2 and its variants

To investigate the pre-steady-state oxygen activation of R383K and D315E PHD2, as well as to determine rates of the consumption of the initial enzyme-substrate complex, stopped-flow UV-vis spectroscopy was employed. Upon mixing anaerobic PHD2.Fe(II).2OG.CODD complexes with O_2-saturated buffer, a transient species absorbing at 307-313 nm was apparent at the maximum time of accumulation of 320 s in the case of WT PHD2 (see Chapter 2). Accumulation of this transient species for R383K and D315E was faster giving maxima at 145 s and 90 s respectively (**Figure 3.19**). Attempts to fit these kinetic traces with a double exponential function describing formation and degradation of the putative intermediate resulted in a poor fit (except for WT) and increasing number of the exponential terms in the fitting function did not significantly improve the fit (**Figure 3.19**). Nonetheless, similar to WT PHD2, low pseudo-first order kinetic rate constants for degradation of the observed transient species (~10^{-4} s^{-1}) suggested that it does not belong to the catalytic pathway, and likely formed due to oxidation of bound or unbound Fe(II) to Fe(III), subsequently to product formation. Thus, consistent with previous report and studies on WT PHD2 (see Chapter 2), accumulation of an Fe(IV)-oxo intermediate on a catalytically relevant time scale for the variant enzymes was not observed [5].

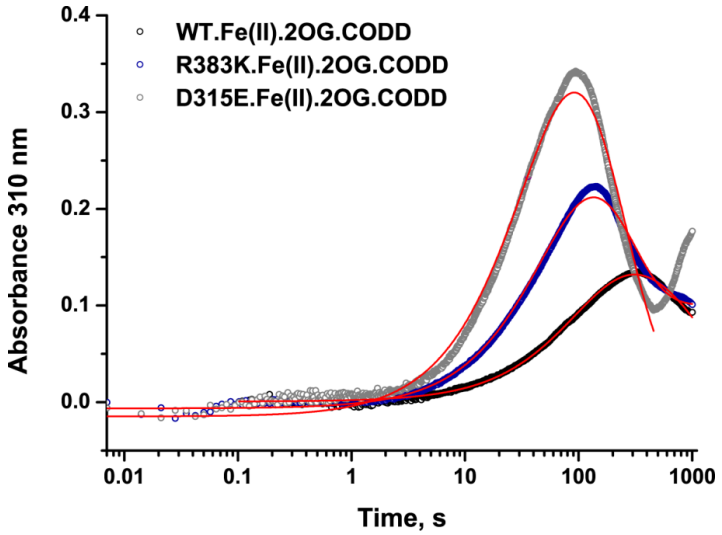


Figure 3.19. Stopped-flow kinetics of the reaction of PHD2 WT, R383K and D315E with oxygen. The reaction mixture in 50 mM HEPES (pH 7.5) containing 0.8 mM apo-PHD2, 0.5 mM Fe(II), 5 mM 2OG and 1 mM CODD was rapidly mixed with O_2-saturated buffer in a 1:1 ratio at 5 °C. Red traces represent fitting with a double exponential function.

Previous studies on other 2OG oxygenases indicated accumulation of another reaction intermediate, which was assigned as a high-spin Fe(II) complex with product(s) [1, 2]. The definitive feature for this intermediate was absorbance decay at 520 nm, where initial enzyme.Fe(II).2OG.substrate complex absorbs (MLCT feature), with the restoration of absorbance after completion of the reaction, as was observed for WT PHD2 (see Chapter 2). A similar absorbance minimum was also observed for the R383K variant (**Figure 3.20**). No change in absorbance at 520 nm was detected for D315E, which is consistent with the absence of an MLCT feature for this variant as shown by static UV-vis spectroscopy experiments (**Figure 3.20c, Figure 3.7**). There was no or little absorbance decay (accumulation of similar intermediate state) in the absence of CODD for both WT and R383K, which is consistent with 'substrate triggering' of O_2 activation of 2OG oxygenases [1-4]. The kinetic traces at 520 nm were fitted with a double-exponential function and determined rate constants (fitting parameters) are summarised in **Table 3.3**. Overall, the R383K variant showed faster absorbance decay than was observed for WT (rate constants: 0.833±0.003 s^{-1} and 0.046±0.001 s^{-1}, respectively, **Figure 3.20**) which suggests a faster oxygen activation for R383K at the initial phase of the catalysis.

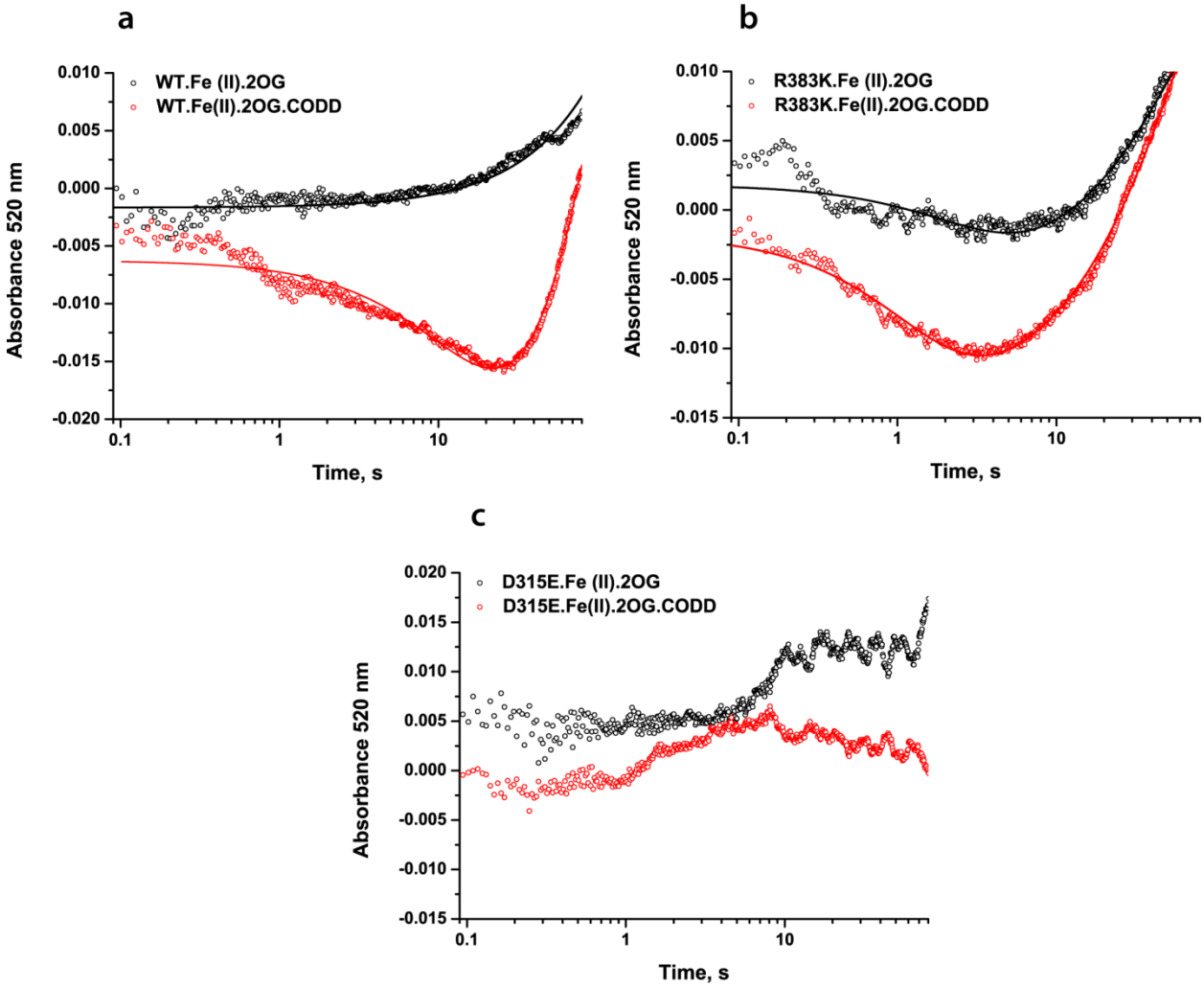


Figure 3.20. Stopped-flow kinetics of the reaction of PHD2 WT, R383K and D315E with oxygen. The reaction mixture in 50 mM HEPES (pH 7.5) containing 0.8 mM apo-PHD2, 0.5 mM Fe(II), 5 mM 2OG and 1 mM CODD was rapidly mixed with O_2-buffer in a 1:1 ratio at 5 °C. Difference spectra of the reaction: **(a)** PHD2 WT 520 nm absorbance, **(b)** R383K 520 nm absorbance, **(c)** D315E 520 nm absorbance. Figure and figure legend are adopted with permission from Tarhonskaya *et al.* Biochem. J. **463**, 363-372.

To validate the kinetics of the observed transient species and their positioning on the catalytic pathway in relation to CODD hydroxylation, rapid quench-flow experiments were performed. The reaction was initiated by mixing the PHD2.Fe(II).2OG.CODD complex with O_2-saturated buffer and was quenched at defined time points by 1 % CF_3COOH. The samples were analysed by MALDI-TOF-MS (hydroxylation) or LC-MS (succinate formation). The rate of CODD hydroxylation was significantly faster for the D315E variant (0.0484±0.006 s^{-1}) compared to WT (0.0095±0.0011 s^{-1}), while R383K did not show any alteration in the kinetics

of product accumulation (0.0120±0.0011 s^{-1}) (**Figure 3.21**). Notably, the determined kinetic rate constants of CODD-OH accumulation (**Table 3**) were comparable to the rate constants of the absorbance recovery for the initial enzyme-substrate complex (absorbance increase at 520 nm, **Figure 3.20**) and formation of the 310 nm absorbance species (**Figure 3.19**). Thus, disruption in the metal binding properties leads to almost 5-fold faster turnover rate of PHD2-catalysed O_2-triggered reaction, while weak interactions with 2OG do not result in a significant change of the overall turnover rates.

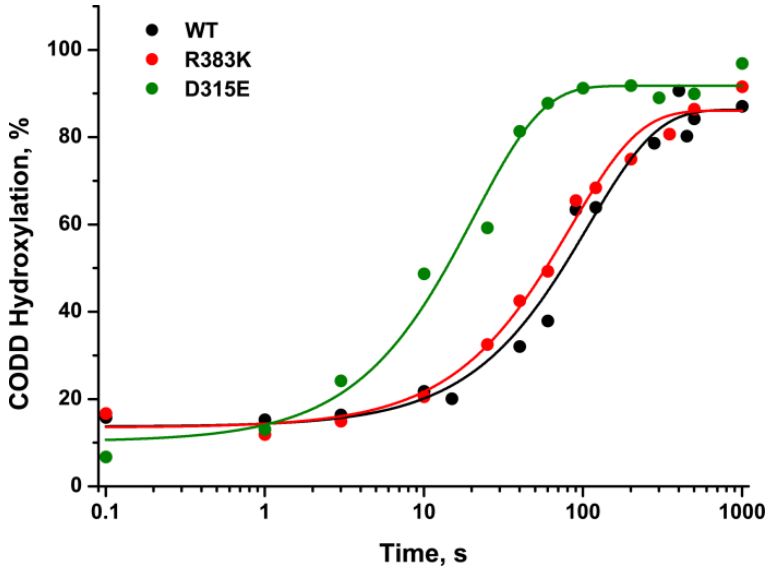


Figure 3.21. Rapid quench-flow studies on PHD2 and its variants. The reaction mixture in 50 mM HEPES (pH 7.5) containing 0.8 mM apo-PHD2, 0.5 mM Fe(II), 5 mM 2OG and 1 mM CODD was rapidly mixed with O_2-saturated buffer in 1:1 ratio at 5 °C and the reaction was quenched with 1 % CF_3COOH at defined time points. CODD hydroxylation was determined by MALDI-TOF-MS. Figure and figure legend are adopted with permission from Tarhonskaya *et al.* Biochem. J. **463**, 363-372.

Table 3.3 Pseudo-first order kinetic rate constants of PHD2-catalysed CODD hydroxylation. The reaction mixture in 50 mM HEPES (pH 7.5) containing 0.8 mM apo-PHD2, 0.5 mM Fe(II), 5 mM 2OG and 1 mM CODD was rapidly mixed with O_2-saturated buffer in a 1:1 ratio at 5 °C. The fitting parameters were obtained using a 2-exponential (for stopped-flow experiments) or a single exponential function (rapid quench-flow experiments). ND – not determined. Table and table legend are adopted with permission from Tarhonskaya *et al.* Biochem. J. **463**, 363-372.

Complex	Stopped-flow, 520 nm		Rapid quench-flow	
	$k_{fall\ phase}$, s^{-1}	$k_{rise\ phase}$, s^{-1}	$k_{hydroxylation}$, s^{-1}	$k_{succinate}$, s^{-1}
WT.Fe(II).2OG.CODD	0.046±0.001	0.0083±0.0060	0.0095±0.0011	0.0064±0.0046
R383K.Fe(II).2OG.CODD	0.833±0.003	0.0165±0.0010	0.0120±0.0011	0.0072±0.0020
D315E.Fe(II).2OG.CODD	ND	ND	0.0484±0.006	0.0472±0.006

Comparison of the stopped-flow and rapid quench-flow results (absorbance decay at 520 nm and product accumulation) revealed that 520 nm intermediate species are likely analogous to those previously observed for other 2OG oxygenases [1, 2] and formed on a catalytically relevant time scale (**Figure 3.22**).

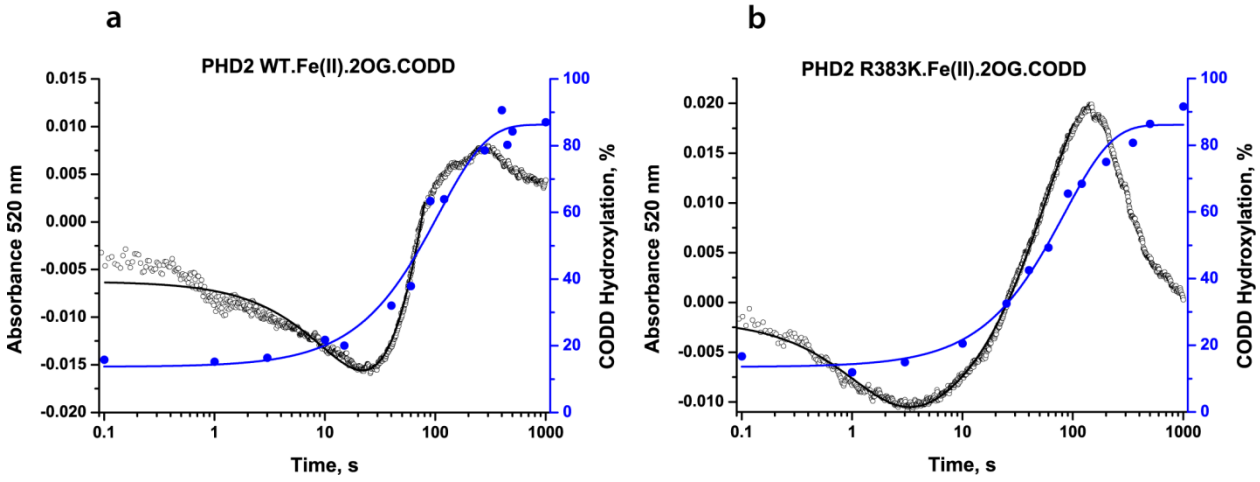


Figure 3.22. Comparison of rapid quench-flow and stopped-flow studies on PHD2 WT and R383K variant. The reaction mixture in 50 mM HEPES (pH 7.5) containing 0.8 mM apo-PHD2, 0.5 mM Fe(II), 5 mM 2OG and 1 mM CODD was rapidly mixed with O_2-saturated buffer in 1:1 ratio at 5 °C and the reaction either quenched with 1 % CF_3COOH after defined time points or observed using a photodiode detector. CODD hydroxylation was determined by MALDI-TOF-MS and compared to changes in absorbance at 520 nm. **(a)** WT, **(b)** R383K.

Previous reports have indicated tight coupling for the PHD2-catalysed CODD hydroxylation and very slow rates of uncoupled 2OG turnover in the absence of a 'prime' substrate [5, 19]. A change in the co-substrate binding affinity (and potentially binding mode) could affect coupling of the catalysed reaction. The rate of succinate formation in the rapid quench-flow experiments was therefore determined using LC-MS. The hydroxylation of CODD was tightly coupled to 2OG oxidation for both R383K and D315E variants (**Figure 3.23**).

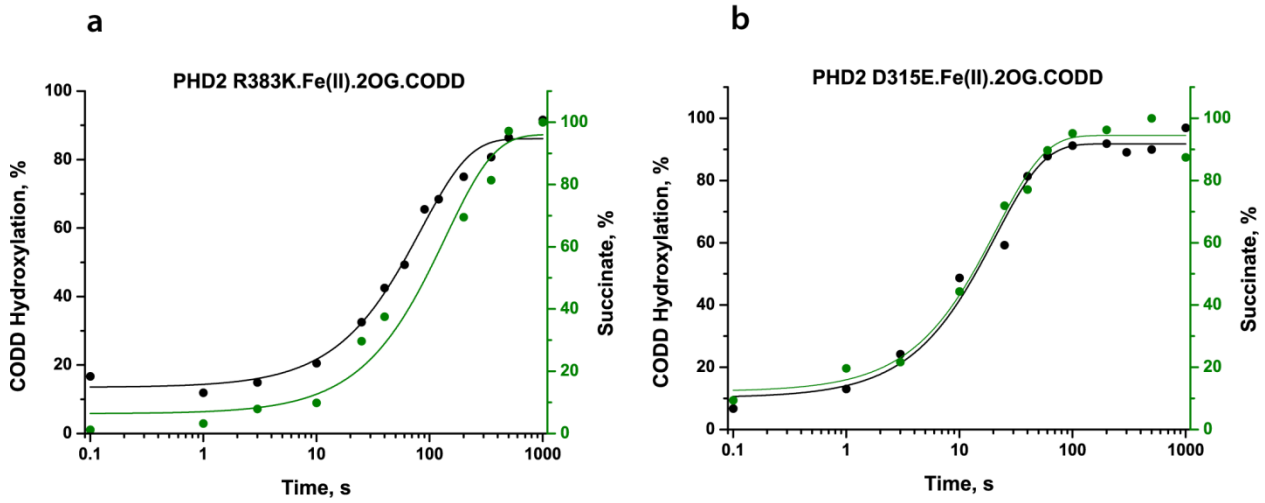


Figure 3.23. Rapid quench-flow studies on the coupling of the turnover of PHD2 and its variants. The reaction mixture in 50 mM HEPES (pH 7.5) containing 0.8 mM apo-PHD2, 0.5 mM Fe(II), 5 mM 2OG and 1 mM CODD was rapidly mixed with O_2-saturated buffer in 1:1 ratio at 5 °C and the reaction was quenched with 1 % CF_3COOH after defined time points. CODD hydroxylation was determined by MALDI-TOF-MS, succinate formation was analysed by LC-MS. Figure and figure legend are adopted with permission from Tarhonskaya *et al.* Biochem. J. **463**, 363-372.

To investigate rates of 2OG oxidative decarboxylation (uncoupled turnover) in the absence of CODD peptide, similar rapid quench-flow experiments were performed. The R383K variant showed little increase in succinate levels during 1000 s period, indicating very slow uncoupled turnover rates (**Figure 3.24**). On the contrary, the D315E variant showed a high rate of uncoupled 2OG oxidation with a rate constant for succinate formation comparable to that in the hydroxylation reaction (0.0472±0.006 s^{-1} and 0.0488±0.0126 s^{-1}, with and without CODD respectively) revealing that presence of substrate does not affect rates of 2OG turnover for this variant. This result, where substrate binding does not trigger faster O_2-activation, suggests that the introduced substitution disrupts the proposed requirement for substrate binding prior to

metal bound water molecule departure (which was proposed to precede a rate-limiting step based on SIE experiments) [6] and consequently promotes faster O_2-activation.

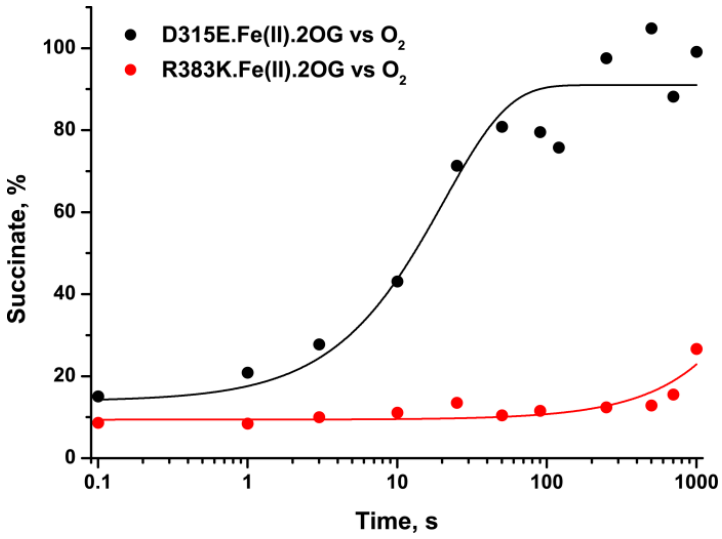


Figure 3.24. Rapid quench-flow studies on uncoupled turnover of PHD2 variants. The reaction mixture in 50 mM HEPES (pH 7.5) containing 0.8 mM apo-PHD2, 0.5 mM Fe(II), 5 mM 2OG was rapidly mixed with O_2-saturated buffer in 1:1 ratio at 5 °C and the reaction was quenched with 1 % CF_3COOH after defined time points. Succinate formation was analysed by LC-MS. Figure and figure legend are adopted with permission from Tarhonskaya *et al.* Biochem. J. **463**, 363-372.

3.2.10. Crystallographic analysis of the D315E variant·

To obtain more information on Fe(II) and 2OG binding to the PHD2 variants, crystallographic experiments were carried out. A crystal structure of the D315E variant in complex with Mn(II) and a bicyclic isoquinolinyl (IOX3 or FG-2216), which is a known 2OG competitor for various 2OG oxygenases [21-23] (substituting Fe(II) and 2OG) was obtained. The structure reveals a similar overall fold to that of WT PHD2 [21] (Cα rmsd: 0.33 Å); however, a E in place of D315 causes local changes in residues (303-323) between DSBH βII and βIII (**Figure 3.25**). Thus, the apparent weaker metal binding properties observed for D315E variant could be due to the increased flexibility of this part of PHD2 structure. Notably, two conformations for the E315 side chain were observed (with 40 % and 60 % occupancy) which could add further flexibility contributing to the weakened metal binding (**Figures 3.25**). The attempts to obtain a crystal structure for the R383K variant were not successful due to poor diffraction quality.

· The crystallography experiments, as well as the analyses of the crystallography data, were performed by Dr R. Chowdhury (University of Oxford, Schofield group).

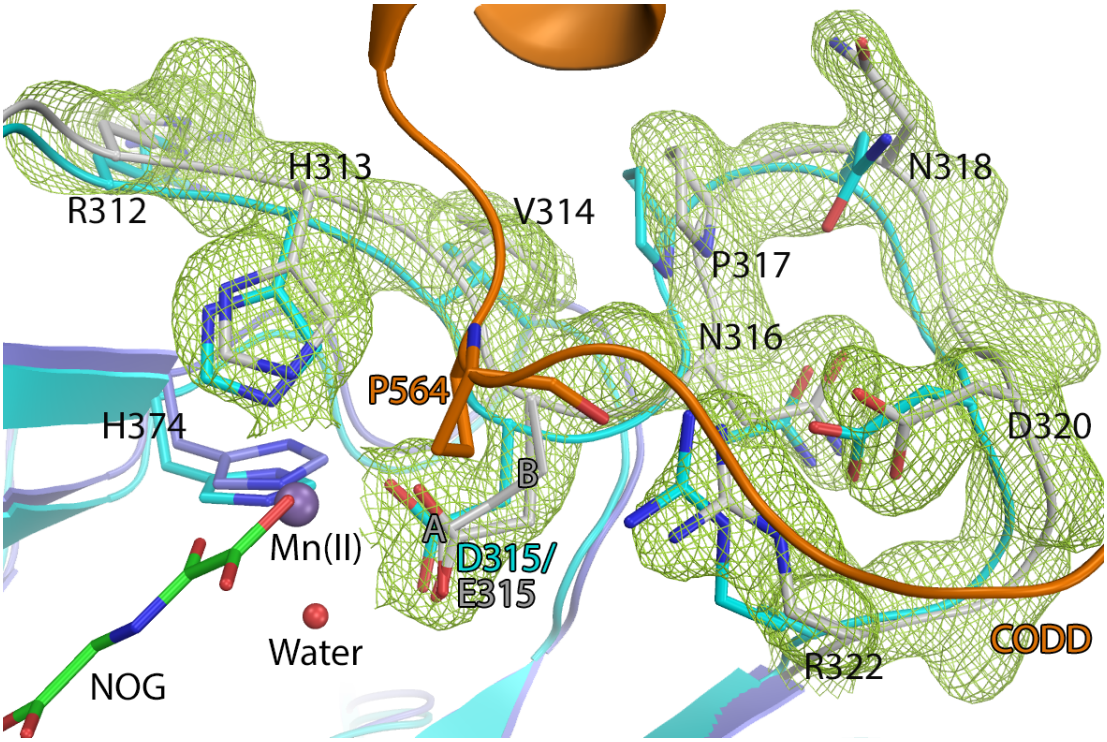


Figure 3.25. Overlay of active site views from structures of PHD2 complexed with CODD (PDB: 3HQR, cyan) and the D315E variant (4UWD, blue). The figure highlights conformational changes in the Cα-backbones and side chain orientations of the residues (303-323, grey) located between DSBH βI and βIII. Two conformations are observed for the E315 side chain. Note that the DSBH βII that contains two of the Fe(II) coordinating residues H313 and D315, do not maintain antiparallel hydrogen-bond pairing between βII and βVII (as also observed in other 2OG oxygenases) even though the ϕ/ψ angles (βII) are within the β-region of the Ramachandran plot. The figure was provided by Dr R. Chowdhury. Figure and figure legend are adopted with permission from Tarhonskaya *et al.* Biochem. J. **463**, 363-372.

Table 3.4. Crystallographic data processing and refinement statistics.

Data Collection	
Space Group	$P6_3$
Cell dimensions a,b,c (Å)	110.52
	110.52
	39.38
Resolution (Å)	47.86 – 1.72 (1.77-1.72)*
No. of unique reflections	29428 (2143)*
Completeness (%)	99.9 (99.9)*
Redundancy	6.6 (6.9)*
R_{sym}**	0.042 (0.670)*
Mean I/σ(I)	20.4 (3.0)*
Refinement	
R_{factor}	0.150
R_{free}	0.174
R.m.s. deviation	
Bond length, Å	0.009
Bond angle, °	1.2

*Highest resolution shell shown in parenthesis.

**$R_{sym} = \sum|I-\langle I\rangle|/\sum I$, where I is the intensity of an individual measurement and $\langle I\rangle$ is the average intensity from multiple observations.

3.3. Discussion

PHD2 has been found to form a very stable complex with Fe(II) and 2OG, which was a characteristic feature for this enzyme and proposed to be important for a tight coupling between HIF-α hydroxylation and 2OG oxidative carboxylation [8]. PHD2 was also shown to undergo an unusually slow activation by oxygen in pre-steady-state kinetic experiments, including in the presence of a 'prime' substrate (CODD HIF-1α) [5]. Furthermore, structural studies indicate unfavorable 2OG positioning in relation to the active site Fe(II) with respect to 'prime' substrate oxidation, possibly complicating oxygen binding [7]. Here it is postulated that these phenomena may be related, and the slow kinetics of PHD2 in its reaction with oxygen are determined by its structural features. Therefore, to probe the molecular features of PHD2.Fe(II).2OG complex formation and their importance in the reaction with O_2, substitutions were introduced to the PHD2 active site in order to obtain variants active in the catalysis of HIF-1α hydroxylation, but differing by their 2OG/Fe(II) binding properties compared to the WT enzyme. Two of the designed variants, D315E and R383K, showed significantly reduced Fe(II) and 2OG binding, respectively, which was reflected in determined binding constants and steady-state kinetics.

According to the PHD2.Mn(II).NOG.CODD crystal structure [7], 2OG binding rearrangements during catalysis can be important and even limit kinetics of PHD2 turnover. Non-denaturing ESI-MS, UV-vis spectroscopy and NMR ligand displacement studies revealed that unlike WT PHD2, 2OG binding for the R383K variant is weak, unless in the presence of the 'prime' substrate. Thus, substitution of the conserved Arg residue forming electrostatic interactions with 2OG significantly influences 2OG binding characteristics, suggesting the structure of the PHD2 active site is adjusted for efficient co-substrate binding.

The influence of 2OG binding affinity to PHD2 on its reaction with oxygen was studied. Although, a faster rate of O_2-activation for R383K variant in stopped-flow experiments was observed compared to WT, significant changes in the kinetics of product accumulation for this variant were not detected under pre-steady-state conditions (including uncoupled turnover), indicating that 2OG binding is not a rate-limiting step in PHD2 catalysis. Structural rationalisation was not possible, as the R383K variant did not form crystals with sufficient diffraction for X-ray structure determination.

In 2OG oxygenases the iron ion is coordinated by a conserved HXD/E…H motif [14]. However, the 2OG-halogenases, e.g. SyrB2, utilise only two H residues [16]. Interestingly, for FIH, another HIF hydroxylase, it has been shown that mutation of the D to G in the FIH iron binding motif does not ablate enzymatic activity [11]. The results described in this Chapter demonstrate that in the case of PHD2, both H residues and one D/E residue are required to ensure effective Fe(II) binding, and unlike for other 2OG oxygenases, disruption to the facial triad-metal interactions can result in full loss of the enzymatic activity. The exception is D315E variant, where weak iron binding does not ablate the enzymatic activity. This result is in agreement with the previously reported loss of PHD2 function caused by a H374R mutation found in patients with erythrocytosis and recurrent paraganglioma [24].

Substitution of D315 to E leads to significantly reduced metal binding, but not to loss of PHD2 enzymatic activity with respect to CODD hydroxylation. This could imply that Fe(II) binding is not limiting for the reaction under the steady-state conditions, when saturating concentrations of Fe(II) are used and/or higher turnover rates of D315E variant make up for sufficient catalysis, even if the content of D315E.Fe(II).2OG complex is significantly lower compared to that for WT PHD2. A crystal structure of D315E variant reveals that the presence of a Glu residue in this position causes local changes in residues (303-323) between DSBH-II and -III (**Figure 3.25**). Thus, the mutation causes an overall increase in the flexibility of the PHD2 structure, which could explain the apparent D315E weaker metal binding properties. However, the origin of the observed effects on the O_2 activation rates could also be mechanistic.

Pre-steady-state kinetic studies on several 2OG oxygenases, which allow observation of the catalytic events on a single turnover scale, have shown that these enzymes are characterised by fast O_2 activation, which is faster in the presence of a 'prime' substrate than in uncoupled turnover ('substrate triggering') [1-4, 25]. This can be rationalised by the necessity to prevent uncoupled 2OG oxidation, which could cause accumulation of succinate and reactive oxidising species in cells [19, 26]. From the perspective of the 2OG oxygenase mechanism, it has been proposed that binding of a 'prime' substrate triggers a weakening of the bond between the Fe(II) and the coordinated H_2O, and therefore shift from iron six- to five-coordinate state [10], thus facilitating release of the water molecule and binding of O_2. As suggested by crystallographic analyses, in PHD2 metal coordinated water molecule is

stabilised by a hydrogen bond with D315, which may be one of the reasons for PHD2 low affinity to O_2 and its slow O_2 activation. Interestingly, mutation of the facial triad D315 to E leads to loss of 'substrate triggering', thus the rate of succinate formation triggered by O_2-activation in the coupled and uncoupled reaction is the same. This would imply an interference of the introduced substitution/weak metal binding with a rate-limiting step of the catalytic cycle preceding the reaction with O_2. Previously, it has been suggested that release of the metal coordinated H_2O should precede the rate-limiting event of the PHD2 catalysis [6]. Thus, structural flexibility in the Fe(II) coordinating environment of D315E variant or loss of sufficient stabilisation of the Fe(II)-bound water molecule due to alteration of the positioning of the E carboxylate group would explain the faster O_2-activation seen for this variant.

Overall, the results suggest that the active site of PHD2 is particularly adapted for tight Fe(II) and 2OG binding, and it has less tolerance than other 2OG oxygenases to conservative (and non-conservative) active site variations. PHD2 is proposed to be the most important of the HIF hydroxylases. Thus, it can be suggested that its active site is especially finely tuned for its physiological O_2-sensing role. The fact that the substitution of the iron binding D to E, although accelerating O_2 activation by a factor of 5, did not increase the rate of O_2-activation to that seen in many other 2OG oxygenases, suggests that there are multiple (structural) features of the PHD2 which collectively contribute to its slow kinetics of O_2 activation.

3.4. References

1. Price, J.C., E.W. Barr, B. Tirupati, J.M. Bollinger, and C. Krebs (2003) *The First Direct Characterization of a High-Valent Iron Intermediate in the Reaction of an α-Ketoglutarate-Dependent Dioxygenase: A High-Spin Fe(IV) Complex in Taurine/α-Ketoglutarate Dioxygenase (TauD) from Escherichia coli.* Biochemistry **42**, 7497-7508.
2. Hoffart, L.M., E.W. Barr, R.B. Guyer, J.M. Bollinger, and C. Krebs (2006) *Direct spectroscopic detection of a C-H-cleaving high-spin Fe(IV) complex in a prolyl-4-hydroxylase.* Proc. Natl. Acad. Sci. U. S. A. **103**, 14738-14743.
3. Galonić, D.P., E.W. Barr, C.T. Walsh, J.M. Bollinger, and C. Krebs (2007) *Two interconverting Fe(IV) intermediates in aliphatic chlorination by the halogenase CytC3.* Nat. Chem. Biol. **3**, 113-116.
4. Matthews, M.L., C.M. Krest, E.W. Barr, F.H. Vaillancourt, C.T. Walsh, M.T. Green, C. Krebs, and J.M. Bollinger (2009) *Substrate-Triggered Formation and Remarkable Stability of the C−H Bond-Cleaving Chloroferryl Intermediate in the Aliphatic Halogenase, SyrB2.* Biochemistry **48**, 4331-4343.
5. Flashman, E., L.M. Hoffart, R.B. Hamed, J.M. Bollinger Jr, C. Krebs, and C.J. Schofield (2010) *Evidence for the slow reaction of hypoxia-inducible factor prolyl hydroxylase 2 with oxygen.* FEBS J. **277**, 4089-4099.
6. Flagg, S.C., N. Giri, S. Pektas, M.J. Maroney, and M.J. Knapp (2012) *Inverse Solvent Isotope Effects Demonstrate Slow Aquo Release from Hypoxia Inducible Factor-Prolyl Hydroxylase (PHD2).* Biochemistry **51**, 6654-6666.
7. Chowdhury, R., M.A. McDonough, J. Mecinović, C. Loenarz, E. Flashman, K.S. Hewitson, C. Domene, and C.J. Schofield (2009) *Structural Basis for Binding of Hypoxia-Inducible Factor to the Oxygen-Sensing Prolyl Hydroxylases.* Structure **17**, 981-989.
8. McNeill, L.A., E. Flashman, M.R.G. Buck, K.S. Hewitson, I.J. Clifton, G. Jeschke, T.D.W. Claridge, D. Ehrismann, N.J. Oldham, and C.J. Schofield (2005) *Hypoxia-inducible factor prolyl hydroxylase 2 has a high affinity for ferrous iron and 2-oxoglutarate.* Mol. BioSyst. **1**, 321-324.
9. McDonough, M.A., C. Loenarz, R. Chowdhury, I.J. Clifton, and C.J. Schofield (2010) *Structural studies on human 2-oxoglutarate dependent oxygenases.* Curr. Opin. Struct. Biol. **20**, 659-672.
10. Pavel, E.G., J. Zhou, R.W. Busby, M. Gunsior, C.A. Townsend, and E.I. Solomon (1998) *Circular dichroism and magnetic circular dichroism spectroscopic studies of the non-heme ferrous active site in clavaminate synthase and its interaction with α-ketoglutarate cosubstrate.* J. Am. Chem. Soc. **120**, 743-753.
11. Hewitson, K.S., S.L. Holmes, D. Ehrismann, A.P. Hardy, R. Chowdhury, C.J. Schofield, and M.A. McDonough (2008) *Evidence That Two Enzyme-derived Histidine Ligands Are Sufficient for Iron Binding and Catalysis by Factor Inhibiting HIF (FIH).* J. Biol. Chem. **283**, 25971-25978.
12. Flashman, E., S.L. Davies, K.K. Yeoh, and C.J. Schofield (2010) *Investigating the dependence of the hypoxia-inducible factor hydroxylases (factor inhibiting HIF and prolyl hydroxylase domain 2) on ascorbate and other reducing agents.* Biochem. J. **427**, 135-142.

13. Flashman, E., E.A.L. Bagg, R. Chowdhury, J. Mecinović, C. Loenarz, M.A. McDonough, K.S. Hewitson, and C.J. Schofield (2008) *Kinetic Rationale for Selectivity toward N- and C-terminal Oxygen-dependent Degradation Domain Substrates Mediated by a Loop Region of Hypoxia-Inducible Factor Prolyl Hydroxylases.* J. Biol. Chem. **283**, 3808-3815.
14. Clifton, I.J., M.A. McDonough, D. Ehrismann, N.J. Kershaw, N. Granatino, and C.J. Schofield (2006) *Structural studies on 2-oxoglutarate oxygenases and related double-stranded [beta]-helix fold proteins.* J. Inorg. Biochem. **100**, 644-669.
15. Hirsilä, M., P. Koivunen, V. Günzler, K.I. Kivirikko, and J. Myllyharju (2003) *Characterization of the Human Prolyl 4-Hydroxylases That Modify the Hypoxia-inducible Factor.* J. Biol. Chem. **278**, 30772-30780.
16. Blasiak, L.C., F.H. Vaillancourt, C.T. Walsh, and C.L. Drennan (2006) *Crystal structure of the non-haem iron halogenase SyrB2 in syringomycin biosynthesis.* Nature **440**, 368-371.
17. Leung, I.K.H., E. Flashman, K.K. Yeoh, C.J. Schofield, and T.D.W. Claridge (2009) *Using NMR Solvent Water Relaxation to Investigate Metalloenzyme−Ligand Binding Interactions.* J. Med. Chem. **53**, 867-875.
18. Leung, I.K.H., M. Demetriades, A.P. Hardy, C. Lejeune, T.J. Smart, A. Szöllössi, A. Kawamura, C.J. Schofield, and T.D.W. Claridge (2013) *Reporter Ligand NMR Screening Method for 2-Oxoglutarate Oxygenase Inhibitors.* J. Med. Chem. **56**, 547-555.
19. Hausinger, R.P. (2004) *Fe(II)/α-Ketoglutarate-Dependent Hydroxylases and Related Enzymes.* Crit. Rev. Biochem. Mol. Biol. **39**, 21-68.
20. Cunliffe, C.J., T.J. Franklin, N.J. Hales, and G.B. Hill (1992) *Novel inhibitors of prolyl 4-hydroxylase. 3. Inhibition by the substrate analog N-oxaloglycine and its derivatives.* J. Med. Chem. **35**, 2652-2658.
21. McDonough, M.A., V. Li, E. Flashman, R. Chowdhury, C. Mohr, B.M.R. Liénard, J. Zondlo, N.J. Oldham, I.J. Clifton, J. Lewis, L.A. McNeill, R.J.M. Kurzeja, K.S. Hewitson, E. Yang, S. Jordan, R.S. Syed, and C.J. Schofield (2006) *Cellular oxygen sensing: Crystal structure of hypoxia-inducible factor prolyl hydroxylase (PHD2).* Proc. Natl. Acad. Sci. U. S. A. **103**, 9814-9819.
22. Warshakoon, N.C., S. Wu, A. Boyer, R. Kawamoto, J. Sheville, S. Renock, K. Xu, M. Pokross, A.G. Evdokimov, R. Walter, and M. Mekel (2006) *A novel series of imidazo[1,2-a]pyridine derivatives as HIF-1α prolyl hydroxylase inhibitors.* Bioorg. Med. Chem. Lett. **16**, 5598-5601.
23. Aik, W., M. Demetriades, M.K.K. Hamdan, E.A.L. Bagg, K.K. Yeoh, C. Lejeune, Z. Zhang, M.A. McDonough, and C.J. Schofield (2013) *Structural Basis for Inhibition of the Fat Mass and Obesity Associated Protein (FTO).* J. Med. Chem. **56**, 3680-3688.
24. Ladroue, C., R. Carcenac, M. Leporrier, S. Gad, C. Le Hello, F. Galateau-Salle, J. Feunteun, J. Pouysségur, S. Richard, and B. Gardie (2008) *PHD2 Mutation and Congenital Erythrocytosis with Paraganglioma.* New Engl. J. Med. **359**, 2685-2692.
25. Sánchez-Fernández, E.M., H. Tarhonskaya, K. Al‑Qahtani, R.J. Hopkinson, J.S.O. McCullagh, C.J. Schofield, and E. Flashman (2013) *Investigations on the oxygen dependence of a 2-oxoglutarate histone demethylase.* Biochem. J. **449**, 491-496.
26. Hewitson, K.S., B.M.R. Liénard, M.A. McDonough, I.J. Clifton, D. Butler, A.S. Soares, N.J. Oldham, L.A. McNeill, and C.J. Schofield (2007) *Structural and*

Mechanistic Studies on the Inhibition of the Hypoxia-inducible Transcription Factor Hydroxylases by Tricarboxylic Acid Cycle Intermediates. J. Biol. Chem. **282**, 3293-3301.

Chapter 4: Mechanistic studies on the reaction of FIH with oxygen

4.1. Introduction

FIH catalyses asparaginyl hydroxylation in HIF-α (Asn803 in the CAD (*C*-terminal activation domain) of HIF-1α and Asn851 in HIF-2α) (see Chapter 1, Section 1.9) [1, 2]. This post-translational modification leads to a reduced interaction of HIF-1/2α with the transcriptional co-activator p300/CBP and so decreases transcription of hypoxia regulated genes [2, 3]. Thus, together with the PHDs (see Chapters 1-3), FIH regulates the hypoxic response in animals [2, 3].

While FIH was identified first as a HIF hydroxylase [2], it has subsequently been found to catalyse hydroxylation of Asn residues in proteins containing ankyrin repeat domains (ARDs). Each ARD comprises repeats of a conserved sequence of ~33 residues, which fold in a helix-turn-helix conformation with a 'β-hairpin' loop connecting individual ARD repeats (**Figure 4.1**, reviewed in [4]). Although ARDs are involved in protein-protein interactions, the function of their post-translational modifications by FIH remains unclear. It has been proposed that hydroxylation of ARDs stabilises the ARD protein fold [5, 6]. Another proposal is that ARD hydroxylation influences the hypoxic regulation of HIF by sequestering FIH [7, 8]. This proposal is supported by recent studies on the gankyrin interaction with FIH (using transgenic mice) showing that gankyrin sequesters FIH under hypoxic conditions, which results in decreased interactions with HIF and promotion of VEGF production [8].

Recent studies have shown that Asn is not the only residue which FIH is able to hydroxylate. FIH has been shown to catalyse hydroxylation of His, Leu and Ser residues [9], in some cases in cells [10]. The sequence of amino acids proximal to the hydroxylated residue has also been shown to play an important role in FIH-catalysed ARD hydroxylation (e.g. substitution of Ala to Pro residue in the position *C*- or *N*-terminal to hydroxylated Asn in Notch-1 results in ARD binding to FIH, but abolishes ARD hydroxylation) [11]. It is proposed that the residues in +1 and -1 positions to Asn participate in substrate binding by making a backbone interaction which helps to project Asn in an orientation optimal for hydroxylation [12].

Although by crystallographic methods HIF and ARD proteins have been shown to bind to FIH in a similar mode [12, 13], there are differences relating to the secondary structure of the different substrates. The CAD of HIF-α is disordered in solution [14, 15], and adopts an extended structured conformation after binding to FIH [13]. ARD substrates exist predominantly in a defined folded state [14] (**Figure 4.1**), and bind to FIH with minor conformational changes. However ARDs must undergo unfolding in order to be hydroxylated [5, 11, 12] (**Figure 4.1b**).

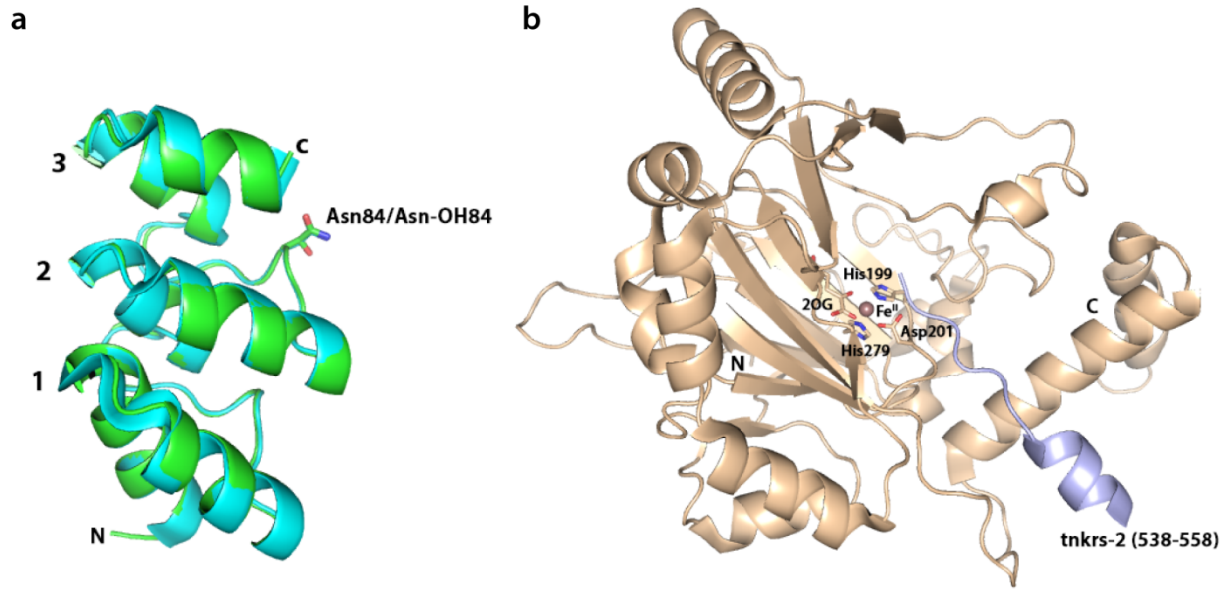


Figure 4.1. Views from crystal structures of (a) 3 ankyrin repeats (3 consensus ankyrin, 3CA) and (b) FIH in complex with a peptide fragment of tankyrase-2 (tnkrs-2, residues 538-558). Ribbon diagram views of **(a)** superimposition of 3CA (cyan, PDB: 2ZGD) and hydroxylated 3CA (green, PDB: 2ZGG). Hydroxylation occurs on Asn84 (on loop 2, 'β-hairpin' type loop) [5]; **(b)** FIH (salmon) in complex with Fe(II), 2OG and fragment of tnkrs-2 (blue, PDB: 2Y0I). There is a conformational change in ARD upon binding to FIH in order to adopt an extended conformation, which results in a proper orientation of a hydroxylated residue for the enzymatic reaction [12].

It has been proposed that ARDs have a higher affinity for FIH compared with HIF-α, as supported by determined steady-state kinetic parameters (lower K_m values for ARD substrates, i.e. <0.2 μM for Notch-1 compared to ~50 μM for HIF-1α [16]). Interestingly, studies on the oxygen dependence of Notch1-3 hydroxylation suggested differences in the affinity of FIH for oxygen, modulated by the substrate [16]; hydroxylation of Notch was maintained at lower oxygen concentrations than hydroxylation of HIF. This observation provides evidence for a potential difference in the regulation of FIH-catalysed post-translational modifications *in vivo*.

Overall, however, no definitive mechanistic differences in the FIH-catalysed ARD versus HIF-α hydroxylation have been identified to date.

The work described in this Chapter focuses on the characteristics of the reaction of FIH with oxygen and compares the results with those obtained for PHD2. The studies aimed to investigate whether the HIF hydroxylases are kinetically suited to act as oxygen sensors, and to investigate the detailed kinetics of the reaction of FIH with oxygen with respect to both its HIF and ARD substrates.

4.2. Results

4.2.1. FIH activity assays in the reaction with HIF-α and ARD substrates

N-terminally His_6-tagged full-length human FIH was produced in *E. coli* and purified using affinity chromatography. This step was followed by His_6-tag cleavage using thrombin and subsequent size exclusion chromatography (see *Materials and Methods*). The enzyme was >95 % pure as assessed by SDS-PAGE analysis and its predicted molecular weight confirmed by LC-MS (40.567 kDa calc., 40.565 kDa found) (**Figure 4.2**).

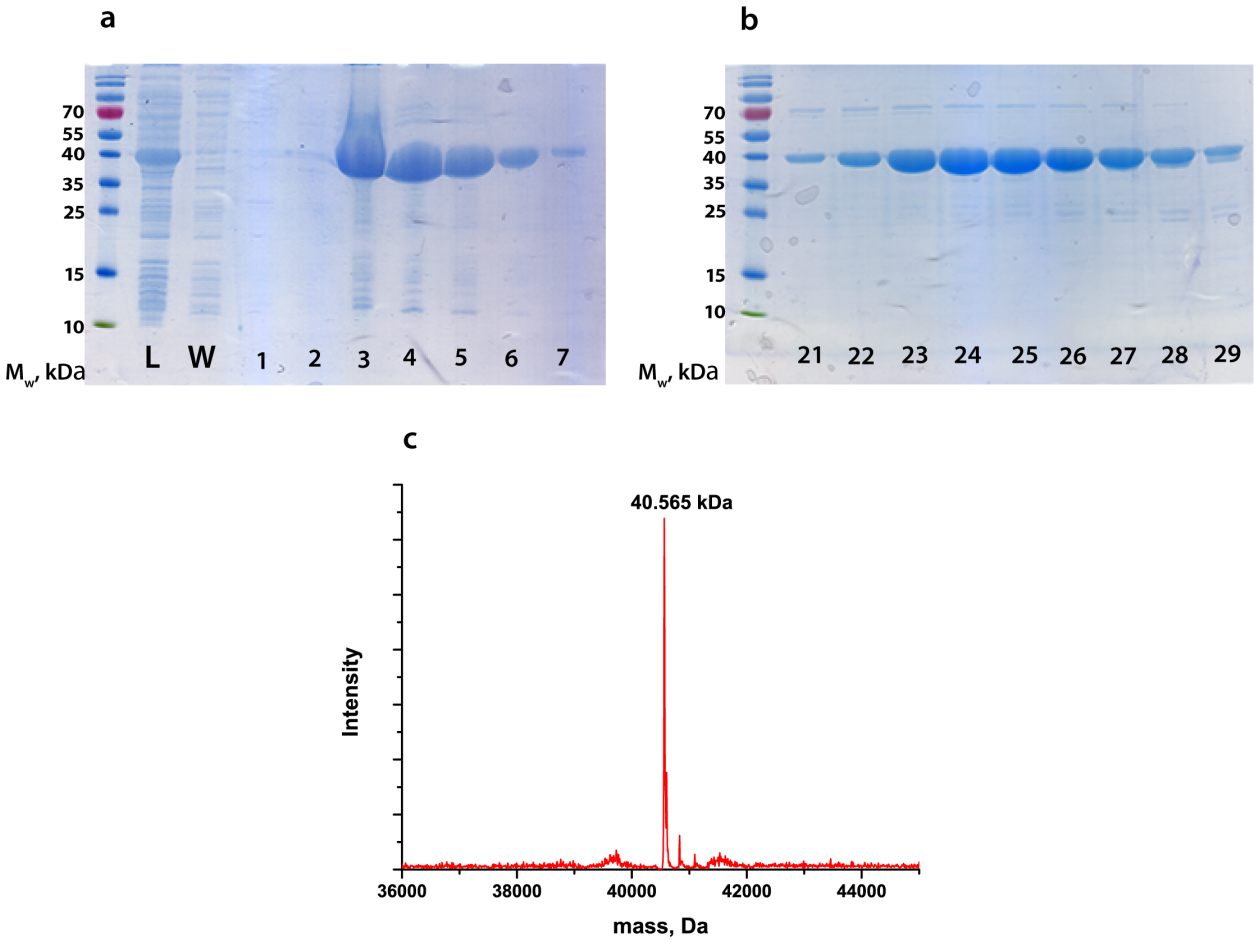


Figure 4.2. SDS-PAGE gels showing purification of FIH. (a) Ni-affinity purification of His_6-FIH. L-lysate, W-wash, 1-7 – fraction numbers. The fractions 3-7 were selected for further purification steps. **(b)** The SDS-PAGE gel showing fractions after size exclusion step. Fractions 21-27 were selected for further experiments. **(c)** The deconvoluted LC-MS spectrum of the purified FIH.

MALDI-TOF-MS assays were performed to investigate FIH activity towards HIF-1/2α CAD fragments and ARD peptide substrates, including a consensus ankyrin repeat 20-mer peptide

($1CA_{20\text{-mer}}$), as well as 20-mer and 35-mer fragments of tankyrase-1 ($tnkrs\text{-}1_{20\text{-mer}}$ and $tnkrs\text{-}1_{35\text{-mer}}$, respectively). Tankyrase is a multifunctional poly(ADP-ribose) polymerase containing 24 ARDs. The observed maximum level of hydroxylation for the CAD HIF-$1\alpha_{19\text{-mer}}$ peptide was much lower than that of the CAD HIF-$1\alpha_{35\text{-mer}}$ peptide, as shown by time course experiments (**Figure 4.3a**), consistent with previous reports indicating insufficient binding of short peptides to FIH [13]. It has also been reported that HIF-2α has a lower affinity for FIH compared to HIF-1α, most likely due to differences in the sequence of the *C*-terminus of CAD [17]. The activity of FIH in its catalysis of CAD HIF-2α hydroxylation using 19-mer and 35-mer peptides under standard assay conditions (as used for HIF-1α CAD) was studied (**Figure 4.3**). Similar to the results with HIF-1α, an increase in the length of the HIF-2α substrate peptide led to an increase of the hydroxylation levels of CAD HIF-2α with no other difference in the reaction time course (**Figure 4.3b**). However, the maximum level of HIF-2α peptide hydroxylation was not more than 25 %, which is consistent with previous reports of low levels of FIH-catalysed HIF-2α hydroxylation *in vivo* [17].

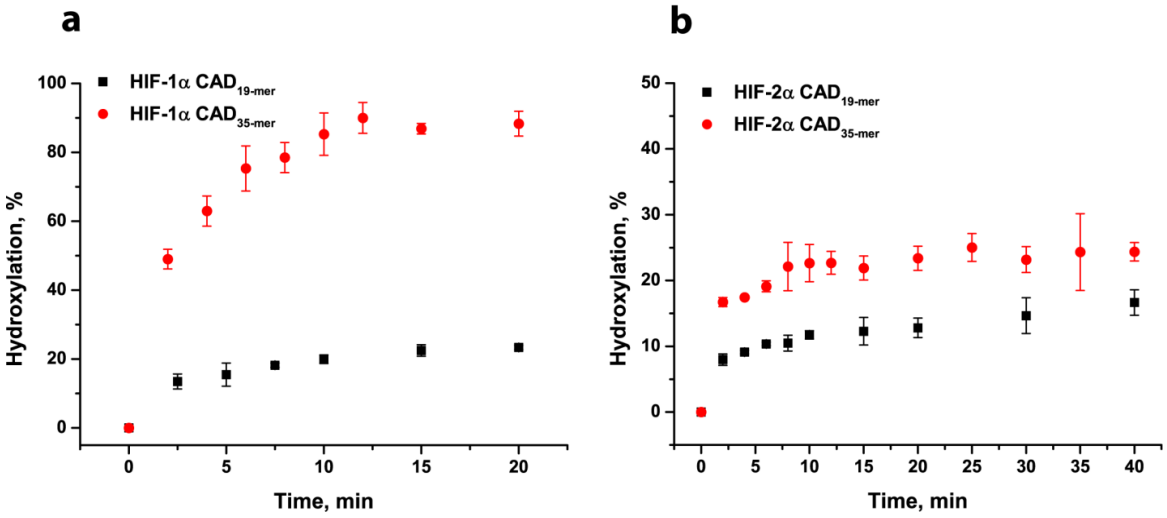


Figure 4.3. FIH-catalysed hydroxylation of the HIF-1/2α peptide fragments. (a) Time course of HIF-1α CAD 19-mer (DESGLPQLTSYDCEVNAPI) and 35-mer (DESGLPQLTSYDCEVNAPIQGSRNLLQGEELLRAL) peptide hydroxylation; **(b)** time course of HIF-2α CAD 19-mer (ESYLLPELTRYDCEVNVPV) and 35-mer (ESYLLPELTRYDCEVNVPVLGSSTLLQGGDLLRAL) peptide hydroxylation. Conditions: 5 μM FIH, 500 μM peptide, 50 μM Fe(II), 500 μM 2OG, 1 mM L-ascorbate in 50 mM HEPES (pH 7.5) were incubated at 37 °C. The different hydroxylation levels were analysed by MALDI-TOF-MS. Error bars represent SD of triplicate assays.

The FIH catalysed hydroxylation of ARD peptides (20-mer), revealed a more efficient reaction than hydroxylation of the HIF-α 20-mer peptides, reaching completion (90 %) after

12-15 minutes. The hydroxylation of the $1CA_{20\text{-mer}}$ was characterised by a very similar hydroxylation time course, compared to tnkrs-$1_{20\text{-mer}}$ (**Figure 4.5a**). To investigate the efficiency of FIH-catalysed hydroxylation in the context of longer ARD peptide substrates, a time course of tnkrs-$1_{35\text{-mer}}$ hydroxylation was also investigated, which showed faster peptide hydroxylation in the presence of the same amount of FIH compared to the 20-mer. The changes were not as profound as may have been expected based on a previous report indicating ~100 fold higher affinity of longer Notch-1 substrates [16] (**Figure 4.5a**).

2CA and 3CA protein constructs were previously designed in the Schofield group as consensus ARD sequences that represent an average of natural ARD substrates. 2CA was designed to contain the second and third 3CA repeats (hydroxylation occurs on the loop of the second repeat, **Figure 4.1a**) for the best comparison with $1CA_{20\text{-mer}}$ peptide and 3CA protein (note, that 2CA used in this study contains a A26H substitution, which does not affect hydroxylation rates as shown using 1CA peptides (Dr A. P. Hardy, unpublished data); hereafter, the 2CA A26H variant is referred to as 2CA).· Analysis of the secondary structures of 2CA and 3CA showed that 3CA is folded, while 2CA is mostly disordered in solution (E. Howe, Schofield group, unpublished data). The His_6-tagged 2CA and 3CA proteins were produced in *E. coli* and purified by Ni-affinity chromatography as described in *Materials and Methods*.

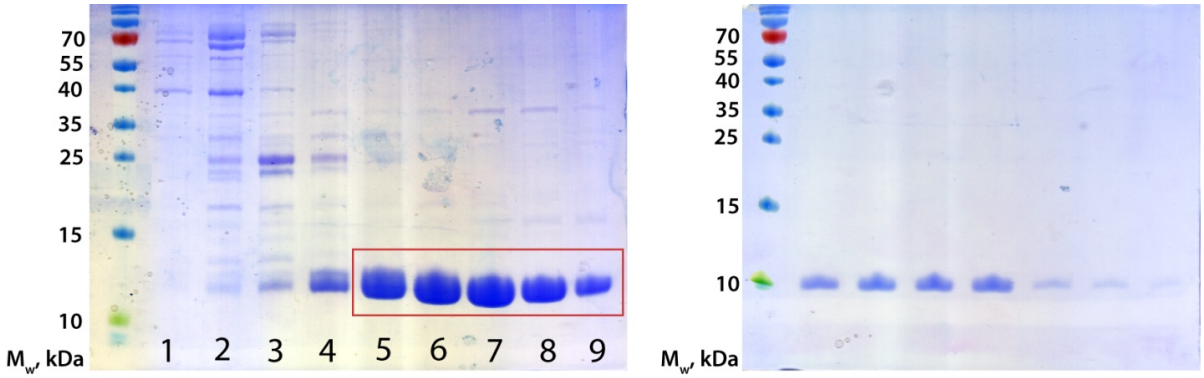


Figure 4.4. SDS-PAGE gels showing purification of 2CA. (a) Ni-affinity purification of His_6-2CA variant. 1-9 – fraction numbers. The fractions 5-9 were selected for further purification steps. **(b)** The SDS-PAGE gel showing fractions after His_6-tag cleavage and a second Ni-affinity purification step to resolved cleaved and uncleaved fractions.

· The design of the 2CA A26H construct was performed by E. Howe (University of Oxford, Schofield group).

Time course analyses of FIH-catalysed hydroxylation of 2CA and 3CA revealed an unexpected result: the rate of product formation increased from 3CA < 1CA < 2CA. (**Figure 4.5b**). To further investigate this observation, steady-state kinetic parameters for the FIH-catalysed reaction were determined.

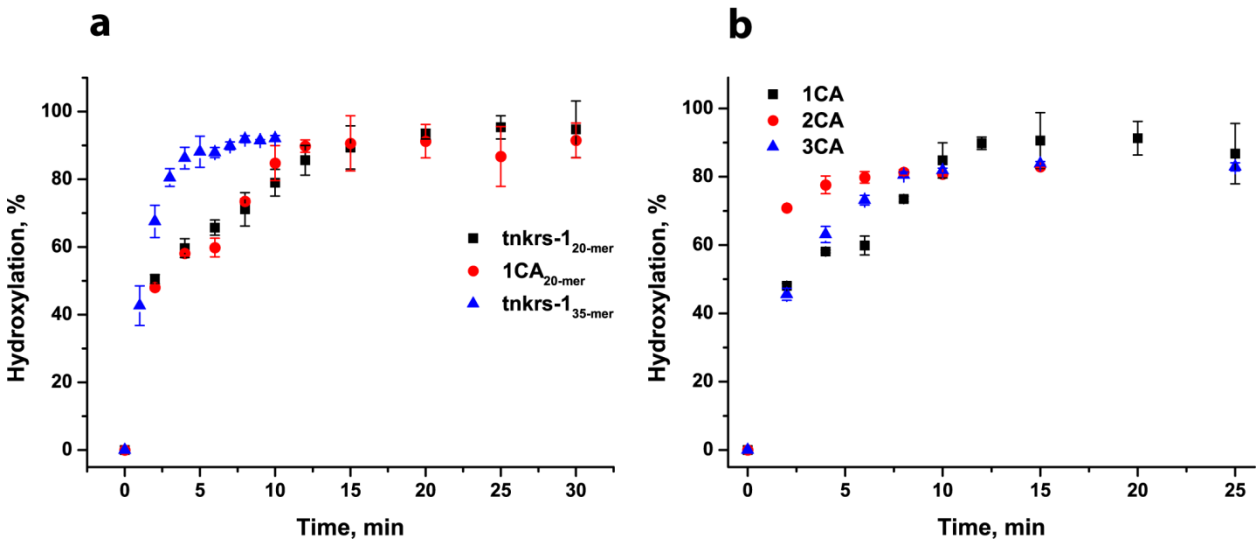


Figure 4.5. FIH-catalysed hydroxylation of the ARD peptides. (a) Time course of 1CA (HLEVVKLLLEAGADVNAQDK), tnkrs-1 20-mer (NLEVAEYLLEHGADVNAQDK) and tnkrs-1 35-mer (AAGYNNLEVAEYLLEHGADVNAQDKGGLIPLHNAA) peptide hydroxylation; **(b)** time course of 1CA, 2CA and 3CA hydroxylation (peptide and protein sequences are listed in Table 7.1). Conditions: 5 µM FIH, 400 µM peptide, 50 µM Fe(II), 500 µM 2OG, 1 mM L-ascorbate in 50 mM HEPES (pH 7.5) were incubated at 37 °C. The different hydroxylation levels were analysed by MALDI-TOF-MS and LC-MS. Error bars represent SD of triplicate assays.

4.2.2. Steady-state kinetic parameters of FIH-catalysed HIF-1/2α and ARD substrate hydroxylation

The initial rates of the FIH catalysed reactions were determined by analysis of substrate hydroxylation time courses at different substrate concentrations, where hydroxylation levels were determined using MALDI-TOF-MS or LC-MS; the data were analysed by fitting the dependence to the Michaelis-Menten equation (non-linear regression fitting). The determined kinetic parameters are summarised in **Table 4.1.** Michaelis-Menten curves are shown in **Figures 4.3 and 4.4**. k_{cat} values were calculated and found to be consistent with the time course activity assays described above, showing higher turnover for longer peptides (**Table 4.1**). The K_m for the HIF-1α CAD was 2-fold lower compared to the HIF-2α CAD (using 35-mer peptides), which is again consistent with the previously reported higher affinity of FIH for

HIF-1α compared to HIF-2α (184±27 μM and 315±40 μM for HIF-1α and HIF-2α, respectively) [17]. When the HIF-2α hydroxylation reaction was conducted under conditions of high 2OG/peptide concentrations, substrate inhibition was observed (>100 μM for 2OG and >700 μM for CAD peptide). Previous studies where FIH activity was analysed using oxygen consumption and [^{14}C] 2OG turnover assays did not identify any substrate inhibition [18, 19]; this observation may be explained by increased uncoupled turnover under conditions of high substrate or 2OG concentrations.

Table 4.1. Steady-state kinetic parameters of FIH-catalysed hydroxylation. Conditions: 0.1-5 μM FIH, peptide (varied), 50 μM Fe(II), 2OG (varied), 1 mM L-ascorbate in 50 mM HEPES (pH 7.5) were incubated at 37 °C. The different hydroxylation levels were analyzed by MALDI-TOF-MS or LC-MS (2CA and 3CA). ND – not determined.

Substrate	K_m2OG, μM	$K_m$substrate, μM	$K_m O_2$, μM	k_{cat}, s^{-1}
1CA	290±50	25±7	40±10	1.6±0.1
2CA	110±30	16±3	56±15	1.7±0.2
3CA	200±60	60±15	120±20	0.6±0.2
tnkrs-$1_{20\text{-mer}}$	370±120	78±11	ND	0.8±0.1
tnkrs-$1_{35\text{-mer}}$	61±7	14±4	50±10	3.0±0.2
HIF-1α $CAD_{35\text{-mer}}$	108±24	184±27	110±30	0.56±0.04
HIF-2α $CAD_{35\text{-mer}}$	19±6*	315±40*	110±10	0.049±0.005

* Substrate inhibition at 2OG concentrations >100 μM and HIF-2α $CAD_{35\text{-mer}}$ concentrations >700 μM was observed.

The steady-state kinetics of ARD substrate hydroxylation were also investigated. The determined K_m values suggested a higher affinity of FIH for ARD substrates compared to HIF-α (25±7 μM and 184±27 μM, for 1CA and HIF-1α $CAD_{35\text{-mer}}$, respectively), consistent with a previous report [16]. In addition, the k_{cat} values were also considerably higher in the case of ARD hydroxylation. Overall, the K_m values for 2OG show that FIH has a lower affinity for 2OG compared to PHD2. The K_m(2OG) values for tnrks-$1_{35\text{-mer}}$ decreased with increasing length of 'prime' substrate, which may reflect easier formation of the FIH.Fe(II).2OG.peptide complex. Determination of the kinetic parameters for $1CA_{20\text{-mer}}$, 2CA and 3CA showed a decrease in substrate and co-substrate K_m values for 2CA compared to $1CA_{20\text{-mer}}$, but an increase in these K_m values in the presence of the 3CA substrate. However,

consistent with the time course experiments in **Figure 4.5b**, for the 3CA substrate a reduction in turnover rate was observed. This result suggests less efficient hydroxylation of folded ARDs, which need to undergo unfolding prior to hydroxylation [5, 12].

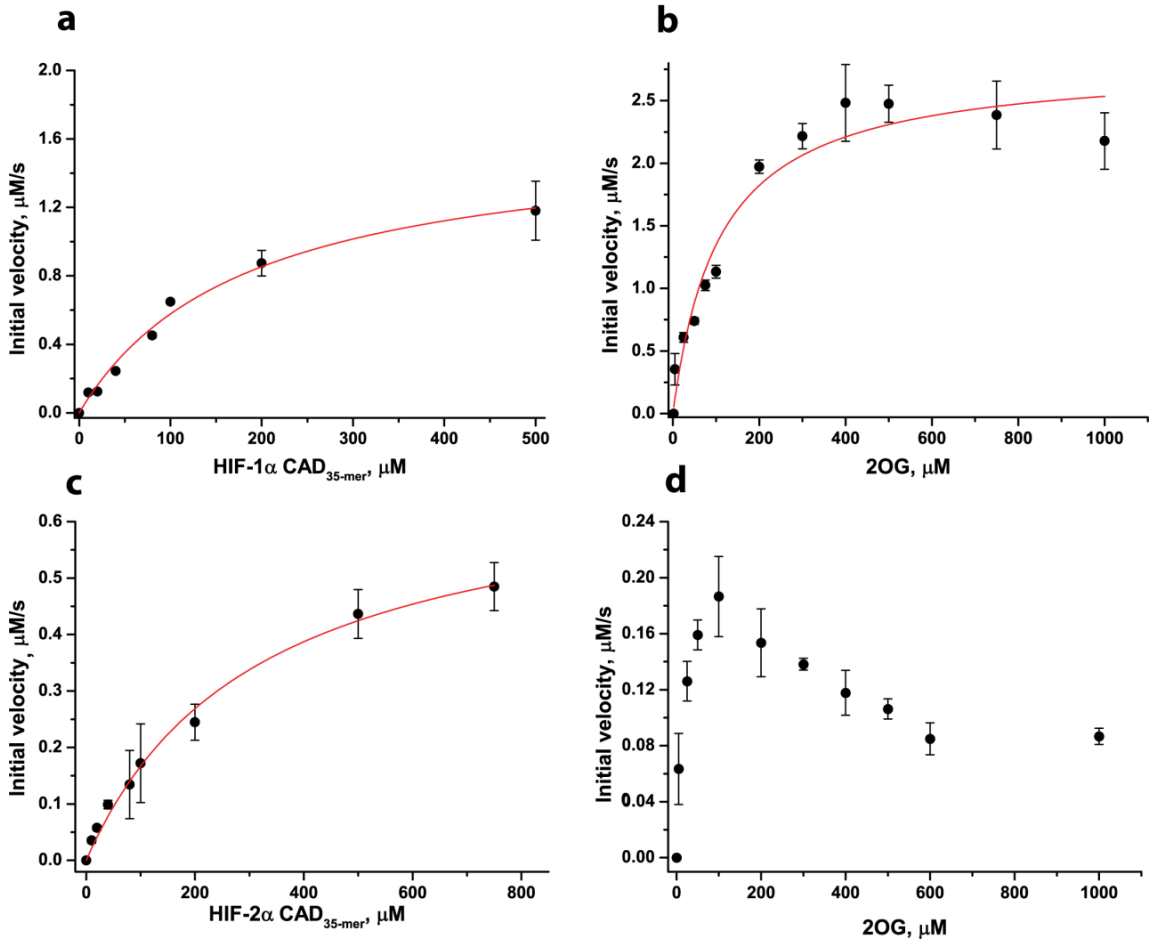


Figure 4.3. Kinetic parameters of the FIH-catalysed hydroxylation of the HIF-1/2α peptide fragments. Conditions: 5 μM FIH, peptide/2OG (varied), 50 μM Fe(II), 1 mM L-ascorbate in HEPES 50 mM (pH 7.5) were incubated at 37 °C. The different hydroxylation levels were analyzed by MALDI-TOF-MS. Error bars represent SD of triplicate assays.

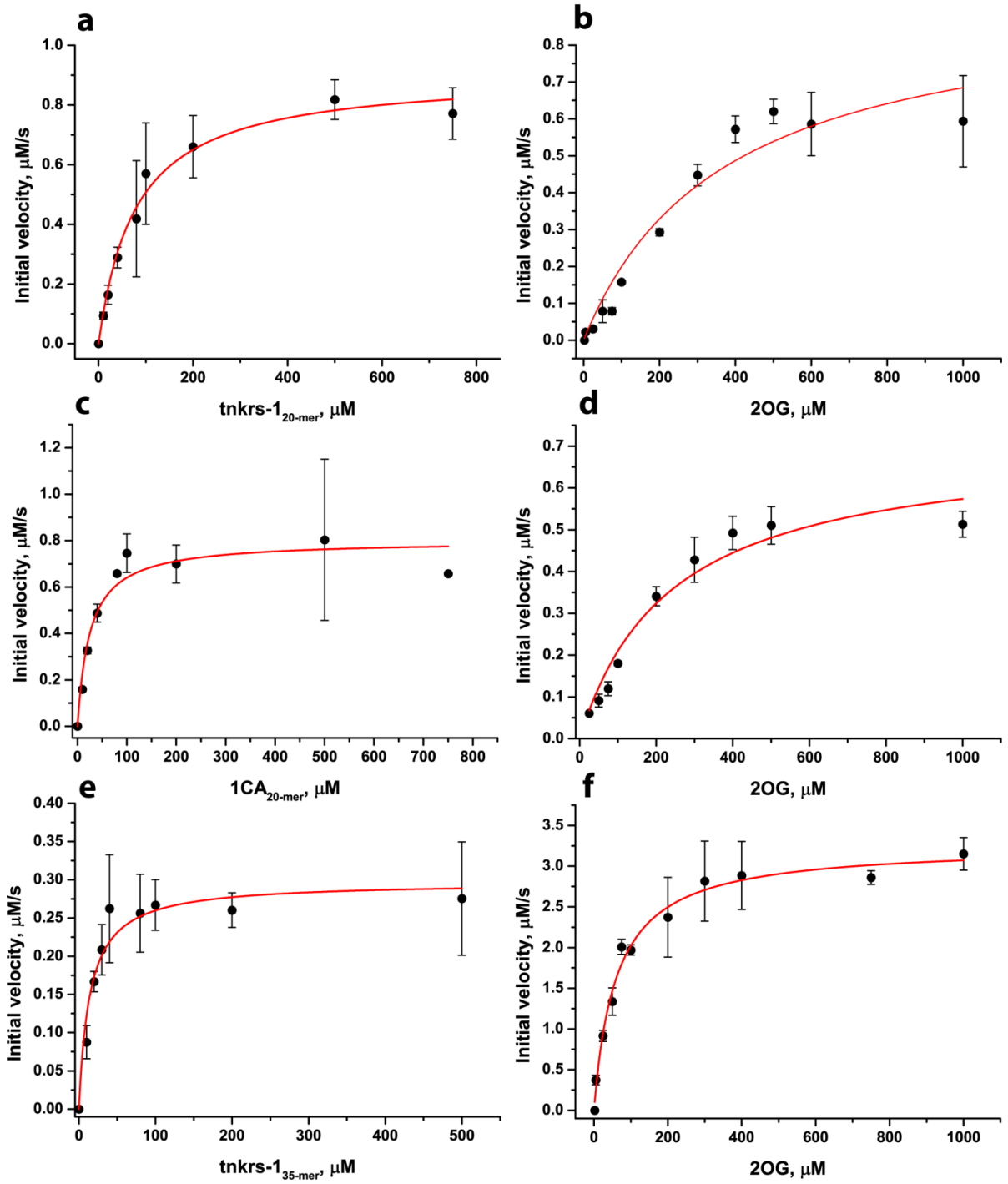


Figure 4.4. Kinetic parameters of the FIH-catalysed hydroxylation of the ARD peptides. (a,b) tankyrase-$1_{20\text{-mer}}$, **(c,d)** 1CA, **(e,f)** tankyrase-$1_{35\text{-mer}}$. Conditions: 2 μM FIH (a,b)/1 μM FIH (f)/0.5 μM FIH (c,d)/0.1 μM FIH (e); peptide/2OG (varied), 50 μM Fe(II), 1 mM L-ascorbate in 50 mM HEPES (pH 7.5) were incubated at 37 °C. The different hydroxylation levels were analysed by MALDI-TOF-MS. Error bars represent SD of triplicate assays. The differences in V_{max} for the same substrate reflect different FIH concentrations used in the assays.

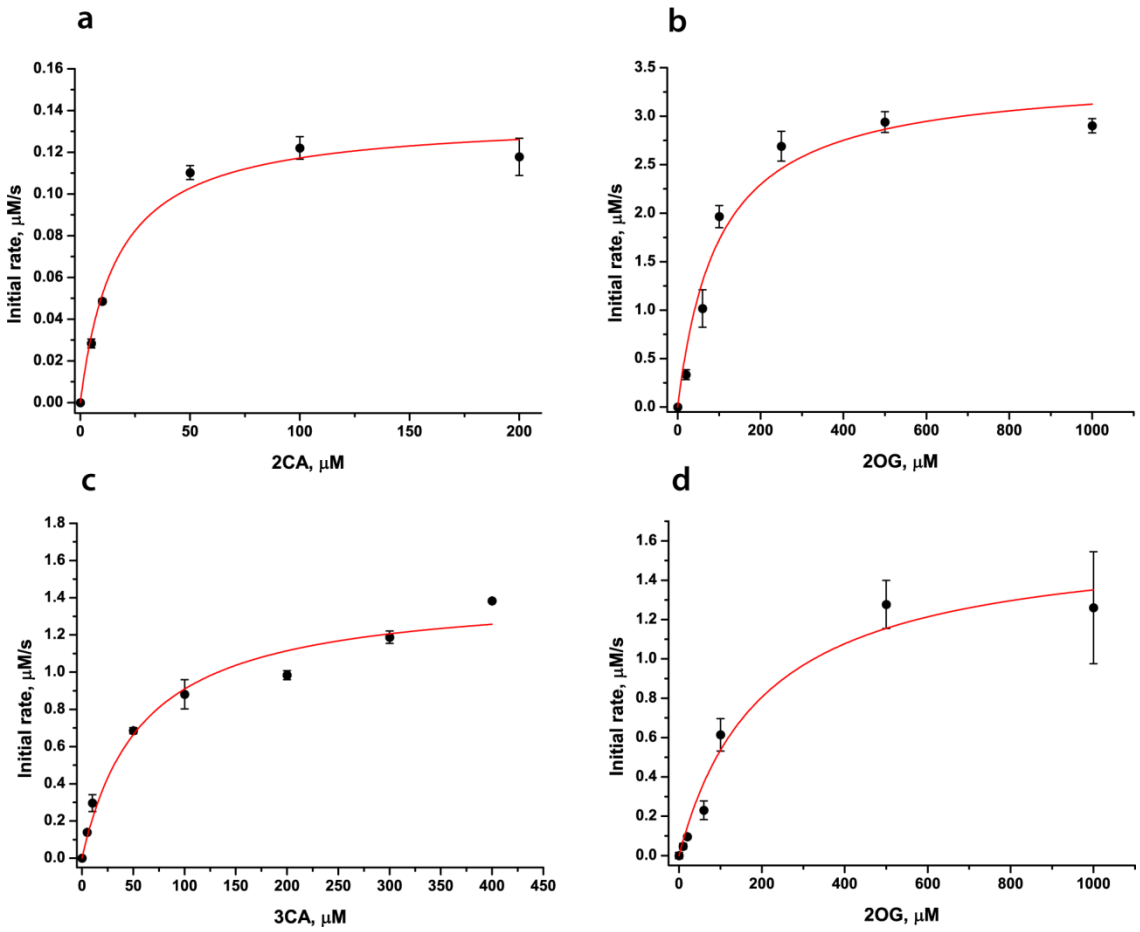


Figure 4.5. Kinetic parameters of the FIH-catalysed hydroxylation of (a,b) 2CA and (c,d) 3CA. Conditions: 0.1 μM FIH (a) or 2 μM FIH (b-d), peptide/2OG (varied), 50 μM Fe(II), 1 mM L-ascorbate in 50 mM HEPES (pH 7.5) were incubated at 37 °C. The different hydroxylation levels were analysed by LC-MS. Error bars represent SD of triplicate assays. The differences in V_{max} for the same substrate reflect different FIH concentrations used in the assays.

4.2.3. Oxygen dependence of the FIH-catalysed hydroxylation

To investigate the oxygen dependence of the FIH-catalysed reactions, initial rates of the reaction were determined (i) using reaction buffer which was pre-equilibrated under different pO_2 in a hypoxic chamber, or (ii) in the reaction, which was conducted under different N_2/O_2 gas mixes with a controlled % of O_2 (see *Materials and Methods*). In the reaction of FIH with CAD HIF-1α the half-saturation of oxygen was achieved at 9-11 %, which gives the $K_m(O_2)$ as 110±30 μM and consistent with previous reports [18, 19]. Despite the differences in the overall turnover rates, there was no influence of the peptide length on the steady-state $K_m(O_2)$ for both 19-mer and 35-mer CAD HIF-1α (the values were the same within error, 90±40 μM

for CAD HIF-1$\alpha_{19\text{-mer}}$, **Figure 4.6**). This could be rationalised by the proposal that the peptide binding step does not affect the rate-limiting step of the reaction when peptide concentrations are saturating. Due to very low levels of hydroxylation of CAD HIF-2$\alpha_{19\text{-mer}}$ only the 35-mer peptide was studied. The O_2-dependence for CAD HIF-2α hydroxylation was characterised by the same K_m value as CAD HIF-1α (110±10 μM). Thus, similar to PHD2, FIH did not show discrimination in its oxygen dependence between HIF-1α and HIF-2α hydroxylation (**Figure 4.7a**, see Chapter 2).

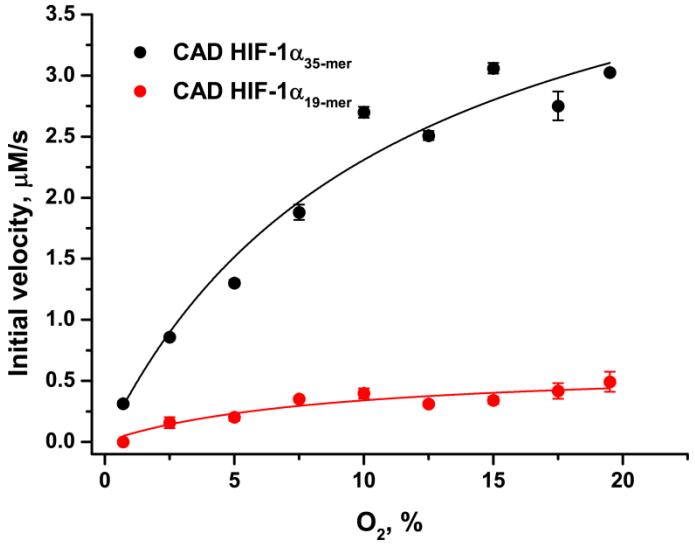


Figure 4.6. Oxygen dependence of the FIH-catalysed hydroxylation of HIF-1α CAD peptides (19-mer vs 35-mer). Conditions: 5 μM FIH, 500 μM peptide, 50 μM Fe(II), 1 mM 2OG, 1 mM L-ascorbate in 50 mM HEPES (pH 7.5) were incubated at 37 °C in a hypoxia workstation under different pO_2. The different hydroxylation levels were analysed by MALDI-TOF-MS. Error bars represent SD of triplicate assays.

A previous study has shown that the $K_m(O_2)$ for FIH can depend on the type of the substrate [16]: the $K_m(O_2)$ values for the ARD-containing proteins Notch1-3 were reported to be 10-fold lower than for CAD HIF-1α [16], suggesting a higher affinity for oxygen in the reaction of ARD-hydroxylation (at least for Notch). To investigate the oxygen dependence of FIH-catalysed ARD hydroxylation, $K_m(O_2)$ values for ARD substrates were determined. The $K_m(O_2)$ for tnkrs-$1_{35\text{-mer}}$ was ~2-fold lower than for CAD HIF-1/2$\alpha_{35\text{-mer}}$ (50±10 μM and 110±10 μM, respectively) in agreement with the previous report [16].

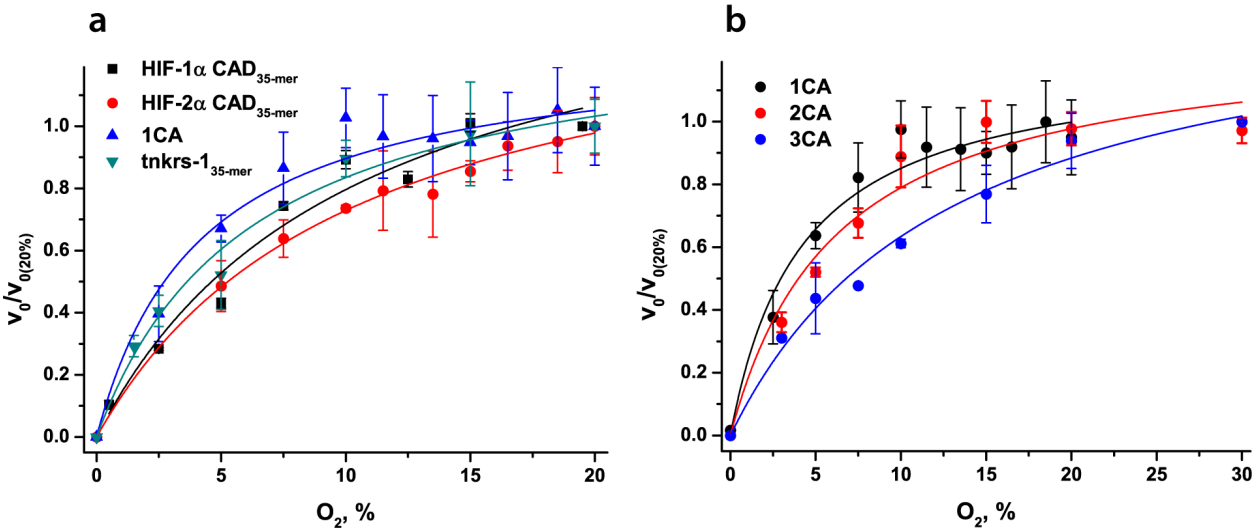


Figure 4.7. Oxygen dependence of the FIH-catalysed hydroxylation of HIF-α and ARD peptides. Conditions: 5 μM FIH, 500 μM peptide, 50 μM Fe(II), 1 mM 2OG, 1 mM L-ascorbate in 50 mM HEPES (pH 7.5) were incubated at 37 °C in a hypoxia workstation under different pO_2. The different hydroxylation levels were analysed by MALDI-TOF-MS, and the relative initial rates (to the initial rate of the reaction at 20 % O_2) are presented. Error bars represent SD of triplicate assays. **(a)** Oxygen dependence for HIF-1/2α, 1CA, tnkrs-$1_{35\text{-mer}}$; **(b)** Comparison of $1CA_{20\text{-mer}}$, 2CA and 3CA.

$K_m(O_2)$ values for 1CA, 2CA and 3CA were determined to be 40±10 μM, 56±15 μM and 120±20 μM, respectively. There was little difference in the FIH affinities to oxygen in the presence of the 1CA and 2CA substrates, however, the $K_m(O_2)$ in the presence of 3CA was 2-fold higher than those for 1CA and 2CA and similar to that of FIH in the presence of its HIF-α substrates (110±30 μM). Thus, an increase in the number of ankyrin repeats and folding of protein do not appear to facilitate the reaction of FIH with oxygen; this may be related to the substrate unfolding process required for catalysis of 3CA hydroxylation.

4.2.4. UV-vis spectroscopy studies on the formation of FIH.Fe(II).2OG.substrate complex

Formation of a 2OG oxygenase-substrate complex is usually characterised by a weakly absorbing feature at 500 nm region due to MLCT (see Chapters 2-3). Upon substrate binding, the Fe(II) (when complexed with 2OG) changes its coordination state from six- to five-coordinate state due to release of a metal-bound water molecule [20, 21]. This is accompanied by a 10 nm shift of λ_{max} of the MLCT feature. In previous crystallographic studies of FIH complexes with HIF-α fragments, no metal-bound water molecule has been observed in the active site; however, all structures with ARD substrates were characterised by the presence of

the water molecule [10, 12, 13]. This water molecule needs to be dissociated before oxygen can bind [20]. Interestingly, solvent isotope studies in the presence of HIF-1α CAD substrate have suggested that the oxygen activation step for the FIH-catalysed reaction most likely occurs after the dissociation of the iron-bound water molecule from the active site [22].

To investigate the mechanistic basis of the difference in the reaction between HIF-α and ARD substrates for FIH, formation of FIH.Fe(II).2OG.substrate complexes was studied using UV-vis spectroscopy. Interestingly, in agreement with previous crystallographic studies, upon addition of either the HIF-1α $CAD_{35\text{-mer}}$ or the HIF-2α $CAD_{35\text{-mer}}$, a ~10 nm shift in the maximum was observed (form λ_{max} 500 nm for FIH.Fe(II).2OG complex to λ_{max}=485 nm and λ_{max}=490 nm for HIF-1α and HIF-2α, respectively), which was not observed for the ARD substrates (λ_{max}=500 nm and λ_{max}=495 nm for 1CA and tnkrs-$1_{20\text{-mer}}$, respectively) (**Figure 4.8**). This would suggest that substrate binding does not change the coordination state of Fe(II) in the case of ARD substrates, and that H_2O may remain coordinated to the active site Fe(II).

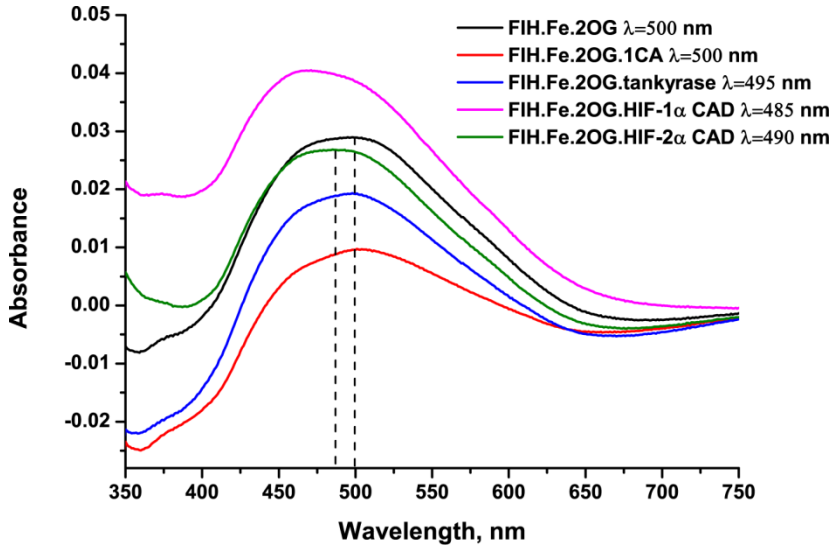


Figure 4.8. UV-vis spectra showing a shift in λ_{max} of the MLCT absorbance feature upon substrate binding to a FIH.Fe(II).2OG complex. Anaerobic 250 μM FIH, 250 μM Fe(II), 1 mM 2OG, 250 μM peptide (HIF-1/2α $CAD_{35\text{-mer}}$/$1CA_{20\text{-mer}}$/tankyrase-$1_{20\text{-mer}}$) in 50 mM HEPES (pH 7.5). The spectrum of FIH only in 50 mM HEPES (pH 7.5) was subtracted from the spectra of the complexes and the difference spectra are presented.

4.2.5. Pre-steady-state kinetics of FIH-catalysed hydroxylation of CAD HIF-1/2α

To investigate the pre-steady-state phase of FIH-catalysed HIF-1/2α hydroxylation, the reaction was studied under conditions close to single turnover. Anaerobic complexes of FIH.Fe(II).2OG.CAD were mixed with O_2-free/O_2-saturated buffer in 1:1 ratio to initiate the reaction in a stopped-flow apparatus and the reaction was observed using a photodiode detector (as for previous analyses on PHD2, see Chapter 2-3, **Figure 4.9**).

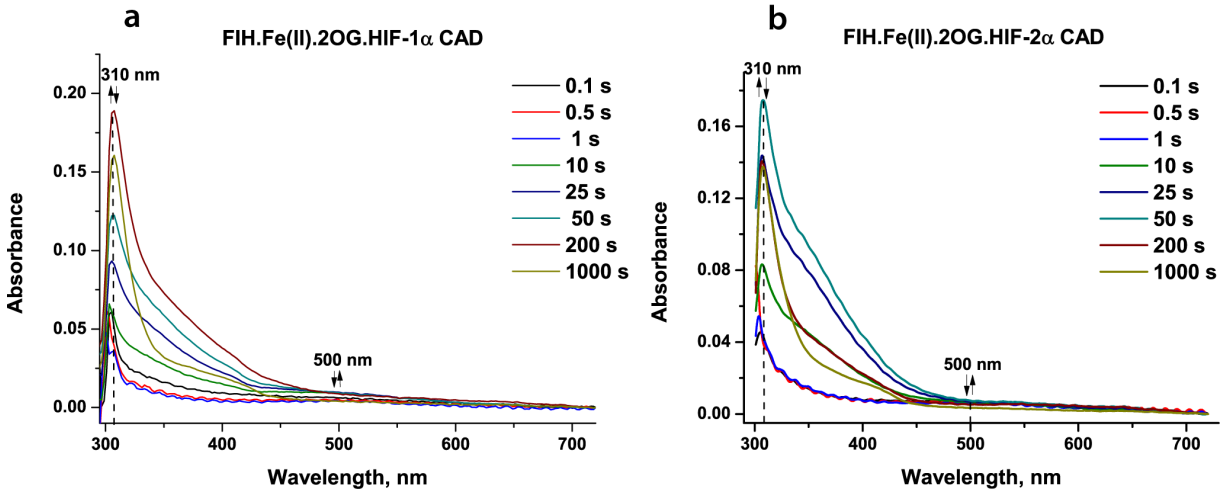


Figure 4.9. Stopped-flow time course of UV-vis absorbance changes during the FIH-catalysed HIF-1/2α hydroxylation. (a) HIF-1α CAD**, (b)** HIF-2α CAD**.** The reaction mixture containing 0.5 mM apo-FIH, 0.4 mM Fe(II), 5 mM 2OG, 1 mM HIF-1/2α $CAD_{35\text{-mer}}$ peptide in 50 mM HEPES (pH 7.5) was rapidly mixed with O_2-saturated buffer in 1:1 ratio and the reaction was observed using a photodiode array detector.

Similar to the time course of the PHD2-catalysed reaction (see Chapters 2-3), formation and degradation of a relatively strongly absorbing species at 300-330 nm region was observed (λ_{max}=310 nm) (**Figure 4.10**). The maximum time of the accumulation of this transient species was ~90 s for CAD HIF-1$\alpha_{35\text{-mer}}$, ~63 s for CAD HIF-2$\alpha_{35\text{-mer}}$, and ~180 s in the absence of peptide substrate. The formation of these species was faster compared to those formed in with PHD2 (~320 s for the reaction with CODD HIF-1α, see Chapter 2), but much slower compared to other studied 2OG oxygenases (~0.1 s for TauD) [23-28]. The kinetic traces at 310 nm representing absorbance changes over time were analysed and fitted with a two-exponential function using Origin 8.51 (**Figure 4.10a**). Similar to PHD2 the obtained fits were poor, likely indicating heterogeneity of the iron species in solution.

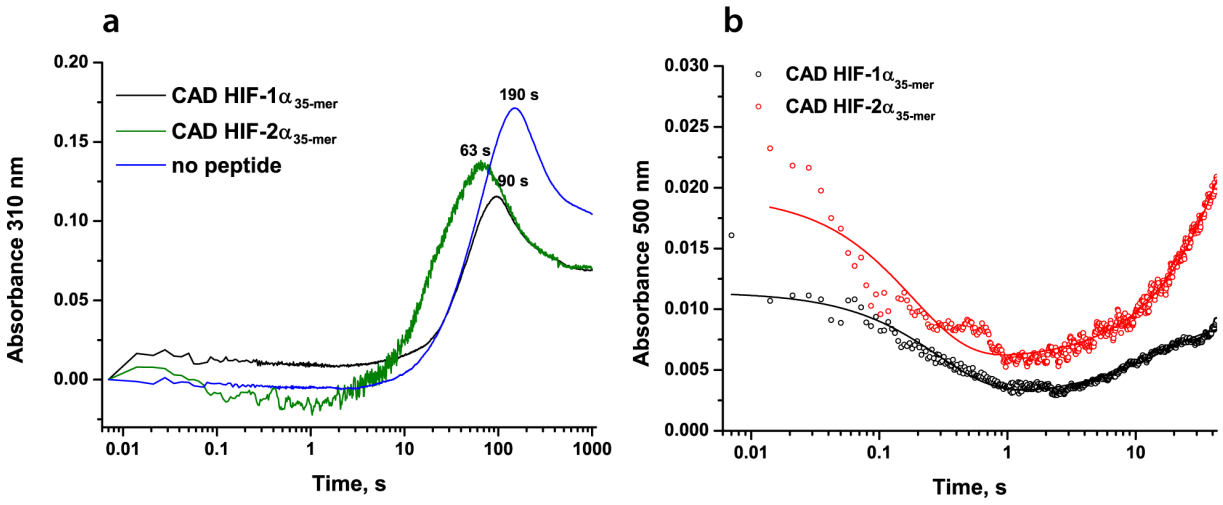


Figure 4.10. Analysis of the kinetic traces at 310 nm and 520 nm for FIH-catalysed HIF-α hydroxylation. (a) 310 nm species; **(b)** 500 nm absorbance decay. The reaction mixture containing anaerobic 0.5 mM apo-FIH, 0.4 mM Fe(II), 5 mM 2OG and 1 mM peptide in 50 mM HEPES (pH 7.5) was rapidly mixed with O_2-saturated buffer in 1:1 ratio at 5 °C and was observed using a photodiode array detector. The data were fitted with a double exponential function.

The absorbance decay at 500 nm was also observed in the FIH-catalysed reaction for both HIF-1α and HIF-2α substrates, similar to PHD2 and other studied 2OG oxygenases (**Figure 4.10b**) [23-28]. The absorbance decay feature was very weak in both cases and developed a minimum much faster compared to PHD2 (~3 s and 22 s for FIH and PHD2, respectively). The kinetic traces at 500 nm were fitted with a double exponential function and the fitting parameters representing the fall and rise phase of the traces are summarised in the **Table 4.2.** Thus, HIF-1α and HIF-2α were characterised by very similar kinetic parameters of oxygen activation as judged by formation of this weakly absorbing species (4.5 s^{-1} and 4.9 s^{-1} for HIF-1α and HIF-2α, respectively) (**Figure 4.10b**).

Table 4.2. Kinetic parameters of pre-steady-state FIH-catalysed hydroxylation. The reaction mixture containing 0.5 mM apo-FIH, 0.4 mM Fe(II), 5 mM 2OG, 1 mM peptide in 50 mM HEPES (pH 7.5) was rapidly mixed with O_2-saturated buffer in 1:1 ratio and then quenched with 1 % CF_3COOH at defined time points or observed by a photodiode array detector. ND- not determined.

Substrate	Stopped-flow, 500 nm		Rapid quench-flow	
	$k_{fall\ phase.}$, s^{-1}	$k_{rise\ phase}$, s^{-1}	$k_{product\ form.}$, s^{-1}	$k_{succinate\ .form.}$ s^{-1}
HIF-1α $CAD_{35\text{-}mer}$	4.5±0.3	0.009±0.005	0.33 ± 0.07	0.31±0.13
HIF-1α $CAD_{19\text{-}mer}$	ND	ND	0.013±0.003	0.016±0.004
HIF-2α $CAD_{35\text{-}mer}$	4.9±0.2	0.02±0.01	0.12±0.01	0.11±0.03
$1CA_{20\text{-}mer}$	17.6±0.1	0.4±0.1	1.3±0.2	0.8±0.3
2CA	11.9±0.2	0.6±0.1	0.48±0.13	ND
3CA	10.5±0.1	1.7±0.3	0.051±0.001	ND
tnkrs-$1_{20\text{-}mer}$	16.7±0.2	0.4±0.2	1.5±0.1	1.0±0.3
tnkrs-$1_{35\text{-}mer}$	14.8±0.2	0.27±0.03	11±3	10±3

To investigate whether the observed stopped-flow absorbance species (310 nm and 500 nm) are positioned on a catalytically relevant time scale and whether they may represent an Fe(IV)-oxo intermediate or high spin FIH.Fe(II).product(s) complexes, rapid quench-flow experiments were performed under the same conditions as the described stopped-flow experiments. Reactions were quenched by 1 % CF_3COOH at defined time points, and hydroxylation of the CAD peptides (CAD HIF-$1\alpha_{19\text{-}mer}$ and CAD HIF-$1/2\alpha_{35\text{-}mer}$) was analysed by MALDI-TOF-MS. Fitting the experimental data with a single exponential function allowed determination of pseudo-first order kinetic constants of product accumulation (**Table 4.2**). The 19-mer peptide substrate stimulates very slow reaction with oxygen (probably due to its poor ability to form a FIH.Fe(II).2OG.substrate complex), with a rate constant of 0.013 s^{-1} similar to those observed for PHD2 (0.0155 s^{-1} for CODD HIF-1α, see Chapter 2). However, the 35-mer peptides were hydroxylated much faster (0.33 s^{-1} and 0.12 s^{-1} for HIF-1α and HIF-2α respectively) compared to PHD2 (note that no change in the pre-steady-state kinetics of PHD2-catalysed hydroxylation of 19-mer CODD/NODD peptides and longer HIF-1α fragments was observed, see Chapter 2). Thus, FIH exhibited much faster oxygen activation and overall turnover compared to PHD2 in the presence of optimal HIF-α CAD substrates.

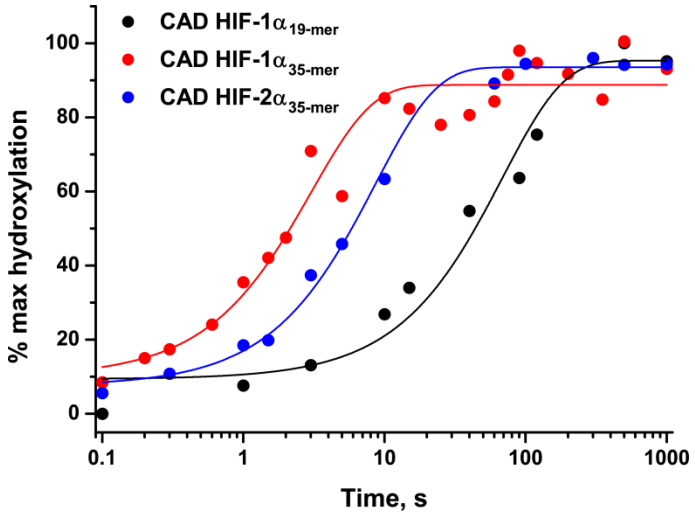


Figure 4.11. Rapid quench-flow experiments showing product accumulation in the FIH-catalysed HIF-α hydroxylation. The reaction mixture containing 0.5 mM apo-FIH, 0.4 mM Fe(II), 5 mM 2OG, 1 mM peptide in 50 mM HEPES (pH 7.5) was rapidly mixed with O_2-saturated buffer in 1:1 ratio at 5 °C and then quenched with 1 % CF_3COOH at defined time points. The data were fitted with *y=a·(1-exp(-bx))+c* function. The hydroxylation levels were assessed by MALDI-TOF-MS.

Rapid quench-flow experiments revealed that the hydroxylation of the peptides was observed simultaneous to/before the formation of the 310 nm species. This result suggests that similarly to PHD2, the observed 310 nm species is non-catalytic and possibly related to iron oxidation (see Chapter 2). There is no accumulation of an Fe(IV)-oxo intermediate during FIH catalysis. However, the observed product accumulation time course correlated to the time of 500 nm decay, suggesting that the observed change in the absorbance of this feature is related to catalytic events (**Figure 4.12**)

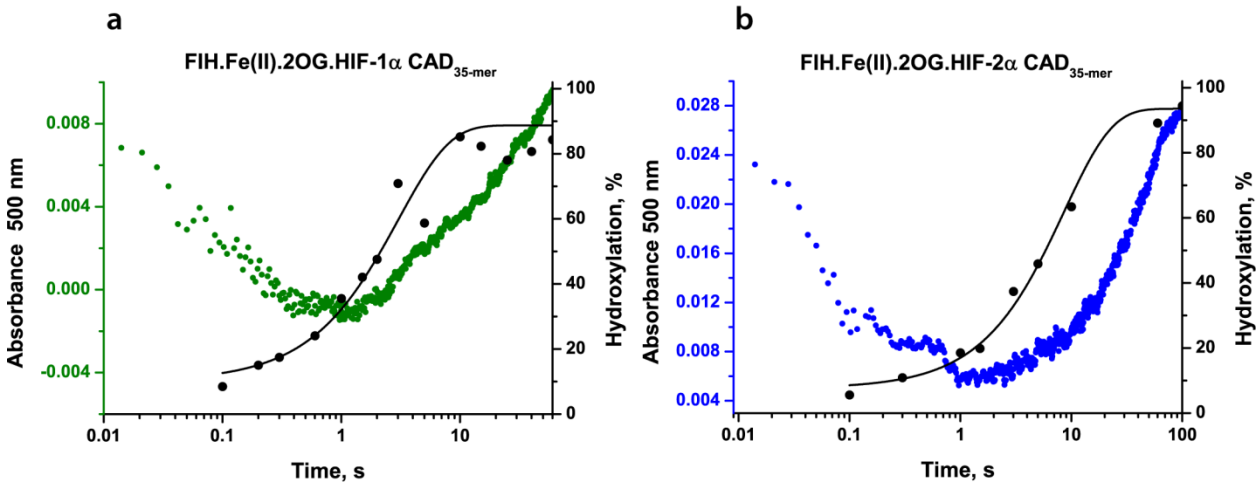


Figure 4.12. Comparison of the pre-steady state kinetics of 500 nm species decay/formation and prime substrate hydroxylation for FIH-catalysed HIF-α hydroxylation. The reaction mixture containing 0.5 mM apo-FIH, 0.4 mM Fe(II), 5 mM 2OG, 1 mM peptide in 50 mM HEPES (pH 7.5) was rapidly mixed with O_2-saturated buffer in 1:1 ratio and then quenched with 1 % CF_3COOH at defined time points or observed by a photodiode array detector. The hydroxylation levels were assessed by MALDI-TOF-MS and the data were fitted with *y=a·(1-exp(-bx))+c* function. Rapid quench-flow results are overlaid with kinetic traces at 500 nm. **(a)** HIF-1α CAD, **(b)** HIF-2α CAD.

To investigate the coupling ratio of the reaction (poor substrates can stimulate increased uncoupled 2OG turnover) [20], LC-MS studies of succinate formation in the rapid quench-flow experiments were performed. Hydroxylation and 2OG oxidation were relatively tightly coupled to hydroxylation of both HIF-1α and HIF-2α peptides, reaching maximum levels at the same time (**Figure 4.13**). The determined rate constants of succinate accumulation were comparable to the hydroxylation constants and are summarised in **Table 4.2.**

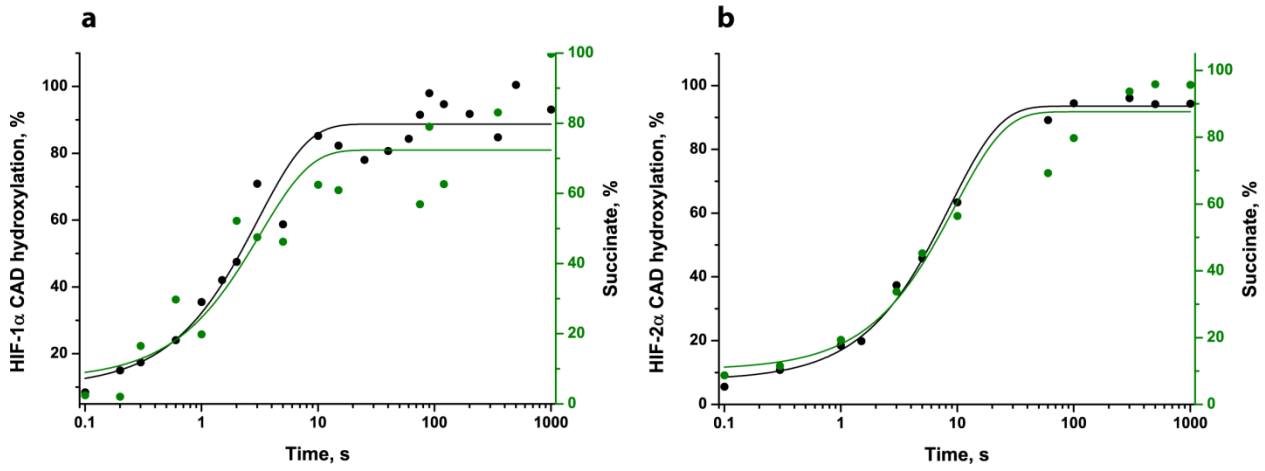


Figure 4.13. Analyses of 'prime' substrate hydroxylation and succinate formation in FIH-catalysed HIF-1/2α hydroxylation. The reaction mixture containing 0.5 mM apo-FIH, 0.4 mM Fe(II), 5 mM 2OG, 1 mM peptide in 50 mM HEPES (pH 7.5) was rapidly mixed with O_2-saturated buffer in 1:1 ratio and then quenched with 1 % CF_3COOH at defined time points. The data were fitted with *y=a·(1-exp(-bx))+c* function. Hydroxylation levels were assessed by MALDI-TOF-MS and succinate concentration was determined using LC-MS.

The determined constants of oxygen activation (the decay of absorbance at 500 nm) could reflect diminished binding affinity of the substrate to FIH, and therefore less strong 'substrate triggering' of the reaction with oxygen. To address this possibility, the dependence of the FIH reaction with oxygen on substrate concentration was investigated (absorbance decay at 500 nm was studied at different FIH:CAD HIF-$1\alpha_{35\text{-mer}}$ ratios, **Figure 4.14**). No absorbance decay at 500 nm was observed at a 1:1 ratio of FIH to peptide, which can be explained by insufficient 'substrate triggering' of the reaction. Saturation of the 500 nm signal was reached at 1:3 ratio, and the profile of the negative absorbance feature did not change with further increase of the substrate concentration. The determined rate constant at 1:3 FIH:CAD HIF-$1\alpha_{35\text{-mer}}$ ratio was 11.3±0.8 s^{-1}.

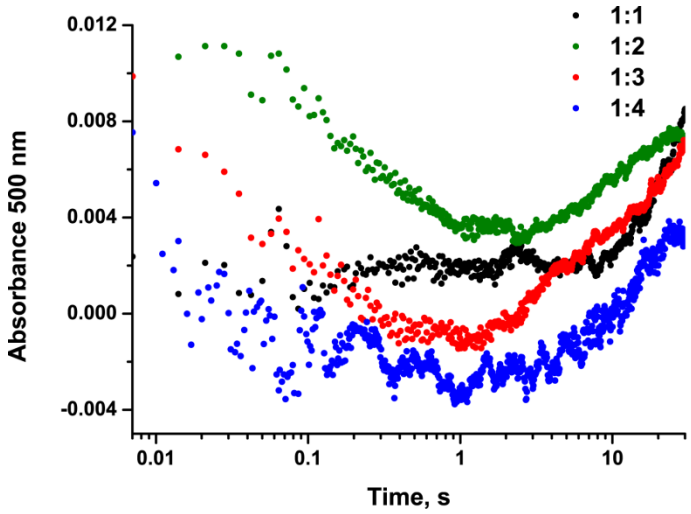


Figure 4.14. Absorbance decay at 500 nm representing enzyme-substrate complex depletion in the FIH-catalysed reaction. The reaction mixture containing anaerobic 0.5 mM apo-FIH, 0.4 mM Fe(II), 5 mM 2OG and 0.5/1/1.25/1.5 mM peptide in 50 mM HEPES (pH 7.5) was rapidly mixed with O_2-saturated buffer in 1:1 ratio and was observed using a photodiode array detector.

4.2.6. Pre-steady-state studies on hydroxylation of ankyrin repeat domain substrates

To study the oxygen-dependence of FIH-catalysed hydroxylation of ARD substrates ($1CA_{20\text{-}mer}$, tnkrs-$1_{20\text{-}mer}$), stopped-flow UV-vis spectroscopy experiments were performed. Similar to the reaction with CAD HIF-1/2α, the formation and degradation of a 310 nm absorbance species was observed, with no significant dependence on the nature of the substrate. The formation and degradation of a 500 nm decay species was also observed, however the rates of formation/degradation of this species were faster in the case of ARD substrates compared to HIF-1/2α (**Figure 4.15**). The amplitude of the absorbance changes at 500 nm during the reaction differed depending on the nature of substrate, which may reflect different efficiencies of substrate binding. Interestingly, given the difference in steady-state kinetic constants for tnkrs-$1_{20\text{-}mer}$ and tnkrs-$1_{35\text{-}mer}$, accumulation of the absorbance decay species at 500 nm for tnkrs-$1_{35\text{-}mer}$ was not faster compared with 20-mer peptides (**Figure 4.16**). The kinetic traces were fitted using a double exponential function and the fitting parameters of the absorbance decay feature formation (the decay at ~500 nm) and degradation are summarised in **Table 4.2**.

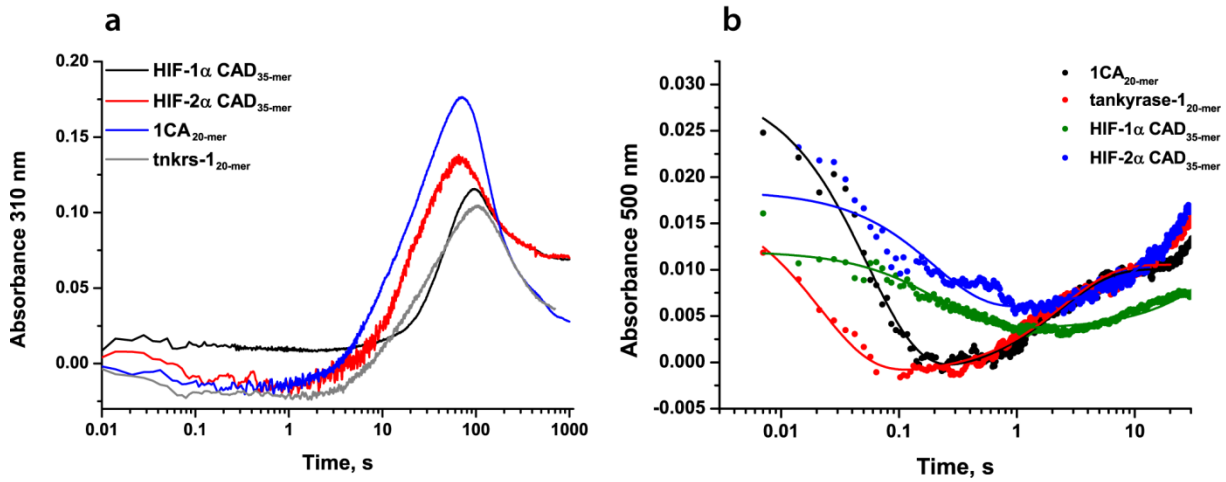


Figure 4.15. Analysis of the kinetic traces at (a) 310 nm and (b) 500 nm for FIH-catalysed ARD substrate hydroxylation. The reaction mixture containing anaerobic 0.5 mM apo-FIH, 0.4 mM Fe(II), 5 mM 2OG and 1 mM peptide in 50 mM HEPES (pH 7.5) was rapidly mixed with O_2-saturated buffer in 1:1 ratio and was observed using a photodiode array detector. The data were fitted with a double exponential function.

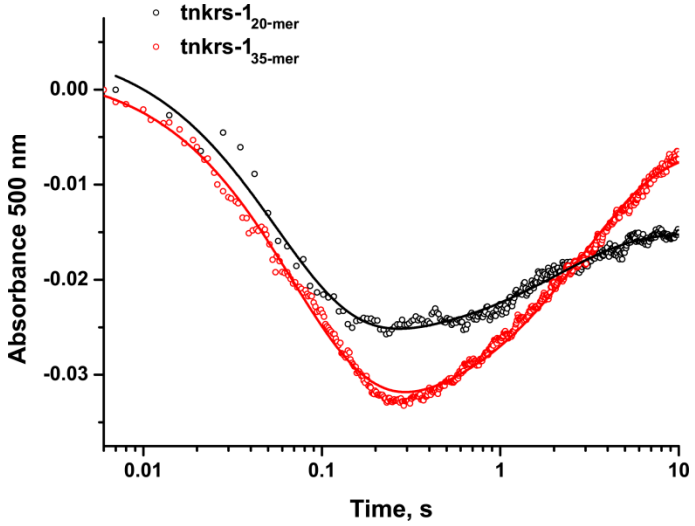


Figure 4.16. Comparison of the kinetic traces at 500 nm for FIH-catalysed tnkrs-$1_{20\text{-mer}}$ and tnkrs-$1_{35\text{-mer}}$ hydroxylation. The reaction mixture containing anaerobic 0.5 mM apo-FIH, 0.4 mM Fe(II), 5 mM 2OG and 1 mM peptide in 50 mM HEPES (pH 7.5) was rapidly mixed with O_2-saturated buffer in 1:1 ratio and was observed using a photodiode array detector. The data were fitted with a double exponential function.

To investigate the pre-steady-state kinetics of product accumulation, rapid quench-flow experiments were performed under the same conditions as for the stopped-flow experiments (**Figure 4.17**). Interestingly, the determined pre-steady-state rate constants of product accumulation suggested a faster reaction upon addition of O_2 in the presence of ARD substrates than that with HIF-α substrates. Upon mixing of FIH.Fe(II).2OG.$1CA_{20\text{-mer}}$ and

FIH.Fe(II).2OG.tnkrs-$1_{20\text{-mer}}$ complexes with O_2-saturated buffer, rapid peptide hydroxylation was observed, and the rate constants were determined to be 1.3±0.2 s^{-1} and 1.5±0.1 s^{-1}, respectively (**Table 4.2**). Thus, oxygen-triggered kinetics of FIH catalysis in the presence of ARDs was approximately 4-fold faster than the equivalent reactions with HIF substrates (0.33±0.07 s^{-1} and 1.3±0.2 s^{-1} for HIF-1α $CAD_{35\text{-mer}}$ and 1CA, respectively). Note, that the studied ARD substrates were only 20-mer peptides, while HIF-1/2α peptides used for comparison were 35-mers; (pre-steady-state kinetics were conducted with HIF-1/2α 35-mers due to their higher substrate efficiency compared to 19-mers). However, the pre-steady-state kinetics of the reaction of a FIH.Fe(II).2OG.tnkrs-$1_{35\text{-mer}}$ complex with oxygen were studied for comparison with those with the HIF-1/2α 35-mer substrates. In contrast to the rate of accumulation of the negative 500 nm species, the rate of hydroxylation of the tankyrase 35-mer upon addition of oxygen was faster compared to the 20-mer peptide. Thus, an increase in the length of the ARD peptide from 20 to 35 residues resulted in a 10-fold faster reaction (determined rate constants 11.4±2.6 s^{-1} for tnkrs-1 35-mer hydroxylation). Consistent with the published report [16], a ~40-fold difference for oxygen-triggered reaction of ARD and HIF-1α substrate hydroxylation was observed (comparing HIF-1α $CAD_{35\text{-mer}}$ and tnkrs-$1_{35\text{-mer}}$).

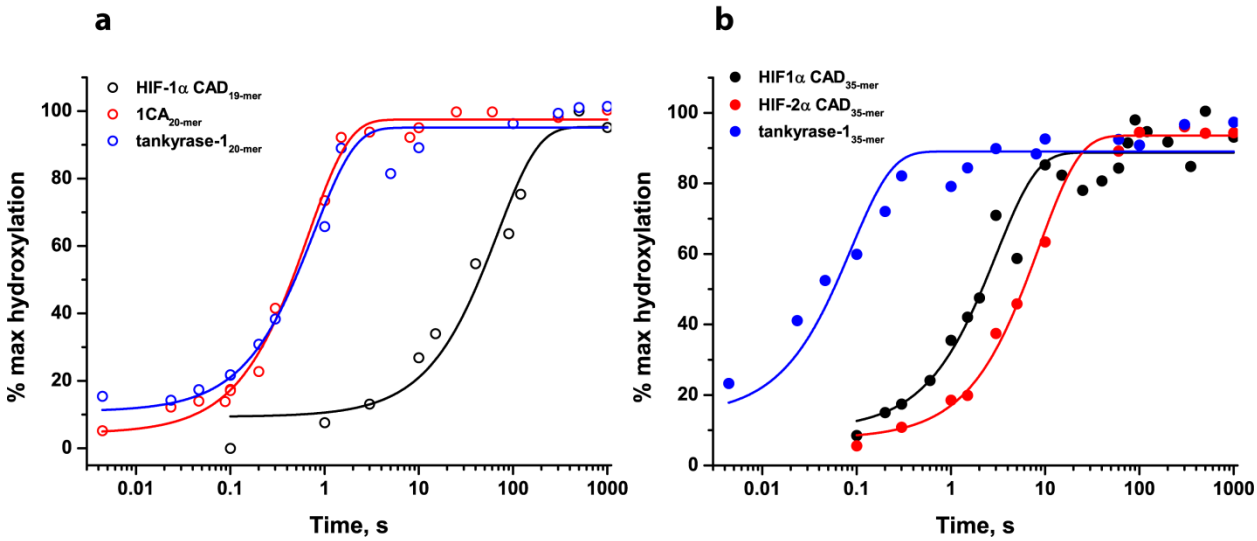


Figure 4.17. Rapid quench-flow results for comparison of the FIH-catalysed ARD and HIF-1/2α hydroxylation. The reaction mixture containing anaerobic 0.5 mM apo-FIH, 0.4 mM Fe(II), 5 mM 2OG and 1 mM peptide in 50 mM HEPES (pH 7.5) was rapidly mixed with O_2-saturated buffer in 1:1 ratio and was quenched by 1 % CF_3COOH at defined time points. The hydroxylation was analysed using MALDI-TOF-MS and the data were fitted with a single exponential function.

To investigate coupling of 2OG oxidation to peptide hydroxylation under the rapid quench-flow experimental conditions, samples were also analysed for succinate formation using LC-MS (**Figure 4.18**). Similar to HIF-α isoforms, the hydroxylation of ARD substrates was fully coupled to succinate formation (determined rate constants are summarised in **Table 4.2**).

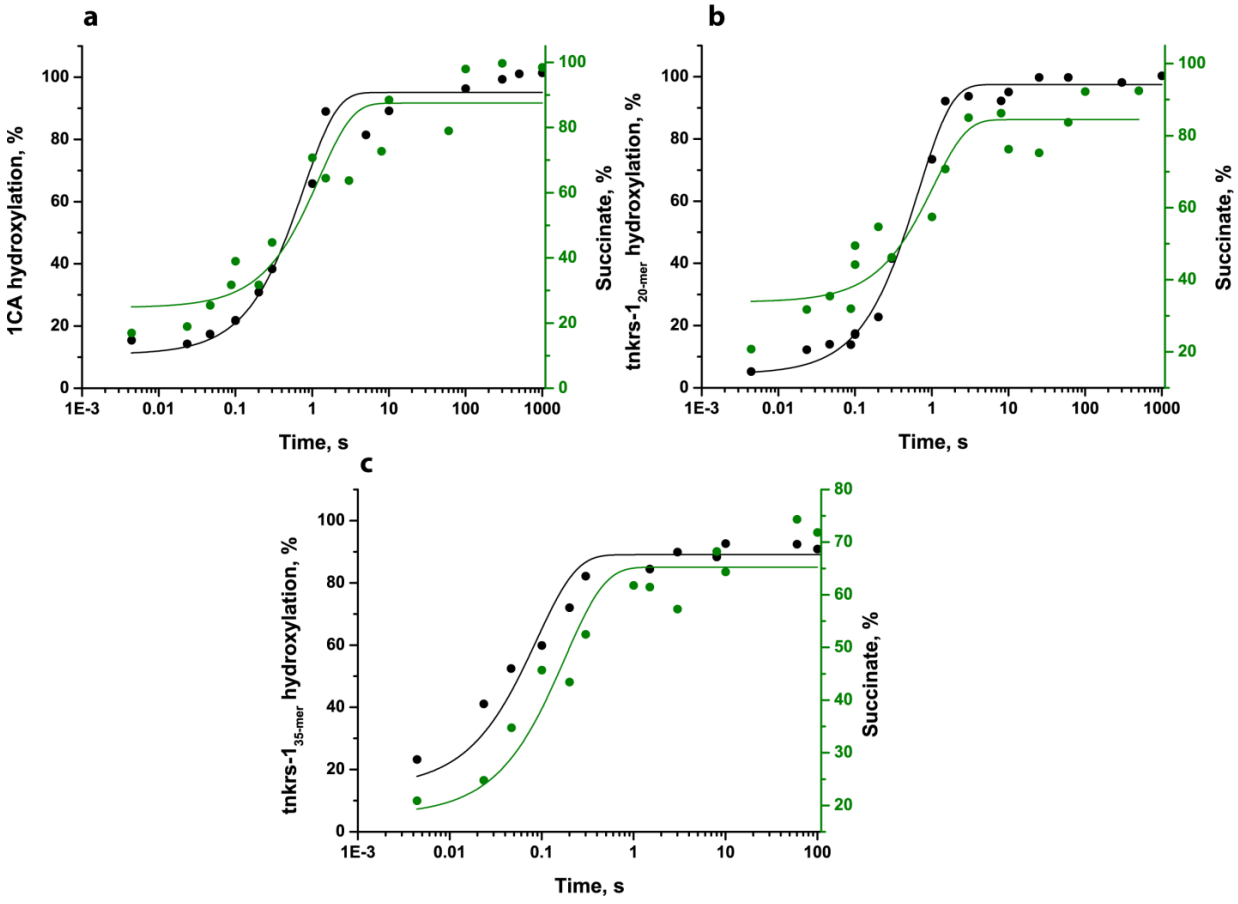


Figure 4.18. Analyses of the hydroxylation and succinate formation in the FIH-catalysed ARD hydroxylation. The reaction mixture containing 0.5 mM apo-FIH, 0.4 mM Fe(II), 5 mM 2OG, 1 mM peptide in 50 mM HEPES (pH 7.5) was rapidly mixed with O_2-saturated buffer in 1:1 ratio and then quenched with 1 % CF_3COOH at defined time points. The data were fitted with $y=a\cdot(1-exp(-bx))+c$ function. The hydroxylation levels were assessed by MALDI-TOF-MS and succinate concentration was determined using LC-MS.

Similar to HIF-α isoforms, the absorbance decay at 500 nm (formation of the negative species) for ARD hydroxylation was consistent with time courses of product accumulation under pre-steady-state conditions (i.e. substrate complex is depleted prior to product formation, **Figure 4.19**). A faster reaction in the case of tankyrase-1 35-mer may be explained by more efficient product release, which is suggested by the simultaneous time course of

product formation and FIH.Fe(II).2OG.substrate complex consumption with the completion of the reaction consistent with the minimum of the 500 nm negative absorbance feature (**Figure 4.19c**).

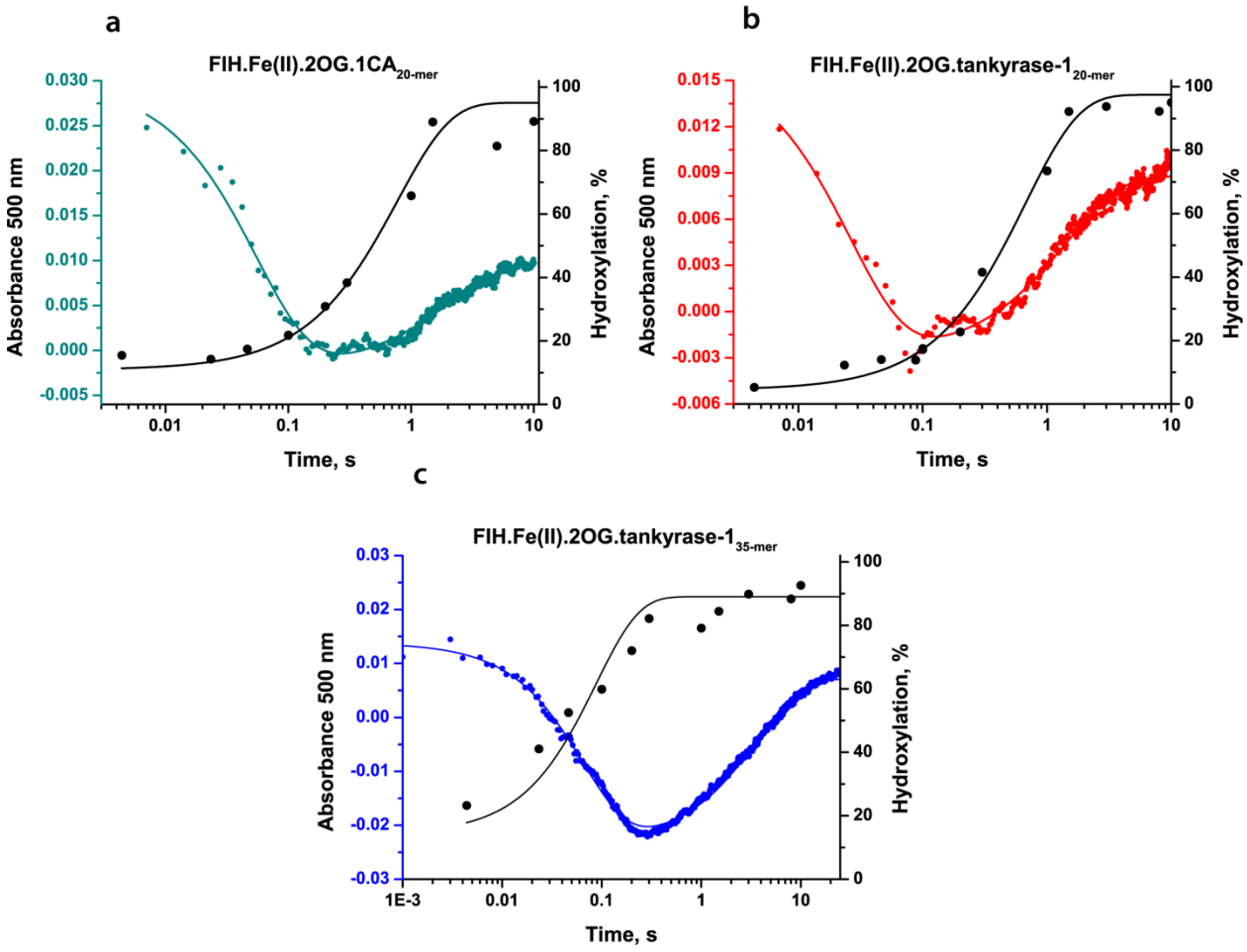


Figure 4.19. Comparison of the rapid quench-flow and stopped-flow experiments for FIH-catalysed ARD hydroxylation, (a) $1CA_{20\text{-mer}}$, (b) $tnkrs\text{-}1_{20\text{-mer}}$, (c) $tnkrs\text{-}1_{35\text{-mer}}$. The reaction mixture containing 0.5 mM apo-FIH, 0.4 mM Fe(II), 5 mM 2OG, 1 mM peptide in 50 mM HEPES (pH 7.5) was rapidly mixed with O_2-saturated buffer in 1:1 ratio and then quenched with 1 % CF_3COOH at defined time points or observed by a photodiode array detector. The hydroxylation levels were assessed by MALDI-TOF-MS and the data were fitted with $y=a\cdot(1-exp(-bx))+c$ function. Rapid quench-flow results are overlaid with kinetic traces at 500 nm.

To investigate the effects of folding of ankyrin repeats on the kinetics of the reaction with oxygen, 1CA was compared to 2CA and 3CA. UV-vis stopped-flow analyses showed that the rate of the absorbance decay at 500 nm decreased with increasing numbers of ankyrin repeats (**Figure 4.20b**, 17.6±0.1 s^{-1}, 11.9±0.2 s^{-1}, 10.5±0.1 s^{-1} for 1CA, 2CA and 3CA, respectively). Similar results were obtained from rapid quench-flow results (**Figure 4.20**). The rate constant

of product accumulation for 1CA hydroxylation was twice as high compared to 2CA (1.3 s^{-1} and 0.48 s^{-1} for 1CA and 2CA, respectively). The rate constant of 3CA hydroxylation showed a ~20–fold decrease (0.051±0.001 s^{-1}) relative to 1CA, indicating that ARD fold stability may be related to this slower reaction with oxygen.

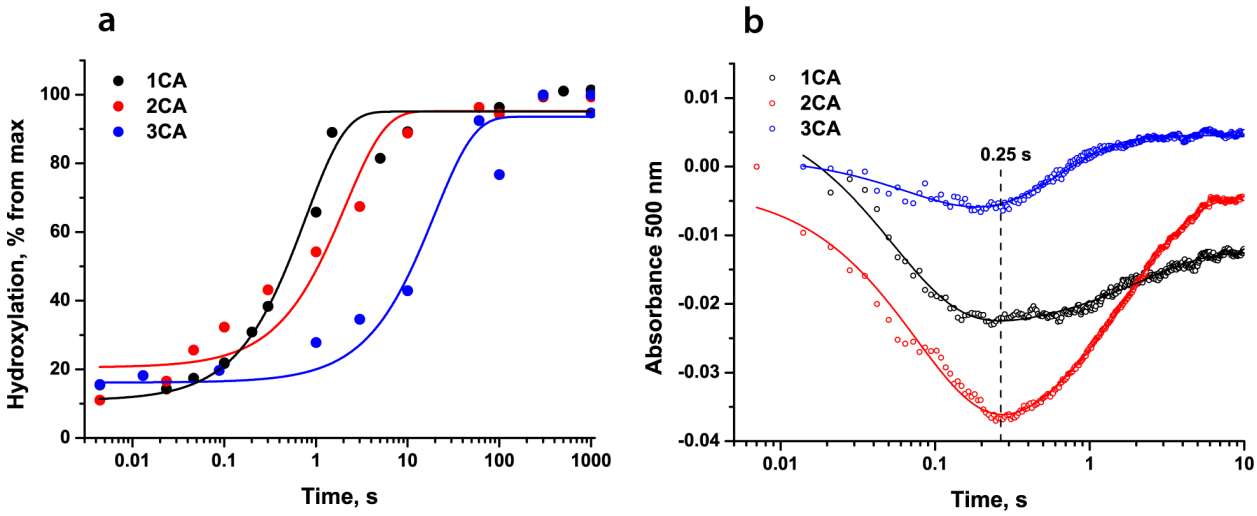


Figure 4.20. Stopped-flow and rapid quench-flow studies of the FIH-catalysed CA hydroxylation. The reaction mixture containing anaerobic 0.5 mM apo-FIH, 0.4 mM Fe(II), 5 mM 2OG and 1 mM ankyrin substrate in 50 mM HEPES (pH 7.5) was rapidly mixed with O_2-saturated buffer in 1:1 ratio at 5 °C and was either observed using a photodiode array detector or rapidly quenched by 1 % CF_3COOH (1CA) or 50 % formic acid. **(a)** Product accumulation time course in rapid quench-flow experiments. The 1CA hydroxylation was analysed by MALDI-TOF-MS; 2CA and 3CA hydroxylation was analysed by protein LC-MS. **(b)** 500 nm decay observed in stopped-flow experiments. The kinetic traces represent the average of triplicate assays.

To investigate whether the observed rates of absorbance decay increase with an increase in substrate concentration, which would suggest that the rate is limited by the peptide binding, the reaction at different FIH:1CA ratios was carried out. Unlike for CAD HIF-$1a_{35\text{-mer}}$, the increase in 1CA did not result in a faster reaction with oxygen, which suggests that binding of ARD peptides is not the limiting factor for the observed rates of the turnover of ARDs (**Figure 4.21**).

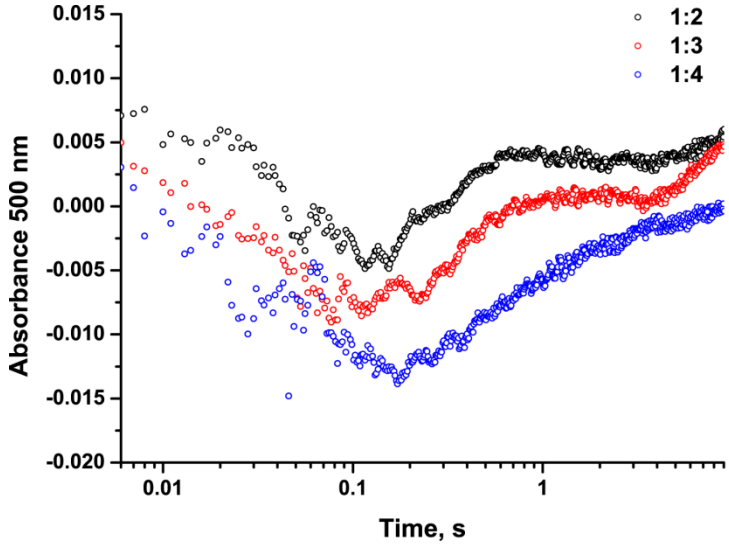


Figure 4.21. Decay at 500 nm representing enzyme-substrate complex depletion in FIH-catalysed 1CA hydroxylation. The reaction mixture containing anaerobic 0.5 mM apo-FIH, 0.4 mM Fe(II), 5 mM 2OG and 1/1.25/1.5 mM peptide in 50 mM HEPES (pH 7.5) was rapidly mixed with O_2-saturated buffer in 1:1 ratio and was observed using a photodiode array detector.

4.3. Discussion

The HIF hydroxylases (PHDs and FIH) are proposed to act as oxygen sensors in cells [29]. While PHD2 exhibits slow oxygen activation of catalysis in its reaction with HIF-α, the FIH reaction with oxygen was significantly faster, with full consumption of the enzyme-substrate complex being observed after ~10 s (approximately 10-fold faster than for PHD2). For both enzymes, accumulation of an Fe(IV)-oxo intermediate was not observed, suggesting that formation and degradation of this reactive species is not rate-limiting for the hydroxylation of HIF-α. Slow oxygen activation of PHD2 and faster reaction of FIH with oxygen were also consistent with lower $K_m(O_2)$ values for FIH compared to PHD2, providing more evidence for establishing a link between a slow pre-steady-state reaction with oxygen and a graded response to changes in oxygen concentration.

PHD2 did not show any substrate-dependent changes in the rate of oxygen activation (PHD2 is known only to hydroxylate HIF-1/2α, and the rates of the reaction with oxygen for these substrates were similar, see Chapter 2). Interestingly however, for FIH oxygen activation appeared to be substrate dependent: FIH reacts much faster with oxygen in the presence of ARD substrates compared to HIF substrates. In addition, further evidence that $K_m(O_2)$ values of FIH are lower with respect to ARD substrates than to HIF substrates was obtained supporting previous observations on Notch1-3 hydroxylation (110±30 μM and 40±10 μM for HIF-1α $CAD_{35\text{-mer}}$ and 1CA respectively) [16]. These observations are of interest from the perspective of understanding the prime biological function of FIH. While FIH is known to be involved in oxygen sensing in cells, the relative importance of its role in ARD hydroxylation is unclear (reviewed in [4]). Taking into account the higher abundance of ARD substrates in cells compared to HIF [30], these results indicate that FIH has a greater potential to hydroxylate ARD substrates under conditions of low oxygen availability. In other words, FIH may not act as an oxygen sensor with respect to ARD hydroxylation. Overall, the substrate dependence of the FIH reaction with oxygen poses a question of whether oxygen sensing is its primary biological function.

It was also observed that the secondary structure of FIH substrates affects the rate of its reaction with oxygen. Previous studies have suggested that while for HIF-α the secondary structure does not affect the efficiency of FIH-catalysed hydroxylation, for ARDs, unfolding

of the substrate prior to hydroxylation is required [11, 12]. It has been proposed that the difference in the efficiency of FIH-catalysed ARD hydroxylation is related to the stability of the protein fold [5]. Thus, four consensus ankyrin repeats are not hydroxylated by FIH, while 3CA is still a substrate [5]. On the other hand, Notch and Iκβα contain >6 ARD and are known to be efficient substrates for FIH [11, 16], including in cells [31]. Thus, the number of repeats in an ARD protein does not necessarily correlate with the hydroxylation efficiency, which is more related to local stability of the hydroxylated region. The observation that ARD folding affects FIH catalysis is in agreement with the observations described in this Chapter, where a slower reaction with a folded ankyrin substrate was observed. It suggests that the unfolding step, which occurs prior to hydroxylation, may be part of the enzymatic mechanism (i.e. may occur after oxygen delivery) and have some impact on the kinetics of the ARD hydroxylation.

In conclusion, the mechanistic studies on the FIH reaction with oxygen revealed interesting features characteristic of catalysis by this enzyme. Although FIH is faster in its reaction with oxygen, it is more similar to PHD2 rather than to other studied 2OG oxygenases in terms of the rate-limiting steps of the reaction. However, the observed influence of enzyme-substrate interactions on the oxygen affinity to FIH suggests that further biological studies, beyond the scope of the work described in this thesis, are required to identify a prime physiological function of FIH. It is also suggests that the proposal that FIH acts as a cellular oxygen sensor should be reviewed.

4.4. References

1. McNeill, L.A., K.S. Hewitson, T.D. Claridge, J.F. Seibel, L.E. Horsfall, and C.J. Schofield (2002) *Hypoxia-inducible factor asparaginyl hydroxylase (FIH-1) catalyses hydroxylation at the beta-carbon of asparagine-803.* Biochem. J. **367**, 571-575.
2. Lando, D., D.J. Peet, D.A. Whelan, J.J. Gorman, and M.L. Whitelaw (2002) *Asparagine Hydroxylation of the HIF Transactivation Domain: A Hypoxic Switch.* Science **295**, 858-861.
3. Mahon, P.C., K. Hirota, and G.L. Semenza (2001) *FIH-1: a novel protein that interacts with HIF-1α and VHL to mediate repression of HIF-1 transcriptional activity.* Genes Dev. **15**, 2675-2686.
4. Cockman, M.E., J.D. Webb, and P.J. Ratcliffe (2009) *FIH-dependent asparaginyl hydroxylation of ankyrin repeat domain-containing proteins.* Ann. N Y Acad. Sci. **1177**, 9-18.
5. Kelly, L., M.A. McDonough, M.L. Coleman, P.J. Ratcliffe, and C.J. Schofield (2009) *Asparagine beta-hydroxylation stabilizes the ankyrin repeat domain fold.* Mol. Biosyst. **5**, 52-58.
6. Hardy, A.P., I. Prokes, L. Kelly, I.D. Campbell, and C.J. Schofield (2009) *Asparaginyl beta-hydroxylation of proteins containing ankyrin repeat domains influences their stability and function.* J. Mol. Biol. **392**, 994-1006.
7. Webb, J.D., A. Muranyi, C.W. Pugh, P.J. Ratcliffe, and M.L. Coleman (2009) *MYPT1, the targeting subunit of smooth-muscle myosin phosphatase, is a substrate for the asparaginyl hydroxylase factor inhibiting hypoxia-inducible factor (FIH).* Biochem. J. **420**, 327-33.
8. Liu, Y., H. Higashitsuji, K. Itoh, T. Sakurai, K. Koike, K. Hirota, M. Fukumoto, and J. Fujita (2013) *Overexpression of gankyrin in mouse hepatocytes induces hemangioma by suppressing factor inhibiting hypoxia-inducible factor-1 (FIH-1) and activating hypoxia-inducible factor-1.* Biochem. Biophys. Res. Commun. **432**, 22-7.
9. Yang, M., A.P. Hardy, R. Chowdhury, N.D. Loik, J.S. Scotti, J.S. McCullagh, T.D. Claridge, M.A. McDonough, W. Ge, and C.J. Schofield (2013) *Substrate selectivity analyses of factor inhibiting hypoxia-inducible factor.* Angew. Chem. Int. Ed. **52**, 1700-1704.
10. Yang, M., R. Chowdhury, W. Ge, R.B. Hamed, M.A. McDonough, T.D. Claridge, B.M. Kessler, M.E. Cockman, P.J. Ratcliffe, and C.J. Schofield (2011) *Factor-inhibiting hypoxia-inducible factor (FIH) catalyses the post-translational hydroxylation of histidinyl residues within ankyrin repeat domains.* FEBS J. **278**, 1086-1097.
11. Wilkins, S.E., S. Karttunen, R.J. Hampton-Smith, I. Murchland, A. Chapman-Smith, and D.J. Peet (2012) *Factor inhibiting HIF (FIH) recognizes distinct molecular features within hypoxia-inducible factor-α (HIF-α) versus ankyrin repeat substrates.* J. Biol. Chem. **287**, 8769-8781.
12. Coleman, M.L., M.A. McDonough, K.S. Hewitson, C. Coles, J. Mecinović, M. Edelmann, K.M. Cook, M.E. Cockman, D.E. Lancaster, B.M. Kessler, N.J. Oldham, P.J. Ratcliffe, and C.J. Schofield (2007) *Asparaginyl Hydroxylation of the Notch Ankyrin Repeat Domain by Factor Inhibiting Hypoxia-inducible Factor.* J. Biol. Chem. **282**, 24027-24038.

13. Elkins, J.M., K.S. Hewitson, L.A. McNeill, J.F. Seibel, I. Schlemminger, C.W. Pugh, P.J. Ratcliffe, and C.J. Schofield (2003) *Structure of Factor-inhibiting Hypoxia-inducible Factor (HIF) Reveals Mechanism of Oxidative Modification of HIF-1α.* J. Biol. Chem. **278**, 1802-1806.
14. Freedman, S.J., Z.-Y.J. Sun, F. Poy, A.L. Kung, D.M. Livingston, G. Wagner, and M.J. Eck (2002) *Structural basis for recruitment of CBP/p300 by hypoxia-inducible factor-1α.* Proc. Natl. Acad. Sci. U. S. A. **99**, 5367-5372.
15. Dames, S.A., M. Martinez-Yamout, R.N. De Guzman, H.J. Dyson, and P.E. Wright (2002) *Structural basis for Hif-1α/CBP recognition in the cellular hypoxic response.* Proc. Natl. Acad. Sci. U. S. A. **99**, 5271-5276.
16. Wilkins, S.E., J. Hyvarinen, J. Chicher, J.J. Gorman, D.J. Peet, R.L. Bilton, and P. Koivunen (2009) *Differences in hydroxylation and binding of Notch and HIF-1alpha demonstrate substrate selectivity for factor inhibiting HIF-1 (FIH-1).* Int. J. Biochem. Cell Biol. **41**, 1563-1571.
17. Loboda, A., A. Jozkowicz, and J. Dulak (2012) *HIF-1 versus HIF-2 — Is one more important than the other?* Vasc. Pharmacol. **56**, 245-251.
18. Ehrismann, D., E. Flashman, D.N. Genn, N. Mathioudakis, K.S. Hewitson, P.J. Ratcliffe, and C.J. Schofield (2007) *Studies on the activity of the hypoxia-inducible-factor hydroxylases using an oxygen consumption assay.* Biochem. J. **401**, 227-234.
19. Koivunen, P., M. Hirsila, V. Gunzler, K.I. Kivirikko, and J. Myllyharju (2004) *Catalytic properties of the asparaginyl hydroxylase (FIH) in the oxygen sensing pathway are distinct from those of its prolyl 4-hydroxylases.* J. Biol. Chem. **279**, 9899-9904.
20. Hausinger, R.P. (2004) *Fe(II)/α-Ketoglutarate-Dependent Hydroxylases and Related Enzymes.* Crit. Rev. Biochem. Mol. Biol. **39**, 21-68.
21. Pavel, E.G., J. Zhou, R.W. Busby, M. Gunsior, C.A. Townsend, and E.I. Solomon (1998) *Circular dichroism and magnetic circular dichroism spectroscopic studies of the non-heme ferrous active site in clavaminate synthase and its interaction with α-ketoglutarate cosubstrate.* J. Am. Chem. Soc. **120**, 743-753.
22. Flagg, S.C., N. Giri, S. Pektas, M.J. Maroney, and M.J. Knapp (2012) *Inverse Solvent Isotope Effects Demonstrate Slow Aquo Release from Hypoxia Inducible Factor-Prolyl Hydroxylase (PHD2).* Biochemistry **51**, 6654-6666.
23. Price, J.C., E.W. Barr, B. Tirupati, J.M. Bollinger, Jr., and C. Krebs (2003) *The first direct characterization of a high-valent iron intermediate in the reaction of an α-ketoglutarate-dependent dioxygenase: a high-spin FeIV complex in taurine/α-ketoglutarate dioxygenase (TauD) from Escherichia coli.* Biochemistry **42**, 7497-7508.
24. Price, J.C., E.W. Barr, L.M. Hoffart, C. Krebs, and J.M. Bollinger, Jr. (2005) *Kinetic dissection of the catalytic mechanism of taurine: α-ketoglutarate dioxygenase (TauD) from Escherichia coli.* Biochemistry **44**, 8138-8147.
25. Hoffart, L.M., E.W. Barr, R.B. Guyer, J.M. Bollinger, Jr., and C. Krebs (2006) *Direct spectroscopic detection of a C-H-cleaving high-spin Fe(IV) complex in a prolyl-4-hydroxylase.* Proc. Natl. Acad. Sci. U. S. A. **103**, 14738-14743.
26. Galonić, D.P., E.W. Barr, C.T. Walsh, J.M. Bollinger, and C. Krebs (2007) *Two interconverting Fe(IV) intermediates in aliphatic chlorination by the halogenase CytC3.* Nat. Chem. Biol. **3**, 113-116.

27. Matthews, M.L., C.M. Krest, E.W. Barr, F.d.r.H. Vaillancourt, C.T. Walsh, M.T. Green, C. Krebs, and J.M. Bollinger (2009) *Substrate-triggered formation and remarkable stability of the C−H bond-cleaving chloroferryl Intermediate in the aliphatic halogenase, SyrB2.* Biochemistry **48**, 4331-4343.
28. Flashman, E., L.M. Hoffart, R.B. Hamed, J.M. Bollinger, Jr., C. Krebs, and C.J. Schofield (2010) *Evidence for the slow reaction of hypoxia-inducible factor prolyl hydroxylase 2 with oxygen.* FEBS J. **277**, 4089-4099.
29. Tian, Y.-M., K.K. Yeoh, M.K. Lee, T. Eriksson, B.M. Kessler, H.B. Kramer, M.J. Edelmann, C. Willam, C.W. Pugh, C.J. Schofield, and P.J. Ratcliffe (2011) *Differential Sensitivity of Hypoxia Inducible Factor Hydroxylation Sites to Hypoxia and Hydroxylase Inhibitors.* J. Biol. Chem. **286**, 13041-13051.
30. Schultz, J., F. Milpetz, P. Bork, and C.P. Ponting (1998) *SMART, a simple modular architecture research tool: Identification of signaling domains.* Proc. Natl. Acad. Sci. U. S. A. **95**, 5857-5864.
31. Cockman, M.E., D.E. Lancaster, I.P. Stolze, K.S. Hewitson, M.A. McDonough, M.L. Coleman, C.H. Coles, X. Yu, R.T. Hay, S.C. Ley, C.W. Pugh, N.J. Oldham, N. Masson, C.J. Schofield, and P.J. Ratcliffe (2006) *Posttranslational hydroxylation of ankyrin repeats in IκB proteins by the hypoxia-inducible factor (HIF) asparaginyl hydroxylase, factor inhibiting HIF (FIH).* Proc. Natl. Acad. Sci. U. S. A. **103**, 14767-14772.

Chapter 5: Mechanistic studies on DAOCS-catalysed ring expansion of penicillin N*

5.1. Introduction

Deacetoxycephalosporin synthase (DAOCS) catalyses the penicillin N (penN) ring expansion to give deacetoxycephalosporin C (DAOC) in prokaryotes (see Chapter 1, Section 1.3) [1-4]. A crystal structure of recombinant DAOCS from *S. clavuligerus* was the first of a 2OG oxygenase to be reported [5]. Subsequent structures of DAOCS in complex with its co-substrate (2OG), penicillins (penG, ampicillin) and byproduct (succinate) were reported [6-8]. The overall folding of DAOCS and its interaction with 2OG are consistent with structures of other 2OG oxygenases [9, 10].

Interestingly, DAOCS occurs in solution predominantly in monomeric form, however it crystallises as a homotrimer. The trimeric oligomerisation results in a partial blockage of the access to the active site due to penetration of the *C*-terminus of one DAOCS molecule to the active site (of the same molecule), thus complicating formation of the complexes of DAOCS with penicillin substrates [5, 7, 11] (**Figure 5.1**). However, crystal structures of the DAOCS complexes with penG and ampicillin were reported in 2004 [8]. These structures revealed interesting binding orientations (more than one) of the penicillin substrates, where their binding sites were overlapping with the 2OG or succinate binding sites. The penicillin binding modes obtained by soaking of the apo-DAOCS crystals first with Fe(II) and then with penicillin substrate, were different from those obtained only in the presence of 2OG. However, in all cases the binding site of penicillin was overlapping with 2OG binding. In addition, steady-state kinetic studies using UV spectrophotometry showed inhibition at high substrate concentrations by both penG and 2OG [8]. Based on these observations, a novel mechanism has been proposed, predicting release of succinate and formation of a stable

· Part of the work described in this Chapter has been published in Tarhonskaya, H., Szöllössi, A., Leung, I.K.H., Bush, J.T., Henry, L., Chowdhury, R., Iqbal, A., Claridge, T.D.W., Schofield, C.J., Flashman E. (2014) *Studies on Deacetoxycephalosporin C Synthase Support a Consensus Mechanism for 2-Oxoglutarate Dependent Oxygenases.* Biochemistry **53**, 2483-2493.

Fe(IV)-oxo intermediate prior to penicillin binding ('ping-pong' mechanism, **Figure 5.2**) [8]. This mechanism was unprecedented in 2OG oxygenase catalysis.

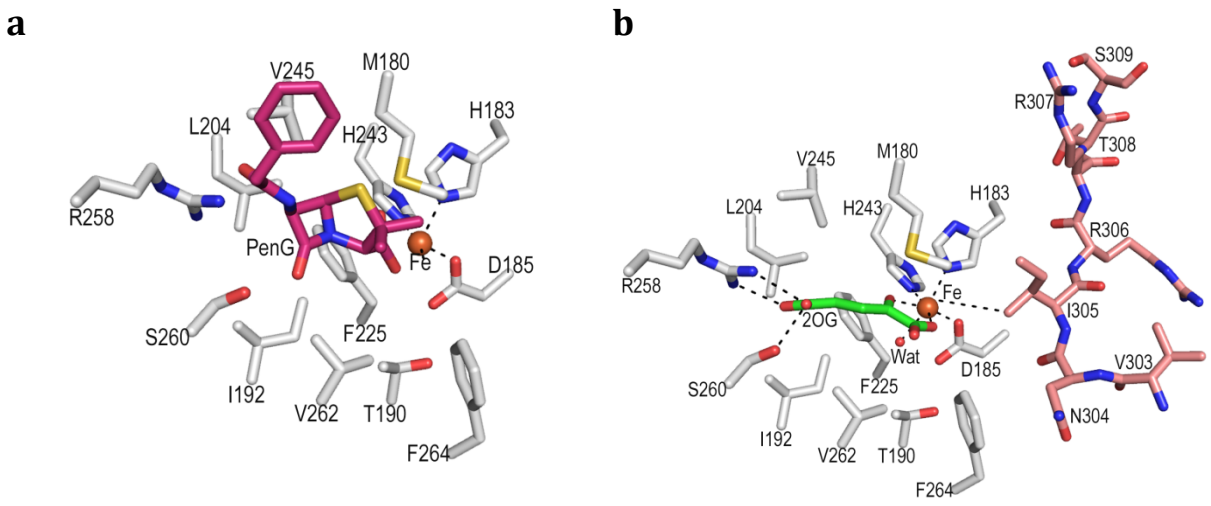


Figure 5.1. View from crystal structures of DAOCS in complex with Fe(II) and penG/2OG. (a) View from a DAOCS structure in complex with Fe(II) and penG (PDB: 1UOF, *H*3 space group) [8]; **(b)** DAOCS structure in complex with Fe(II) and 2OG (PDB: 1RXG) showing how the monomer *C*-terminus protrudes into the active site. The figure was provided by R. Chowdhury.

NMR and mass spectrometry experiments on DAOCS were previously carried out in the Schofield group (by Andrea Szöllössi) [12]. These showed the possibility of ternary complex (DAOCS.Fe(II).2OG.penicillin) formation during the DAOCS-catalysed reaction (in contrast to the proposed mechanism described above [8]). Using [^{13}C]-labeled penG and [^{13}C]-2OG it was shown that no (co-)substrate displacement occurs during addition of penG to DAOCS.Zn(II).[^{13}C]-2OG or 2OG to the mixture of DAOCS.Zn(II) with [^{13}C]-penG. In addition, by determination of the binding constants for different ligands (binding to a DAOCS.Mn(II) complex) in the presence or absence of 2OG, it was shown that the natural substrate penN is a much stronger binder compared to the unnatural substrate penG. No penG or penN binding to the DAOCS.Mn(II) complex in the absence of 2OG was observed within the limits of detection. Simultaneous observation (by NMR) of succinate formation and penicillin ring expansion showed that penG turnover is shifted towards uncoupled reaction at low penG concentrations, while penN ring expansion is fully coupled to 2OG oxidative decarboxylation [12].

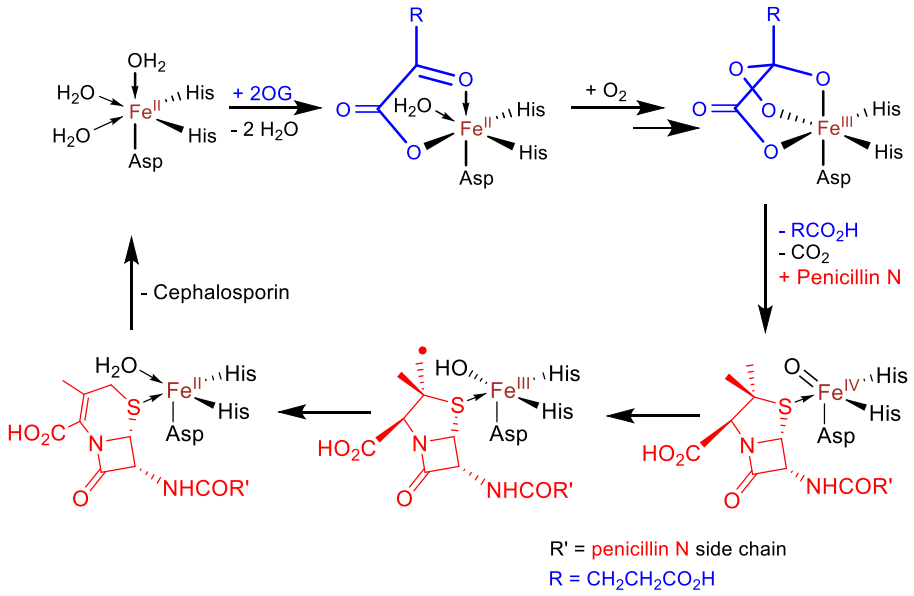


Figure 5.2. The outline of the proposed 'ping-pong' mechanism for DAOCS. Binding of dioxygen to DAOCS.Fe(II).2OG complex occurs with subsequent formation of an Fe(IV)-oxo species, and release of succinate and CO_2 followed by penicillin binding [8].

Thus, the contradiction of different experimental studies, as well as the significant difference of the proposed 'ping-pong' mechanism from that of the consensus 2OG oxygenases suggested that the DAOCS mechanism requires further investigation. The work described in this Chapter focuses on binding and kinetic studies on DAOCS aiming to determine its mechanism.

5.2. Results·

5.2.1. Non-denaturing mass spectrometry studies of a ternary complex formation

Recombinant DAOCS from *S. clavuligerus*, cloned into pet-24a(+) vector, was produced in *E. coli* BL21(DE3) strain in 2 TY medium with induction by 1 mM IPTG (28 °C, 4 h) in the presence of kanamycin (see *Materials and Methods*, Section 7.9 for more details). The enzyme was purified using anion exchange chromatography followed by a size exclusion step [13]. The elution of DAOCS during size exclusion chromatography resulted in up to 90 % pure protein (as shown by SDS-PAGE); however, higher purity was not achieved, likely due to the formation of enzyme aggregates leading to decreased yields (**Figure 5.3)**.

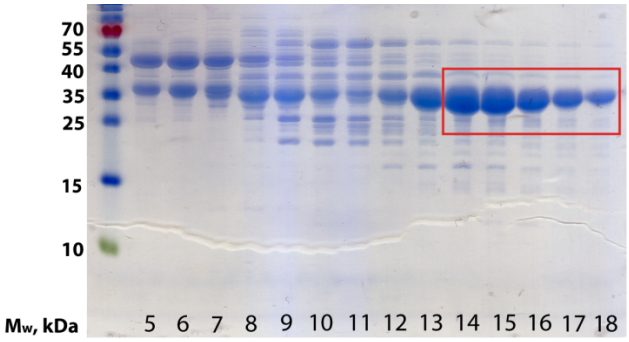


Figure 5.3. Purification of DAOCS. SDS-PAGE gel obtained after size exclusion purification step. 5-18 are fractions obtained after size-exclusion purification step. Fractions in the red frame were selected for further assays.

To investigate formation of an enzyme-substrate complex, non-denaturing ESI-MS studies were first carried out. As a prelude, the metal binding to apo-DAOCS was studied. Titration of DAOCS with Fe(II) showed, that addition of more than 2 equivalents of Fe(II) leads to multiple iron binding **(Figure 5.4a)** (most likely in a non-specific manner), while one equivalent of Fe(II) was not sufficient to convert all apo-DAOCS to the DAOCS.Fe(II) complex, and instead resulted in formation of apo-DAOCS and DAOCS.Fe(II) peaks with almost equivalent intensities. Increasing the cone voltage sould decrease the stability of the complexes, thus one would expect to observe reduced metal binding (including reduced non-specific interactions) and binding of only one equivalent of iron(II) ion to DAOCS with increased cone voltage. However, changes in the cone voltage from 80 V to 120 V did not

· Penicillin N used in these studies was synthesised by Jacob T. Bush (University of Oxford, Schofield group).

affect the multiple metal binding pattern in the case of DAOCS. The ratio of 2 equivalents of Fe(II) relative to apo-DAOCS was chosen for further experiments, because under these conditions the maximum intensity of the DAOCS.Fe(II) complex peak relative to the apo-DAOCS peak was observed (**Figure 5.4a**).

Next, 2OG binding was studied. Addition of 2OG to the DAOCS.Fe(II) resulted in formation of an extra peak, with a mass corresponding to the DAOCS.Fe(II).2OG complex (**Figure 5.4b**). Titration experiments showed that a 5-fold excess of 2OG was required for efficient formation of a DAOCS.Fe(II).2OG complex, while further increasing the 2OG concentration led to a decrease in quality of the spectra. In contrast to Fe(II), multiple binding for 2OG was not observed.

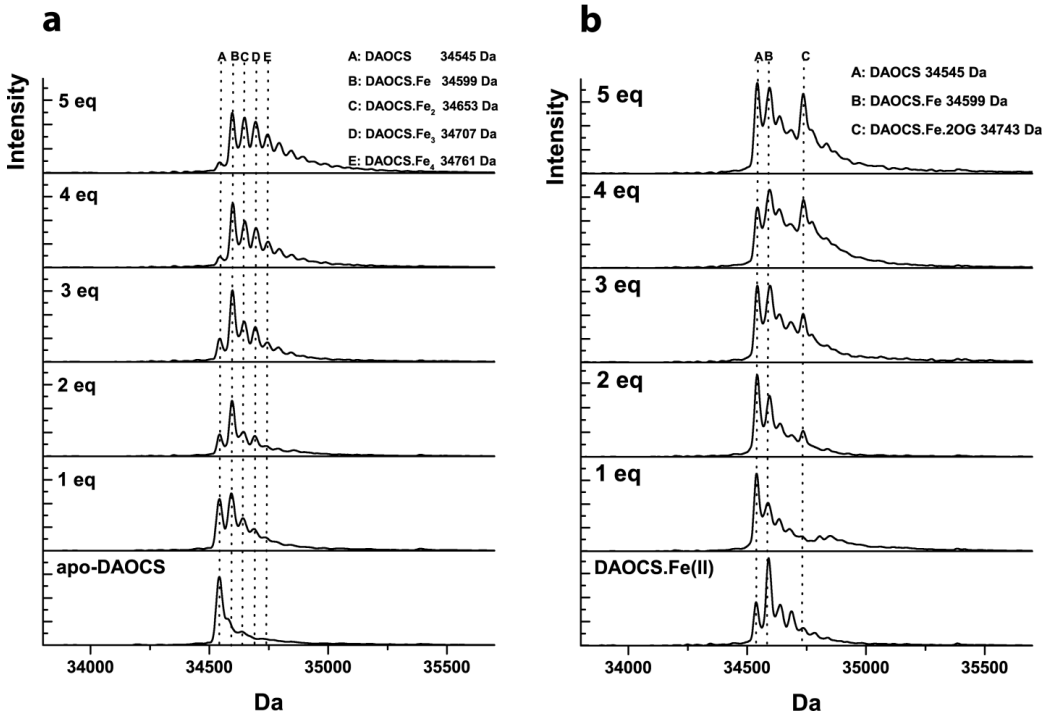


Figure 5.4. Deconvoluted non-denaturing MS spectra showing formation of the DAOCS complex with (a) Fe(II) and (b) 2OG. (a) Conditions: 15 µM DAOCS in 15 mM ammonium acetate buffer (pH 7.5) was mixed with different ratio of Fe(II); cone voltage was 80 V (increasing or decreasing the cone voltage did not affect the number of peaks present in a spectrum). A – DAOCS (34545 Da), B – DAOCS.Fe(II) (34599 Da), C – DAOCS.2Fe(II) (34653 Da), D – DAOCS.3Fe(II) (34707 Da), E – DAOCS.4Fe(II) (34761 Da). 1 equivalent of Fe(II) does not result in disappearance of the apo-DAOCS peak. **(b)** Conditions: 15 µM of DAOCS in 15 mM ammonium acetate buffer (pH 7.5) was mixed with 30 µM of Fe(II) and different concentrations of 2OG; cone voltage: 60 V. A – DAOCS (34545 Da), B – DAOCS.Fe(II) (34599 Da), C – DAOCS.Fe(II).2OG (34743 Da). Figure and figure legend are adapted with permission from Tarhonskaya *et al.* (2014) Biochemistry **53**, 2483-2493 [14]. Copyright (2014) American Chemical Society.

To study penicillin binding, inhibition of catalysis was required. Thus, Fe(II) was substituted with catalytically inactive Mn(II) and Zn(II) at a 1:2 DAOCS to metal ratio. Mn(II) showed weaker intensity of DAOCS.metal(II) complex compared to Fe(II), while Zn(II) was a much stronger binder with no apo-enzyme peak observed in its presence (**Figure 5.5**). Again in all cases multiple metal binding was observed.

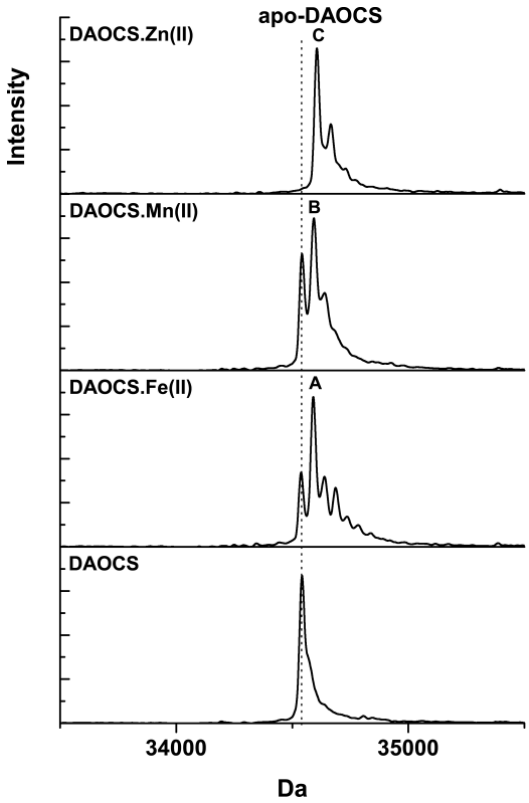


Figure 5.5. Deconvoluted non-denaturing MS spectra showing formation of DAOCS complexes with different metals. Conditions: 15 µM of DAOCS in 15 mM ammonium acetate buffer (pH 7.5) was mixed with 30 µM of Fe(II)/Mn(II)/Zn(II) (1:2 ratio); cone voltage: 80 V. The most stable complex was observed with Zn(II), however, the presence of multiple binding of metal-ions was apparent in all cases. A – DAOCS.Fe(II), B – DAOCS.Mn(II), C - DAOCS.Zn(II). Figure and figure legend are adapted with permission from Tarhonskaya *et al.* (2014) Biochemistry **53**, 2483-2493 [14]. Copyright (2014) American Chemical Society.

As an alternative method to prevent penicillin turnover when trying to observe a full DAOCS.substrate complex, the 2OG analogue inhibitor, *N*-oxalylglycine (NOG) was used. NOG showed stronger binding to the DAOCS.Fe(II) complex compared with 2OG, with only 1 equivalent required for sufficient complex formation (**Figure 5.6a**) compared to 5 equivalents for 2OG (**Figure 5.4b**).

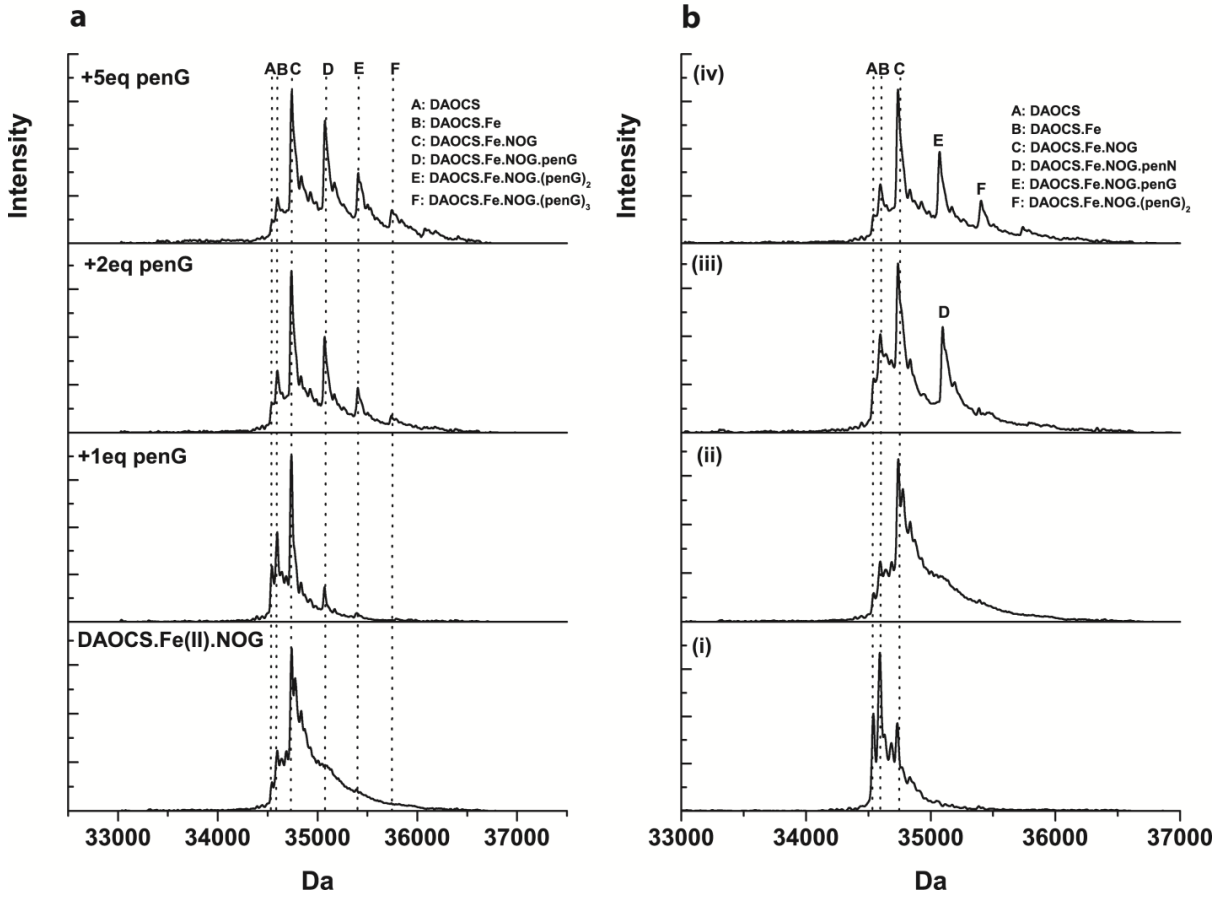


Figure 5.6. Deconvoluted non-denaturing MS spectra showing formation of ternary complexes of DAOCS with Fe(II), NOG and penG. Conditions: the ratio of DAOCS:Fe(II):NOG was 1:2:1 (1 equivalent - 15 μM), cone voltage was 60 V. **(a)** Titration of penG into the assay mixture containing DAOCS:Fe(II):NOG complex. A – DAOCS (34545 Da), B – DAOCS.Fe(II) (34599 Da), C – DAOCS.Fe(II).NOG (34746 Da), D – DAOCS.Fe(II).NOG.penG (35078 Da), E – DAOCS.Fe(II).NOG.2penG (35411 Da), F – DAOCS.Fe(II).2OG.3penG (35744 Da). Non-specific binding of more than 1 molecule of penG is apparent. **(b)** Binding of penN and penG to DAOCS:Fe(II):NOG complex. Conditions: the ratio of DAOCS:Fe(II):NOG:penG/penN was 1:2:1:2 (1 equivalent - 15 μM), cone voltage was 60 V. (i) DAOCS, Fe(II); (ii) DAOCS, Fe(II), NOG; (iii) DAOCS, Fe(II), NOG, penG; (iv) DAOCS, Fe(II), NOG, penN. (A – DAOCS (34545 Da), B – DAOCS.Fe(II) (34599 Da), C – DAOCS.Fe(II).NOG (34745 Da), D – DAOCS.Fe(II).NOG.penN (35105 Da), E – DAOCS.Fe(II).NOG.penG (35078 Da), F – DAOCS.Fe(II).NOG.2penG (35411 Da)). Figure and figure legend are adapted with permission from Tarhonskaya *et al.* (2014) Biochemistry **53**, 2483-2493 [14]. Copyright (2014) American Chemical Society.

Binding of penG (an analogue of the natural substrate, penN) and penN to the DAOCS.Fe(II).NOG complex was also examined. At a 2-fold excess of penG or penN (relative to DAOCS), the formation of a peak corresponding to the mass of a ternary DAOCS.Fe(II).NOG.penicillin complex (**Figure 5.4b**) was observed. At higher concentrations of penG, but not penN, additional peaks corresponding to multiple molecules

of penG binding were apparent, which probably represent non-specific/catalytically non-productive binding (**Figure 5.6a**). This is consistent with previously reported substrate inhibition by penG in the DAOCS-catalysed reaction [8].

5.2.2. Presence of a substrate results in a shift of MLCT absorbance maximum

UV-vis spectroscopy was then employed to study ternary complex formation [15]. Under anaerobic conditions 2OG oxygenases usually show MLCT features, centered in the 500 nm region, which represent the interaction of Fe(II) with 2OG in the enzyme.Fe(II).2OG complex (as described in previous chapters). Formation of broad absorbance features was apparent after addition of Fe(II) to an anaerobic solution containing DAOCS and 2OG (λ_{max}=523 nm). Addition of 2OG to DAOCS prior to Fe(II) did not result in the appearance of an MLCT feature. Plotting an absorbance at λ_{max} versus concentration allowed determination of the Fe(II)/DAOCS complex ratio and K_d(Fe(II)). Saturation of Fe(II) binding was achieved at 0.73 Fe(II)/DAOCS complex ratio, which is similar to previously reported values for TauD [16, 17]. The determined K_d(Fe(II)) was 5.0±3.7 μM (**Figure 5.7**).

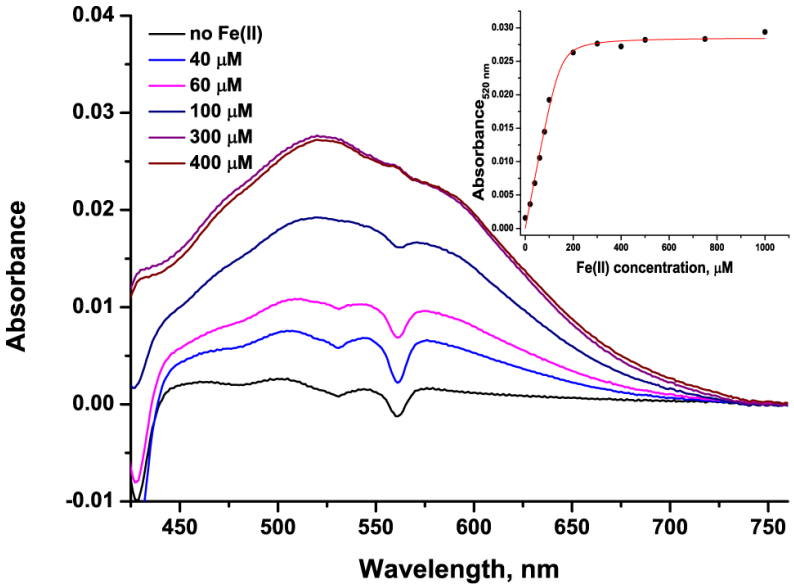


Figure 5.7. UV-vis spectra showing formation of a DAOCS.Fe(II).2OG complex. Formation of MLCT features was observed with maxima at 520 nm. Conditions: 200 μM DAOCS in 50 mM HEPES (pH 7.5) was mixed with 1 mM 2OG under anaerobic conditions and titrated with Fe(II). The inset shows absorbance at 520 nm plotted as a function of Fe(II) concentration and analysis of the dependence allowed determination of K_d(Fe(II))=5.0±3.7 μM. Figure and figure legend are adapted with permission from Tarhonskaya *et al.* (2014) Biochemistry **53**, 2483-2493 [14]. Copyright (2014) American Chemical Society.

The influence of substrate binding on the position of the MLCT maximum of the DAOCS.Fe(II).2OG complex was also studied to assess whether the observed penG/N binding occurred in the active site region in solution (binding of a 'prime' substrate triggers a 10 nm shift in λ_{max}, see Chapters 1,3). Addition of penG resulted in a slight shift of the maximum from λ_{max}=523 nm to 519 nm. In contrast, binding of penN resulted in a clear shift of the maximum to 514 nm (**Figure 5.8**). This shift is similar to those observed upon a 'prime' substrate binding to other 2OG oxygenases (e.g. from 530 nm to 520 nm for TauD) [15], and is usually associated with a change from six-coordinate to five-coordinate Fe(II) state [16]. Thus the UV-vis spectroscopy studies were consistent with the ESI-MS and NMR studies and they supported the proposal that both penN and penG can bind to the DAOCS.Fe(II).2OG complex in the active site region, but the latter binds much more weakly [14].

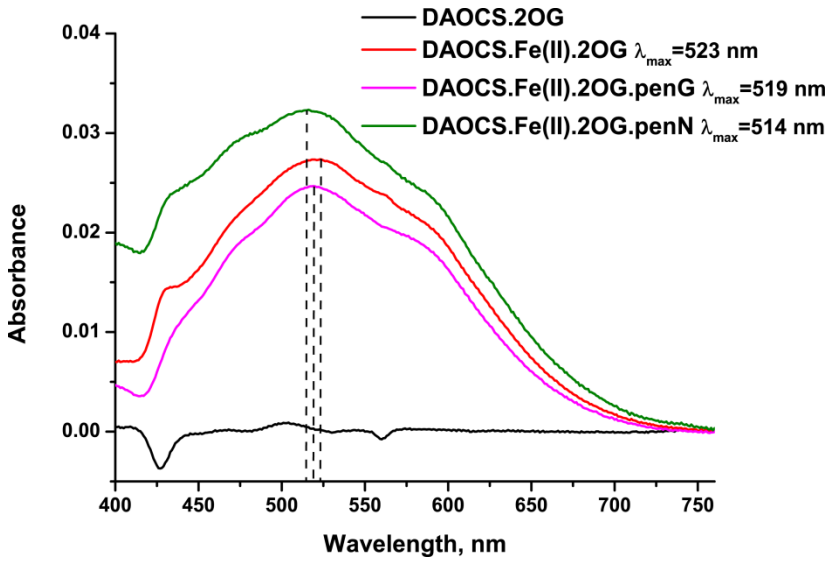


Figure 5.8. UV-vis spectra showing formation of DAOCS.Fe(II).2OG and DAOCS.Fe(II).2OG.penicillin G/N complexes. Formation of MLCT features was observed with maxima at ~520 nm. Conditions: 200 µM DAOCS in 50 mM HEPES (pH 7.5) was mixed with 1 mM 2OG, 200 µM Fe(II) and 2 mM penG/penN under anaerobic conditions. A shift of the MLCT feature maxima was observed upon addition of penicillin substrates indicating a change in Fe(II) coordination. Figure and figure legend are adapted with permission from Tarhonskaya *et al.* (2014) Biochemistry **53**, 2483-2493 [14]. Copyright (2014) American Chemical Society.

5.2.3. Stopped-flow kinetic studies on the DAOCS-catalysed reaction

The proposed 'ping-pong' mechanism for DAOCS (**Figure 5.2**) suggests that binding of the penicillin substrate to the DAOCS.Fe(IV)-oxo intermediate occurs after the release of

succinate from the active site [8]. Thus, one may expect observation of a stable Fe(IV)-oxo intermediate by UV-vis spectroscopy. Moreover, the intermediate formation should not be affected by the presence or absence of the penicillin substrates. To investigate this, stopped-flow UV-vis spectroscopy studies were carried out. Anaerobically prepared mixtures of DAOCS, Fe(II), 2OG with and without penN/penG were rapidly mixed with O_2-free/O_2-saturated buffer, and the reaction was observed using a photodiode array detector at 5 °C. The data were processed as described in *Materials and Methods* and the previous Chapters.

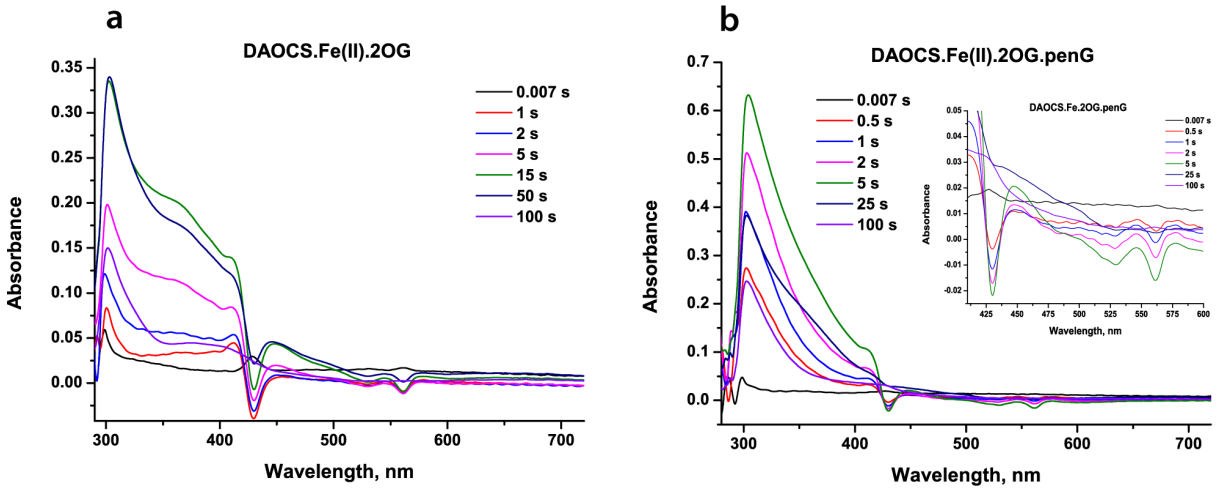


Figure 5.9. Stopped-flow UV-vis time courses. (a) Uncoupled DAOCS-catalysed turnover; **(b)** penG ring expansion (the inset represents 500 nm region). Conditions: anaerobically prepared mixture of (a) 0.8 mM DAOCS in 50 mM HEPES (pH 7.5), 0.7 mM Fe(II), 5 mM 2OG, and (b) 0.8 mM DAOCS in 50 mM HEPES (pH 7.5), 0.7 mM Fe(II), 5 mM 2OG, 1 mM penG was rapidly mixed with O_2-free/O_2-saturated buffer. Difference spectra are presented. Formation and degradation of absorbance species with maximum at 310 nm was apparent as previously observed for other 2OG oxygenases (at 318 nm [16]). Figure and figure legend are adapted with permission from Tarhonskaya *et al.* (2014) Biochemistry **53**, 2483-2493. [14]. Copyright (2014) American Chemical Society.

Consistent with previous pre-steady-state studies on 2OG oxygenases, a transient species centered at 310 nm (318 in the studies on the TauD-catalysed reaction [16]) was observed in the reaction of DAOCS.Fe(II).2OG.penG/penN complexes with O_2-saturated buffer, which was not apparent in the absence of oxygen [16-18]. Thus, the differences between spectra representing the reaction after mixing with O_2-free and O_2-saturated buffer were analysed (**Figure 5.9**). Formation of an absorbance decay feature was observed in the 500 nm region, again consistent with previous kinetic studies on 2OG oxygenases (**Figure 5.9, inset**) [16-20]. The 310 nm species was apparent with a maximum time of accumulation of 2 s (penN), 10 s

(penG) and 25 s (uncoupled turnover). To investigate whether the 310 nm species may represent oxidation of free iron(II) in solution, control experiments with Fe(II) and Fe(II)/2OG were carried out. An increase in absorbance due to the oxidation of free Fe(II) to Fe(III) was not observed on the same time scale as formation of the 310 nm species (**Figure 5.10**).

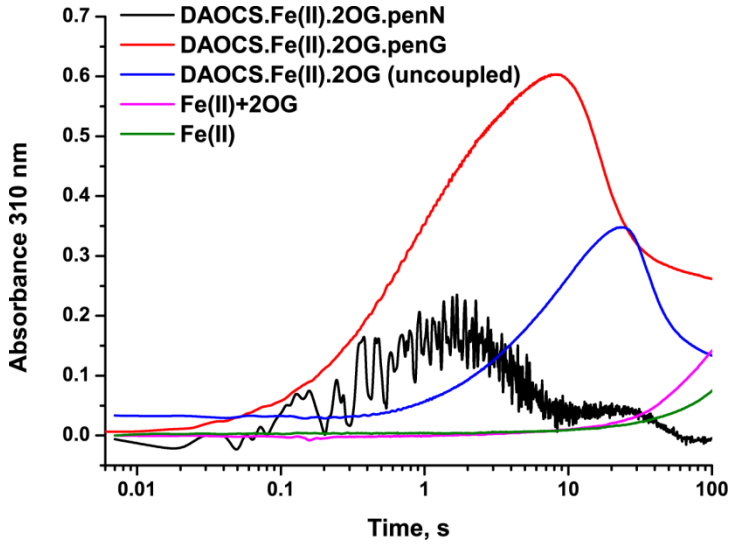


Figure 5.10. Stopped-flow kinetic traces showing changes in absorbance at 310 nm. Conditions: anaerobically prepared mixture of 0.8 mM DAOCS in 50 mM HEPES (pH 7.5), 0.7 mM Fe(II), 5 mM 2OG and 1 mM penG/penN (if present) was rapidly mixed with O_2-free/O_2-saturated buffer. Difference spectra were analysed. Changes in absorbance in non-enzyme controls show that observed transient species likely represent enzymatic reaction. Figure and figure legend are adapted with permission from Tarhonskaya *et al.* (2014) Biochemistry **53**, 2483-2493 [14]. Copyright (2014) American Chemical Society.

The kinetic traces obtained for penN were fitted with a 2-exponential function yielding apparent rate constants of the putative 310 nm intermediate formation and degradation of 1.7 s^{-1} and 0.24 s^{-1}, respectively (**Figure 5.11**). It was not possible to obtain a good fit for the reaction with penG or the reaction in the absence of substrate, which suggests a certain degree of heterogeneity of the studied systems. Fitting of the uncoupled turnover kinetic trace (i.e. reaction in the absence of penicillin) did not improve by increasing the number of exponential terms in the fitting function. The use of a double exponential function to fit the data for the reaction of penG ring expansion also gave a very poor fit (**Figure 5.11**), while a three-exponential function allowed simulation of a species formation rate, but not degradation. Thus, in the case of penG, the profile of the 310 nm species seems to consist of two highly

overlapping peaks, further complicating kinetic analysis and possibly reflecting both the reaction of penG ring expansion and uncoupled turnover.

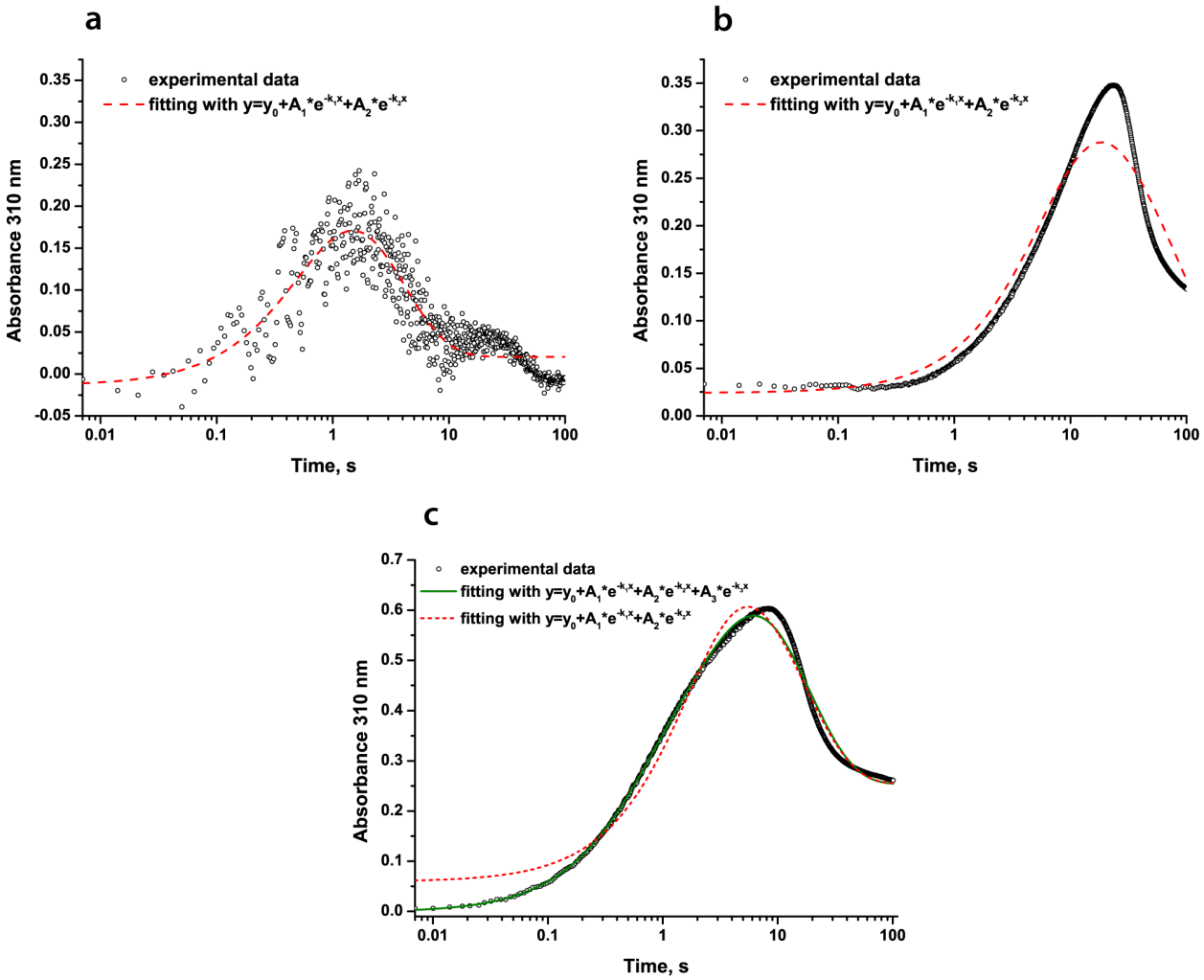


Figure 5.11. Fitting of the stopped-flow traces representing formation and degradation of 310 nm species. Conditions: anaerobically prepared mixture of 0.8 mM DAOCS in 50 mM HEPES (pH 7.5), 0.7 mM Fe(II), 5 mM 2OG and 1 mM penG/penN (if present) was rapidly mixed with O_2-free/O_2-saturated buffer. Difference spectra were analysed. Analytical fitting of the kinetic traces at 310 nm (a putative Fe(IV)-oxo intermediate) [16, 17, 21], to determine kinetic constants of the formation and degradation of the 310 nm species, was attempted using double or triple exponential functions. **(a)** DAOCS-catalysed penN ring expansion. **(b)** DAOCS-catalysed uncoupled turnover. **(c)** DAOCS-catalysed penG ring expansion.

In addition to the formation and degradation of the 310 nm species, a decrease in absorbance at a wavelength corresponding to the maximum of the MLCT features, representing initial enzyme-substrate complex, was observed (520 nm for DAOCS.Fe(II).2OG complex, 519 nm for the DAOCS.Fe(II).2OG.penG complex, and 514 nm for the DAOCS.Fe(II).2OG.penN

complex) (**Figure 5.12a**). Analogous to previous reports on other 2OG oxygenases, this intermediate may be attributed to the high spin Fe(II) enzyme-product(s) complex, which absorbs less than the initial enzyme-substrate complex, therefore its accumulation leads to an overall decrease in absorbance [17]. Formation of a 514 nm decay intermediate was concurrent to 310 nm intermediate degradation (0.24 s^{-1} and 0.26 s^{-1} for 310 nm species degradation and 514 nm decay, respectively), thus suggesting a similar order of catalytic events to that previously reported for other 2OG oxygenases (**Figure 5.12b**) [16, 17]. There was very little decrease in 514-520 nm absorbance in the absence of the penicillin 'prime' substrate (uncoupled turnover), which is again consistent with the previously observed 'substrate triggering' of oxygen activation under pre-steady-state conditions [18].

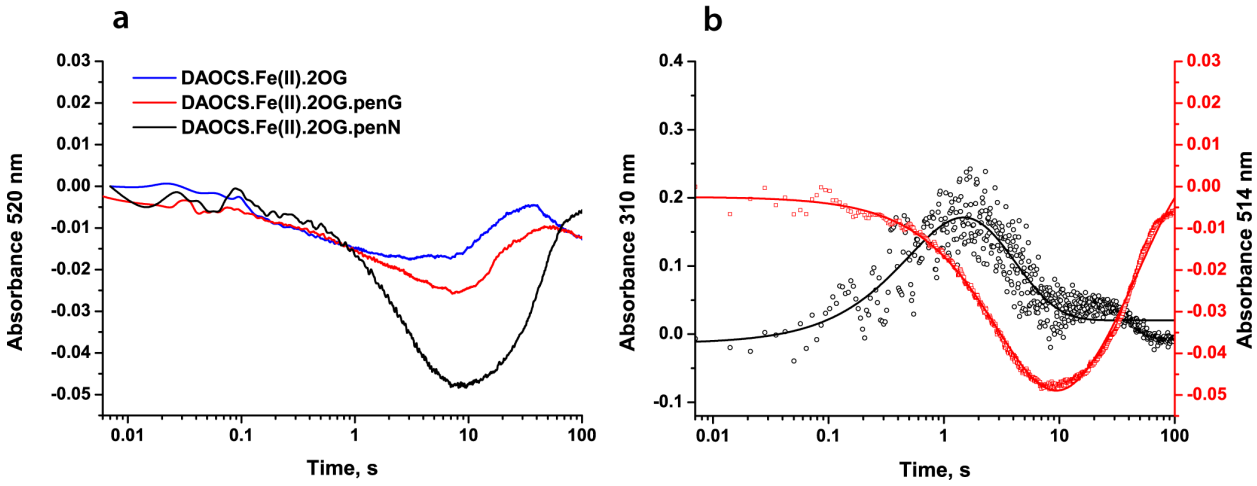


Figure 5.12. Transient kinetic studies showed faster formation of the putative Fe(IV)-oxo intermediate in the presence of penN compared to uncoupled turnover. Conditions: anaerobically prepared mixture of 0.8 mM DAOCS in 50 mM HEPES (pH 7.5), 0.7 mM Fe(II), 5 mM 2OG and 1 mM penG/penN (if present) was rapidly mixed with O_2-free/O_2-saturated buffer. Difference spectra were analysed and kinetic traces at **(a)** 520 nm and **(b)** 310 nm species vs 520 nm decay for DAOCS-catalysed ring expansion. The data were fitted with a double exponential function. Figure and figure legend are adapted with permission from Tarhonskaya *et al.* (2014) Biochemistry **53**, 2483-2493 [14]. Copyright (2014) American Chemical Society.

5.2.4. Rapid quench-flow studies on DAOCS-catalysed reaction

To investigate the kinetics of product formation and compare these to the formation and degradation of the intermediates observed in stopped-flow experiments, rapid quench-flow experiments were carried out. The reaction was performed under the same conditions as the stopped-flow experiments and quenched at defined time points with 1 % CF_3CO_2H. On

account of the instability of penicillin substrates under acidic conditions, only succinate formation was analysed (by LC-MS), carrying out the reaction in the presence and absence of the penicillin substrate. The resulting kinetic curves were fitted with a single exponential function. In the presence of penN, faster succinate formation was observed (determined rate constant (fitting parameter) was 0.063 s^{-1}) compared to uncoupled turnover (determined rate constant (fitting parameter) was <0.01 s^{-1}) (**Figure 5.13**). In the case of uncoupled succinate accumulation, the reaction was not complete within 1000 s, thus it was not possible to accurately determine the rate constant in this case. Nonetheless, DAOCS-catalysed uncoupled 2OG turnover is much slower than 2OG turnover in the presence of penN, yet faster than for other studied 2OG oxygenases, such as PHD2 and FIH (see Chapters 2-4).

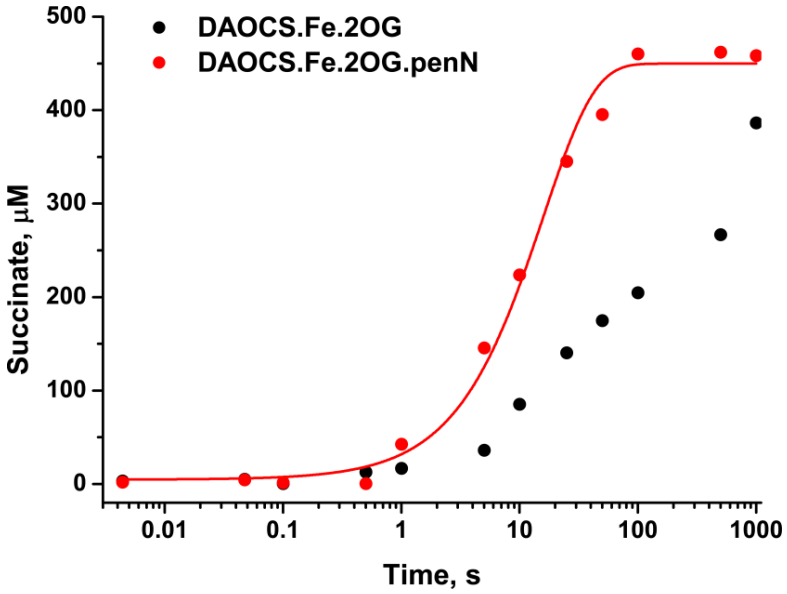


Figure 5.13. Pre-steady-state kinetic studies showed faster formation succinate in the presence of penN compared to uncoupled turnover. Conditions: anaerobically prepared mixture of 0.8 mM DAOCS in 50 mM HEPES (pH 7.5), 0.7 mM Fe(II), 5 mM 2OG and 1 mM penN (if present) was rapidly mixed with O_2-saturated buffer and quenched at defined time points by 1 % CF_3CO_2H. Succinate accumulation was detected using LC-MS, and succinate concentration was determined by comparison with an external calibration curve. Figure and figure legend are adapted with permission from Tarhonskaya *et al.* (2014) Biochemistry **53**, 2483-2493 [14]. Copyright (2014) American Chemical Society.

The time course of succinate accumulation was consistent with that of the formation and degradation of the intermediates observed during the stopped-flow experiments (**Figure 5.14**). Thus, the succinate accumulation starts simultaneously with restoration of the absorbance of the initial enzyme-substrate complex. In addition, faster 2OG oxidation in the presence of a

'prime' substrate is very common for 2OG oxygenase catalysis, and again suggests similarity in the employed DAOCS catalytic mechanism to other members of the enzymatic family [19].

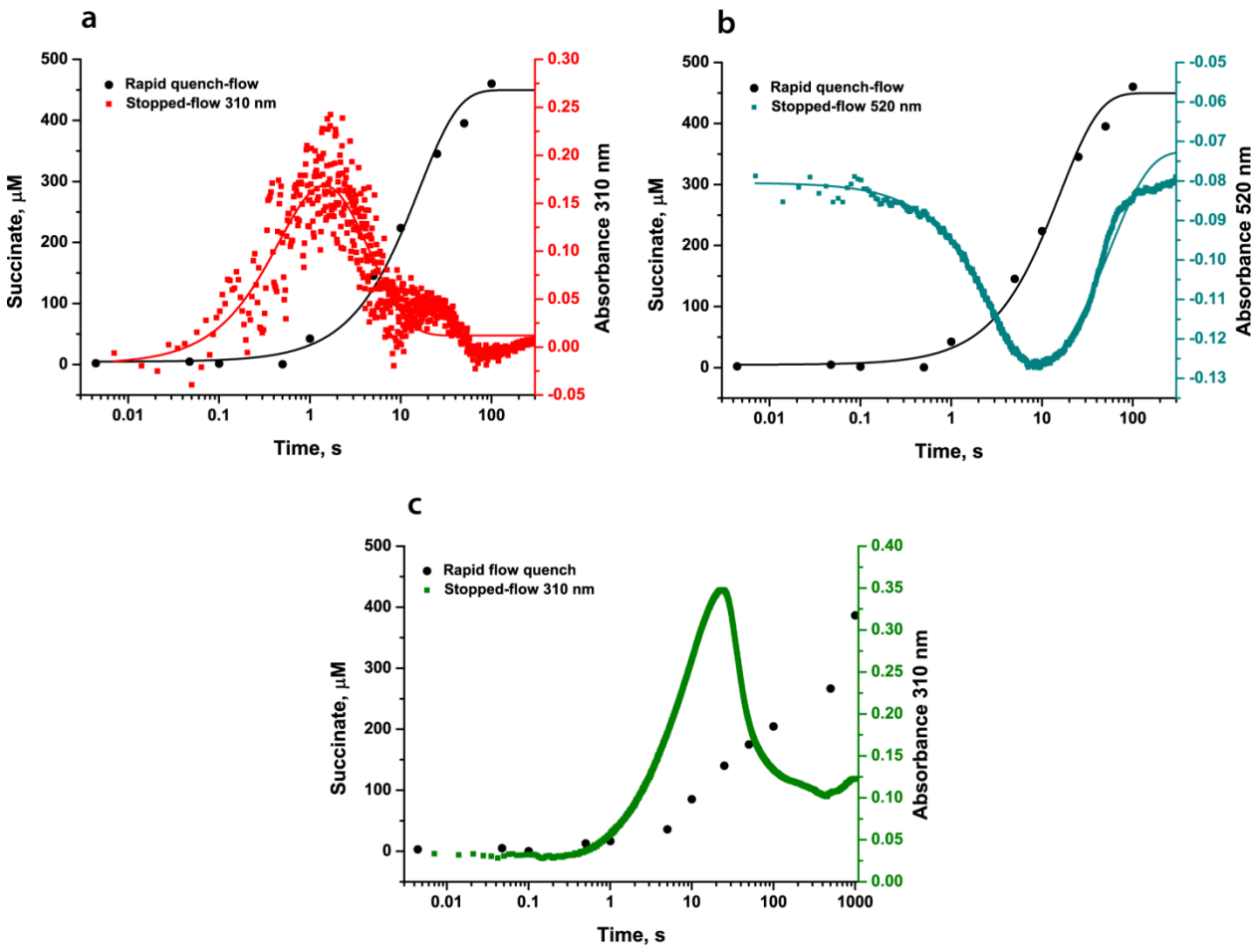


Figure 5.14. Transient kinetic studies reveal faster formation of the putative Fe(IV)-oxo intermediate and succinate in the presence of penN compared to uncoupled turnover. Conditions: anaerobically prepared mixture of 0.8 mM DAOCS in 50 mM HEPES (pH 7.5), 0.7 mM Fe(II), 5 mM 2OG and 1 mM penN (if present) was rapidly mixed with O_2-saturated buffer and observed by a photodiode array detector/quenched at defined time points by 1 % CF_3CO_2H. **(a)** penN ring expansion, the kinetic trace at 310 nm vs succinate accumulation; **(b)** penN ring expansion, the kinetic trace at 520 nm vs succinate accumulation; **(c)** uncoupled DAOCS-catalysed 2OG turnover, the kinetic trace at 310 nm vs succinate accumulation.

5.3. Discussion

Overall, the combined biophysical and kinetic analyses suggest the employment of the consensus 2OG oxygenase mechanism in DAOCS catalysis and reveal the viability of an enzyme.Fe(II).2OG.penN complex formation for DAOCS. However, there is still a possibility that non-productive substrate binding, at least for unnatural penicillin substrates, can occur, based on the observation of the unusual penicillin substrate binding modes in structural studies [8]. During investigations described in this thesis, no evidence was accrued for the proposed 'ping-pong' mechanism, in which succinate is released prior to penN binding [8]. The results of the binding studies demonstrate that 2OG and penN can bind simultaneously to DAOCS. In addition, UV-vis spectroscopy results were consistent with those of the NMR analyses [12], in which the differences in paramagnetic water relaxation times obtained upon addition of penN to the DAOCS.Mn(II).2OG complex demonstrate binding of penN at the metal binding region of the active site without 2OG displacement [14]. Thus, these results imply that the order of substrate binding in DAOCS catalysis follows the same sequence as for other studied 2OG oxygenases [19, 22].

Notably, there were differences in the binding of penN and penG to DAOCS. The ESI-MS studies demonstrated that penG binds to DAOCS with much lower affinity compared to penN, which is consistent with the reported higher K_m value for penG (14-36 μM and 0.7-2.6 mM, for penN and penG respectively) [6, 23, 24]. The ESI-MS studies also suggest that more than one molecule of penG can bind to DAOCS, thus there is a possibility of penG binding in a non-catalytically productive orientation. Observation of uncoupled 2OG turnover stimulation by non-optimal substrate binding is well-precedented with 2OG oxygenases [22, 25]. In the view of potential applications of DAOCS for the production of hydrophobic cephalosporin antibiotics, optimisation of the ratio of 2OG and penG coupling is an important parameter both with respect to catalytic efficiency and to minimisation of oxidative damage which could be caused by uncoupled turnover (reviewed in [24]).

The pre-steady-state kinetics of DAOCS catalysis showed very similar features to those observed for other 2OG oxygenases [16-21, 25]. Thus, formation and degradation of a species with maximum at 310 nm was apparent with similar kinetics as the Fe(IV)-oxo intermediate (absorbing at 318 nm for TauD [16]) previously characterised for TauD and other 2OG

oxygenases [16, 19]. Development of an absorbance decay feature at 520 nm after the 310 nm species was also observed, as with other 2OG oxygenases (see Chapters 2-4) [19]. This 520 nm species was previously assigned as a high spin Fe(II) complex with products [16, 17, 19]. The Fe(IV)-oxo intermediate has been reported to absorb in a visible region (including 520 nm, where the enzyme.Fe(II).2OG.substrate complex absorbs), while a second intermediate lacks the chromophoric absorbance properties of an initial enzyme-substrate complex. The observed accumulation of the intermediate with an absorbance decay feature at 520 nm occurs after degradation of the Fe(IV)-oxo intermediate [16, 17, 19]. The sequence of the catalytic events in DAOCS catalysis was consistent with this proposal (**Figure 5.14**), and the rate constants for the degradation of the 310 nm intermediate and the decay of the absorbance at 520 nm were very similar (0.24 s^{-1} and 0.26 s^{-1}, respectively). The observations described in this Chapter thus suggest that DAOCS employs a mechanism similar to other 2OG oxygenases.

Rapid quench-flow studies on DAOCS confirmed the proposal that the 310 nm intermediate is analogous to that previously reported [16, 17, 20, 21] showing that the time course of succinate accumulation is consistent with degradation of the 310 nm species. Notably, formation of the 310 nm species was faster in the presence of penN compared to uncoupled turnover, and to a lesser extent with penG. PenG was previously shown to have lower affinity to DAOCS than penN and higher rates of uncoupled turnover [12]. These observations again support the proposal of the consensus order of (co-)substrate binding for DAOCS since, in the proposed 'ping-pong' mechanism, the rate of formation of an Fe(IV)-oxo intermediate species would be independent of penicillin binding [8]. Moreover, rapid quench-flow analyses of coupled and uncoupled turnover suggest that the succinate accumulation rate depends on the presence of penN, which implies that succinate release does not occur prior to penicillin binding (**Figure 5.13**). Thus, it was observed that succinate formation is faster in the presence of penN, again within the consensus mechanism in which 'prime' substrate binding weakens chelation of an Fe(II)-coordinated water to enable oxygen binding [18, 19].

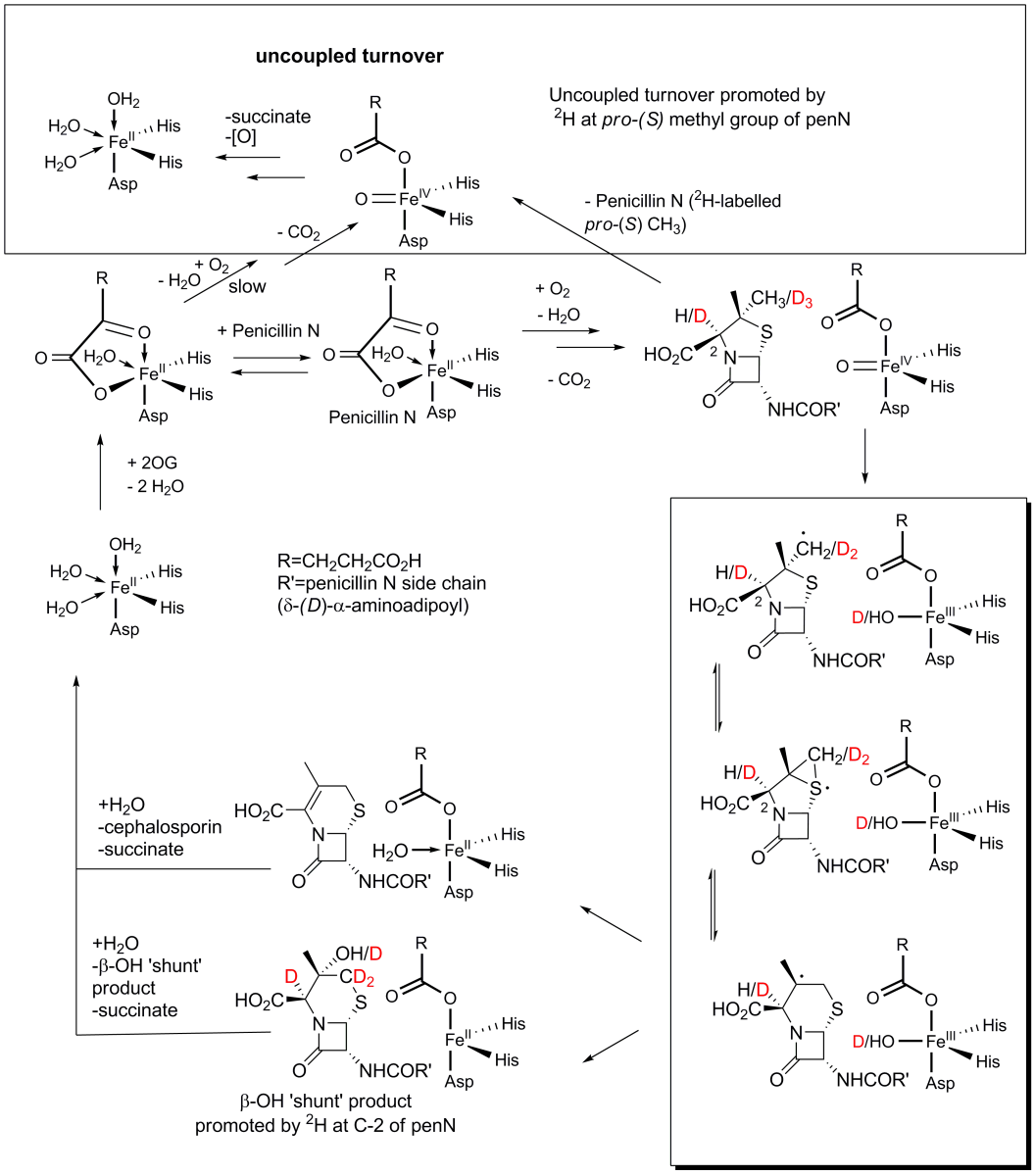


Figure 5.15. The outline of the proposed consensus mechanisms for DAOCS catalysis. Binding of dioxygen to the DAOCS.Fe(II).2OG.penicillin N complex results in the oxidative decarboxylation of 2OG and generation of an Fe(IV)-oxo species that enables oxidative rearrangement of the substrate via initial hydrogen abstraction on the methyl group of the penicillin. Based on studies with DAOC/DACS, we propose that when penN is labelled with deuterium at its (*pro-S*) *β*-methyl group, the deuterated substrate can be preferentially released from the active site at the stage of the Fe(IV)-oxo penicillin intermediate due to the relative difficulty in cleaving the C-^{2}H bond compared to C-^{1}H bond [26], i.e. promoting uncoupled turnover. C-2 deuteration promotes formation of a C-3 hydroxycepham, a 'shunt' product, that arises from hydroxylation rather than desaturation of the cepham radical intermediate [26]. Note, there is evidence that exchange of oxygen (incorporated into Fe(IV)-oxo intermediate from O_2) with that of solvent H_2O can occur [27]. Figure and figure legend are adapted with permission from Tarhonskaya *et al.* (2014) Biochemistry **53**, 2483-2493 [14]. Copyright (2014) American Chemical Society.

The main difference between the reaction of the HIF hydroxylases and DAOCS is the observation of accumulation of the presumed Fe(IV)-oxo intermediate (at 310 nm) [25]. In addition, formation and degradation of this intermediate occur relatively fast in the case of DAOCS, which suggests that the DAOCS-catalysed reaction undergoes fast oxygen activation compared to PHD2. Differences in the observation of a putative Fe(IV)-oxo intermediate imply that while for PHD2 and FIH oxygen activation is a rate limiting step, for DAOCS this step occurs at a much faster rate, and degradation of the Fe(IV)-oxo intermediate could be limiting for the catalysis. This is consistent with the discussed isotopic studies (see Chapter 1, Section 1.3, **Figure 5.15**) [28]. Thus, the evidence suggest that despite the proposal that 2OG oxygenases employ a similar mechanism, alterations to their kinetics may have developed in order to adjust to a performed biological function.

Overall, DAOCS oxygen activation rates were consistent with some other studied 2OG oxygenases [17, 19-21]. However, the observed kinetics of DAOCS catalysis was slightly different compared to PHD2 and FIH with respect to the accumulation of the putative Fe(IV)-oxo intermediate. These results contribute to the data on the pre-steady-state kinetics of the 2OG oxygenases and suggest that the nature of the rate limiting step of their catalysis differs, possibly in a manner related to biological function.

5.4. References

1. Baldwin, J.E., R.M. Adlington, J.B. Coates, M.J. Crabbe, N.P. Crouch, J.W. Keeping, G.C. Knight, C.J. Schofield, H.H. Ting, and C.A. Vallejo (1987) *Purification and initial characterization of an enzyme with deacetoxycephalosporin C synthetase and hydroxylase activities.* Biochem. J. **245**, 831-841.
2. Dotzlaf, J.E. and W.K. Yeh (1987) *Copurification and characterization of deacetoxycephalosporin C synthetase/hydroxylase from Cephalosporium acremonium.* J. Bacteriol. **169**, 1611-1618.
3. Kovacevic, S., B.J. Weigel, M.B. Tobin, T.D. Ingolia, and J.R. Miller (1989) *Cloning, characterization, and expression in Escherichia coli of the Streptomyces clavuligerus gene encoding deacetoxycephalosporin C synthetase.* J. Bacteriol. **171**, 754-760.
4. Baker, B.J., J.E. Dotzlaf, and W.K. Yeh (1991) *Deacetoxycephalosporin C hydroxylase of Streptomyces clavuligerus. Purification, characterization, bifunctionality, and evolutionary implication.* J. Biol. Chem. **266**, 5087-5093.
5. Valegård, K., A.C.T. van Scheltinga, M.D. Lloyd, T. Hara, S. Ramaswamy, A. Perrakis, A. Thompson, H.-J. Lee, J.E. Baldwin, C.J. Schofield, J. Hajdu, and I. Andersson (1998) *Structure of a cephalosporin synthase.* Nature **394**, 805-809.
6. Lee, H.-J., M.D. Lloyd, K. Harlos, I.J. Clifton, J.E. Baldwin, and C.J. Schofield (2001) *Kinetic and crystallographic studies on deacetoxycephalosporin C synthase (DAOCS).* J. Mol. Biol. **308**, 937-948.
7. Öster, L.M., A.C.T. van Scheltinga, K. Valegård, A.M. Hose, A. Dubus, J. Hajdu, and I. Andersson (2004) *Conformational Flexibility of the C Terminus with Implications for Substrate Binding and Catalysis Revealed in a New Crystal Form of Deacetoxycephalosporin C Synthase.* J. Mol. Biol. **343**, 157-171.
8. Valegård, K., A.C.T. van Scheltinga, A. Dubus, G. Ranghino, L.M. Öster, J. Hajdu, and I. Andersson (2004) *The structural basis of cephalosporin formation in a mononuclear ferrous enzyme.* Nat. Struct. Mol. Biol. **11**, 95-101.
9. Aik, W., M.A. McDonough, A. Thalhammer, R. Chowdhury, and C.J. Schofield (2012) *Role of the jelly-roll fold in substrate binding by 2-oxoglutarate oxygenases.* Curr. Opin. Struct. Biol. **22**, 691-700.
10. Clifton, I.J., M.A. McDonough, D. Ehrismann, N.J. Kershaw, N. Granatino, and C.J. Schofield (2006) *Structural studies on 2-oxoglutarate oxygenases and related double-stranded β-helix fold proteins.* J. Inorg. Biochem. **100**, 644-669.
11. van Scheltinga, T.A.C., K. Valegård, S. Ramaswamy, J. Hajdu, and I. Andersson (2001) *Multiple isomorphous replacement on merohedral twins: structure determination of deacetoxycephalosporin C synthase.* Acta Crystallogr. Sect. D **57**, 1776-1785.
12. Szöllössi, A. MPhil thesis, University of Oxford.
13. Lloyd, M.D., H.-J. Lee, K. Harlos, Z.-H. Zhang, J.E. Baldwin, C.J. Schofield, J.M. Charnock, C.D. Garner, T. Hara, T.A.C. van Scheltinga, K. Valegård, J.A.C. Viklund, J. Hajdu, I. Andersson, Å. Danielsson, and R. Bhikhabhai (1999) *Studies on the active site of deacetoxycephalosporin C synthase.* J. Mol. Biol. **287**, 943-960.
14. Tarhonskaya, H., A. Szöllössi, I.K.H. Leung, J.T. Bush, L. Henry, R. Chowdhury, A. Iqbal, T.D.W. Claridge, C.J. Schofield, and E. Flashman (2014) *Studies on Deacetoxycephalosporin C Synthase Support a Consensus Mechanism for 2-Oxoglutarate Dependent Oxygenases.* Biochemistry **53**, 2483-2493.

15. Ryle, M.J., R. Padmakumar, and R.P. Hausinger (1999) *Stopped-Flow Kinetic Analysis of Escherichia coli Taurine/α-Ketoglutarate Dioxygenase: Interactions with α-Ketoglutarate, Taurine, and Oxygen.* Biochemistry **38**, 15278-15286.
16. Price, J.C., E.W. Barr, B. Tirupati, J.M. Bollinger, and C. Krebs (2003) *The First Direct Characterization of a High-Valent Iron Intermediate in the Reaction of an α-Ketoglutarate-Dependent Dioxygenase: A High-Spin Fe(IV) Complex in Taurine/α-Ketoglutarate Dioxygenase (TauD) from Escherichia coli.* Biochemistry **42**, 7497-7508.
17. Hoffart, L.M., E.W. Barr, R.B. Guyer, J.M. Bollinger, and C. Krebs (2006) *Direct spectroscopic detection of a C-H-cleaving high-spin Fe(IV) complex in a prolyl-4-hydroxylase.* Proc. Natl. Acad. Sci. U. S. A. **103**, 14738-14743.
18. Krebs, C., D. Galonić Fujimori, C.T. Walsh, and J.M. Bollinger (2007) *Non-Heme Fe(IV)–Oxo Intermediates.* Acc. Chem. Res. **40**, 484-492.
19. Bollinger, J.M., J.C. Price, L.M. Hoffart, E.W. Barr, and C. Krebs (2005) *Mechanism of Taurine: α-Ketoglutarate Dioxygenase (TauD) from Escherichia coli.* Eur. J. Inorg. Chem. **2005**, 4245-4254.
20. Matthews, M.L., C.M. Krest, E.W. Barr, F.d.r.H. Vaillancourt, C.T. Walsh, M.T. Green, C. Krebs, and J.M. Bollinger (2009) *Substrate-Triggered Formation and Remarkable Stability of the C−H Bond-Cleaving Chloroferryl Intermediate in the Aliphatic Halogenase, SyrB2.* Biochemistry **48**, 4331-4343.
21. Sánchez-Fernández, E.M., H. Tarhonskaya, K. Al-Qahtani, R.J. Hopkinson, J.S.O. McCullagh, C.J. Schofield, and E. Flashman (2013) *Investigations on the oxygen dependence of a 2-oxoglutarate histone demethylase.* Biochem. J **449**, 491-496.
22. Hausinger, R.P. (2004) *Fe(II)/α-Ketoglutarate-Dependent Hydroxylases and Related Enzymes.* Crit. Rev. Biochem. Mol. Biol. **39**, 21-68.
23. Lee, H.-J., C.J. Schofield, and M.D. Lloyd (2002) *Active Site Mutations of Recombinant Deacetoxycephalosporin C Synthase.* Biochem. Biophys. Res. Commun. **292**, 66-70.
24. Goo, K.-S., C.-S. Chua, and T.-S. Sim (2009) *Directed evolution and rational approaches to improving Streptomyces clavuligerus deacetoxycephalosporin C synthase for cephalosporin production.* J. Ind. Microbiol. Biotechnol. **36**, 619-633.
25. Flashman, E., L.M. Hoffart, R.B. Hamed, J.M. Bollinger Jr, C. Krebs, and C.J. Schofield (2010) *Evidence for the slow reaction of hypoxia-inducible factor prolyl hydroxylase 2 with oxygen.* FEBS J. **277**, 4089-4099.
26. Baldwin, J.E., R.M. Adlington, N.P. Crouch, C.J. Schofield, N.J. Turner, and R.T. Aplin (1991) *Cephalosporin biosynthesis: A branched pathway sensitive to an isotope effect.* Tetrahedron **47**, 9881-9900.
27. Baldwin, J.E., R.M. Adlington, N.P. Crouch, and I.A.C. Pereira (1993) *Incorporation of ^{18}O-labelled water into oxygenated products produced by the enzyme deacetoxy/deacetylcephalosporin C synthase.* Tetrahedron **49**, 7499-7518.
28. Baldwin, J.E., R.M. Adlington, R.T. Aplin, N.P. Crouch, G. Knight, and C.J. Schofield (1987) *Cephalosporin C biosynthesis; a branched pathway sensitive to a kinetic isotope effect.* J. Chem. Soc., Chem. Commun., 1651-1654.

Chapter 6: Mechanism of 2-hydroxyglutarate oxidation*

6.1. Introduction

Substitutions to the enzymes of the tricarboxylic (TCA) cycle, such as isocitrate dehydrogenase (IDH1/2) have been associated with particular types of cancers [1-4]. IDH1/2 catalyses the conversion of isocitrate to 2OG, which then serves as a co-substrate for 2OG oxygenases, among many other functions. 'Gain-of-function' mutations to IDH1/2 lead to accumulation of (*R*)-2-hydroxyglutarate ((*R*)-2HG), rather than 2OG, in high concentrations (up to 10 mM) [5]. It is proposed that accumulated TCA cycle metabolites, including (*R*)-2HG, can inhibit 2OG oxygenases causing pro-oncogenic effects [3, 4, 6].

It has indeed been shown that both (*S*)- and (*R*)-2HG can inhibit a number of 2OG oxygenases including histone demethylases and enzymes responsible for nucleic acid modification [6-9]. In contrast, one report has suggested that (*R*)-2HG can activate the PHDs, but not other 2OG oxygenases, in a stereospecific manner [10]. Thus, it has been proposed that (*R*)-2HG, but not (*S*)-2HG, is oxidised in the active site of PHDs to 2OG, which is subsequently utilised in catalysis (Koivunen *et al.* [10]). The suggested mechanism of this transformation includes (*R*)-2HG oxidation via an Fe(III)-superoxide intermediate [10]. An Fe(III)-superoxo species is a proposed active intermediate in the catalysis by enzymes related to 2OG oxygenases, which do not utilise 2OG as a co-substrate (e.g. isopenicillin N synthase (IPNS)) [11]. Although C-H cleavage in a 'prime' substrate performed by Fe(III)-superoxo intermediates is known for enzymes related to 2OG oxygenases, (co-)substrate C-H cleavage in 2OG oxygenases is unprecedented [11]. The proposed mechanism of 2HG oxidation by 2OG oxygenases [10] is intriguing, as it would suggest that PHD2 can perform a novel mechanism, which does not require 2OG as a co-substrate and/or utilises a small molecule both as a co-substrate and a 'prime' substrate.

*Part of the work described in this Chapter has been published in Tarhonskaya, H., Rydzik, A.M., Leung, I.K.H., Loik, N.D., Chan, M.C., Kawamura, A., McCullagh, J.S.O., Claridge, T.D.W., Flashman, E., Schofield, C.J. *Non-enzymatic chemistry enables 2-hydroxyglutarate-mediated activation of 2-oxoglutarate oxygenases*, (2014) Nature Communications, **5** http://dx.doi.org/10.1038/ncomms4423

To elucidate whether 2HG oxidation to 2OG indeed occurs enzymatically, the mechanism of this reaction was investigated and the results are described in this Chapter.

6.2. Results

6.2.1. Enzymatic assays on 2HG-promoted PHD2 catalysis of CODD hydroxylation

Studies on the ability of (*R*)-2HG to promote PHD2-catalysed HIF-1α CODD hydroxylation were performed using MALDI-TOF-MS based assays. Firstly, the time course of the reaction (2 min - 20 hours) was investigated. To ensure that Met oxidation, which usually results in a background +16 Da peak in CODD hydroxylation analysis (~5-10 %), does not interfere with the results, a CODD peptide where Met was replaced with Ala was used in all enzymatic assays described in this Chapter. CODD hydroxylation was not observed after short incubations in the presence of 2HG under the standard assay conditions (4 μM PHD2, 200 μM CODD, 5 mM 2HG, 4 mM ascorbate, 50 μM Fe(II), see *Materials and Methods*), consistent with previously reported inhibition studies [6]. However, CODD hydroxylation was observed after 20 hours of assay mixture incubation at 37 °C, notably, without discrimination between (*R*)- and (*S*)-2HG (**Figure 6.1b,c**)

PHD2 catalysis is known to depend on the presence of reducing agents *in vitro*, such as L-ascorbate [12-14]. L-Ascorbate is usually included as a component of an assay, to ensure sufficient promotion of PHD2 activity, including in the conditions used by Koivunen *et al.* [6, 10, 15] (the assay conditions used in the different studies are summarised in **Table 6.1.**). Thus, the influence of the reducing agent concentration on the reaction was investigated. Using longer incubation times (20 hours) 2HG-promoted CODD hydroxylation was shown to be dependent on the concentration of L-ascorbate with up to 20 % CODD hydroxylation observed in the presence of 10 mM L-ascorbate (**Figure 6.1c,d**). Again, there was no difference between (*R*)- and (*S*)-2HG in the reaction, which was in contrast to the results of Koivunen *et al.* [10] CODD hydroxylation was not observed in the absence of both 2HG and 2OG [6].

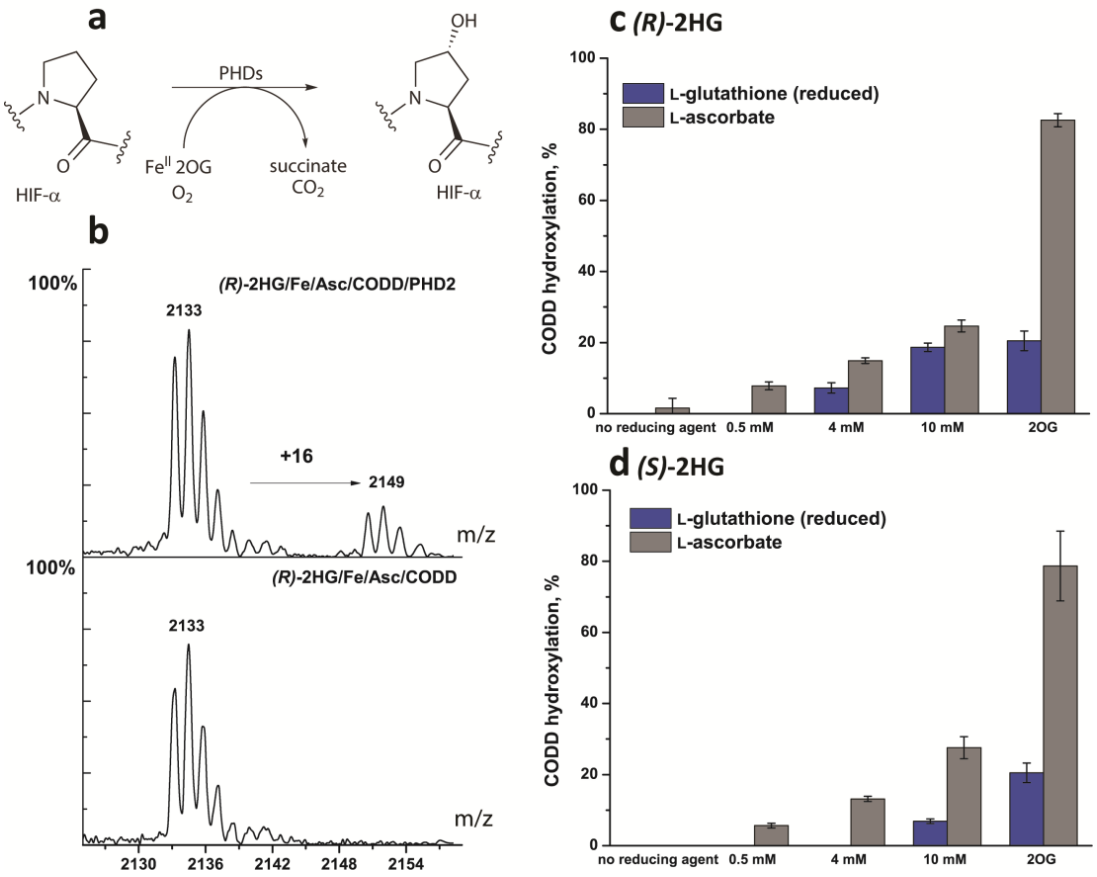


Figure 6.1. PHD2/2HG catalysed prolyl hydroxylation of hypoxia-inducible factor is enabled by reducing agents. Samples containing 4 μM PHD2, 200 μM *C*-terminal oxygen dependent degradation domain (CODD) peptide, 5 mM (*R*)- or (*S*)-2HG, 50 μM Fe(II), 0/0.5/4/10 mM L-ascorbate in 50 mM HEPES (pH 7.5) were incubated for 20 hours (37 °C) and then analysed by MALDI-TOF-MS or subjected to amino acid analysis. Error bars represent SD of the mean of triplicate assays. 2OG control incubations contained 300 μM 2OG instead of 2HG. **(a)** The PHD2-catalysed reaction. **(b)** Typical MALDI-TOF-MS spectra of CODD-OH (upper, CODD was incubated with PHD2/(*R*)-2HG/Fe(II)/L-ascorbate) and CODD (lower, a control without PHD2). **(c)** Dependence of the PHD2/(*R*)-2HG-catalysed CODD hydroxylation reaction on L-ascorbate and GSH, as determined by MALDI-TOF-MS. **(d)** Dependence of the PHD2/(*S*)-2HG-catalysed CODD hydroxylation reaction on L-ascorbate and GSH, as determined by MALDI-TOF-MS. Figure and figure legend are adapted with permission from Tarhonskaya *et al.* (2014) Nature Communications **5** http://dx.doi.org/10.1038/ncomms4423 [16].

Table 6.1. Summary of the conditions used in the PHD2 enzymatic assays in this study and earlier work Table and table legend are adapted with permission from Tarhonskaya *et al.* (2014) Nature Communications **5** http://dx.doi.org/10.1038/ncomms4423 [16].

	Conditions	Incubation time	Method
This study	4 μM $PHD2_{181-426}$, 200 μM CODD peptide, 5 mM (*R*)- or (*S*)-2HG, 0-10 mM L-ascorbate, 50 μM Fe(II).	20 hours	MALDI-TOF-MS
This study	10 μM $PHD2_{181-426}$, 10 μM CODD peptide, 5 mM (*R*)- or (*S*)-2HG, 2 mM L-ascorbate, 50 μM Fe(II).	10 min	MALDI-TOF-MS
[10]*	1 μM PHD2, 0.08-0.36 μM L-[2,3,4,5-^{3}H]Pro-labelled HIF-1α ODDD, 5 mM (*R*)-2HG, 5 μM Fe(II), 2 mM L-ascorbate, 60 μg mL^{-1} catalase, 0.1 mM DTT, 2 mg mL^{-1} BSA.	Not specified	Radioactive assay (^{3}H detection)
[10]	5 mM (*R*)-2HG, 50 μM CODD peptide, other components not specified.	20 hours	LC-MS
[10]*	PHDs – concentration not specified, 5 mM (*R*)-2HG, 50 μM CODD peptide, 5 μM Fe(II), 2 mM L-ascorbate, 60 μg mL^{-1} catalase, 0.1 mM DTT, 2 mg mL^{-1} BSA, 80 μM [^{14}C]-labelled 2OG.	Not specified	[^{14}C]-radioactive assay

(*) Detailed conditions are described in ref. [15]

As L-ascorbate was shown to promote the reaction, the influence of another reducing agent – L-glutathione was studied. Glutathione (GSH) is a biologically important antioxidant that participates in cellular protection against oxidative stress [17]. GSH was also found to promote PHD2-catalysed CODD hydroxylation, however, at higher concentrations compared to L-ascorbate (**Figure 6.1c,d**). This result can be rationalised by the fact that GSH has a lower ability to stimulate PHD2 activity *in vitro* as has been previously shown [18]. Control assays without either 2HG or 2OG again revealed no hydroxylation. Similar to the results with L-ascorbate, no difference between the two 2HG enantiomers was observed.

Physiological concentrations of L-ascorbate are known to be lower (0.1-0.4 mM) than those used in the standard *in vitro* assay conditions described in this Chapter [19]. Thus, promotion of the PHD2-catalysed reaction by low L-ascorbate concentrations was studied. The observed levels of modification were low suggesting that the concentration of the reducing agent is one of the crucial factors for the reaction. However, the observed trend was consistent with the previously revealed dependence of the product (CODD-OH) formation on the presence of reducing agent (**Figure 6.2**).

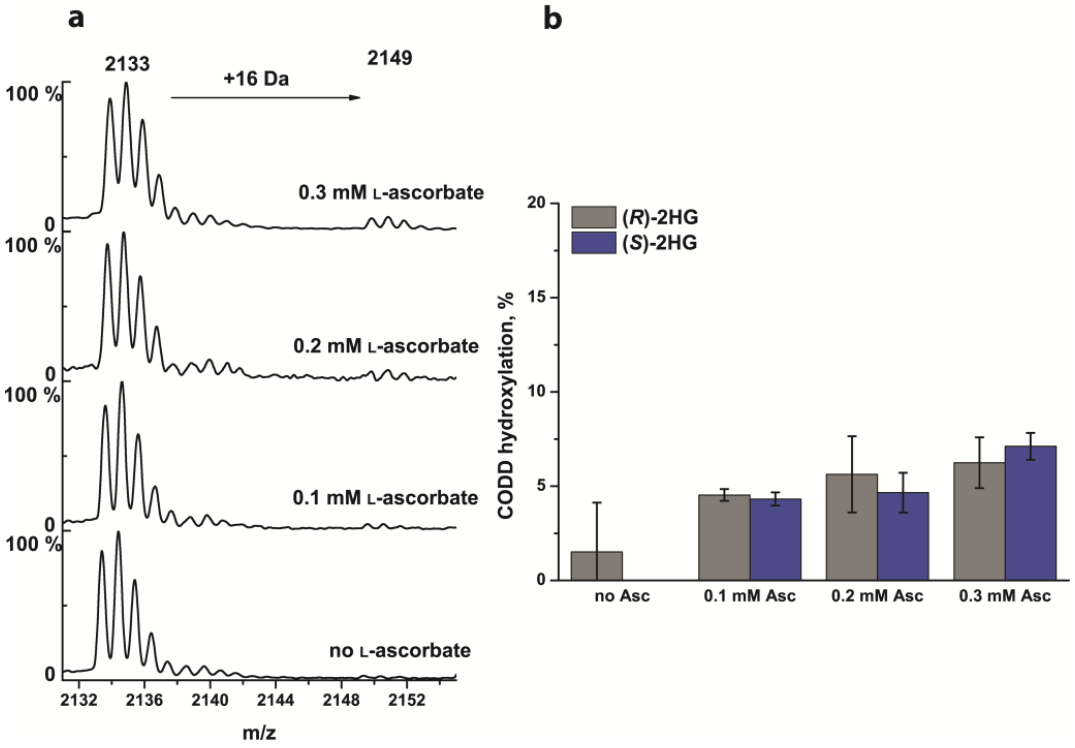


Figure 6.2. PHD2/2HG catalysed prolyl hydroxylation of HIF is enabled by reducing agents (0.1 mM – 0.4 mM L-ascorbate). Samples containing 4 µM PHD2, 200 µM *C*-terminal oxygen dependent degradation domain (CODD) peptide, 5 mM (*R*)- or (*S*)-2HG, 50 µM Fe(II), 0.1-0.4 mM L-ascorbate in 50 mM HEPES (pH 7.5) were incubated for 20 hours (37 ^{o}C) and then analysed by MALDI-TOF-MS. Error bars represent SD of the mean of triplicate assays. **(a)** MALDI-TOF-MS spectra obtained after 20 hours of incubation of the assay mixture. **(b)** Dependence of the PHD2/2HG-catalysed CODD hydroxylation reaction on L-ascorbate, as determined by MALDI-TOF-MS. Figure and figure legend are adapted with permission from Tarhonskaya *et al.* (2014) Nature Communications **5** http://dx.doi.org/10.1038/ncomms4423 [16].

2OG oxygenases can produce reactive oxidising species (ROS) in a substrate uncoupled manner, which could non-specifically oxidise CODD in the absence of actual enzymatic reaction. To investigate whether the observed CODD modification was due to interaction with

ROS 'leaking' from the PHD2 active site, assay mixtures were examined after addition of up to 100 μM H_2O_2 instead of the enzyme. No CODD +16 Da shift was observed in the MS spectra in this case. Furthermore, to confirm 2HG-mediated prolyl hydroxylation of CODD, amino acid analyses were performed. Hydrolysed assay mixtures of (*R*)- or (*S*)-2HG, PHD2, Fe(II), CODD and L-ascorbate were shown to contain *trans*-4-hydroxylated proline confirming formation of CODD-OH (**Figure 6.3**).

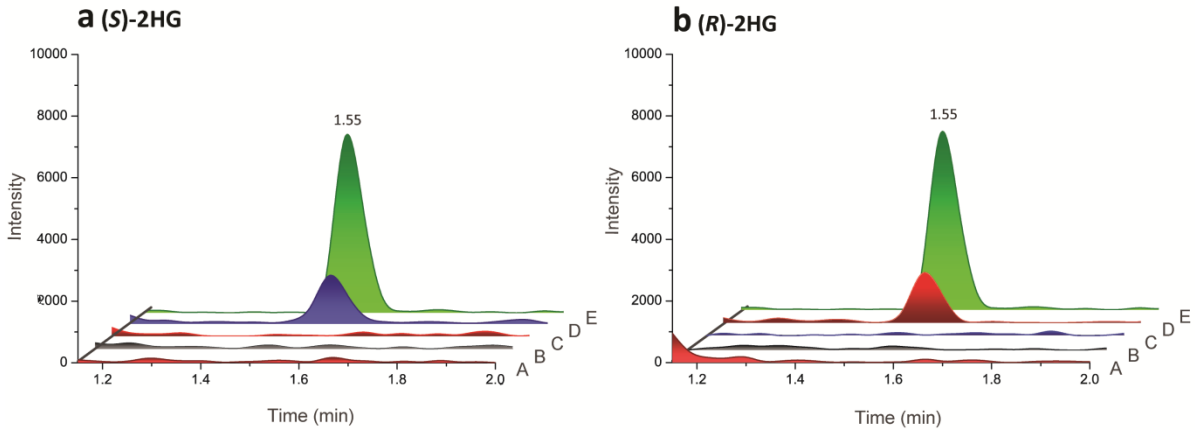


Figure 6.3. Amino acid analyses on PHD2/2HG catalysed prolyl hydroxylation of HIF. Samples containing 4 μM PHD2, 200 μM *C*-terminal oxygen dependent degradation domain (CODD) peptide, 5 mM (*S*)- **(a)** or (*R*)-2HG **(b)**, 50 μM Fe(II), 0/0.5/4/10 mM L-ascorbate in 50 mM HEPES (pH 7.5) were incubated for 20 hours (37 °C) and then subjected to amino acid analysis. (A. 2HG, Fe(II), L-ascorbate; B. CODD, 2HG, Fe(II), L-ascorbate; C. PHD2, 2HG, Fe(II), L-ascorbate; D. PHD2, CODD, 2HG, Fe(II), L-ascorbate; E. standard containing *trans*-4-hydroxyproline amino acid). Figure and figure legend are adapted with permission from Tarhonskaya *et al.* (2014) Nature Communications **5** http://dx.doi.org/10.1038/ncomms4423 [16].

6.2.2. Studies of 2HG binding to PHD2

In order to be oxidised to 2OG enzymatically as proposed [10], 2HG must, at least transiently, form a complex with PHD2. To investigate the likelihood of enzymatic 2HG oxidation, a range of methods were used to try and observe formation of such a complex. As described in previous chapters, 2OG oxygenases have a characteristic absorbance feature for an enzyme.Fe(II).2OG complex due to a metal to ligand charge transfer (MLCT, 530 nm for PHD2) [20]. Thus, UV-vis spectroscopy was used to probe for the formation of an MLCT band in the case of 2HG binding. An anaerobic PHD2.Fe(II).2OG complex showed a broad absorbance peak at 520-530 nm region as expected [12]. However, addition of (*R*)- or (*S*)-2HG to PHD2.Fe(II) under anaerobic conditions did not result in the formation of any

observable MLCT band (**Figure 6.4**). This suggests either the absence of (or very weak) 2HG binding to PHD2 or differences in the interaction of 2HG with the active site metal compared with 2OG.

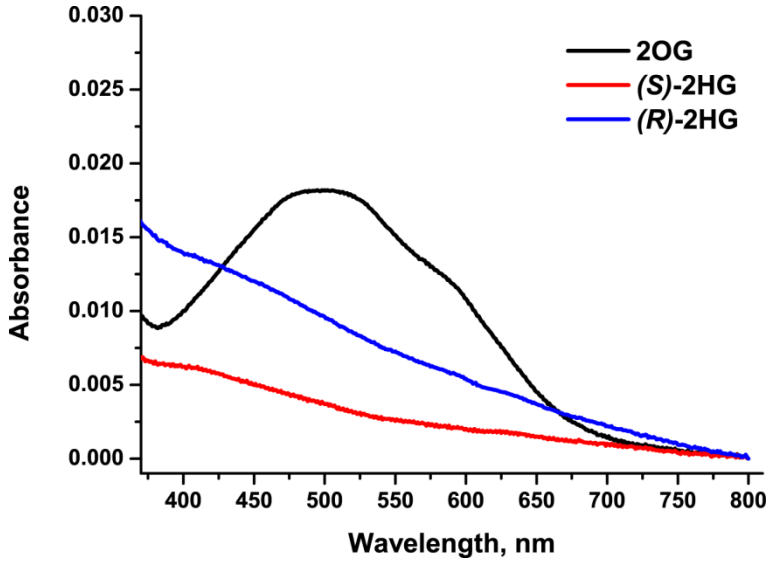


Figure 6.4. UV-vis spectra of the formation of PHD2.Fe(II).2OG/2HG complexes. Absorption spectra were acquired using a Cary Varian 4000 UV-vis spectrophotometer at room temperature with 0.1 mM PHD2, 0.1 mM Fe(II) and 0.5 mM 2OG or (*R*)/(*S*)-2HG in deoxygenated 50 mM HEPES (pH 7.5). The broad features with a maximum at 500-530 nm are characteristic of the metal to ligand charge transfer (MLCT) for the PHD2.Fe(II).2OG complex [12] (black line). In contrast to 2OG, there was no MLCT UV-vis absorbance observed for either (*R*)-2HG (blue line) or (*S*)-2HG (red line). Figure and figure legend are adapted with permission from Tarhonskaya *et al.* (2014) Nature Communications **5** http://dx.doi.org/10.1038/ncomms4423 [16].

Next, non-denaturing ESI-MS studies were conducted to observe possible formation of a PHD2.Fe(II).(*R*)-2HG complex. No complex with (*R*)-2HG was observed within the limits of detection (in contrast with 2OG) (**Figure 6.5**). CODD binding is known to induce conformational changes in PHD2 [21]. Thus binding in the presence of CODD was also investigated. Neither PHD2.Fe(II).(*R*)-2HG.CODD, nor enzymatic 2HG-promoted turnover was observed by non-denaturing ESI-MS. Overall, no evidence for binding of (*R*)-2HG to the PHD2.Fe(II) complex was acquired.

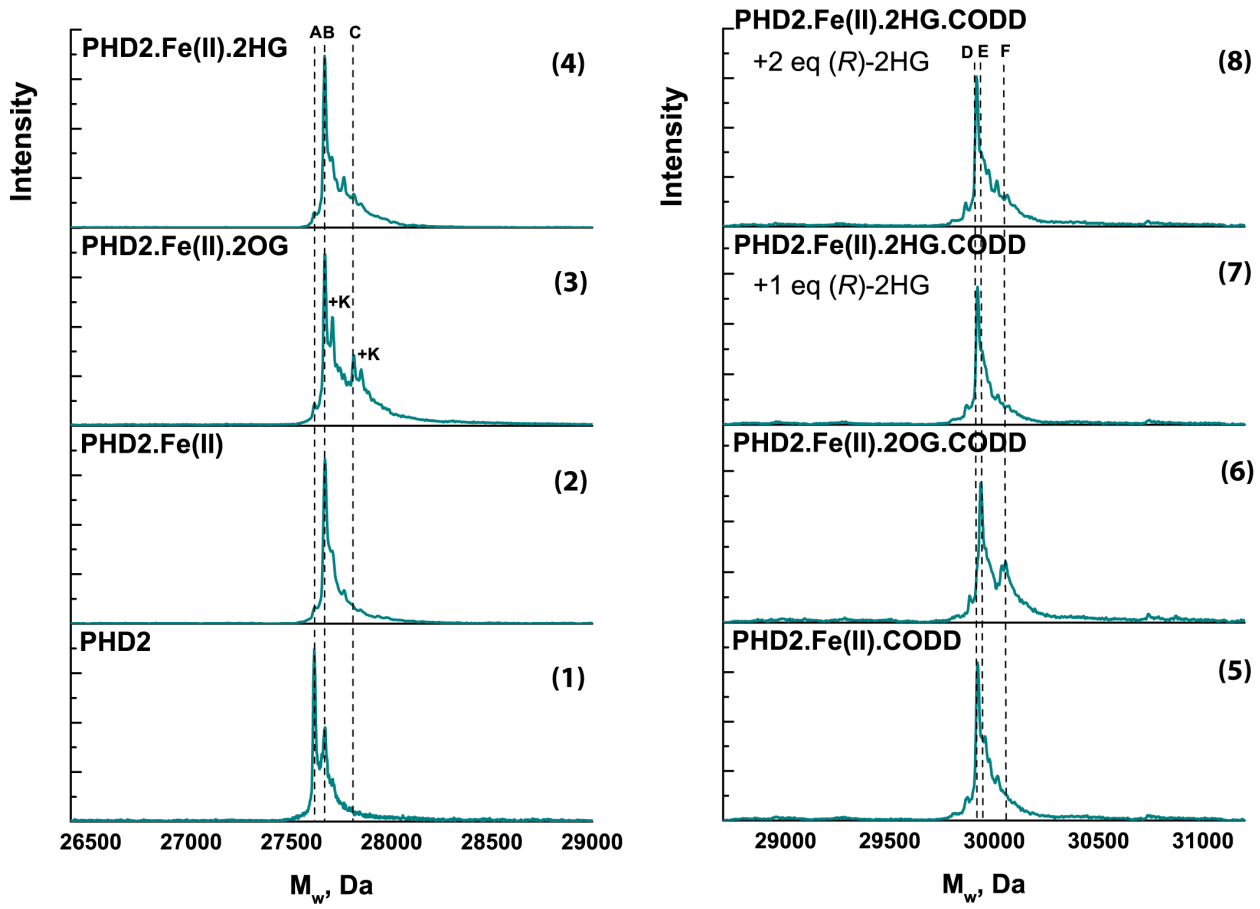


Figure 6.5. Non-denaturing MS does not reveal (*R*)-2HG binding to PHD2 +/- Fe(II)/CODD within limits of detection. Conditions: 15 µM PHD2 in 15 mM ammonium acetate buffer (pH 7.5) was mixed with 15 µM Fe(II) and then with 15 µM 2OG/(*R*)-2HG/CODD; cone voltage for the acquisition of the spectra was 60 V. The mixtures contained **(1)** PHD2; **(2)** PHD2 and Fe(II) (1:1); **(3)** PHD2, Fe(II), 2OG (1:1:1); **(4)** PHD2, Fe(II), (*R*)-2HG (1:1:1); **(5)** PHD2, Fe(II), CODD (1:1:1); **(6)** PHD2, Fe(II), CODD, 2OG (1:1:1:1); **(7)** PHD2, Fe(II), CODD, (*R*)-2HG (1:1:1:1); **(8)** PHD2, Fe(II), CODD, (*R*)-2HG (1:1:1:2). A – PHD2 (27614 Da), B – PHD2.Fe(II) (27670 Da), C – PHD2.Fe(II).2OG (27815 Da), D – PHD2.Fe(II).CODD (29923 Da), E – PHD2.Fe(II).CODD-OH (29939 Da), F – PHD2.Fe(II).CODD-OH.succinate (30052 Da). Figure and figure legend are adapted with permission from Tarhonskaya *et al.* (2014) Nature Communications **5** http://dx.doi.org/10.1038/ncomms4423 [16].

6.2.3. Non-enzymatic nature of 2HG oxidation

All the obtained evidence suggests that it is unlikely that 2HG is oxidised to 2OG in the active site of PHD2. Given the ability of reducing agents (L-ascorbate and GSH) to stimulate the 2HG-mediated reaction discussed above, the possibility of non-enzymatic oxidation of 2HG to 2OG was investigated. Assay mixtures of Fe(II)/2HG with different concentrations of reducing agents were incubated for 20 hours to match the conditions of the enzymatic assays, and were subsequently analysed by LC-MS (2OG determination, see *Materials and Methods*). 2OG elution was observed at ~2.35 min, and the concentration of the analyte in samples was determined by comparison with an external calibration curve. 2OG formation was observed in all samples, again with no discrimination between (*R*)- and (*S*)-2HG (**Figure 6.6**). To better understand the non-enzymatic processes which may take place during the incubation, the reaction with the oxidised form of glutathione (GSSG) and dehydroascorbate was investigated. 2OG formation was not observed in the presence of GSSG, indicating the importance of the –SH group of GSH for the promotion of the reaction; incubation with dehydroascorbate led to the observation of small levels of 2OG, possibly due to its partial reduction to L-ascorbate under the assay conditions (**Figure 6.6**).

Further LC-MS assays showed that the commercial (*R*)-2HG, which was used in the assays, contained background levels of 2OG (~1 μM in 5 mM (*R*)-2HG)), while no background was observed in (*S*)-2HG (**Figure 6.7**). Thus, the possibility of 2OG contamination of commercial batches of (*R*)- and (*S*)-2HG as a source of 2OG to elicit CODD hydroxylation was considered next. NMR analyses showed contamination of commercial batches of (*R*)-2HG with 2OG up to 0.02% (by molarity), but not of (*S*)-2HG (**Figure 6.7**).

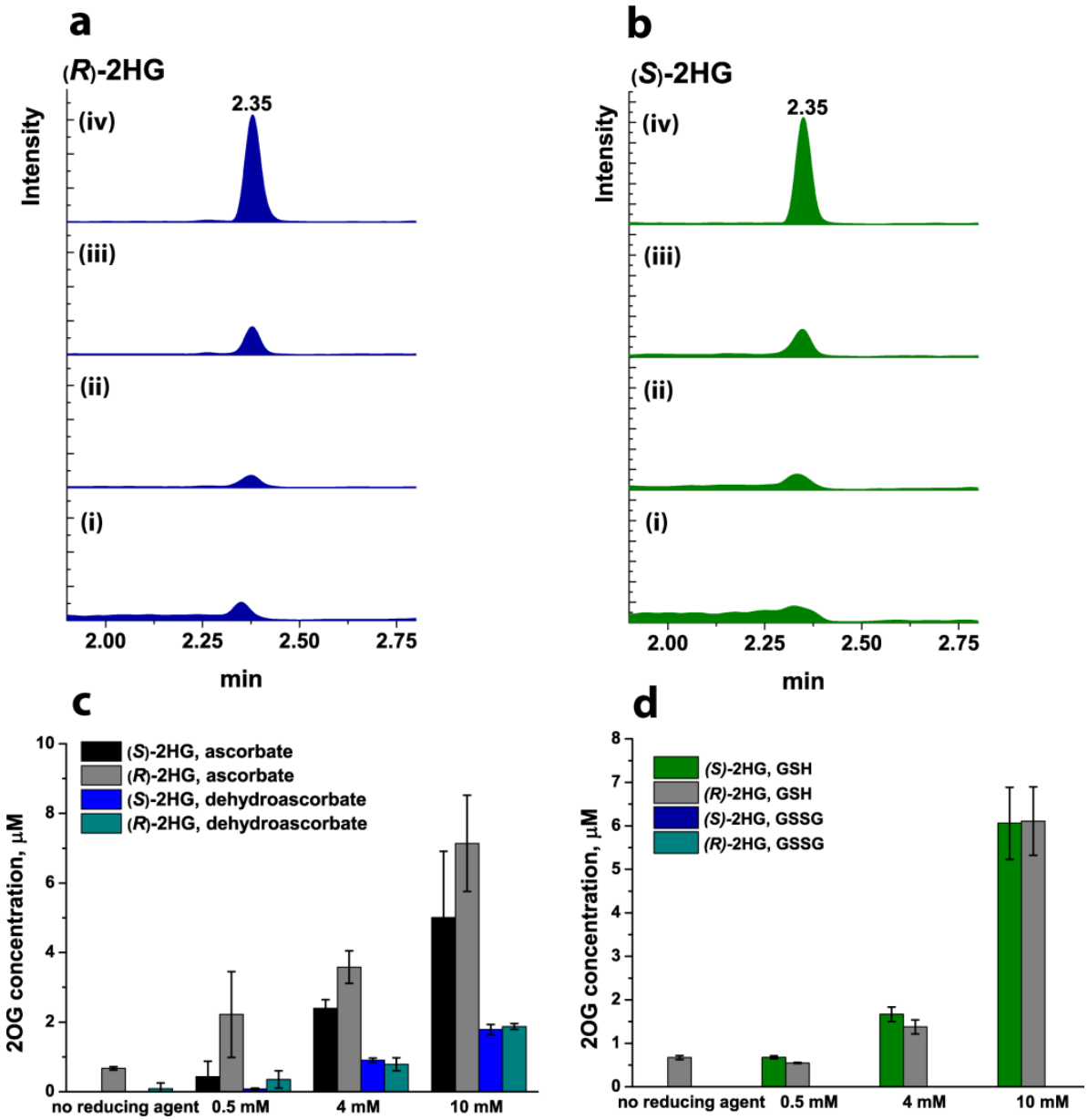


Figure 6.6. LC-MS detection of non-enzymatic 2HG conversion to 2OG catalysed by Fe(II) and reducing agents. Amounts of 2OG were determined after incubation of 2HG with Fe(II) and different reducing agents. **(a), (b)** LC-MS chromatograms showing 2OG formation under non-enzymatic conditions in the presence of GSH. The reaction mixture was incubated for 20 hours (37 °C) and contained 5 mM (*R*)- or (*S*)-2HG, 50 µM Fe(II), reducing agent (**(i)** no reducing agent, **(ii)** 0.5 mM, **(iii)** 4 mM, **(iv)** 10 mM reducing agent). All panels in one stack (**(i)-(iv)**) have the same range of ion intensity ($0 – 6.5 \cdot 10^5$). **(c), (d)** Amounts of 2OG formed with different reducing agents. Error bars represent SD of the mean of triplicate assays. Figure and figure legend are adapted with permission from Tarhonskaya *et al.* (2014) Nature Communications **5** http://dx.doi.org/10.1038/ncomms4423 [16].

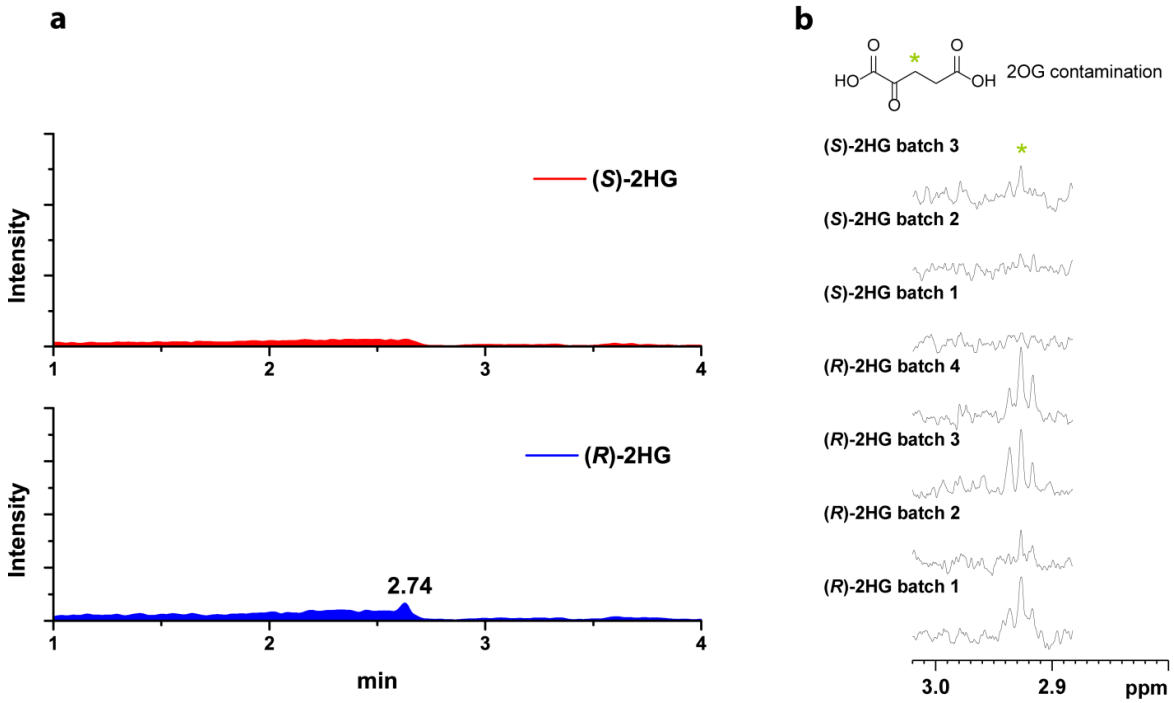


Figure 6.7. LC-MS and ^{1}H NMR analyses of commercial 2HG batches for the presence of 2OG. (a) LC-MS chromatograms of (*S*)- and (*R*)-2HG (detection of ions with 145 m/z (negative ionisation mode)). **(b)** ^{1}H NMR analyses of 2HG batches.· Figure and figure legend are adapted with permission from Tarhonskaya *et al.* (2014) Nature Communications **5** http://dx.doi.org/10.1038/ncomms4423 [16].

To probe whether the observed level of 2OG contamination in 2HG is sufficient to sustain PHD2 catalysis, the assays were conducted under single turnover conditions (10 μM CODD and 10 μM PHD2) (**Figure 6.8**). The results were consistent with previously observed 2OG contamination levels, giving 10 % of CODD hydroxylation, which is equivalent to the level of CODD hydroxylation seen on addition of 1 μM 2OG. This result supports the proposal that the previously reported observation of PHD2/2HG-mediated catalysis of HIF hydroxylation *in vitro* could result from (*R*)-2HG contamination by low levels of 2OG. (Note that the conditions used in the previous study were close to single turnover **Table 6.1.** [10])

· The NMR experiments described in this Chapter were performed by Dr I. K. H. Leung (analysis of 2HG purity) and Dr A. M. Rydzik (University of Oxford, Schofield group).

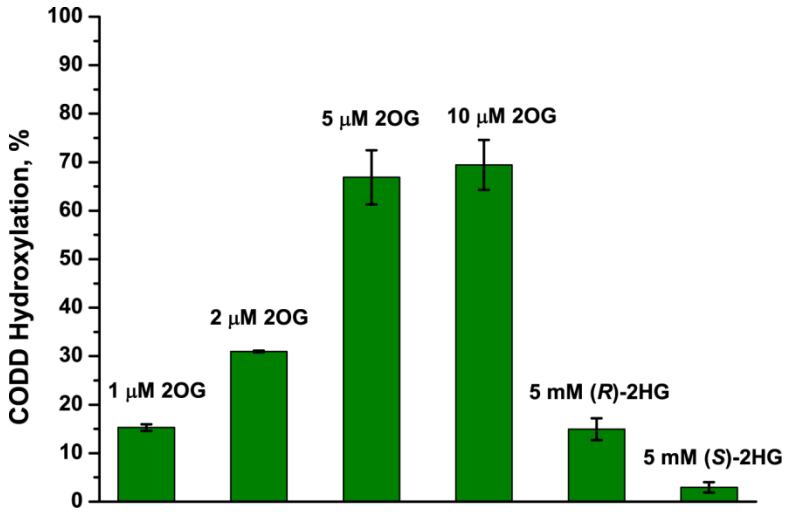


Figure 6.8. PHD2/2HG-mediated prolyl hydroxylation of HIF under single turnover conditions. Samples containing 10 μM PHD2, 10 μM CODD peptide, 2OG (varied)/5 mM (*R*)- or (*S*)-2HG (commercially supplied, unpurified), 50 μM Fe(II), 2 mM L-ascorbate in 50 mM HEPES (pH 7.5) were incubated for 10 min (37 °C) and then analysed by MALDI-TOF-MS. Error bars represent SD of the mean of triplicate assays. Figure and figure legend are adapted with permission from Tarhonskaya *et al.* (2014) Nature Communications **5** http://dx.doi.org/10.1038/ncomms4423 [16].

The importance of Fe(II) for the non-enzymatic reaction was next investigated. LC-MS was used to analyse 2OG production following incubation of 2HG/metal/ascorbate for 20 hours (37 °C). These experiments revealed that Fe(III) also catalyses the conversion of 2HG to 2OG (**Figure 6.9**), but that other transition metals, such as Zn(II), Mn(II), Co(II), Ni(II), Cu(II) did not promote the oxidation (i.e. only addition of Fe(II)/Fe(III) resulted in 2HG oxidation to 2OG). Investigation of the dependence of the reaction on Fe(II) concentration showed that the conversion does not occur at low Fe(II) concentrations (within the limits of detection), and at least 5 μM Fe(II)/Fe(III) is required to efficiently promote the reaction. This was also confirmed by NMR assays (**Figure 6.9**).

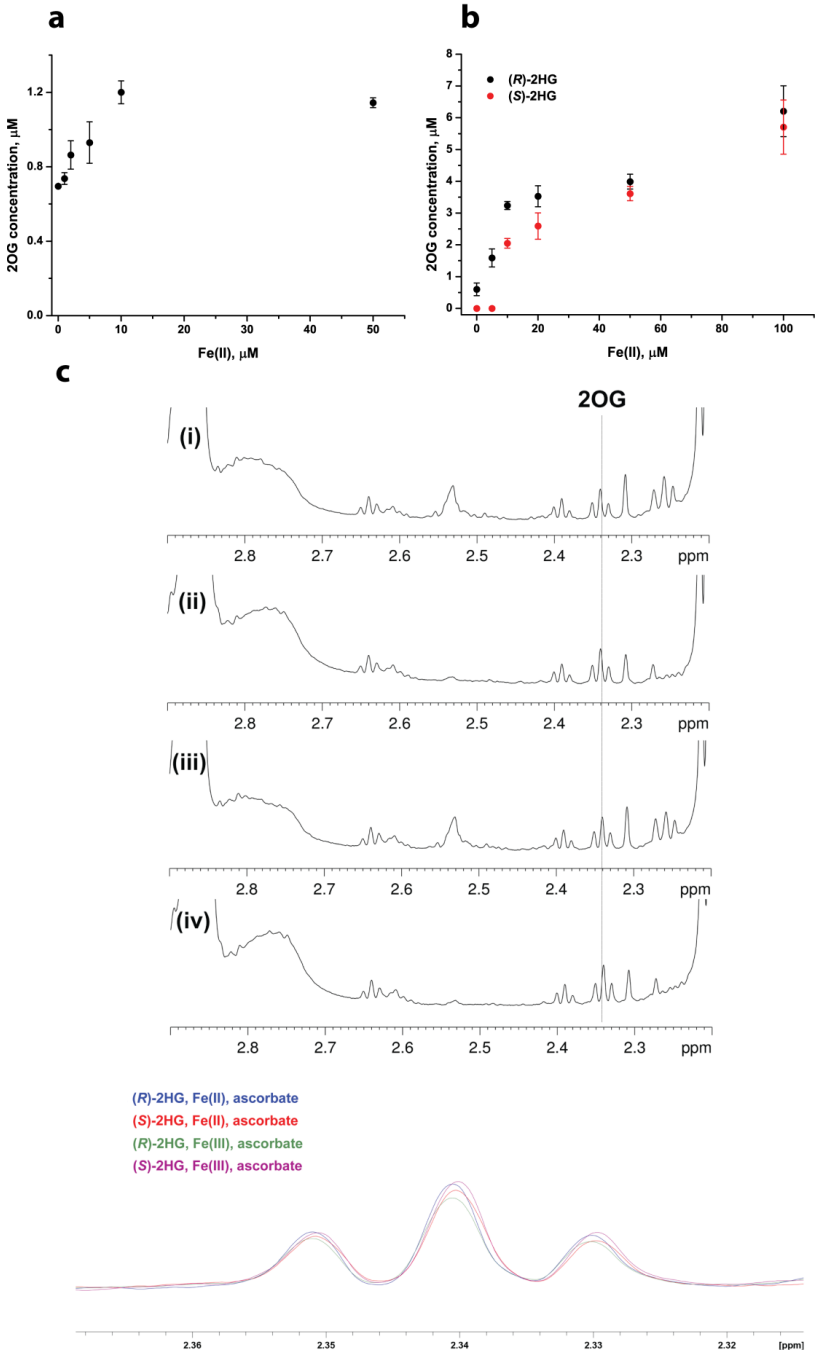


Figure 6.9. 2HG oxidation to 2OG is iron-mediated. LC-MS detection of 2OG in samples which were incubated (20 hours) in 50 mM HEPES (pH 7.5) at 37 °C under the following conditions: **(a)** 5 mM (*R*)-2HG, Fe(II) (variable), 2 mM GSH; **(b)** 5 mM (*R*)- (black circles) or (*S*)-2HG (red circles), Fe(II) (variable), 10 mM L-ascorbate, 50 mM HEPES (pH 7.5). Error bars represent SD for triplicate assays. **(c)** ^{1}H NMR detection of 2OG in samples which were incubated (20 hours) in 50 mM Tris-*d11* (pH 7.5) at 37 °C . (i) 5 mM (*R*)-2HG, 50 µM Fe(II), 10 mM L-ascorbate; (ii) 5 mM (*S*)-2HG, 50 µM Fe(II), 10 mM L-ascorbate; (iii) 5 mM (*R*)-2HG, 50 µM Fe(III), 10 mM L-ascorbate; (iv) 5 mM (*S*)-2HG, 50 µM Fe(III), 10 mM L-ascorbate. Figure and figure legend are adapted with permission from Tarhonskaya *et al.* (2014) Nature Communications **5** http://dx.doi.org/10.1038/ncomms4423 [16].

6.2.4. NMR studies on non-enzymatic 2HG oxidation

The requirement of both reducing agent and Fe(II)/Fe(III) for 2HG oxidation suggested that these reactions might be enabled by the mechanisms of Fenton chemistry (Fenton type chemistry is viable for α-hydroxyacid oxidation) [22-24]. During Fenton chemistry reactions, ROS are produced [24], thus the viability of the non-enzymatic reaction in the presence of H_2O_2 was studied. Interestingly, in the presence of 5 mM H_2O_2, non-enzymatic oxidation of 2HG was observed leading to the formation of 2OG, succinate and another oxidation product which was assigned as succinic semialdehyde (SSA) by comparison with standards.· It was also found that addition of either Fe(II) or Fe(III) is required for the reaction. As has been shown above, 2HG is oxidised relatively slowly in the presence of Fe(II)/Fe(III) and reducing agent (16-20 hours or more), however, the oxidation was much faster under peroxo conditions (2OG formation was apparent by NMR after 1 hour of incubation). Notably, the ratio between formation of 2OG and SSA was dependent on the amount of H_2O_2 present (**Figure 6.10**).

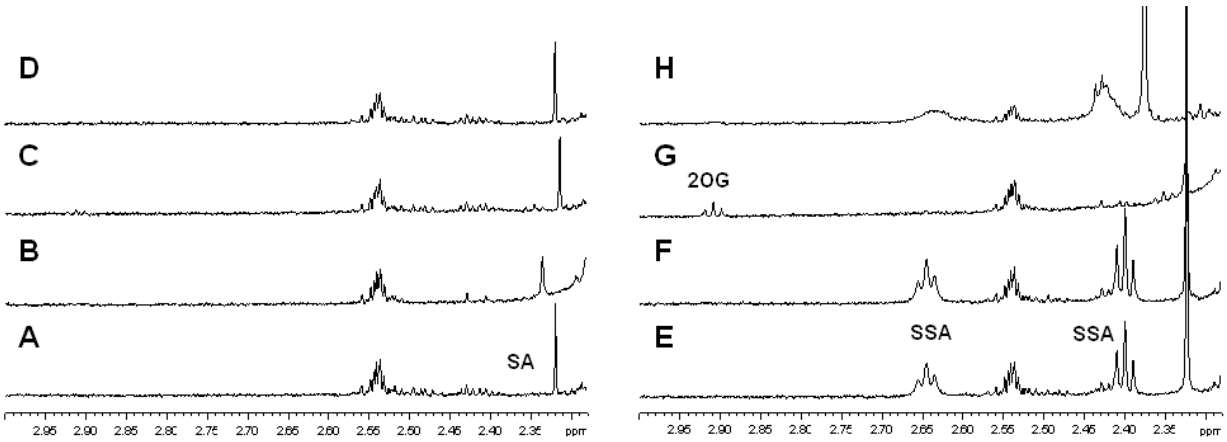


Figure 6.10. ^{1}H NMR studies of (*R*)-2HG oxidation mediated by H_2O_2. Reaction of (*R*)-2HG H_2O_2 in a 90 % water 10 % D_2O mixture

A. 5 mM (*R*)-2HG;
B. 5 mM (*R*)-2HG, 50 μM Fe(II);
C. 5 mM (*R*)-2HG, 10 mM L-ascorbate;
D. 5 mM (*R*)-2HG, 5 mM H_2O_2;
E. 5 mM (*R*)-2HG, 50 μM Fe(II), 5 mM H_2O_2;
F. 5 mM (*R*)-2HG, 10 mM L-ascorbate, 5 mM H_2O_2;
G. 5 mM (*R*)-2HG, 50 μM Fe(II), 10 mM L-ascorbate;
H. 5 mM (*R*)-2HG, 50 μM Fe(II), 10 mM L-ascorbate, 5 mM H_2O_2.

Incubation of (*R*)-2HG with Fe(II)/H_2O_2 or L-ascorbate/H_2O_2 for 20 hours led to observation of succinic semialdehyde. The figure was provided by Dr A. M. Rydzik.

· The SSA used for these experiments was synthesised by Dr A. M. Rydzik.

While in the presence of reducing agent the reaction was shifted towards formation of 2OG rather than SSA, in the presence of H_2O_2, formation of SSA was preferably observed. SSA concentrations also decreased under very high H_2O_2 concentrations, suggesting further possible oxidative conversion. Thus, SSA could have been a product of 2OG oxidation, or could have been produced from 2HG via an alternative oxidative pathway. NMR analyses of the assay mixtures where 2OG was incubated with Fe(II) and H_2O_2 yielded only succinate formation. Thus, 2OG was not oxidised to SSA. In addition, SSA oxidation to succinate was not observed under these conditions. Therefore the 2HG oxidation reaction most likely proceeds via an iron-complex formation, and two coordinating moieties in a ligand are required for metal coordination (**Figure 6.11**) [16].

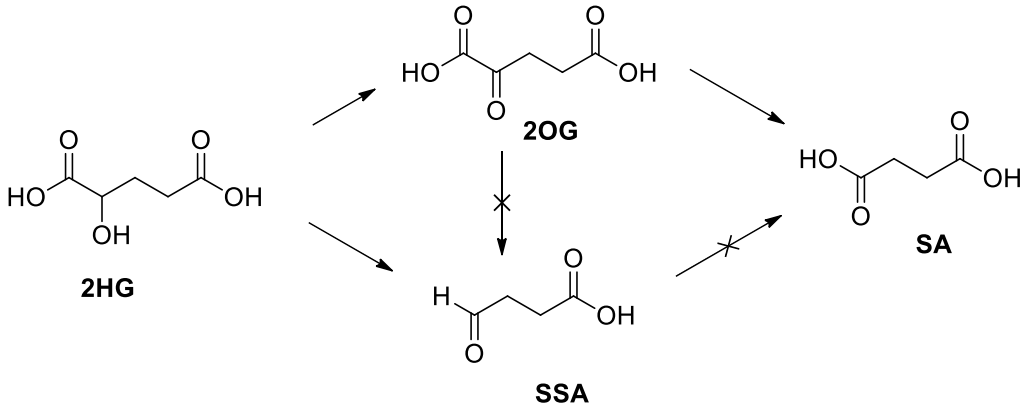


Figure 6.11. Summary of the oxidation processes occurring with the 2HG/Fe(II)/H_2O_2 system. 2HG – 2-hydroxyglutarate, 2OG – 2-oxoglutarate, SA – succinic acid, SSA – succinic semialdehyde. Under conditions of 5 mM (*R*)-2HG, 50 μM Fe(II), 5 mM H_2O_2 2HG is converted into 2OG and SSA, and 2OG can further be oxidised to SA. The transformation of 2OG to SA and SSA to SA was not observed under the conditions studied, therefore it is proposed that the reaction requires the presence of two Fe-coordinating moieties in the molecule to be coordinated by Fe(II) or Fe(III).

To further investigate the role of Fe(II) in the catalysis of the 2HG oxidative conversion, stopped-flow UV-vis spectroscopy analyses were employed. The reaction was triggered by mixing Fe(II) +/- 2HG mixture with H_2O_2, and was tracked using a photodiode array detector (**Figure 6.12**). Transient absorbance features were apparent (240-340 nm) during the reaction of the 2HG/Fe(II) mixture with H_2O_2, which likely represent transition between different oxidation states of iron (**Figure 6.12**) [25]. The time courses for the Fe(II) and Fe(II)/2HG mixtures demonstrated similar slight increases in the region of 280-450 nm (broad features), most likely due to Fe(II) oxidation in solution to Fe(III). The Fe(II)/H_2O_2 mixture showed a broad increase in absorbance in the same region, again most likely due to Fe(III) formation.

Only in the case of the 2HG/Fe(II)/H_2O_2 reaction formation of a transient species with maxima at 240 nm and 320 nm (relatively broad) was apparent (**Figure 6.12d**). The rate of formation and degradation of the transient species was dependent on the concentration of H_2O_2 (**Figure 6.13**), and the reaction occurred over 5 min, consistent with the NMR 2HG oxidation time course studies [16].

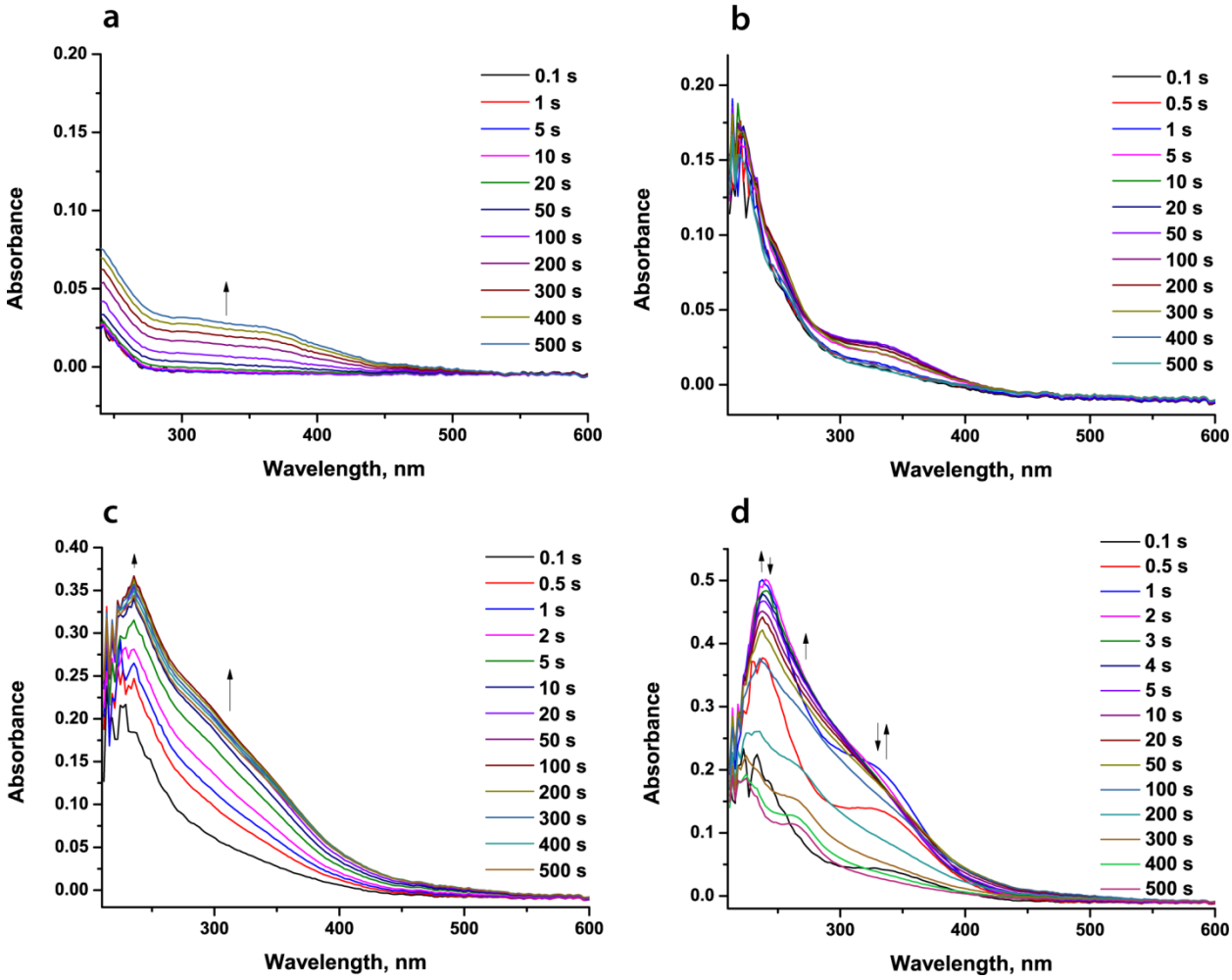


Figure 6.12. Stopped-flow UV-vis absorbance time course of 2HG oxidation by H_2O_2. Stopped-flow UV-vis absorbance time courses were obtained under the following conditions **(a)** 100 µM Fe(II), **(b)** 5 mM (*R*)-2HG, 100 µM Fe(II), **(c)** 100 µM Fe(II), 2 mM H_2O_2, **(d)** 5 mM (*R*)-2HG, 100 µM Fe(II), 2 mM H_2O_2. Figure and figure legend are adapted with permission from Tarhonskaya *et al.* (2014) Nature Communications **5** http://dx.doi.org/10.1038/ncomms4423 [16].

The isolated kinetic traces taken at maximum absorbance wavelength of the observed transients showed formation of two peaks during the 5 min reaction time course. Increasing the H_2O_2 concentration resulted in faster formation of the first peak and more pronounced

formation of a second peak (**Figure 6.13**). There was no decrease in absorbance at the end of the reaction under the conditions of excess H_2O_2, suggesting irreversible oxidation of Fe(II) to Fe(III) in solution. All traces form two unresolved peaks indicating that at least one of the transient species absorbs in the whole 240-340 nm region. Although it was not possible to assign the oxidation states of the observed absorbance species based on the stopped-flow experiments, the results support the proposal of iron-mediated conversion of 2HG to 2OG by correlation of the observed iron-transient species (by stopped-flow spectroscopy) and formation of 2HG oxidation products (by NMR).

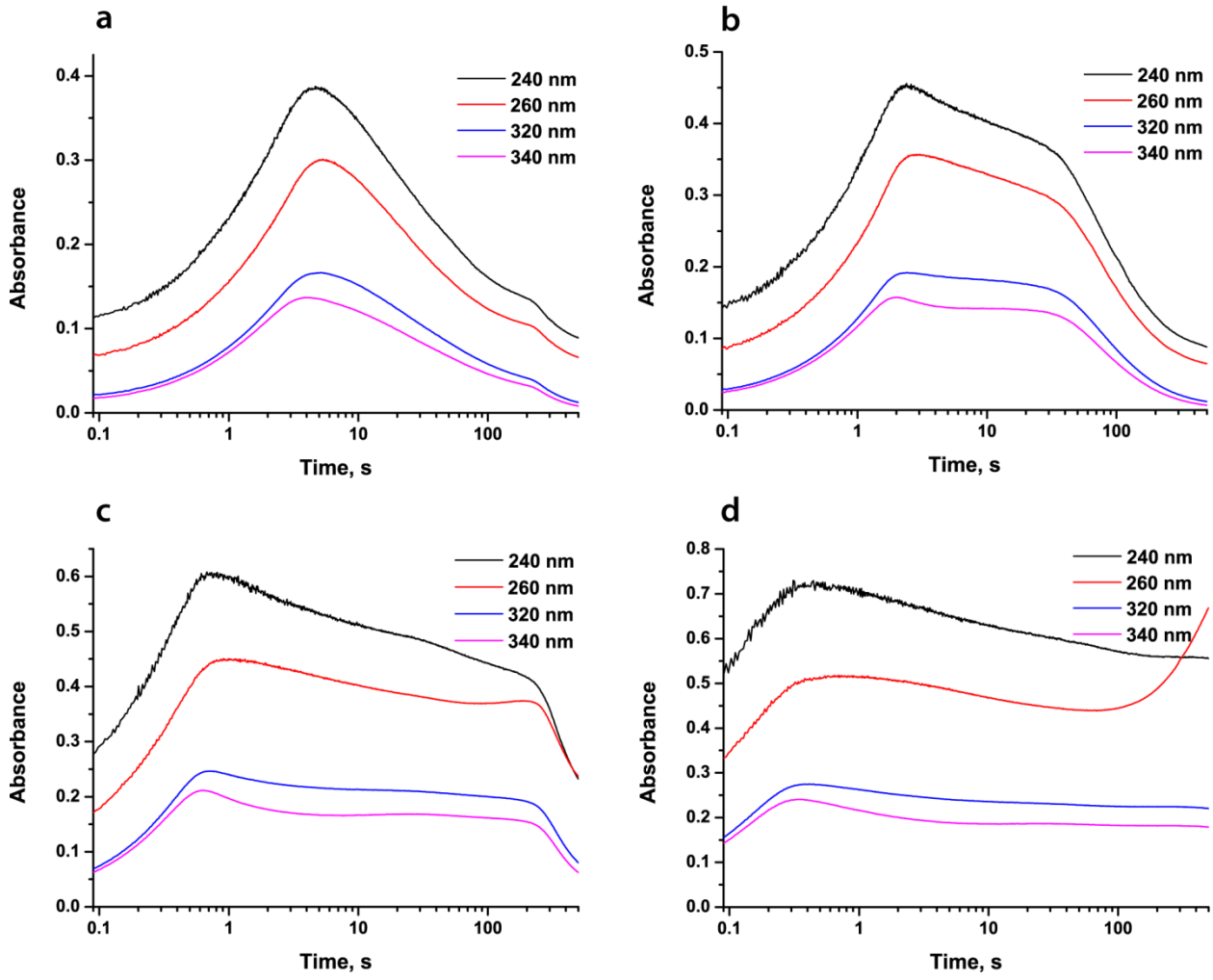


Figure 6.13. Stopped-flow UV vis absorbance spectra of iron(II)/(III)-species. Spectra representing changes of absorbance at 240, 260, 320, 340 nm were obtained under the following conditions: **(a)** 5 mM (*R*)-2HG, 100 µM Fe(II), 0.25 mM H_2O_2; **(b)** 5 mM (*R*)-2HG, 100 µM Fe(II), 0.5 mM H_2O_2; **(c)** 5 mM (*R*)-2HG, 100 µM Fe(II), 1 mM H_2O_2; **(d)** 5 mM (*R*)-2HG, 100 µM Fe(II), 5 mM H_2O_2. Figure and figure legend are adapted with permission from Tarhonskaya *et al.* (2014) Nature Communications **5** http://dx.doi.org/10.1038/ncomms4423 [16].

6.2.5. 2HG-promoted activation of other 2OG oxygenases

Given the apparent ability of (*R*)-2HG to activate the PHDs, but not other 2OG oxygenases [10], the possibility of 2HG-dependent promotion of the reaction for other 2OG oxygenases was then investigated. According to a previous report [6], 2HG is a very weak inhibitor not only for the PHDs, but also for FIH and BBOX1 (γ-butyrobetaine (GBB) oxygenase, which catalyses the final step in L-carnitine biosynthesis; IC_{50} values are 1.5 mM and 13.2 mM for (*R*)-2HG, and 189 μM and 142 μM for (*S*)-2HG, respectively [6]). In contrast, 2HG inhibits some histone demethylases with relative potency (IC_{50} values ~20 μM for both 2HG enantiomers) [6]. Thus, activity assays were conducted in the presence of 2HG and L-ascorbate for other human 2OG oxygenases including BBOX1, FIH and JMJD2A· (or KDM4A, an N^{ϵ}-methyl lysine demethylase). NMR detection of BBOX1 activity revealed that 2HG enables carnitine formation from GBB (**Figure 6.14**). The levels of formed carnitine were slightly higher in the presence of (*R*)-2HG than in the presence of (*S*)-2HG, which is consistent with the lower inhibitory potency for the (*R*)-isomer, compared to (*S*)-2HG [6]. Consistent with non-enzymatic oxidation of 2HG to 2OG, BBOX1 added to a 2HG/Fe(II)/L-ascorbate mixture, previously incubated for 20 hours (and probably containing non-enzymatically formed 2OG as was discussed above), showed higher levels of carnitine, compared with those assays where BBOX1 was incubated together with substrate and 2HG/Fe(II)/L-ascorbate. Interestingly, no enzymatic reaction was observed with FIH. This could be explained by the sensitivity of FIH to ROS, which are potentially formed during the reaction [26]. JMJD2A previously has been shown to be inhibited by both 2HG enantiomers. Nonetheless activity of JMJD2A in 2HG-promoted catalysis was investigated. Consistent with Koivunen *et al.* no demethylation was observed in the presence of (*R*)- and (*S*)-2HG [10].

· The JMJD2A enzyme was provided by Dr A. Kawamura (University of Oxford).

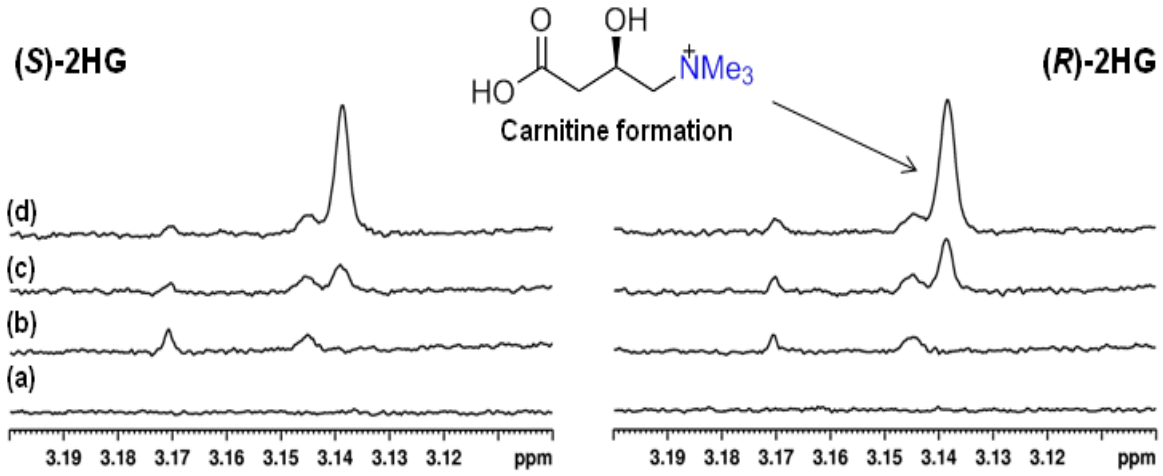


Figure 6.14. ^{1}H NMR spectra showing carnitine formation catalysed by BBOX1 in the presence of 2HG. (a) Standards of (*S*)-2HG and (*R*)-2HG; **(b)** (*S*)-2HG or (*R*)-2HG incubated in the assay mixture for 24 hours prior to analysis; **(c)** (*S*)-2HG or (*R*)-2HG incubated in the assay mixture with BBOX1 for 24 hours prior to analysis; **(d)** (*S*)-2HG or (*R*)-2HG incubated in the assay mixture for 24 hours, then treated with BBOX1 and Fe(II) (1:1) and incubated for further 2 hours prior to analysis. The standard assay mixture contained 100 µM GBB (γ-butyrobetaine), 4 mM L-ascorbate, 50 µM Fe(II), 80 mM KCl in 50 mM Tris-*d11* (pH 7.5) containing 10 % D_2O. BBOX1 concentration was 100 nM. (*S*)-2HG and (*R*)-2HG were used at a final concentration of 5 mM. The figure was provided by Dr A. M. Rydzik. Figure and figure legend are adapted with permission from Tarhonskaya *et al.* (2014) Nature Communications **5** http://dx.doi.org/10.1038/ncomms4423 [16].

As trace contamination of 2OG was found in (*R*)-2HG, IC_{50} values for PHD2 inhibition by 2HG were re-determined. (*R*)-2HG was subjected to high pressure liquid chromatography (HPLC) to remove 2OG contamination prior to re-determination of the IC_{50} values (**Figure 6.15**). It was found that (*R*)- and (*S*)-2HG are both very weak inhibitors of PHD2 (IC_{50} values are 23 mM and 6 mM for (*R*)- and (*S*)-2HG, respectively), which is consistent with a previous report [6]. Although, both (*R*)- and (*S*)-2HG are weak inhibitors, IC_{50} values show that there is 4-fold difference in their potency.

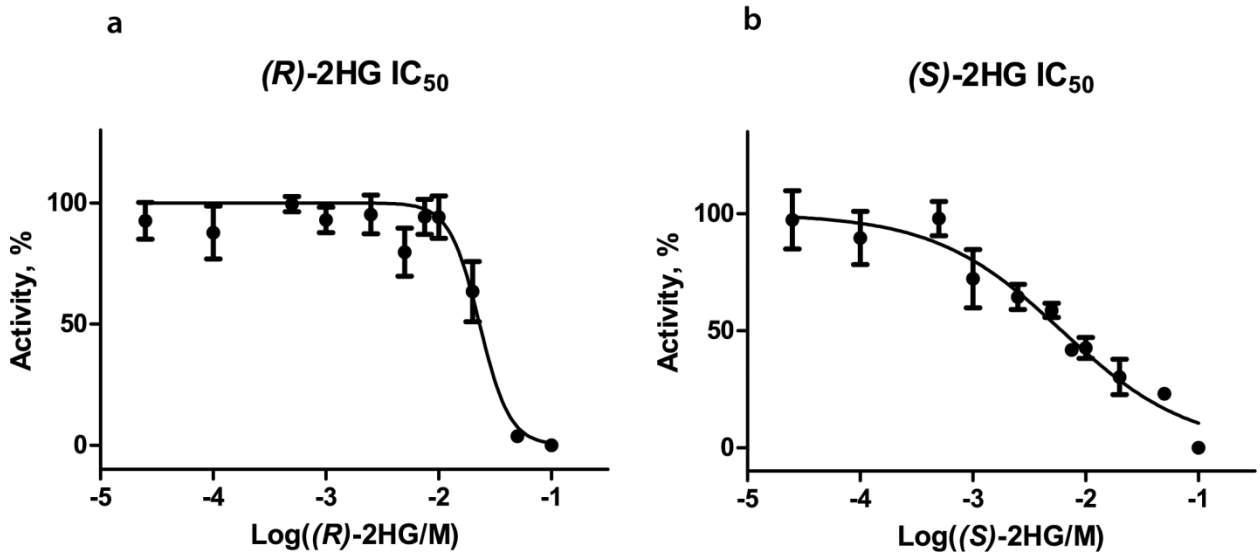


Figure 6.15. Inhibition of PHD2 by re-purified 2HG. The reaction mixtures containing 4 μM PHD2, 100 μM CODD peptide (DLDLEALAPYIPADDDFQL), 25 μM 2OG, 4 mM L-ascorbate, 50 μM Fe(II) and variable concentrations of (*R*)- or (*S*)-2HG were incubated at 37 °C and subsequently analysed by MALDI-TOF-MS. Error bars represent SD for triplicate assays. Determined IC_{50} values are 23 mM for (*R*)-2HG (18–29 mM, 95 % confidence interval), 6.1 mM for (*S*)-2HG (4.3–8.7 mM, 95 % confidence interval). (*R*)-2HG used in this experiment was additionally HPLC-purified to remove 2OG background. Figure and figure legend are adapted with permission from Tarhonskaya *et al.* (2014) Nature Communications **5** http://dx.doi.org/10.1038/ncomms4423 [16].

SSA was observed as one of the products of 2HG oxidation, therefore studies of its potential activity as a 2OG oxygenase inhibitor were carried out. Inhibition of PHD2, FIH, JMJD2A and BBOX1 was investigated using the same conditions as in a previous report [6]. SSA was shown to be a very weak inhibitor with IC_{50} values in the mM range (4.5 mM, 2.9 mM, 2.8 mM and 267 μM for FIH, PHD2, JMJD2A and BBOX1, respectively (**Figure 6.16**).

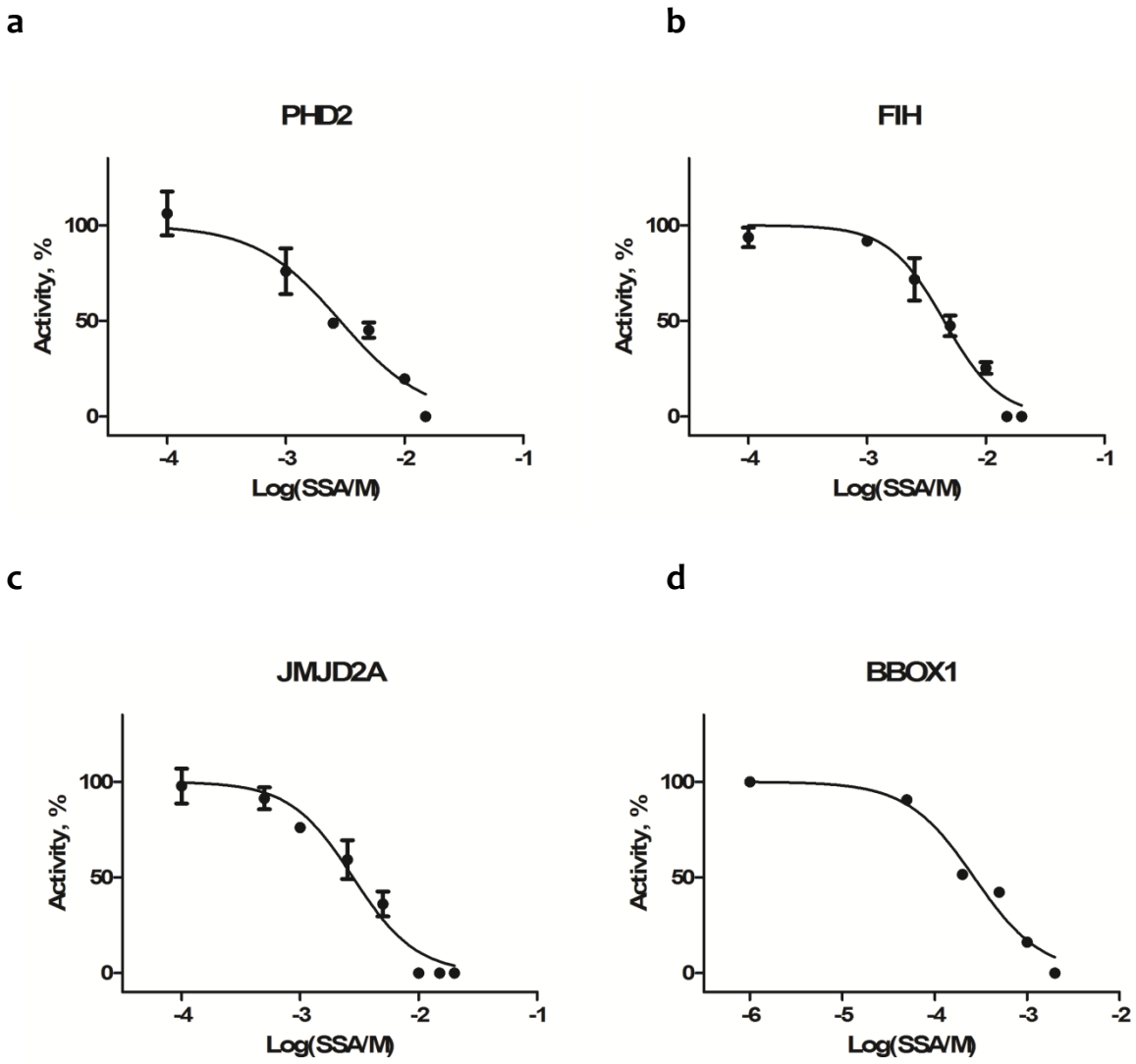


Figure 6.16. Inhibition of 2OG oxygenases by succinic semialdehyde (SSA). Determined IC_{50} values are 2.9 mM for PHD2 (1.7–4.9 mM 95 % confidence interval), 4.5 mM for FIH (3.4–5.8 mM 95 % confidence interval), 2.8 mM JMJD2A (2.1–3.8 mM 95 % confidence interval), 267 µM for BBOX1 (166-431 µM 95 % confidence interval). The conditions used were as reported [6] and samples were analysed by MALDI-TOF-MS. Figure and figure legend are adapted with permission from Tarhonskaya *et al.* (2014) Nature Communications **5** http://dx.doi.org/10.1038/ncomms4423 [16].

6.3. Discussion

The results described in this Chapter demonstrate that it is unlikely that the reported activation of PHDs by (*R*)-2HG is due to the enzymatic conversion of (*R*)-2HG to 2OG. In addition, the results clearly show that non-enzymatic conversion of 2HG to 2OG can occur. This reaction is promoted by reducing agents (L-ascorbate, GSH), and also requires Fe(II)/Fe(III). Moreover, biophysical studies imply that (*R*)-2HG is a very weak binder for PHD2, therefore the PHD2.Fe(II).(*R*)-2HG complex/characteristic absorbance band was not observed by ESI-MS and UV-vis spectroscopy (**Figure 6.4, Figure 6.5**). Non-enzymatic studies showed that 2OG levels produced in the reaction could support catalysis by PHD2, as observed in the previous report [10]. Overall, no evidence for the enzyme catalysed oxidation of 2HG to 2OG was obtained.

One would expect non-enzymatic 2HG oxidation to occur without discrimination between (*R*)- and (*S*)-2HG enantiomers. This proposal is consistent with the observations based on the results described here. However, Koivunen *et al.* observed the PHD activation only in the presence of (*R*)-, but not (*S*)-2HG. Inhibition analyses on PHD2 show that, although both 2HG enantiomers are very weak inhibitors, (*S*)-2HG is a better inhibitor than (*R*)-2HG. At high concentrations of 2HG compared to PHD2 (as occurs under the assay conditions), the inhibitory effects of (*S*)-2HG may be pronounced relative to the inhibition by (*R*)-2HG. In addition, a background contamination of 2OG in (*R*)-2HG, but not (*S*)-2HG, was observed in all commercially available batches, purchased from the same source as was used by Koivunen *et al.* [10]. Thus, the previously observed stereospecifity of the effects of PHD activation could be due to the difference in inhibition potency of 2HG enantiomers and/or low levels of 2OG being present in (*R*)-2HG.

The reported activation of PHD2 by (*R*)-2HG was claimed to be selective among 2OG oxygenases [10]. However, the results described in this Chapter suggest that the reaction is possible not only for PHD2, but also for other 2OG oxygenases for which 2HG enantiomers do not show high inhibition potency. An increased activity for BBOX1 was observed with (*R*)-2HG compared to the (*S*)-enantiomer, which is consistent with reported IC_{50} values. The possibility of the JMJD2A-catalysed demethylation in the presence of 2HG was also tested, and consistent with the reported μM inhibition range for both 2HG enantiomers, the reaction

was not observed [6]. However, one would expect 2HG-promoted catalysis in the case of FIH. Consistent with the reported FIH sensitivity to ROS, including H_2O_2, which are likely to be produced during the Fenton type chemistry reactions, 2HG-promoted catalysis by FIH was not observed [6, 26]. Thus, although the 2HG oxidation to 2OG is mostly enabled by non-enzymatic reaction, the apparent inhibition potency of 2HG is one of the factors which defines the possibility of the 2HG-promoted enzymatic reaction.

Non-enzymatic 2HG oxidation most likely proceeds via Fenton type chemistry mechanisms, which involve formation of iron-bound ROS [23, 24]. The higher rates observed in the presence of H_2O_2 compared to reducing agents suggest that generation of ROS could be crucial for the reaction [24]. Given the complexity of 2HG metabolism, it is difficult to distinguish between non-enzyme and enzyme-catalysed reactions in cells (**Figure 6.17**) [1]. Thus, it is possible that the reactions observed in this study could contribute to the network of 2HG metabolism. Also as the non-enzymatic 2HG conversion is promoted by H_2O_2, the effect of this chemistry could be more important under conditions of oxidative stress, if the 2HG conversion occurs in cells.

Recent work on IDH mutated mice indicated a reduction in antioxidant concentrations compared to wild-type mice [8]. It is also proposed that 'gain-of-function' IDH-mutations may result in perturbation in the $NADP^+$/NADPH ratio [4]. It is thus possible that Fenton type chemistry, including reactions observed in this study, may be involved in the regulation of these processes.

IDH1/2 mutations leading to accumulation of (*R*)-2HG were identified in many cancers. However, the relation of (*R*)-2HG to tumorigenesis is still unclear [4]. Although the balance of current knowledge mostly suggests that it is unlikely that (*R*)-2HG levels can influence the activity of the HIF hydroxylases, inhibition of chromatin modifying enzymes remains plausible. It has also been shown that (*R*)-2HG, but not (*S*)-2HG, promotes cytokine independence and blocks differentiation in hematopoietic cells [27]. These transformations were linked to the activity of TET enzymes (TET enzymes catalyse hydroxylation of 5-methylcytosine in mammals), although the direct relation between the inhibition of TETs and the observed transformations was not formally proven.

SSA is a metabolite produced by oxidation/transamination of γ-aminobutyric acid (GABA) [28] (**Figure 6.17**). Deficiency in SSA dehydrogenase is a pathological condition which occurs as a result of a genetic disorder and leads to accumulation of SSA in cells, because it cannot be further oxidised to succinic acid and utilised in the TCA cycle metabolism [29]. Thus, formation of SSA as a result of the oxidative conversion of 2HG is of biological interest. In addition, the reactive nature of SSA suggests that its potential involvement in tumorigenesis merits investigation. The inhibition activity for a number of 2OG oxygenases (PHD2, JMJD2A, FIH, BBOX1) was tested. The results reveal that, although SSA is a weak inhibitor of 2OG oxygenases, in some cases it is a more potent inhibitor than (*R*)-2HG. Thus, the possibility of SSA formation from 2HG under the conditions of the oxidative stress would complicate the metabolic network of (*R*)-2HG in IDH1/2 mutated organisms even further (**Figure 6.17**).

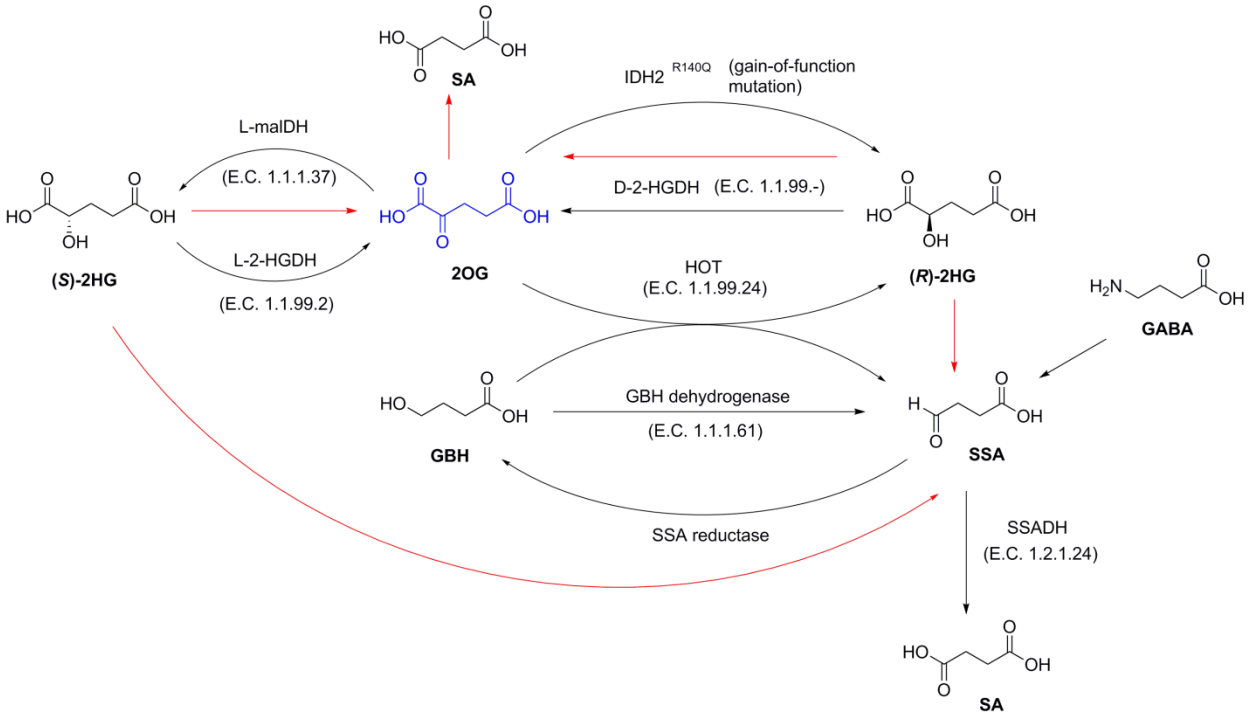


Figure 6.17. Metabolic pathways of (*R*)- and (*S*)-2HG. Red arrows represent non-enzymatic transformations observed in this study, black arrows represent identified literature metabolic pathways [1]. L-malDH - L-malate dehydrogenase; L-2-HGDH - L-2-hydroxyglutarate dehydrogenase; IDH2 - isocitrate dehydrogenase 2; D-2HGDH - D-2-hydroxyglutarate dehydrogenase; HOT - hydroxyacid-oxoacid transhydrogenase enzyme; GBH - γ-hydroxybutyrate; SSA reductase - succinic semialdehyde reductase enzyme; SSADH - succinic semialdehyde dehydrogenase; GABA - γ-aminobutyric acid. Figure and figure legend are adapted with permission from Tarhonskaya *et al.* (2014) Nature Communications **5** http://dx.doi.org/10.1038/ncomms4423 [16].

The results presented in this Chapter have consequences for the interpretation of the cellular observations of Koivunen *et al.* [10]. It has been reported that, compared to wild type cells, levels of both HIF-1α and HIF-2α were lower in mid-passage (passage 20) astrocyte cells, in which mutant IDH1 R132H protein was present, indicating possible activation of PHD enzymes. The observed non-enzymatic 2HG oxidation suggests that these effects are unlikely to arise due to the use of (*R*)-2HG as a co-substrate by PHDs [8, 30]. However, other factors could be responsible for PHD activation in cells. One possibility is that 2OG concentration is increased to a certain level in IDH1 mutant cells, which is the result either of enzymatic conversion of 2HG to 2OG (not by PHDs) or of the non-enzymatic chemistry observed in this study. However, significant increases in 2OG levels were not observed in the previous cell biology studies [30]. Another possibility is that the observed effects on HIF levels in cells resulted from inhibition of JmjC demethylases and TET enzymes ((*R*)-2HG was shown to be an inhibitor for these enzymes [6]). In addition, it has been reported that HIF-α levels were normalised in later passages, which suggests that at least some of the observed effects in IDH mutant cell lines could have been mediated via 'epigenetic processes'.

In summary, no evidence for a novel mechanism to be employed by PHD2 resulting in enzymatic oxidation of (*R*)-2HG to 2OG was obtained, which again supports the proposal that 2OG oxygenases employ a consensus mechanism. However, the non-enzymatic chemistry which could enable this transformation is of interest by itself, because of its potential relevance to the physiological conditions in oxidative stress. Therefore, further biological studies, which are beyond the scope of the work described in this thesis, could inform on the actual mechanisms of 2HG-mediated activation of the PHDs *in vivo*.

6.4. References

1. Kranendijk, M., E. Struys, G. Salomons, M. van der Knaap, and C. Jakobs (2012) *Progress in understanding 2-hydroxyglutaric acidurias.* J. Inherited Metab. Dis. **35**, 571-587.
2. Matsunaga, H., A. Futakuchi-Tsuchida, M. Takahashi, T. Ishikawa, M. Tsuji, and O. Ando (2012) *IDH1 and IDH2 have critical roles in 2-hydroxyglutarate production in D-2-hydroxyglutarate dehydrogenase depleted cells.* Biochem. Biophys. Res. Commun. **423**, 553-556.
3. Yang, H., D. Ye, K.-L. Guan, and Y. Xiong (2012) *IDH1 and IDH2 Mutations in Tumorigenesis: Mechanistic Insights and Clinical Perspectives.* Clin. Cancer. Res. **18**, 5562-5571.
4. Ichimura, K. (2012) *Molecular pathogenesis of IDH1/2 mutations in gliomas.* Brain Tumor Pathol. **29**, 131-139.
5. Dang, L., D.W. White, S. Gross, B.D. Bennett, M.A. Bittinger, E.M. Driggers, V.R. Fantin, H.G. Jang, S. Jin, M.C. Keenan, K.M. Marks, R.M. Prins, P.S. Ward, K.E. Yen, L.M. Liau, J.D. Rabinowitz, L.C. Cantley, C.B. Thompson, M.G. Vander Heiden, and S.M. Su (2009) *Cancer-associated IDH1 mutations produce 2-hydroxyglutarate.* Nature **462**, 739-742.
6. Chowdhury, R., K.K. Yeoh, Y.-M. Tian, L. Hillringhaus, E.A. Bagg, N.R. Rose, I.K.H. Leung, X.S. Li, E.C.Y. Woon, M. Yang, M.A. McDonough, O.N. King, I.J. Clifton, R.J. Klose, T.D.W. Claridge, P.J. Ratcliffe, C.J. Schofield, and A. Kawamura (2011) *The oncometabolite 2-hydroxyglutarate inhibits histone lysine demethylases.* EMBO Rep. **12**, 463-469.
7. Zhao, S., Y. Lin, W. Xu, W. Jiang, Z. Zha, P. Wang, W. Yu, Z. Li, L. Gong, Y. Peng, J. Ding, Q. Lei, K.-L. Guan, and Y. Xiong (2009) *Glioma-Derived Mutations in IDH1 Dominantly Inhibit IDH1 Catalytic Activity and Induce HIF-1α.* Science **324**, 261-265.
8. Sasaki, M., C.B. Knobbe, M. Itsumi, A.J. Elia, I.S. Harris, I.I.C. Chio, R.A. Cairns, S. McCracken, A. Wakeham, J. Haight, A.Y. Ten, B. Snow, T. Ueda, S. Inoue, K. Yamamoto, M. Ko, A. Rao, K.E. Yen, S.M. Su, and T.W. Mak (2012) *D-2-hydroxyglutarate produced by mutant IDH1 perturbs collagen maturation and basement membrane function.* Genes Dev. **26**, 2038-2049.
9. Sasaki, M., C.B. Knobbe, J.C. Munger, E.F. Lind, D. Brenner, A. Brustle, I.S. Harris, R. Holmes, A. Wakeham, J. Haight, A. You-Ten, W.Y. Li, S. Schalm, S.M. Su, C. Virtanen, G. Reifenberger, P.S. Ohashi, D.L. Barber, M.E. Figueroa, A. Melnick, J.-C. Zuniga-Pflucker, and T.W. Mak (2012) *IDH1(R132H) mutation increases murine haematopoietic progenitors and alters epigenetics.* Nature **488**, 656-659.
10. Koivunen, P., S. Lee, C.G. Duncan, G. Lopez, G. Lu, S. Ramkissoon, J.A. Losman, P. Joensuu, U. Bergmann, S. Gross, J. Travins, S. Weiss, R. Looper, K.L. Ligon, R.G.W. Verhaak, H. Yan, and W.G. Kaelin Jr (2012) *Transformation by the (R)-enantiomer of 2-hydroxyglutarate linked to EGLN activation.* Nature **483**, 484-488.
11. van der Donk, W.A., C. Krebs, and J.M. Bollinger Jr (2010) *Substrate activation by iron superoxo intermediates.* Curr. Opin. Struct. Biol. **20**, 673-683.
12. Flashman, E., L.M. Hoffart, R.B. Hamed, J.M. Bollinger Jr, C. Krebs, and C.J. Schofield (2010) *Evidence for the slow reaction of hypoxia-inducible factor prolyl hydroxylase 2 with oxygen.* FEBS J. **277**, 4089-4099.

13. Myllylä, R., K. Majamaa, V. Günzler, H.M. Hanauske-Abel, and K.I. Kivirikko (1984) *Ascorbate is consumed stoichiometrically in the uncoupled reactions catalyzed by prolyl-4-hydroxylase and lysyl hydroxylase.* J. Biol. Chem. **259**, 5403-5405.
14. Hausinger, R.P. (2004) *Fe(II)/α-Ketoglutarate-Dependent Hydroxylases and Related Enzymes.* Crit. Rev. Biochem. Mol. Biol. **39**, 21-68.
15. Koivunen, P., M. Hirsilä, K.I. Kivirikko, and J. Myllyharju (2006) *The Length of Peptide Substrates Has a Marked Effect on Hydroxylation by the Hypoxia-inducible Factor Prolyl 4-Hydroxylases.* J. Biol. Chem. **281**, 28712-28720.
16. Tarhonskaya, H., A.M. Rydzik, I.K.H. Leung, N.D. Loik, M.C. Chan, A. Kawamura, J.S.O. McCullagh, T.D.W. Claridge, E. Flashman, and C.J. Schofield (2014) *Non-enzymatic chemistry enables 2-hydroxyglutarate-mediated activation of 2-oxoglutarate oxygenases*. Nat. Commun. **5**, DOI: 10.1038/ncomms4423.
17. Townsend, D.M., K.D. Tew, and H. Tapiero (2003) *The importance of glutathione in human disease.* Biomed. Pharmacother. **57**, 145-155.
18. Flashman, E., S.L. Davies, K.K. Yeoh, and C.J. Schofield (2010) *Investigating the dependence of the hypoxia-inducible factor hydroxylases (factor inhibiting HIF and prolyl hydroxylase domain 2) on ascorbate and other reducing agents.* Biochem. J. **427**, 135-142.
19. Du, J., J.J. Cullen, and G.R. Buettner (2012) *Ascorbic acid: Chemistry, biology and the treatment of cancer.* BBA - Rev. Cancer **1826**, 443-457.
20. Price, J.C., E.W. Barr, B. Tirupati, J.M. Bollinger, and C. Krebs (2003) *The First Direct Characterization of a High-Valent Iron Intermediate in the Reaction of an α-Ketoglutarate-Dependent Dioxygenase: A High-Spin Fe(IV) Complex in Taurine/α-Ketoglutarate Dioxygenase (TauD) from Escherichia coli.* Biochemistry **42**, 7497-7508.
21. Chowdhury, R., M.A. McDonough, J. Mecinović, C. Loenarz, E. Flashman, K.S. Hewitson, C. Domene, and C.J. Schofield (2009) *Structural Basis for Binding of Hypoxia-Inducible Factor to the Oxygen-Sensing Prolyl Hydroxylases.* Structure **17**, 981-989.
22. Walling, C. and K. Amarnath (1982) *Oxidation of mandelic acid by Fenton's reagent.* J. Am. Chem. Soc. **104**, 1185-1189.
23. Stadtman, E.R. (1993) *Oxidation of Free Amino Acids and Amino Acid Residues in Proteins by Radiolysis and by Metal-Catalyzed Reactions.* Annu. Rev. Biochem **62**, 797-821.
24. Buettner, G.R. and B.A. Jurkiewicz (1996) *Catalytic Metals, Ascorbate and Free Radicals: Combinations to Avoid.* Radiat. Res. **145**, 532-541.
25. Knight, R.J. and R.N. Sylva (1975) *Spectrophotometric investigation of iron(III) hydrolysis in light and heavy water at 25°C.* J. Inorg. Nucl. Chem. **37**, 779-783.
26. Masson, N., R.S. Singleton, R. Sekirnik, D.C. Trudgian, L.J. Ambrose, M.X. Miranda, Y.-M. Tian, B.M. Kessler, C.J. Schofield, and P.J. Ratcliffe (2012) *The FIH hydroxylase is a cellular peroxide sensor that modulates HIF transcriptional activity.* EMBO Rep. **13**, 251-257.
27. Losman, J.-A., R.E. Looper, P. Koivunen, S. Lee, R.K. Schneider, C. McMahon, G.S. Cowley, D.E. Root, B.L. Ebert, and W.G. Kaelin (2013) *(R)-2-Hydroxyglutarate Is Sufficient to Promote Leukemogenesis and Its Effects Are Reversible.* Science **339**, 1621-1625.

28. Kim, K.J., P.L. Pearl, K. Jensen, O.C. Snead, P. Malaspina, C. Jakobs, and K.M. Gibson (2011) *Succinic semialdehyde dehydrogenase: biochemical-molecular-clinical disease mechanisms, redox regulation, and functional significance.* Antioxid. Redox Signaling **15**, 691-718.
29. Pearl, P.L., E.J. Novotny, M.T. Acosta, C. Jakobs, and K.M. Gibson (2003) *Succinic semialdehyde dehydrogenase deficiency in children and adults.* Ann. Neurol. **54**, S73-S80.
30. Xu, W., H. Yang, Y. Liu, Y. Yang, P. Wang, S.-H. Kim, S. Ito, C. Yang, P. Wang, M.-T. Xiao, L.-x. Liu, W.-q. Jiang, J. Liu, J.-y. Zhang, B. Wang, S. Frye, Y. Zhang, Y.-h. Xu, Q.-y. Lei, K.-L. Guan, S.-m. Zhao, and Y. Xiong (2011) *Oncometabolite 2-Hydroxyglutarate Is a Competitive Inhibitor of a-Ketoglutarate-Dependent Dioxygenases.* Cancer Cell **19**, 17-30.

Chapter 7: Materials and Methods*

7.1. Materials

All chemicals, unless otherwise stated, were obtained in the highest quality available from Sigma-Aldrich.

Pfu Turbo DNA polymerase and competent cells XL10-Gold were from Stratagene.

Bacto tryptone, yeast extract and bacto agar for use in culture media were from OXOID; sodium chloride for culture media was from Fisher BioReagents.

Isopropyl β-D-1-thiogalactopyranoside (IPTG) was from Apollo Scientific.

Water was purified using a Millipore Elix 10 system equipped with 0.22 μm filter (ultra pure water, 18.2 MΩ·cm). Water was sterilized for DNA applications by autoclaving.

Competent cells

E. coli strains were used with the following genotypes (Stratagene, Competent Cells Brochure):

XL10-Gold Transformation of mutagenesis plasmid product, commercially obtained.

BL21 (DE3) Protein expression, prepared in-house (see below).

* Some of the developed experimental procedures described in this Chapter have been published (see footnotes to Chapters 2-6); Other published procedures, developed previously and used for experimental work on this thesis, are referenced throughout.

Peptide sequences

The peptides were obtained from Peptide Protein Research Ltd. (Fareham, UK) or GL Biochem Ltd, (Shanghai, China).

Table 7.1. Sequences of the peptides used in this thesis.

Peptide	Sequence
CODD HIF-1$\alpha_{556-574}$	DLDLEMLA**P**YIPMDDDFQL
CODD HIF-2$\alpha_{523-541}$	ELDLETLA**P**YIPMDGEDFQ
NODD HIF-1$\alpha_{395-413}$	DALTLLA**P**AAGDTIISLDF
NODD HIF-2$\alpha_{398-416}$	EELAQLA**P**TPGDAIISLDF
CAD HIF-1$\alpha_{789-806}$	DESGLPQLTSYDCEV**N**API
CAD HIF-1$\alpha_{789-822}$	DESGLPQLTSYDCEV**N**APIQGSRNLLQGEELLRAL
CAD HIF-2$\alpha_{832-850}$	ESYLLPELTRYDCEV**N**VPV
CAD HIF-2$\alpha_{832-866}$	ESYLLPELTRYDCEV**N**VPVLGSSTLLQGGDLLRAL
1CA$_{20\text{-mer}}$	HLEVVKLLLEAGADV**N**AQDK
tankyrase-1$_{849-868}$	NLEVAEYLLEHGADV**N**AQDK
tankyrase-1$_{844-886}$	AAGYNNLEVAEYLLEHGADV**N**AQDKGGLIPLHNAA
2CA	SDKNGSTPLHLAARNGHLEVVKLLLEHGADVNAQDKWGKT AFDISIDNGNEDLAEILQ
3CA	GSHMGSDLGKKLLEAARAGQDDEVRILMANGADVAAKDKN GSTPLHLAARNGHLEVVKLLLEAGADVNAQDKFGKTAFDISI DNGNEDLAEILQ

7.2. General experimental procedures

pH Measurements

The pH of solutions was determined using a Jenway pH Meter 3305, with Aldrich glass/calomel combination electrode. Prior to measurements calibration was carried out between pH 4.0-7.0 or pH 7.0-10.0 with buffer solutions of phthalate (pH 4.0), phosphate (pH 7.0) and borate (pH 10.0) from Fisher Scientific. Electrodes were stored in a 4 M potassium chloride solution.

Centrifugation

Samples of volume less than 1.5 mL were centrifuged at room temperature using Beckman Coulter Ltd. benchtop centrifuge (Microfuge 22R) at 13,000 rpm (14,000 x g). Cell growth cultures and cell lysates were centrifuged in a Beckmann Avanti J-25, and protein was concentrated using a Beckmann Allegra X-30R, all at 4 °C.

7.3. Site-directed mutagenesis (PHD2)

Table 7.2. PHD2 primers.

Variant	Sequence (5'-3')
H313D	GGTTATGTACGTGATGTTGATAATCCAAATGG
D315E	TGTACGTCATGTTGAAAATCCAAATGGAGATG
D315H	TGTACGTCATGTTCATAATCCAAATGGAGATG
H374E	CGTCGCAACCCTGAAGAAGTACAACCAGCATATG
R383K	GCATAT GCTACACACTACGCAATAACTGTTTG

Preparation of oligonucleotides

Oligonucleotides were from Sigma-Aldrich Ltd. as lyophilised pellets on a 0.025 µmol scale (no extra purification, except desalting). Before use, the oligonucleotides were resuspended in sterile Milli-Q water to give a 100 µM stock solution, which was then diluted to 10 µM with sterile Milli-Q water for use in PCR experiments.

Polymerase chain reaction (PCR) protocol

Stratagene's QuikChange site-directed mutagenesis protocol (Stratagene Instruction Manual #200518) was used to make point mutations. The forward and reverse primers, each incorporating the mutation and complementary to opposite strands of the vector were used to amplify the sequence in opposite directions by PCR. A typical PCR was set up according to Stratagene's QuikChange ® Site-Directed Mutagenesis protocol:

dsDNA template (10 ng/µL)	1 µL
Forward primer (10 µM)	2 µL
Reverse primer (10 µM)	2 µL

10 × reaction buffer	5 µL
dNTP mixture (2 mM)	5 µL
Sterile Milli-Q H_2O	34 µL
*Pfu*Turbo DNA polymerase (2.5 U/µL)	1 µL

The final volume of the reaction was maintained at 50 µL. The PCR mixture was heated to 95 °C for 1 minute to denature the DNA. Further thermal cycling (16 cycles) with the mutagenic primers yielded an amplified and mutated plasmid. Typical cycling parameters for the QuikChange Site-Directed Mutagenesis were as follows:

Temperature	**Time**	**Step**
95 °C	1 min	Denaturation
55 °C	1 min	Annealing
68 °C	7 min	Extension

A final extension was carried out at 68 °C for 10 minutes and the mixture was then cooled to 4 °C.

The annealing temperature was varied from 55 to 60 °C depending on the binding of mutagenic primers to the template as verified later by DNA sequencing (Geneservice Ltd., Department of Biochemistry, University of Oxford).

Dpn I digestion of the PCR products

The PCR reactions yielded product mixtures containing mutated plasmids and parental (nonmutated) dsDNA templates. It was necessary to remove the non-modified templates before transformation since they both contain the same antibiotic resistance gene. This was achieved by digesting the PCR products with the Dpn I restriction enzyme (Stratagene Instruction Manual #200518). Dpn I digests methylated/hemimethylated DNAs; the plasmid DNA templates were isolated from a dam + *E. coli* strain so the parent DNA could be digested. Dpn I (1 µL) was added to the PCR products and gently mixed before being digested for 3 hours at 37 °C.

Transformations of competent cells

For transformation, an aliquot of competent cells (35 µL) was transferred to a 1.5 mL sterile Eppendorf vial and the plasmid/PCR product (1 or 2 µL) was added with gentle mixing. The transformation mixture was chilled on ice for 15 minutes, followed by a heat shock for 30 (for XL10-Gold cells) or 45 seconds (for BL21(DE3) cells) at 42 °C to induce DNA uptake. In order to allow the bacterial cells to recover from the heat shock, the cells were incubated at 37 °C for an hour with 200 µL SOC medium and plated on LB-agar plates containing kanamycin at 30 µg/mL. Finally the plates were incubated at 37 °C overnight.

7.4. Preparation of competent cells BL21 (DE3)

100 mL sterile 2 TY medium was inoculated with a single colony and cell culture was grown in a shaking incubator (220 rpm) at 37 °C overnight. 400 mL sterile growth medium was inoculated with 800 µL of the starting culture and grown (220 rpm, 37 °C) to OD_{600} 0.6-0.8. Then cells were centrifuged at 750 x g, 4 °C for 5 minutes and gently resuspended in 200 mL sterile 100 mM $CaCl_2$/20% (v/v) glycerol solution. The suspension was incubated on ice for 20 minutes and again centrifuged at 750 x g, 4 °C for 5 minutes. The cell pellets were gently resuspended in 8 mL of 100 mM $CaCl_2$/20% (v/v) glycerol solution. The suspension of cells was aliquoted in sterile Eppendorf vials and stored immediately at -80 °C.

7.5. Preparation of media

2 Tryptone/Yeast extract (2 TY) medium (per 1L)

The components were dissolved in 0.9 L Milli-Q water. After mixing the components, Milli-Q water was added up to 1 L, and the mixture was autoclaved.

Table 7.3. 2 TY medium.

Reagent	Mass (g)
Tryptone	16.0
Yeast extract	10.0
NaCl	5.0

Luria-Bertani (LB) agar medium (per 0.5 L)

After mixing the components, Milli-Q water was added up to 0.5 L and the mixture was autoclaved.

Table 7.4. LB agar medium.

Reagent	Mass (g)
Tryptone	5
Yeast extract	2.5
Agar	10
NaCl	5

SOC Medium (per 100 mL)

After mixing the components, Milli-Q water was added up to 100 mL and the mixture was autoclaved. 0.5 mL sterile 2 M $MgCl_2$ and 20 mM sterile glucose were added afterwards.

Table 7.5. SOC medium.

Reagent	Mass/Volume
Tryptone	2 g
Yeast extract	0.5 g
NaCl	0.058 g
KCl	0.019 g
NaOH (1M)	0.4 mL

7.6. Plasmid purification

A single colony resulting from transformation was inoculated into 10 mL 2 TY medium containing kanamycin at 30 μg/mL. The starter culture was grown overnight at 37 °C with shaking at 220 rpm. Plasmid DNA was purified from the culture using the Qiagen Miniprep Kit following the manufacturer's protocol. The integrity of the mutations was confirmed by sequencing performed by Geneservice Ltd., Department of Biochemistry, University of Oxford.

7.7. Preparation of glycerol freeze

100 mL of 2 TY medium containing kanamycin at 30 µg/mL were inoculated with a single colony and then were grown in a shaking incubator (220 rpm) overnight at 37 °C. 1 mL of the cell culture was centrifuged at 13,000 rpm (14,000 x g) for 2 min and then resuspended in 400 µL of sterile 2 TY medium followed by addition of 400 µL sterile glycerol stock solution, and frozen at -80 °C.

Table 7.6. Glycerol stock solution.

Reagent	Concentration
Glycerol	65 % (v/v)
$MgSO_4$	0.1 M
Tris·HCl (pH 7.6)	0.025 M

7.8. Protein expression trials

A starter culture was grown overnight at 37 °C with shaking at 220 rpm. 100 mL 2 TY medium were inoculated with 1 mL of starter culture and grown to at 37 °C with shaking at 220 rpm until OD_{600} reached 0.6-0.7 and induced then with 100 µL IPTG (final concentration 0.5 mM). The flasks were incubated at 18, 28 and 37 °C, 220 rpm for 3 hours and overnight. Cells were harvested at 4000 rpm (1800 x g), 4 °C for 10 minutes, and the wet cell pellets were stored at -80°C.

For expression trials cell pellets were resuspended in 5 mL 50 mM Tris·HCl pH 7.5 and then lysed by sonication with a Soniprep 150 sonicator (2 x 30 sec sonication with 30 sec rest in between). The crude lysates were centrifuged at 13000 rpm (14,000 x g) for 2 minutes and the supernatant was transferred into Eppendorf vials. Cell pellets were resuspended in 1 mL 50 mM Tris·HCl pH 7.5. Samples were analysed for the presence and level of the expressed protein with SDS-PAGE.

7.9. Full-scale protein expression

Plasmid constructs used in this study

cDNA sequences encoding tPHD2 have previously been inserted into the pET-28a(+)/pET-24a(+) vectors (Novagen), by Dr K. S. Hewitson and Dr E. Flashman [1], to yield tPHD2 (catalytic domain of $PHD2_{181-426}$) protein with/without an *N*-terminal His_6-tag. These constructs were used as templates for further mutagenesis experiments. Constructs for the Y303F, Y329F, and H374R PHD2 variants were previously prepared by Dr. R. Chowdhury [1].

A full–length FIH sequence was previously inserted into the pET-28a(+) vector in the Schofield group, to yield a protein with an *N*-terminal His_6-tag. A full-length DAOCS construct in the pET-24a(+) vectors was previously designed in the Schofield group [2]. cDNA sequences encoding 2CA A26H have been designed and inserted into the pNIC28 vector by E. Howe, to yield a protein with an *N*-terminal His_6-tag. The 3CA was previously encoded into pET-28a(+) vector, to yield a protein with an *N*-terminal His_6-tag (Schofield group).

General expression procedure

Large scale growth was initiated by adding 7.5 mL of overnight starter culture to 600 mL of 2 TY media supplemented with kanamycin at 30 μg/mL. Cells were grown at 37 °C with shaking at 220 rpm until OD_{600} reached 0.6-0.7; and the expression of protein was induced by addition of IPTG (at the temperature optimum for expression, **Table 7.7**). After expression (see **Table 7.7** for the expression time) cells were harvested at 7000 rpm, 4 °C for 8 minutes. The supernatant was discarded; the cells were collected and frozen at -80 °C.

Table 7.7. Protein expression conditions.

Protein	Temperature, °C	IPTG, mM	Time, hours
PHD2	28/18	0.5	overnight
FIH	37	0.5	4
DAOCS	28	1	4
2CA	18	0.2	overnight
3CA	37	0.5	4

7.10. Protein purification

Enzymes were purified at 4 °C using an AKTA Fast Protein Liquid Chromatography (FPLC) System, Amersham Pharmacia Biotech (Liquid Chromatography Controller UPC-900 with high precision P-920 pump). The FPLC system was controlled from a PC running UNICORN v. 4.00. All buffers were freshly prepared with Milli-Q water and filtered through a 0.2 μm Millipore filter before use.

Purification of WT PHD2 and the R383K variant

Cation exchange chromatography

The cell pellet was resuspended in 100 mL of 0.1 M MES buffer pH 5.8 containing 1 mM $MgCl_2$ and DNAse I (0.02 mg/mL) at 4 °C. The cell suspension was lysed by sonication on ice (4 x 45 sec sonication, 45 sec rest in between), using a SONICS VibraCell 150 sonicator, with a microtip at 60 % amplitude. The cell lysate was then centrifuged at 24,000 rpm (25,000 x g), 4 °C for 30 minutes, and filtered through a 0.45 μm Millipore filter. The cleared lysate was then loaded onto a Sepharose SP 50 mL column pre-equilibrated with 2 column volumes (CV, 1CV~50 mL) of Milli-Q water, 2 CV of 1 M NaCl and 2 CV of 0.1 M MES pH 5.8. After loading of the lysate, the column was washed with 3-4 CV of 0.1 M MES pH 5.8. Protein was eluted over 30 minutes with a gradient (0-100 %, 4 mL/min) of 0.1 M MES 1 M NaCl pH 5.8 buffer. The fractions containing target protein were determined by SDS-PAGE.

EDTA incubation

To obtain apo-enzymes, the PHD2 fractions obtained after cation exchange chromatogtaphy were incubated with 0.2 M EDTA in ammonium acetate (15 mM, pH 7.5) with a final protein concentration of approx. 1 mg/mL.

Size exclusion chromatography

A Superdex S75 column, 300 mL was equilibrated with 1 CV of water and 1 CV of buffer (100 mM Tris·HCl, 100 mM NaCl, pH 7.5) at a flow rate of 2.0 mL/min. The proteins were concentrated to around 2.2 mL using an Amicon ultra-15 Millipore centrifugal filter membrane (10 kDa M_W cut-off) and loaded onto the column using a 2 mL loop at 0.5 mL/min. After loading of proteins the flow rate was increased to 2 mL/min with UV base corrected to zero. The protein fractions were collected by an automatic fraction collector when the UV

peak level rose above 10 mAU, in typical fractions of 5 mL. The eluted fractions were analysed for purity by SDS-PAGE. The procedure usually yielded proteins of >90 % purity by SDS-PAGE. The fractions containing pure protein were pooled together and buffer exchanged into 50 mM Tris·HCl pH 7.5, concentrated to ~1 mL using Amicon ultra-15 Millipore centrifugal filter membrane (10 kDa M_W cut-off) and stored in aliquots of 20 μL at -80 °C. The molecular weight of the purified PHD2 variants was determined by LC-MS and was consistent with calculated values.

Purification of the Y303, H313, D315, Y329, H374 PHD2 variants (His_6-tagged proteins)

The cell extracts were prepared according to the same procedure as used for ion exchange purification with the difference that in this case frozen cell pellets were resuspended in Protino Ni-TED lysis-equilibration-wash (LEW) buffer (0.5 M NaCl, 20 mM Tris·HCl, pH 7.5). The crude cell lysate was filtered through a Millipore 0.45 μm filter and then applied on a TED (Tris-carboxymethyl ethylene diamine) column pre-equilibrated with 10 CV (CV~10 mL) of Milli-Q water and 10 CV LEW buffer. Lysate loading was followed by 10 CV wash with LEW buffer and elution over 30 min with a gradient (0-100 %) of the elution buffer (0.5 M NaCl, 0.5 M imidazole, 20 mM Tris·HCl, pH 7.5). The procedure yielded His_6-tagged proteins of >95 % purity by SDS-PAGE. The protein was concentrated by ultrafiltration (10 kDa M_W cut-off, Amicon ultra-15, Millipore) and either subjected to buffer exchange or thrombin cleavage.

Cleavage of His_6-tag (thrombin)

High grade thrombin (Novagen) was used to remove the His_6-tag from the *N*-terminus of a fusion protein according to the standard manufacturer's instructions (1 U of thrombin to 1 mg of protein). The thrombin protein mixture was incubated for 24-28 hours at 4 °C and then resolved by size exclusion chromatography as described above.

FIH purification

The cell pellet was resuspended in 100 mL of 50 mM HEPES 500 mM NaCl 5 mM imidazole (pH 7.5) buffer (binding buffer) containing 1 mM $MgCl_2$ and DNAse I (0.02 mg/mL) at 4 °C. The cell suspension was lysed by sonication on ice (10 x 30 sec sonication, 40 sec rest between pulses), using a SONICS VibraCell 150 sonicator, with a microtip at 60 % amplitude.

Then the cell lysate was centrifuged at 24,000 rpm (25,000 x g), 4 °C for 30 minutes, and filtered through a 0.45 µm Millipore filter. The cleared lysate was then loaded onto a Ni-NTA column (GE Healthcare Life Sciences, Little Charlton, UK) pre-equilibrated with 3 column volumes (CV, 1 CV~5 mL) of binding buffer (**Table 7.8**). After loading of the lysate, the column was washed with 8 CV of binding buffer and 15 CV of wash buffer (**Table 7.8**). Proteins were eluted over 30 minutes with 100 % elution buffer (no gradient, **Table 7.8**). The fractions containing target protein were determined by SDS-PAGE.

Table 7.8. Buffers used for Ni-affinity purification.

Buffer	Composition
Binding buffer	50 mM HEPES 500 mM NaCl 5 mM imidazole (pH 7.5)
Wash buffer	50 mM HEPES 500 mM NaCl 30 mM imidazole (pH 7.5)
Elution buffer	50 mM HEPES 500 mM NaCl 500 mM imidazole (pH 7.5)

Cleavage of His_6-tag (thrombin)

High grade thrombin (Novagen) was used to remove the His_6-tag from the *N*-terminus of a fusion protein according to the standard manufacturer's instructions (1 U of thrombin to 4 mg of protein). The thrombin protein mixture was incubated overnight at 4 °C and then resolved by size exclusion chromatography.

Size exclusion chromatography

A Superdex S200 column, 300 mL was equilibrated with 1 CV of water and 1 CV of buffer (100 mM HEPES, 100 mM NaCl, pH 7.5) at a flow rate of 2.0 mL/min. The proteins were concentrated to around 2.2 mL using an Amicon ultra-15 Millipore centrifugal filter membrane (30 kDa M_W cut-off) and loaded onto the column using a 2 mL loop at 0.5 mL/min. After loading of proteins the flow rate was increased to 2 mL/min with UV base corrected to zero. The protein fractions were collected by an automatic fraction collector when the UV peak level rose above 10 mAU, in typical fractions of 5 mL. The eluted fractions were analysed for purity by SDS-PAGE. The procedure usually yielded proteins of >95 % purity by SDS-PAGE. The fractions containing pure protein were pooled together and buffer exchanged

into 50 mM HEPES pH 7.5, concentrated to ~1 mL using Amicon ultra-15 Millipore centrifugal filter membrane (30 kDa M_W cut-off), then stored in aliquots (100 µL) at -80 °C.

DAOCS purification

Ion exchange chromatography

The cell pellet was resuspended in 100 mL of 50 mM Tris·HCl buffer pH 7.5 containing 1 mM $MgCl_2$ and DNAse I (0.02 mg/mL) at 4 °C. The cell suspension was lysed by sonication on ice (5 x 30 sec sonication, 40 sec rest in between), using a SONICS VibraCell 150 sonicator, with a microtip at 60 % amplitude. Then the cell lysate was centrifuged at 24,000 rpm (25,000 x g), 4 °C for 30 minutes, and filtered through a 0.45 µm Millipore filter. The cleared lysate was then loaded onto a Sepharose FF 50 mL column pre-equilibrated with 2 column volumes (CV, 1CV~50 mL) of Milli-Q water, 2 CV of 1 M NaCl and 2 CV of 50 mM Tris·HCl 1 mM EDTA buffer pH 7.5. After loading of the lysate, the column was washed with 3-4 CV of 50 mM Tris·HCl 1 mM EDTA pH 7.5 buffer. Protein was eluted over 60 minutes (2 mL/min) with a gradient (0-50 %) 50 mM Tris·HCl 1 mM EDTA 0.3 M NaCl buffer pH 7.5. The fractions containing target protein were determined by SDS-PAGE

Size exclusion chromatography

A Superdex S75 column, 300 mL was equilibrated with 1 CV of water and 1 CV of buffer (100 mM Tris·HCl 100 mM NaCl, pH 7.5) at a flow rate of 2.0 mL/min. The proteins were concentrated to around 2.2 mL using Amicon ultra-15 Millipore centrifugal filter membrane (10 kDa M_W cut-off) and loaded onto the column using 2 mL loop at 0.5 mL/min. After loading of proteins the flow rate was increased to 2 mL/min with the UV base corrected to zero. The protein fractions were collected using an automatic fraction collector when UV peak level rose above 10 mAU, in typical fractions of 5 mL. The eluted fractions were analysed for purity by SDS-PAGE. The procedure usually yielded proteins of >95 % purity by SDS-PAGE. The fractions containing pure protein were pooled together and buffer exchanged into 50 mM Tris·HCl pH 7.5, concentrated to ~1 mL using Amicon ultra-15 Millipore centrifugal filter membrane (30 kDa M_W cut-off) and stored in aliquots of 100 µL at -80 °C.

2CA (2 consensus ankyrin repeats) purification

The cell pellet was resuspended in 100 mL of 50 mM HEPES 500 mM NaCl 5 mM imidazole (pH 7.5) buffer (binding buffer) containing 1 mM $MgCl_2$ and DNAse I (0.02 mg/mL) at 4 °C. The cell suspension was lysed by sonication on ice (10 x 30 sec sonication, 40 sec rest in between), using a SONICS VibraCell 150 sonicator, with a microtip at 60 % amplitude. Then the cell lysate was centrifuged at 24,000 rpm (25,000 x g), 4 °C for 30 minutes, and filtered through a 0.45 μm Millipore filter. The cleared lysate was then loaded onto a 5 mL Ni-NTA column (GE Healthcare Life Sciences, Little Charlton, UK) pre-equilibrated with 3 column volumes (CV, 1CV~5 mL) of the binding buffer (**Table 7.8**). After loading of the lysate, the column was washed with 8 CV of binding buffer and 15 CV of wash buffer (50 mM HEPES 500 mM NaCl 30 mM imidazole (pH 7.5) buffer). Protein was eluted over 60 minutes (14 CV) with 0-100 % elution buffer gradient (**Table 7.8**). The fractions containing target protein were determined by SDS-PAGE.

To cleave the His_6-tag the 2CA fractions were incubated overnight at 4 °C with the TEV-1 protease (1:10 ratio by molarity). The mixture was then purified using a 5 mL Ni-NTA column to give untagged protein. The protein fractions were assessed for purity by SDS-PAGE and buffer exchanged into 50 mM HEPES pH 7.5 using Amicon ultra-15 Millipore centrifugal filter membrane (3 kDa M_W cut-off) and stored in aliquots of 100 μL at -80 °C.

3CA (3 consensus ankyrin repeats) purification

3CA purification was carried out according to the same protocol as that used for FIH using a 5 mL Ni-NTA column (GE Healthcare Life Sciences, Little Charlton, UK) that used no gradient during elution. Amicon ultra-15 Millipore centrifugal filter membrane (3 kDa M_W cut-off) concentrators were used to concentrate the protein. The 3CA concentration was determined using Bradford reagent.

7.11. SDS-PAGE

SDS-PAGE gel preparation

The buffers for SDS-PAGE gel preparation were made according to the following recipes:

2 x SDS-PAGE separating gel buffer (per 0.5 L)

Tris·HCl 750 mM pH 8.8

SDS 0.2 % (w/v)

2 x SDS-PAGE stacking gel buffer (per 0.5 L)

Tris·HCl 250 mM pH 6.8

SDS 0.2 % (w/v)

Polyacrylamid gels were prepared using the Bio-Rad Mini-Protean Tetra Electrophoresis System. The compositions of the gels was the following:

Table 7.9. Separating gel.

Reagent	Volume
30 % Acrylamide	2.5 mL
2 x SDS-PAGE separating buffer	2.5 mL
TEMED	10 µL
25 % (w/v) APS	30 µL

Table 7.10. Stacking gel.

Reagent	Volume
30 % Acrylamide	300 µL
2 x SDS-PAGE stacking buffer	1 mL
Milli-Q H_2O	700 µL
TEMED	5 µL
25 % (w/v) APS	15 µL

Electrophoresis was typically conducted at a constant voltage of 200 V. Samples were prepared by addition of 2 x loading buffer (10 µL) to 10 µL of protein sample followed by heating on the hot block at 100 °C for 5 minutes and then loaded to give ~10 µg of protein per well. Molecular weight marker was obtained from Invitrogen. The gels were stained for 5 minutes in staining solution and then destained until clear.

Table 7.11. 10 x SDS-PAGE running buffer (1 L)

Reagent	Mass/Volume
Tris base	30.2 g
Glycine	144 g
10 % (w/v) SDS	100 mL
Milli-Q H_2O	900 mL

Table 7.12. 2 x SDS-PAGE loading buffer (100 mL)

Reagent	Mass/Volume
Tris·HCl	0.5 M, pH 6.8
Bromophenol blue	0.2 g
10 % (w/v) SDS	20 mL
Glycerol	12 mL
β-mercaptoethanol	5 mL
Milli-Q H_2O	up to 100 mL

Table 7.13. SDS-PAGE staining solution.

Reagent	Concentration
Acetic acid (glacial)	10 %
Methanol	20 %
Coomassie brilliant blue R250	0.1 %

Table 7.14. SDS-PAGE destaining solution.

Reagent	Concentration
Acetic acid (glacial)	10 %
Methanol	25 %

7.12. MALDI-TOF-MS-based hydroxylation assays

PHD2 enzymatic assays

Enzymatic assays were performed in 50 mM Tris·HCl pH 7.5 buffer or 50 mM HEPES pH 7.5 at 37 °C with typically the following reagent concentrations:

Table 7.15. Conditions used for PHD2 assays.

Reagent	Concentration
PHD2	4 μM
peptide	100 μM
2OG	300 μM
L-ascorbate	4 mM
Fe(II)	50 μM

The 19-mer peptides were from Peptide Protein Research Ltd. (Fareham, UK) or GL Biochem Ltd, (Shanghai, China) and then dissolved to 1 mM stock concentration in 50 mM Tris·HCl, pH 7.5 buffer. $Fe(NH_4)_2(SO_4)_2 \cdot 7H_2O$ was dissolved in 20 mM HCl at a concentration of 250 mM. Fe(II) stock solution was then diluted with Milli-Q water to give the final concentration of 2.5 mM. 2OG was dissolved in buffer to 6 mM stock concentration, ascorbate was dissolved to 100 mM stock solution. The master mixture was prepared with the above working reagents concentrations. Enzyme was diluted with buffer to 40 μM and the reaction was started by the addition of enzyme to the reaction mixture. After appropriate time points the reaction was quenched by 1 % formic acid in 1:1 proportion, followed by sample freezing in liquid nitrogen. All reactions were carried out in triplicate.

FIH enzymatic assays

The enzymatic assays were performed in 50 mM HEPES pH 7.5 buffer at 37 °C with typically the following reagents concentrations:

Table 7.16. Conditions used for FIH assays.

Reagent	Concentration
FIH	5 μM
peptide	400 μM
2OG	500 μM
L-ascorbate	1 mM
Fe(II)	50 μM

Peptides for FIH assays were from GL Biochem Ltd, (Shanghai, China) and then dissolved to 1 mM stock concentration in 50 mM HEPES, pH 7.5 buffer. $Fe(NH_4)_2(SO_4)_2 \cdot 7H_2O$ was dissolved in 20 mM HCl at a concentration of 250 mM. Fe(II) stock solution was then diluted with Milli-Q water to give the final concentration of 2.5 mM. 2OG was dissolved in buffer to 10 mM stock concentration, ascorbate was dissolved to 100 mM stock solution. The master mixture was prepared with the above working reagents concentrations. Enzyme was diluted with buffer to 50 μM and the reaction was started by the addition of enzyme to the reaction mixture. After appropriate time points the reaction was quenched by 100 mM EDTA in 1:1 proportion, followed by sample freezing in liquid nitrogen. All reactions were carried out in triplicate.

Preparation of MALDI samples and analysis

1 μL of α-cyano-4-hydroxycinnamic acid (CHCA MALDI matrix) was spotted onto the MALDI plate and then mixed with 1 μL of sample. Samples were analysed in reflectron negative mode and data were processed with MASSLYNX 4.0 (Waters).

The percentage of hydroxylated peptide was calculated using the following formula (described using CODD HIF-1α as example).

$$\%CODD-OH = \frac{\frac{P_3}{TIC}}{(\frac{P_3}{TIC} + \frac{P_2}{TIC} - (\frac{P_1^{'}}{TIC^{'}} - \frac{P_1}{TIC})},$$

where P_1 is the intensity of the peak of a CODD impurity (M_w 2239 g/mol), P_2 is the intensity of the CODD peak, and P_3 is the intensity of the COOD-OH peak, TIC is the total ion count of

the spectrum. P_1' is the peak intensity of the impurity in a control sample, which was not incubated with enzyme, and TIC' is the total ion count for the control. During the reaction, CODD impurity undergoes hydroxylation, and as it has molecular weight equal to CODD -16, hydroxylated impurity contributes to the intensity of the unhydroxylated CODD peak. Thus, to exclude this effect the difference between content of impurity in the control was subtracted.

7.13. Non-denaturing ESI-MS

For non-denaturing analyses PHD2 WT and its variants were desalted using Bio-Spin 6 Columns (Bio-RAD, Hemel Hempstead, UK) into 15 mM ammonium acetate (pH 7.5). The stock solution was diluted with the same buffer to a final concentration of 100 μM. $Fe(NH_4)_2(SO_4)_2 \cdot 7H_2O$ was dissolved in 20 mM HCl at a concentration of 100 mM and then diluted with Milli-Q water to give final concentration of 100 μM. The protein was mixed with Fe(II) and 2OG to give final working concentrations of 15 μM, 15 μM Fe(II), and in particular cases 15 μM 2OG.

Data were acquired using a Q-TOF mass spectrometer (Q-TOF micro, Micromass, Altrincham, UK) interfaced with a Nanomate (Advion Biosciences, Ithaca, NY, USA) with a chip voltage of 1.80 kV and a delivery pressure of 0.5 psi (1 psi=6.81 kPa). The sample cone voltage was typically 60 V with a source temperature of 40 °C and an acquisition/scan time 10 s/1s. Calibration and sample acquisition were performed in positive ion mode in the range 500-5000 m/z. The pressure at the interface between the atmospheric source and the high vacuum region was fixed at 6.20 mbar. External instrument calibration was achieved using sodium iodide. Data were processed with MASSLYNX 4.0 (Waters).

7.14. UV-vis spectroscopy studies

UV-vis spectroscopy experiments were performed using a Varian Cary 4000 UV-vis spectrophotometer in the wavelength range of 200 nm - 800 nm. Sample preparation was typically carried out in an anaerobic glove box (Belle Technologies, Weymouth, U.K.) as described [3, 4]. 50 mM HEPES pH 7.5 buffer and Milli-Q water were deoxygenated by repeated rounds of vacuum/argon purging, then sealed with a rubber septum and parafilm. $Fe(NH_4)_2(SO_4)_2 \cdot 7H_2O$ was dissolved in deoxygenated Milli-Q water, 2OG and CODD 19-mer were dissolved in deoxygenated 50 mM HEPES pH 7.5 buffer. The enzyme solution was

gently deoxygenated on ice by about 30 short rounds of vacuum/argon purging and sealed with a rubber septum and parafilm.

In the case of PHD2, samples typically contained 100 μM PHD2 (WT or its variant) and either 90 μM Fe(II) followed by titration with 50 mM 2OG solution or 1 mM 2OG followed by titration with 5 mM Fe(II) solution (adding 1 μL titrant to the solution of the enzyme with Fe(II)/2OG). In particular cases the sample also contained 125 μM CODD.

In the case of FIH, samples typically contained 250 μM FIH, 1 mM 2OG, 250 μM Fe(II) and 500 μM peptide in 50 mM HEPES pH 7.5.

In the case of DAOCS, samples typically contained 200 μM DAOCS, 1 mM 2OG, 300 μM Fe(II) and 2 mM penicillin N/G in 50 mM HEPES pH 7.5. For K_d(Fe(II)) determination samples contained 200 μM DAOCS, 1 mM 2OG and Fe(II) were titrated from 10 mM or 50 mM stock.

To expose the MLCT feature, a spectrum of the apo-enzyme was subtracted from the obtained spectra of the complexes. K_d values were calculated by fitting the dependence of the metal ligand charge transfer feature (MLCT) at λ_{max} plotted against ligand concentration using the following formula:

$$\Delta A = \frac{1}{2 \cdot P_{tot}} \Delta A_{\max}((P_{tot} + x + K_d) - \sqrt{(P_{tot} + x + K_d)^2 - 4xP_{tot}}),$$

where ΔA is absorbance at the wavelength of MLCT maximum, ΔA_{max} – maximum absorbance reached after saturation, P_{tot} – a concentration of an enzyme.

7.15. Steady-state oxygen-dependence studies

Studies of peptide hydroxylation reactions were initially performed in an "Invivo Hypoxia workstation 500" with variable oxygen concentrations (0-20 %). The reaction buffer and Milli-Q water were pre-equilibrated in the hypoxic chamber under different partial pressure of oxygen at 37 °C for 12 hours. The assays were conducted as previously described above with all reagents except enzyme solution dissolved in pre-equilibrated buffer. Reactions were stopped by spotting 1 μL of reaction mixture onto a MALDI plate followed by addition of

CHCA MALDI matrix (SA matrix was used for 35-mer peptides). MALDI analysis of samples was performed as previously described for the MALDI hydroxylation assay.

To investigate oxygen dependence under conditions of >20 % O_2, mass flow controllers (Brooks Instrument, UK) were used to fix O_2 concentrations. Peptide solutions (94 µL) were equilibrated for 10 min at 37 °C with the O_2:N_2 ratio at desired values in septa sealed glass vials, before addition of solutions of 2OG/L-ascorbate (2 µL), Fe(II) (2 µL) and PHD2 (2 µL) using gas-tight Hamilton syringes, to give final reaction conditions as described above. The reaction was stopped by 1 % formic acid (PHD2 assays) or by 100 mM EDTA. The ratio between hydroxylated and unhydroxylated substrate was analysed either by MALDI-TOF-MS or by LC-MS (for 2CA and 3CA).

7.16. Stopped-flow UV-vis spectroscopy

Preparation of O_2-free/O_2-saturated buffer

To prepare O_2-free buffer 50 mM HEPES pH 7.5 buffer and Milli-Q water were deoxygenated by repeating rounds of vacuum/argon purging, then sealed with a rubber septum and parafilm. To prepare O_2-saturated buffer, 50 mM HEPES pH 7.5 was subjected to rounds of vacuum/oxygen purging (on ice).

Stopped-flow analyses

Stopped-flow UV-vis spectroscopy experiments were performed as previously described [3]. An anaerobically prepared solution of enzyme, peptide, $Fe(NH_4)_2(SO_4)_2 \cdot 7H_2O$, and 2OG in 50 mM HEPES pH 7.5 was rapidly mixed with O_2-free/O_2-buffer in 1:1 ratio. Spectra were recorded over 1000 s using a photodiode array detector measuring absorbance changes over a wavelength range of 300-720 nm. The O_2-free spectra were subtracted from the spectra with O_2-saturated buffer obtained under analogous conditions. The kinetic traces at the wavelength of interest were analysed using Origin™ 8.51 software.

Table 7.17. Conditions used for stopped-flow UV-vis assays.

	Enzyme, mM	Substrate, mM	2OG, mM	Fe(II), mM
PHD2	0.8	1	5	0.5
FIH	0.5	1	5	0.4
DAOCS	0.8	1	5	0.7

7.17. Rapid quench-flow studies

Rapid flow-quench experiments were performed using the same conditions and an assay mixture preparation procedure as in stopped-flow experiments. Rapid quench flow equipment (RQF-63, TG-K Scientific, UK) was set in an anaerobic glove box (Belle Technologies, Weymouth, UK). Samples were quenched with 1 % (v/v) CF_3COOH and analysed using MALDI-TOF-MS (peptide hydroxylation) as described above or LC-MS (succinate formation).

For further MALDI-TOF-MS analyses samples were diluted to 50 μM peptide concentrations by 15 mM ammonium citrate and spotted onto the MALDI target plate as described above. To prepare samples for LC-MS succinate determination, enzyme was filtered out using an Amicon ultra-15 Millipore centrifugal filter membrane (3 kDa M_W cut-off).

The obtained data were analysed using Origin™ 8.51 software and fitted with a single exponential function.

7.18. LC-MS 2OG/succinate determination

Chromatographic separation was performed at 50 °C using a Waters ACQUITY BEH Amide 1.7 μm 2.1x100 mm column on a Waters ACQUITY™ ultra-performance liquid chromatography (UPLC) system. The following eluents were used: mobile phase A: 10 % H_2O, 90 % acetonitrile (v/v), 10 mM ammonium formate; mobile phase B: 50 % H_2O, 50 % (v/v) acetonitrile, 10 mM ammonium formate.

For succinate determination and quantification in rapid flow quench experiments, the elution gradient was 0 – 5.0 min linear from 10 % to 50 % B, and 5.0 – 7.0 min at 10 % B for re-equilibration of the column. A constant flow rate of 0.4 mL/min was used. Analytes were detected in negative ionisation mode using single reaction monitoring (SRM) on a Quattro

triple quadruple mass spectrometer (Waters, USA) with a cone voltage of 15 V and a capillary voltage of 3.0 kV. The desolvation temperature was set to 250 °C and the source temperature to 120 °C

For 2OG determination (Chapter 6), reaction mixtures typically contained 5 mM (*R*)- or (*S*)-2HG, 50 μM $(NH_4)_2Fe(SO_4)_2$ and variable concentrations (0–10 mM) L-ascorbate/GSH prepared in 50 mM HEPES (pH 7.5), and were incubated for 20 h (37 °C). 2OG production was subsequently measured. The elution gradient was 0–10.0 min linear from 10–30 % B, and 10.0–12.0 min at 10 % B for re-equilibration of the column. A constant flow rate of 0.4 mL/ min was used. This was directly coupled to a Waters Quattro micro (Micromass UK Ltd) triple quadrupole mass spectrometer in the negative ionization mode. The desolvation temperature was set to 250 °C and the source temperature to 120 °C.

7.19. Protein LC-MS

Samples obtained in kinetic assays on 2CA and 3CA were diluted to a protein concentration of 5 μM in MilliQ water for MS analysis. They were analysed using a Waters® LCT classic mass spectrometer by electrospray ionisation in positive ion mode. An Agilent HP1100 liquid chromatography system was used and samples were run through a Phenomenex® Aeris Widepore 3.6μ XB-C8 150x2.1 mm column at 0.5 mL/ min in a gradient of phase A: 95 % H_2O/5 % CH_3CN/0.01 % FA; phase B: 95 % CH_3CN/5 % H_2O/0.01 % FA. Gradient was carried out according to Table 7.17. for 2CA and 3CA samples. Data were collected and analysed using MassLynx 4.0. Spectra were deconvoluted using MaxEnt 1 across an appropriate mass range.

Table 7.18. The gradient used for analyses of 2CA and 3CA hydroxylation.

Time	Phase A	Phase B
0	100	0
1.5	100	0
12	0	100
14	0	100
15	100	0
19	100	0

7.20. Amino acid analysis [5]

Peptides were acid hydrolysed before analysis. An excess of 6 M HCl was added to each sample, which were then incubated for 24 h at 110 °C under vacuum. All samples were concentrated in a vacuum centrifuge (Speed-Vac, Heto). Hydrolysed peptides were reconstituted in borate buffer pH 9.5 (100 µL) and a solution of 6-aminoquinolyl-*N*-hydroxysuccinimidyl carbamate (AQC) in CH_3CN (50 µL, twice concentrated in comparison with AccQTag Solution Protocol, Waters). The mixture was reacted for 10 min at 55 °C. LC-MS analyses were performed using Waters Acquity (Waters, USA) ultra-performance liquid chromatography system coupled to a Waters Quattro micro (Micromass UK Ltd) triple quadrupole mass spectrometer equipped with an electrospray ionisation source. Separations were performed using a AccQ-Tag Ultra column (1.7 µm, 100 x 2.1 mm; column temperature set at 55 °C) with flow rate of 0.7 mL/min. The injection volume was 1 µL. Samples were kept at 4 °C in an autosampler. The mobile phase A composition was 95 % (v/v) H_2O, 5% AccQTag Eluent A concentrate, the mobile phase B: 100 % CH_3CN, 1.3 % (v/v) formic acid. The gradient conditions used for separation are given in **Table 7.19**. The conditions for ESI-MS detection were as follows: positive-ion mode, desolvation temperature at 150 °C, source temperature at 120 °C, capillary voltage at 3000 V, sample cone voltage at 25 V, cone and desolvation gas flow at 30 and 800 L/min respectively. The extracted ion chromatogram was created at the mass corresponding to AQC-derivatized hydroxyproline (304±0.2 Da). Three chromatograms were acquired for every sample. The limit of detection for the method is approximately 1 pmol/µL.

Table 7.19. The gradient used for amino acid analyses.

Time, min	Phase A, %
0	100
25.0	75.0
25.5	40.0
27.5	40.0
28.0	100.0
30.0	100.0

7.21. CD spectroscopy

CD-spectra were recorded using a Chirascan CD/Fluorimeter (Applied Photophysics, UK) spectrometer. Measurements were carried out at 20 ºC in a 0.1-cm path length quartz cuvette, with an enzyme concentration of 0.125 mg/mL in 5 mM Na-phosphate buffer, pH 8.0. Spectra were recorded in the wavelength range of 260 to 190 nm at 0.5 nm intervals, and each spectrum represents an average of 3 scans. Spectra were baseline-corrected by subtraction of the buffer spectrum. Data were expressed as the mean residue ellipticity ([θ], $deg \cdot cm^2 \cdot dmol^{-1}$).

Thermal denaturation experiments were performed under the same conditions. The ellipticity at 220 nm (θ_{220}) was monitored from 10 to 90 ºC. Origin 8.5 software was employed to fit the data to a boltzmann sigmoidal curve and estimate apparent T_m values.

7.20. References

1. Chowdhury, R., M.A. McDonough, J. Mecinović, C. Loenarz, E. Flashman, K.S. Hewitson, C. Domene, and C.J. Schofield (2009) *Structural Basis for Binding of Hypoxia-Inducible Factor to the Oxygen-Sensing Prolyl Hydroxylases.* Structure **17**, 981-989.
2. Lloyd, M.D., H.-J. Lee, K. Harlos, Z.-H. Zhang, J.E. Baldwin, C.J. Schofield, J.M. Charnock, C.D. Garner, T. Hara, A.C. Terwisscha van Scheltinga, K. Valegård, J.A.C. Viklund, J. Hajdu, I. Andersson, Å. Danielsson, and R. Bhikhabhai (1999) *Studies on the active site of deacetoxycephalosporin C synthase.* J. Mol. Biol. **287**, 943-960.
3. Price, J.C., E.W. Barr, B. Tirupati, J.M. Bollinger, and C. Krebs (2003) *The First Direct Characterization of a High-Valent Iron Intermediate in the Reaction of an α-Ketoglutarate-Dependent Dioxygenase: A High-Spin Fe(IV) Complex in Taurine/α-Ketoglutarate Dioxygenase (TauD) from Escherichia coli.* Biochemistry **42**, 7497-7508.
4. Flashman, E., L.M. Hoffart, R.B. Hamed, J.M. Bollinger Jr, C. Krebs, and C.J. Schofield (2010) *Evidence for the slow reaction of hypoxia-inducible factor prolyl hydroxylase 2 with oxygen.* FEBS J. **277**, 4089-4099.
5. Yang, M., A.P. Hardy, R. Chowdhury, N.D. Loik, J.S. Scotti, J.S. McCullagh, T.D. Claridge, M.A. McDonough, W. Ge, and C.J. Schofield (2013) *Substrate selectivity analyses of factor inhibiting hypoxia-inducible factor.* Angew. Chem. Int. Ed. **52**, 1700-1704.

Chapter 8: Summary and conclusions

The Fe(II)/2OG oxygenases are a widespread enzymatic group, which perform a variety of biological functions (see Chapter 1, **Figure 1.1**) [1, 2]. Members of the Fe(II)/2OG oxygenases have conserved active site structures and overall folding. Despite the diversity of the performed enzymatic reactions, significant evidence has been obtained to support the proposal that 2OG oxygenases employ a consensus mechanism [1]. This thesis aimed to address whether the mechanisms of individual 2OG oxygenases are tailored to their specific roles. The work addressed proposed deviations from the consensus mechanism [3, 4], and/or whether the different steps of catalysis of individual 2OG oxygenases were kinetically regulated in a manner related to their biological roles.

PHD2 is a Fe(II)/2OG-dependent HIF hydroxylase which is proposed to act as an oxygen sensor and which has been shown to react slowly with oxygen [5]. Mutagenesis and kinetic studies of PHD2 were performed to identify a molecular rationale for its slow reaction with oxygen. The work described in this thesis found that very tight Fe(II)/2OG binding contributes to the unusual kinetics of PHD2. The slow reaction of PHD2 with oxygen was confirmed including with of all its HIF substrates (no differences between kinetics of oxygen-triggered hydroxylation of peptides representing NODD/CODD sites in HIF-1/2α were observed); it was proposed that the activation of the active site Fe(II) by oxygen is a rate-limiting step in PHD2 catalysis. Although the rate of reaction with oxygen was increased by substituting the Fe(II)/H_2O coordinating D315 residue, the relatively minor rate increase suggests that tight Fe(II)/2OG binding is not the only molecular feature that contributes to the kinetics of PHD2 reaction with oxygen: there are probably other molecular features enabling the fine tuning of PHD2 to its biological function.

As well as investigating the molecular rationale for the unusual rate of reaction of PHD2 with oxygen, the unusual proposal that PHD2 can utilise (*R*)-2HG as a co-substrate and oxidise it in the active to 2OG [4] was also examined. The work described in this thesis did not find any evidence to support this proposal. However, it was found that (*R*)-2HG can be non-enzymatically converted to 2OG in solution in the presence of Fe(II/III) and reducing agents.

The results rationalise the reported 2HG-promoted catalysis by PHD2 *in vitro*, and suggest that the observed non-enzymatic chemistry might be of biological interest. Overall, the mechanistic studies on PHD2 described in this thesis confirm that this enzyme functions similarly to other 2OG oxygenases, employing the consensus mechanism for this enzyme family. The activity of PHD2, however, is limited by the rate of its reaction with oxygen, thus tailoring it to its biological role as an oxygen sensor.

FIH is another HIF hydroxylase that is proposed to act as a cellular oxygen sensor. However, the reported $K_m(O_2)$ values for FIH are lower than for PHD2, and cellular data indicate it remains active in hypoxia [6, 7]. The results described here show that the characteristics of the FIH pre-steady-state kinetics are different from those of PHD2. FIH reacts much faster with oxygen, so combined with its lower $K_m(O_2)$ value, this is consistent with the proposal that the pre-steady-state rate of reaction with oxygen may be related to oxygen-sensing capacity. Furthermore, the rate of oxygen activation was dependent on the type of the substrate. Thus, FIH reacts significantly faster with oxygen in the presence of ARD substrates compared to HIF substrates; this is again consistent with known lower $K_m(O_2)$ values for FIH with ARD substrates. More biological studies could clarify if these results have implications for the biological function of FIH. However, at least *in vitro*, there is evidence that FIH might not exhibit the characteristics required for an oxygen sensing enzyme. Although, the kinetic studies of FIH are consistent with the general consensus mechanism, its reaction with oxygen appears to be less tailored to an oxygen sensing role than PHD2, and it can also be modulated by the nature of its substrate.

DAOCS is a Fe(II)/2OG oxygenase involved in the ring expansion of penicillin N. It has been proposed that DAOCS deviates from the standard consensus 2OG oxygenase mechanism and instead employs a ‘ping-pong’ mechanism whereby the product of 2OG decarboxylation leaves the active site prior to ‘prime’ substrate binding [3]. The work described in this thesis used kinetic and biophysical analyses to probe this proposal, and the results suggest that DAOCS does in fact employ a mechanism similar to other 2OG oxygenases, where binding of 2OG and a penicillin substrate can occur at the same time with the formation of a ternary DAOCS.Fe(II).2OG.penicillin complex. Mechanistic studies (by pre-steady-state kinetic techniques, UV-vis spectroscopy and ESI-MS) of DAOCS catalysis were also consistent with those previously reported for other studied 2OG oxygenases, suggesting formation and

degradation of similar catalytic intermediates, and employment of the consensus mechanism by DAOCS in solution. The 'ping-pong' mechanism previously proposed for DAOCS was based significantly on crystallographic work showing overlapping binding sites of 2OG and penG [3]. It is possible that the active site interactions with the DAOCS *C*-terminus in the crystal form alter the DAOCS active site such that it is not longer catalytically representative. In addition, multiple binding of penG to DAOCS suggests that some of the binding modes for unnatural penicillin substrates might be not catalytically productive.

Although all three enzymes studied in this thesis (PHD2, FIH and DAOCS) were found to employ the consensus mechanism for 2OG oxygenases, differences in the kinetics of individual steps in their catalysis were observed. PHD2 and FIH were not found to accumulate an Fe(IV)-oxo intermediate, while DAOCS does exhibit accumulation of an absorbance feature similar to the characterised (in the case of other 2OG oxygenases [8]) Fe(IV)-oxo intermediate. These results suggest that differences in the arrangement of active sites of 2OG oxygenases can significantly affect rate-limiting steps of the catalysis. This may also suggest a difference in the interaction with oxygen for 2OG oxygenases modifying small molecule substrates to those which act as protein hydroxylases. However, more studies on other protein modifying 2OG oxygenases are required to validate such a proposal.

Overall, despite the significant variation for 2OG oxygenases in their substrates and biological functions, the available evidence is that the conserved structures and active site arrangements result in very similar overall mechanisms. However, clear differences are observed in the rates of individual steps in catalysis. These differences must arise from variations in their sequences and structures, which are proposed to cause the adjustment of 2OG oxygenases to their biological function.

References

1. Hausinger, R.P. (2004) *Fe(II)/α-Ketoglutarate-Dependent Hydroxylases and Related Enzymes.* Crit. Rev. Biochem. Mol. Biol. **39**, 21-68.
2. Loenarz, C. and C.J. Schofield (2011) *Physiological and biochemical aspects of hydroxylations and demethylations catalyzed by human 2-oxoglutarate oxygenases.* Trends Biochem. Sci **36**, 7-18.
3. Valegård, K., A.C.T. van Scheltinga, A. Dubus, G. Ranghino, L.M. Oster, J. Hajdu, and I. Andersson (2004) *The structural basis of cephalosporin formation in a mononuclear ferrous enzyme.* Nat. Struct. Mol. Biol. **11**, 95-101.
4. Koivunen, P., S. Lee, C.G. Duncan, G. Lopez, G. Lu, S. Ramkissoon, J.A. Losman, P. Joensuu, U. Bergmann, S. Gross, J. Travins, S. Weiss, R. Looper, K.L. Ligon, R.G.W. Verhaak, H. Yan, and W.G. Kaelin Jr (2012) *Transformation by the (R)-enantiomer of 2-hydroxyglutarate linked to EGLN activation.* Nature **483**, 484-488.
5. Flashman, E., L.M. Hoffart, R.B. Hamed, J.M. Bollinger Jr, C. Krebs, and C.J. Schofield (2010) *Evidence for the slow reaction of hypoxia-inducible factor prolyl hydroxylase 2 with oxygen.* FEBS J. **277**, 4089-4099.
6. Koivunen, P., M. Hirsilä, V. Günzler, K.I. Kivirikko, and J. Myllyharju (2004) *Catalytic Properties of the Asparaginyl Hydroxylase (FIH) in the Oxygen Sensing Pathway Are Distinct from Those of Its Prolyl 4-Hydroxylases.* J. Biol. Chem. **279**, 9899-9904.
7. Tian, Y.-M., K.K. Yeoh, M.K. Lee, T. Eriksson, B.M. Kessler, H.B. Kramer, M.J. Edelmann, C. Willam, C.W. Pugh, C.J. Schofield, and P.J. Ratcliffe (2011) *Differential Sensitivity of Hypoxia Inducible Factor Hydroxylation Sites to Hypoxia and Hydroxylase Inhibitors.* J. Biol. Chem. **286**, 13041-13051.
8. Bollinger, J.M., J.C. Price, L.M. Hoffart, E.W. Barr, and C. Krebs (2005) *Mechanism of Taurine: α-Ketoglutarate Dioxygenase (TauD) from Escherichia coli.* Eur. J. Inorg. Chem. **2005**, 4245-4254.

Appendix: Data processing (stopped-flow kinetics)

The data obtained in the pre-steady-state kinetic studies were processed according to the following procedure.

1. To avoid any non-specific effects, the time-resolved spectra obtained after mixing of the enzyme-substrate complexes with O_2-*free* buffer (**Figure 9.1a**) were subtracted from the time-resolved spectra obtained after mixing of the enzyme-substrate complexes with O_2-*saturated* buffer (**Figure 9.1b**). The resulting difference spectra (**Figure 9.1c**) were analysed for the presence of transient species.

2. The time dependence of absorbance changes at wavelengths of interest were analysed to determine kinetic constants of formation and degradation of the species. Analytical fitting of the experimental data was performed using exponential functions (**Figures 9.2 and 9.3**). If the fit of the experimental data was poor, the number of exponential terms was increased (up to 4 terms). The goodness of the fit was assessed using residuals and Chi-Sqr value as criteria.

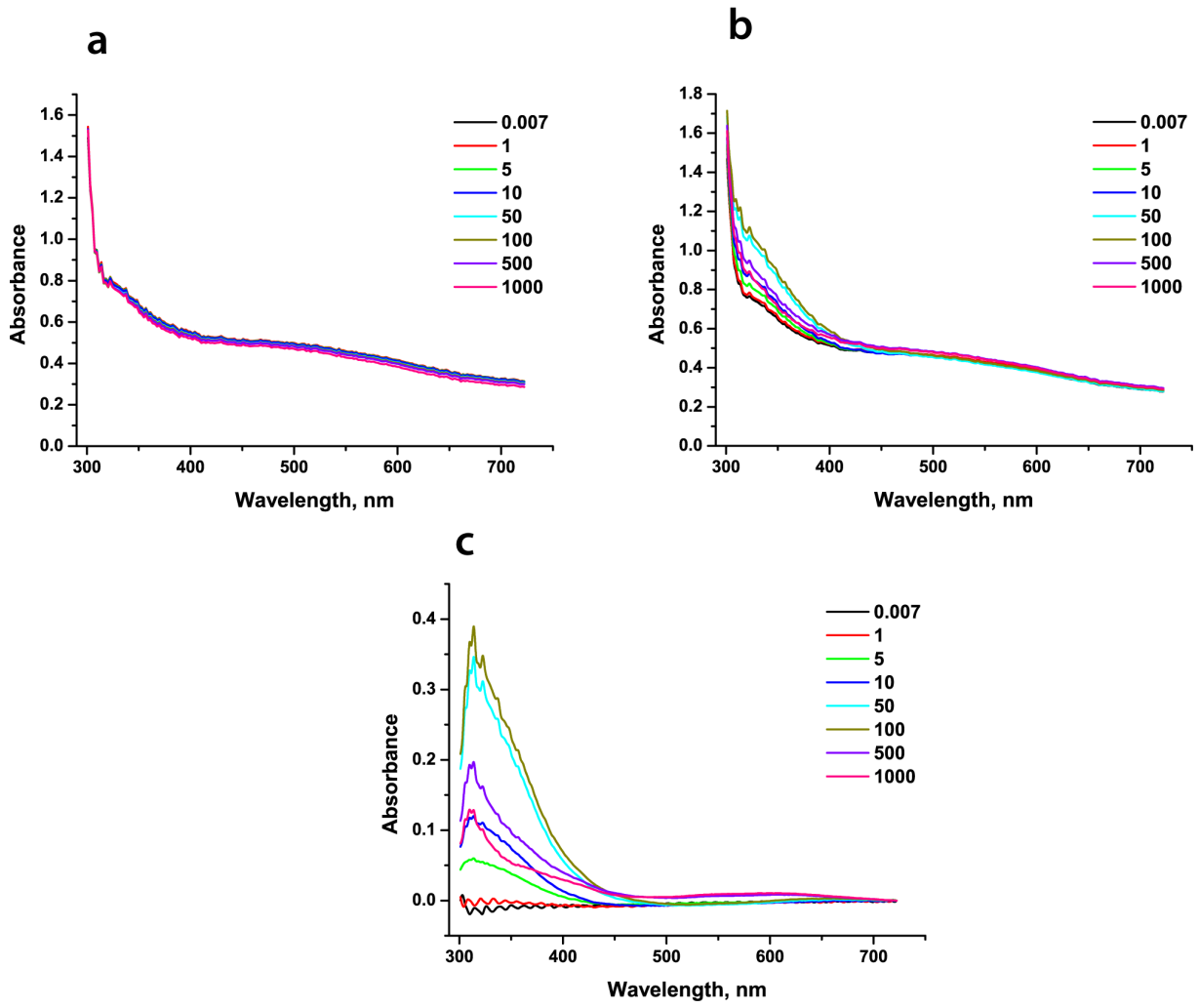


Figure 9.1. Stopped-flow absorbance spectra showing time course of the PHD2-catalysed reaction. **(a)** The absorbance spectra representing reaction after mixing PHD2.Fe(II).2OG.NODD complex with O_2-free buffer. **(b)** The absorbance spectra representing reaction after mixing PHD2.Fe(II).2OG.NODD complex with O_2-saturated buffer. **(c)** The difference spectra: O_2-free buffer spectra were subtracted from O_2-saturated buffer spectra. Changes in absorbance with maxima at 310 nm and 520 nm became apparent.

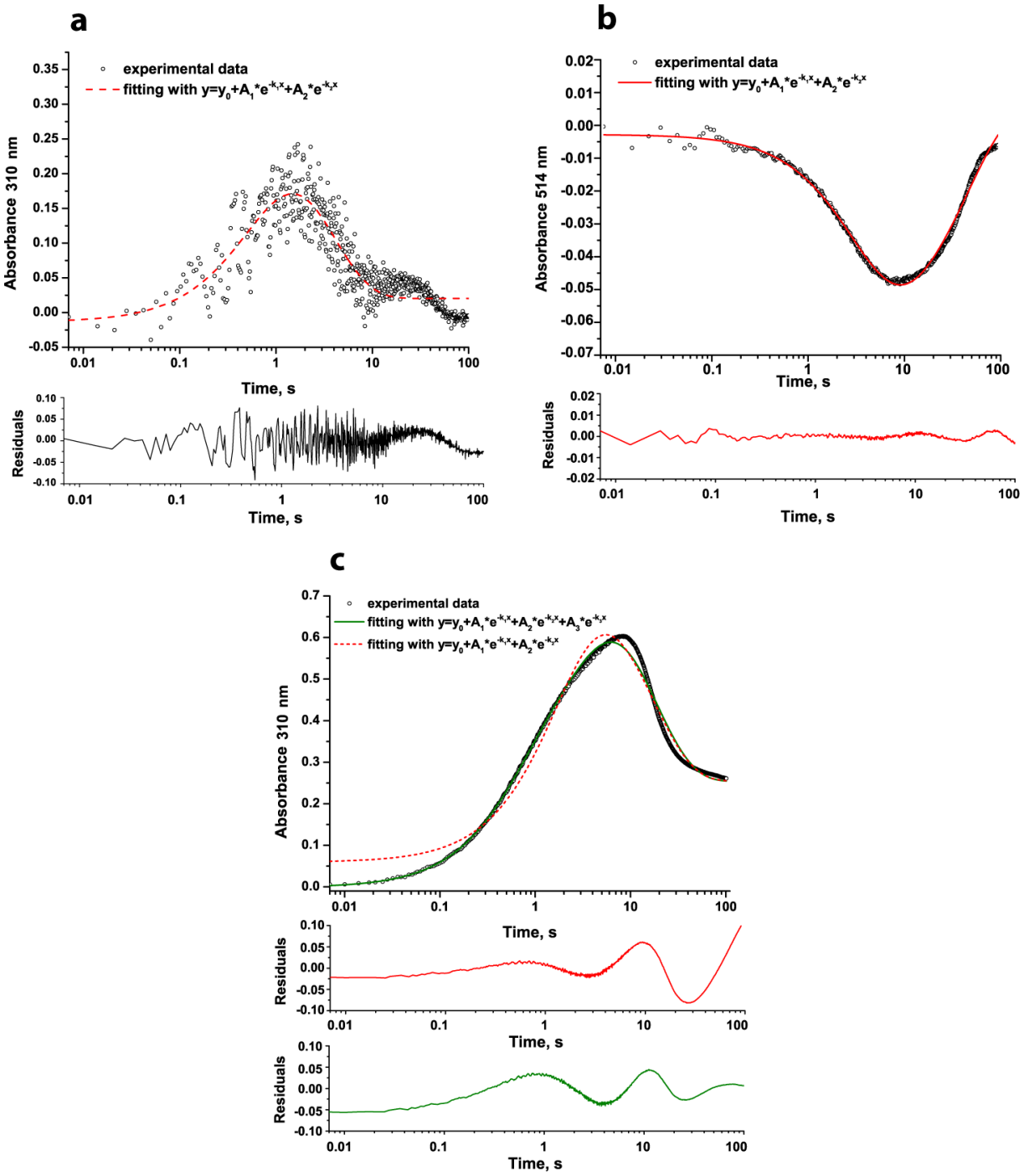


Figure 9.2. Fitting of the stopped-flow traces representing formation and degradation of absorbance species in the DAOCS-catalysed reaction. (a) DAOCS-catalysed penN ring expansion, 310 nm species. The residuals indicate a good fit up to 10 s (the residuals are scattered with no dependence). **(b)** DAOCS-catalysed penN ring expansion, 514 nm absorbance change. The residuals indicate a good fit up to ~50 s (the residuals are scattered with no dependence, the level of noise is low). **(c)** DAOCS-catalysed penG ring expansion, 310 nm species. The residuals indicate a poor fit in the case of both double and triple exponential functions (the residuals look dependent over time and don't show required random scattering).

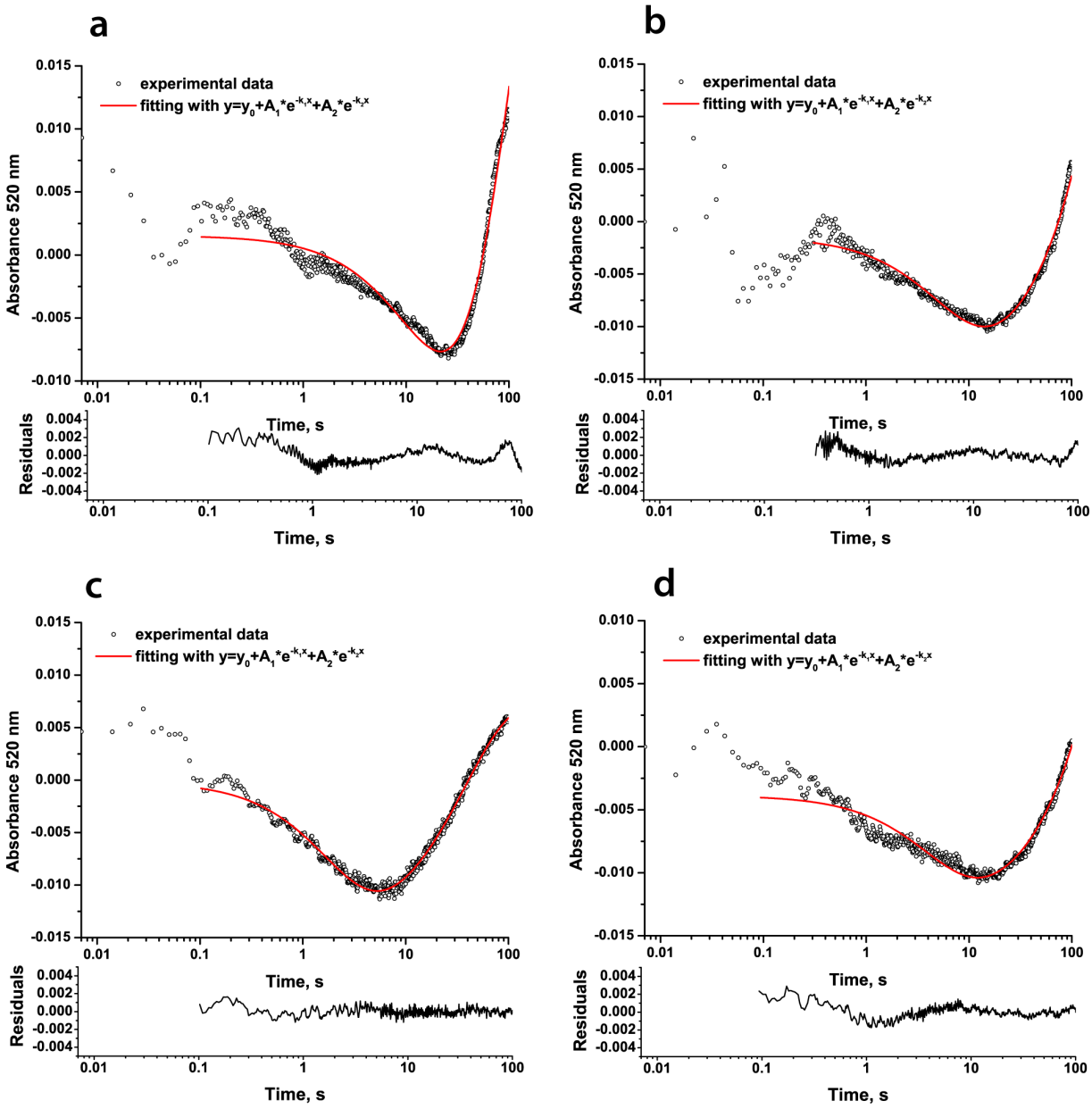


Figure 9.3. Fitting of the stopped-flow traces representing formation and degradation of 520 nm absorbance species in the PHD2-catalysed reactions. (a) PHD2-catalysed hydroxylation of CODD HIF-1α. **(b)** PHD2-catalysed hydroxylation of NODD HIF-1α. **(c)** PHD2-catalysed hydroxylation of CODD HIF-2α. **(d)** PHD2-catalysed hydroxylation of NODD HIF-2α.